MONOPROPELLANT ENGINE INVESTIGATION FOR SPACE SHUTTLE REACTION CONTROL SYSTEM

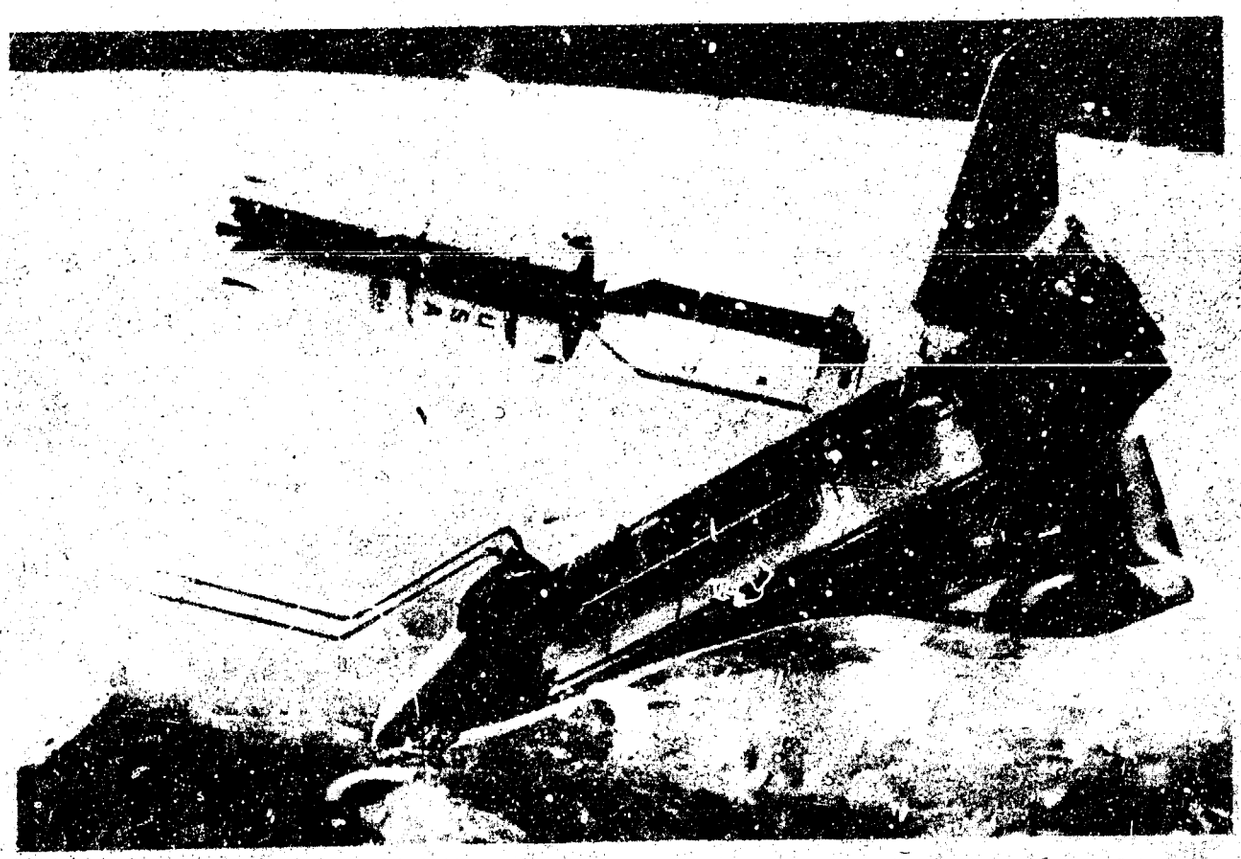

CONTRACT NAS 8-2-8950
NASA/JSC

FINAL REPORT
75-R-460
Volume I

Rocket Research Corporation
Redmond, Washington

TABLE OF CONTENTS

LIST OF FIGURES

LIST OF FIGURES (Concluded)

LIST OF TABLES

FOREWORD

This document is Volume I of the final report of a program conducted by Rocket Research Corporation for NASA-JSC (Contract NAS 8-28950) entitled "Monopropellant Engine Investigation for the Space Shuttle Reaction Control System." An additional task added during the course of the program was the detailed design, analysis, and testing of a catalytic gas generator for the Space Shuttle APU. Results of the gas generator task are presented in a separate document, Volume II, of this final report.

The project manager for the program was Dr. Don L. Emmons. Mr. Douglas D. Huxtable was responsible for the technical direction of the design, analysis, and experimental efforts. Major contributors to the program included K. W. Arasim, M. Archer, C. Cunningham, J. Daly, Dr. J. D. Rockenfeller, T. O. Roubidoux, Dr. E. W. Schmidt, I. Stewart, and the many manufacturing personnel involved in the RCS fabrication and assembly. Mr. D. R. Blevins, NASA-JSC, was the technical monitor.

1.0 INTRODUCTION

1.1 GENERAL

Presented herein are the results of an investigation to determine the capability of a monopropellant hydrazine thruster to meet the requirements specified for the Space Shuttle RCS. Of those requirements (Table 1-1), the major concern was whether the 100,000 seconds life could be achieved at thrust levels within the specified range. Although burn times in excess of 200,000 seconds have been demonstrated at low thrust levels, the corresponding total impulse values have been substantially lower than that required for the Space Shuttle RCS. Two other areas of concern, involving the catalyst, were: 1) the effects of the relatively high vehicle vibration levels on catalyst attrition and 2) the effect of exposure of the catalyst to air during atmospheric reentry of the vehicle. The goal of the present program was to investigate these problem areas, as well as others defined below, and then design, fabricate and demonstrate the life/performance capability of a monopropellant hydrazine RCS engine.

Table 1-1
SPACE SHUTTLE RCS SPECIFIED REQUIREMENTS

Thrust	400 – 1,100 lbf
Feed pressure	300 psia
Minimum impulse bit	30 lbf-sec
Maximum pulse frequency	5 Hz
Maximum steady state burn	600 sec
Burn-time per mission	1,000 sec
Pulses per mission	2,000
Life:	
Total on-time	100,000 sec
Total impulse (min.)	40×10^6 lbf-sec
Environment:	
Random vibration	28 *g* rms

1.2 PROGRAM SCOPE AND OBJECTIVES

In order to accomplish the overall objective the program was divided into the following five major tasks:

- Task I – Preliminary Design Investigation
- Task II – Engine Detailed Design and Analysis
- Task III – Hardware Fabrication, Test, and Evaluation
- Task IV – Hardware Refurbishment and Delivery
- Task V – Post-Test Disassembly and Inspection

The overall flow of the program is shown in Figure 1-1. The scope and objectives of each task are presented in the ensuing paragraphs.

1.2.1 Task I – Preliminary Design Investigation

The objective of Task I was to establish a cost-effective design approach which ensured maximum confidence that the specified engine requirements could be achieved with high reliability and minimum development/operational costs. To achieve this objective, the Task I effort was divided into subtasks with the following objectives.

Bed Retention Design Studies – The objective of these studies was to optimize the design of compartmented catalyst beds to withstand the vibration/acoustic/shock and acceleration environments experienced by the Space Shuttle during launch and reentry. Parametric tests were conducted to evaluate various compartment geometries under simulated mission conditions. Results from these studies included the effect on catalyst attrition of compartment dimensions and total time of exposure of the bed to the launch/reentry environment.

Material Studies – The objective of these studies was to select materials for fabrication of the engine components capable of meeting the specified engine life requirements. Tests were conducted to evaluate effects of nitridation, oxidation, and corrosion due to high temperature operation and exposure to humid salt air. Results were obtained of material nitridation/corrosion characteristics as a function of time of exposure to the above environments at various thermal conditions.

Engine Optimization Studies – The objective of these studies was to analytically evaluate the effect of chamber pressure and bed loading on engine weight, cost, life, and operating/performance characteristics with the goal of selecting the optimum engine operating conditions. In support of these studies subscale tests were conducted with the objective of determining the optimum catalyst composition (i.e., ratio of spontaneous to nonspontaneous catalyst) to minimize catalyst cost consistent with meeting the specified engine performance and life requirements. The primary result from this effort was the selection of the optimum engine operating conditions (chamber pressure and bed loading) and the corresponding catalyst bed composition.

Preliminary Engine Design Studies – The objective of this subtask was to generate preliminary designs of various engine configurations using the results obtained from the previous subtasks. The engine designs varied primarily in the injector design approach and an all-welded design versus a replaceable catalyst bed design.

Design Selection – The objective of this task was to conduct the necessary preliminary analyses and design studies required to select an optimum engine design for the Task II effort based on development/operational cost, reliability, weight, and servicing/maintenance requirement considerations.

Catalyst Studies – In addition to the above subtasks, tests were conducted on in-house funds to evaluate the catalyst oxidation contamination problem and to establish the catalyst thermal

MONOPROPELLANT ENGINE INVESTIGATION FOR A SPACE SHUTTLE RCS
SUMMARY PROGRAM APPROACH

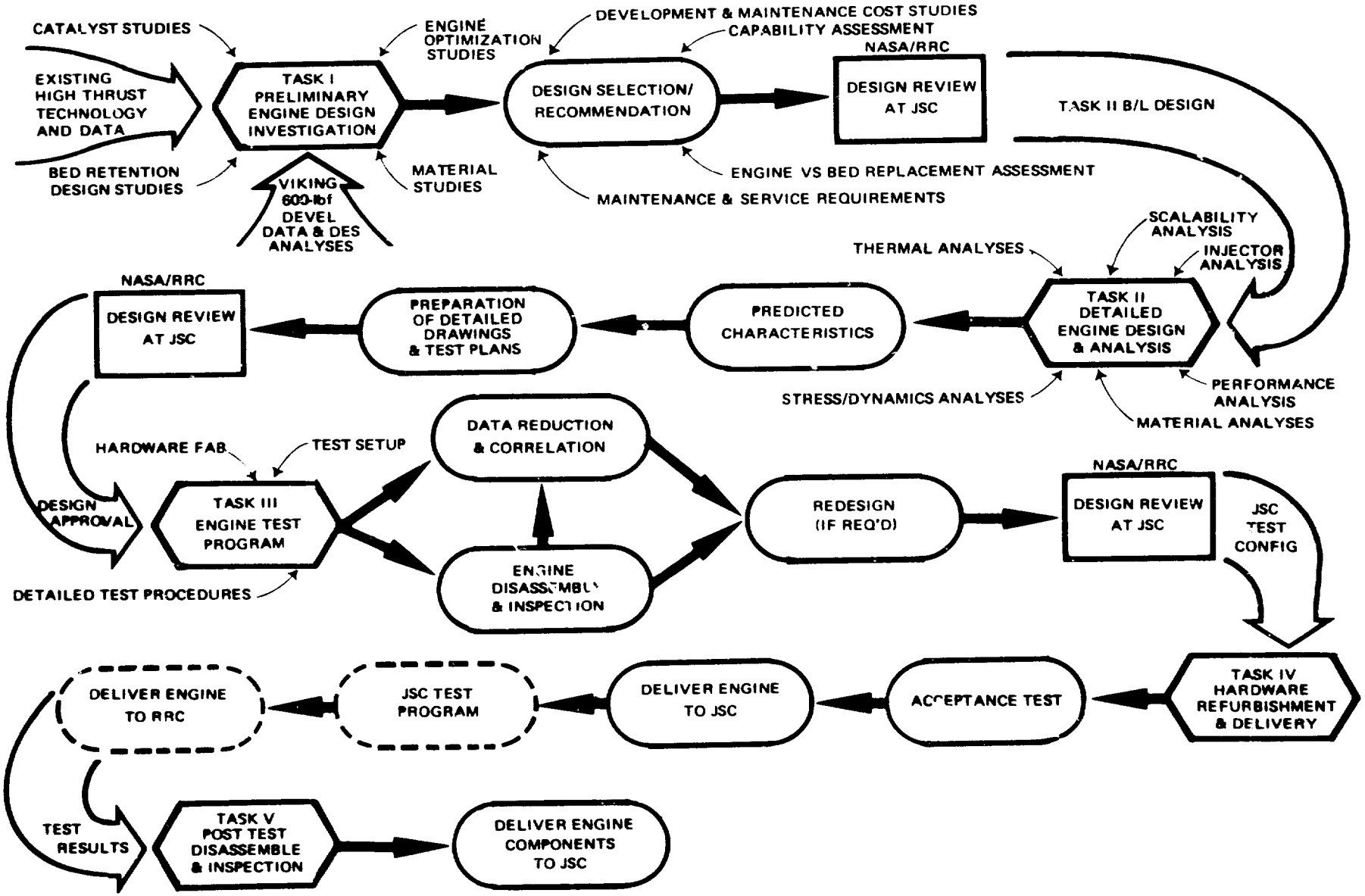

Figure 1-1

expansion characteristics. Results from these experiments consisted of: 1) effect of temperature and pressure on catalyst oxidation; 2) effect of humid, salt air on catalyst activity and life; and 3) effects of temperature and catalyst bed geometry on thermal expansion characteristics.

1.2 Task II – Engine Detailed Design and Analysis

The primary objective of this task was to establish a detailed design of the selected engine supported with thorough analytical studies. The goal of the design and analytical studies was to ensure that the RCS engine design submitted to test fully demonstrates the capability of monopropellant technology to meet the Space Shuttle requirements. The end result of this effort was preparation of detailed engineering drawings of the engine suitable for fabrication. Additional results consisted of justification for the selection of specific engine design features/materials and prediction of the engine performance, thermal, hydraulic, and stress characteristics. Service, maintainability, and checkout requirements were also defined as were potential safety concerns.

1.2.3 Task III – Hardware Fabrication, Test, and Evaluation

The primary objective of this task was to demonstrate by test the applicability and limitations of monopropellant hydrazine RCS engines for the Space Shuttle using current technology. Specific objectives of the test program were to: 1) verify the engine design, and 2) demonstrate the engine capability to meet the stated design requirements and goals. Results to be obtained from the test program consisted of: 1) demonstration of engine life capability under simulated mission conditions; 2) demonstration of number of starts obtained with a preheated bed; 3) measured performance characteristics; 4) sensitivity of washout during long steady state burns; 5) vibration damage susceptibility to the catalyst and engine components; 6) thermal performance; 7) performance during off-limits operation; 8) effects of the test firings on wear of the injector and catalyst bed assembly, catalyst contamination, nitriding of screens, etc., and catalyst condition; 9) post-test calibration data for the injector and valve; and 10) general servicing and handling characteristics.

During the course of the program an additional task (Task IIIA) was established with the objective of evaluating potential improvements of the engine designed in Task II.

A third subtask was added with the objective of evaluating the capability of the Space Shuttle engine configuration to satisfy the Viking 600-lb$_f$ engine life, performance, and flow rate requirements. This was to be accomplished using subscale hardware. Results of the tests are presented in Reference 1-1.

1.2.4 Task IV – Hardware Refurbishment and Delivery

The objective of this task was to deliver an engine to NASA that was refurbished including any design modifications recommended and approved as a result of the Task III effort.

1.2.4.1 Task IV A – Design, Fabrication, Test, and Delivery of a Gas Generator Assembly

During the program an additional task was undertaken for the design and evaluation of a catalytic gas generator capable of meeting the Space Shuttle APU requirements. The details of that investigation are presented in Volume II of this final report.

1.2.5 Task V – Post-Test Disassembly and Inspection

The initial objective of this task was to establish the effects of the test firings conducted by NASA on the RCS engine components. The task was revised, however, to accomplish the same objective on the Transtage engine tested by NASA. Results of the investigation are reported in Reference 1-2.

2.0 SUMMARY OF RESULTS

The major results of the RCS investigation are summarized in this section of the report. Results of the gas generator investigation are presented in Volume II.

2.1 TASK I – PRELIMINARY DESIGN INVESTIGATION

Preliminary Design Studies – During the Task I effort, studies were conducted to determine the optimum RCS design approach for meeting the Space Shuttle requirements. It was concluded that a radial outflow bed design was optimum and that the bed should be compartmented to minimize catalyst attrition. On the basis of analysis, it was determined that the RCS chamber pressure and catalyst bed loading should be 153 psia and 0.045 lbm/in.^{2}-sec, respectively, for optimum life, weight, cost, and engine size.

Catalyst Bed Retention – A series of tests was conducted using various catalyst bed compartment configurations to establish the effect of random vibration on breakup of the catalyst granules. Two catalyst containers, one simulating a radial bed design and the other an axial bed design, were subjected to vibration (29 g rms) in each of the three orthogonal axes for a total duration of 300 minutes. Test variables included: 1) catalyst bed size, 2) packing density, and 3) particle size. The effect of voids in the bed was investigated by preloading the bed with initial voids of 5 and 10 percent. Maximum breakup rate was 0.02 percent per minute of vibration at 29 g rms. It was determined that an initial void in the bed had negligible effect on breakup rate. Used catalyst had the highest breakup rate. It was concluded that the effect of vehicle launch vibration on catalyst attrition was probably not a serious problem.

Catalyst Studies – Laboratory experiments were conducted wherein Shell 405 catalyst was exposed to flowing air for 30 minutes at temperatures ranging from 200 to 1,700°F. Tests were also conducted with an ozone/air mixture (15 ppm O_3) typical of the upper atmosphere. Following exposure, the catalyst sample was tested for ignition delay and hydrogen chemisorption.

The results showed that a marked change occurred in both ignition delay and hydrogen chemisorption at a temperature of approximately 1,200°F. The ignition delay characteristics indicated very little oxygen damage at exposure temperatures below 1,200°F, whereas, hydrogen chemisorption indicated a continual decrease in surface area with increasing temperature. The results obtained with the ozone/air mixture had the same trend, although showing somewhat more degradation than that obtained with atmospheric air. It was postulated, however, that catalyst damage during reentry of the Space Shuttle was not likely to occur due to outgassing effects. This hypothesis was verified in tests conducted both at RRC and NASA-JSC wherein air was directed into the nozzle of thrusters following a firing. On the basis of these test results, it was concluded that outgassing provides sufficient protection to prevent catalyst oxidation damage for the Space Shuttle application.

Materials Studies – An extensive materials investigation was undertaken to provide the necessary data for selection of satisfactory materials for fabrication of the RCS components. Tests were conducted on several candidate materials for oxidation, corrosion, and nitriding resistance. The material nitriding tests were conducted for a 30-hour duration using a synthetic gas mixture at 1,800°F. Tests were also conducted for the same duration with the nitriding environment at 1,650 and 1,900°F. These tests consisted of exposing sample materials to a flowing gas mixture of ammonia and nitrogen. After exposure to the nitriding environment, the samples were tested for weight change, hardness, ductility, and depth of nitriding. Most of the materials evaluated showed excellent resistance to nitridation.

Oxidation and salt corrosion tests were also conducted using nitrided samples. The oxidation tests were performed by cyclically exposing the sample material to an air atmosphere at 1,600°F for a total of five cycles. Each cycle was 30 minutes in duration followed by a rapid air quench.

The salt corrosion tests (30 days) were conducted per ASTM Specification B117. Samples used for this test were previously nitrided for 6 hours at 1,800°F. In general, those materials with iron in their composition showed less resistance to corrosion. It was postulated that nitriding reduced the corrosion resistance of all the samples evaluated.

On the basis of results of the above studies, as well as a consideration of material physical properties, Hastelloy B was selected for fabrication of the RCS components. Its high strength at elevated temperature and low coefficient of thermal expansion were significant factors in the selection.

Subscale Testing – A cost-effective test technique was developed which used a small wedge-shaped chamber configured to the exact size and geometry of a single catalyst compartment. The subscale bed assembly consisted of an injector element, inner catalyst bed, and outer catalyst bed. The bed assembly was installed in a chamber which incorporated a nozzle sized for the desired operating pressure. This subscale test technique provided direct scalability of subscale test results to the full-scale engine providing a technique for conducting optimization studies at low cost. Subscale tests were conducted to: 1) evaluate various low cost outer bed catalysts, 2) evaluate various compartmentation techniques, 3) determine the minimum acceptable quantity of Shell 405 for the inner bed, and 4) determine life capability of the catalyst during simulated mission firings.

Life tests conducted with the LCH-101 catalyst (containing iron, nickel, and cobalt) revealed degradation due to long term exposure to the high temperature decomposition products. An RRC proprietary catalyst (LCH-202) was subsequently evaluated and found to be a superior catalyst for use in the outer bed. A total of 26.3 hours firing time was accumulated on this catalyst during subscale testing.

Two separate techniques for compartmentation of the catalyst bed were evaluated using the subscale test technique. The two compartmentation techniques included: 1) conventional and 2)

scalloped methods of catalyst containment. The conventional approach was based on use of the Viking bed design with spacers to provide compartmentation. The scalloped technique was based on: 1) the use of slots in the bedplates to eliminate screen wires and 2) a bedplate design approach to minimize thermal expansion effects. A total of 9.7 hours was accumulated on the subscale engine incorporating the scalloped bedplate design. This approach was subsequently adopted for the full-scale RCS engine.

Tests were conducted with varying quantities of Shell 405 in the inner bed to establish the minimum quantity required for the RCS engine. A minimum quantity of Shell 405, corresponding to 25 percent of the total catalyst, was found to provide acceptable performance. Based on life considerations a value of 35 percent was recommended for the RCS engine.

2.2 TASK II – ENGINE DETAILED DESIGN AND ANALYSIS

Using the results of the Task I studies the detailed design of the RCS was initiated. The final design of the engine is shown in Figure 2-1. A design summary is presented in Table 2-1. Photographs of the components in various stages of assembly are shown in Figures 2-2 through 2-5. The propellant valve used in the test program was a throttling valve developed by E-Systems, Inc. for the Viking Lander engine, modified to perform as an on-off valve.

The engine incorporated a number of unique design features including:

Slotted Bedplates – Eliminated the requirement of screen wires conventionally used for catalyst retention.

Compartmented Catalyst Bed – Incorporated 12 separate catalyst compartments to minimize differential thermal expansion effects.

Low Injection Momentum – Incorporated 24 injection elements to minimize injection momentum and maximize propellant distribution to the catalyst.

Low Cost Catalyst – Shell 405 catalyst (25 to 30 mesh) was used in the inner bed and an RRC proprietary low-cost catalyst (14 to 18 mesh) was used in the outer bed, with the Shell 405 comprising 35 percent of the total catalyst weight.

Thrust Chamber Liner – Used between chamber wall and catalyst bed to minimize heat transfer during start transients and reduce temperature gradients in the thrust chamber walls.

Cavitating Venturi – Incorporated in the valve outlet to reduce surge flow during start-up and maintain uniform flow rate/thrust throughout life.

Refurbishable Catalyst Bed – Incorporated removable end closures to permit refurbishment of catalyst bed without replacing bedplates or injector body.

Detailed analyses were conducted for the RCS with predictions made of the thermal, structural, and performance characteristics of the engine. In addition, a design safety and reliability assessment was conducted, and maintenance requirements of the RCS defined.

11064-37A

SPACE SHUTTLE RCS TECHNOLOGY ENGINE

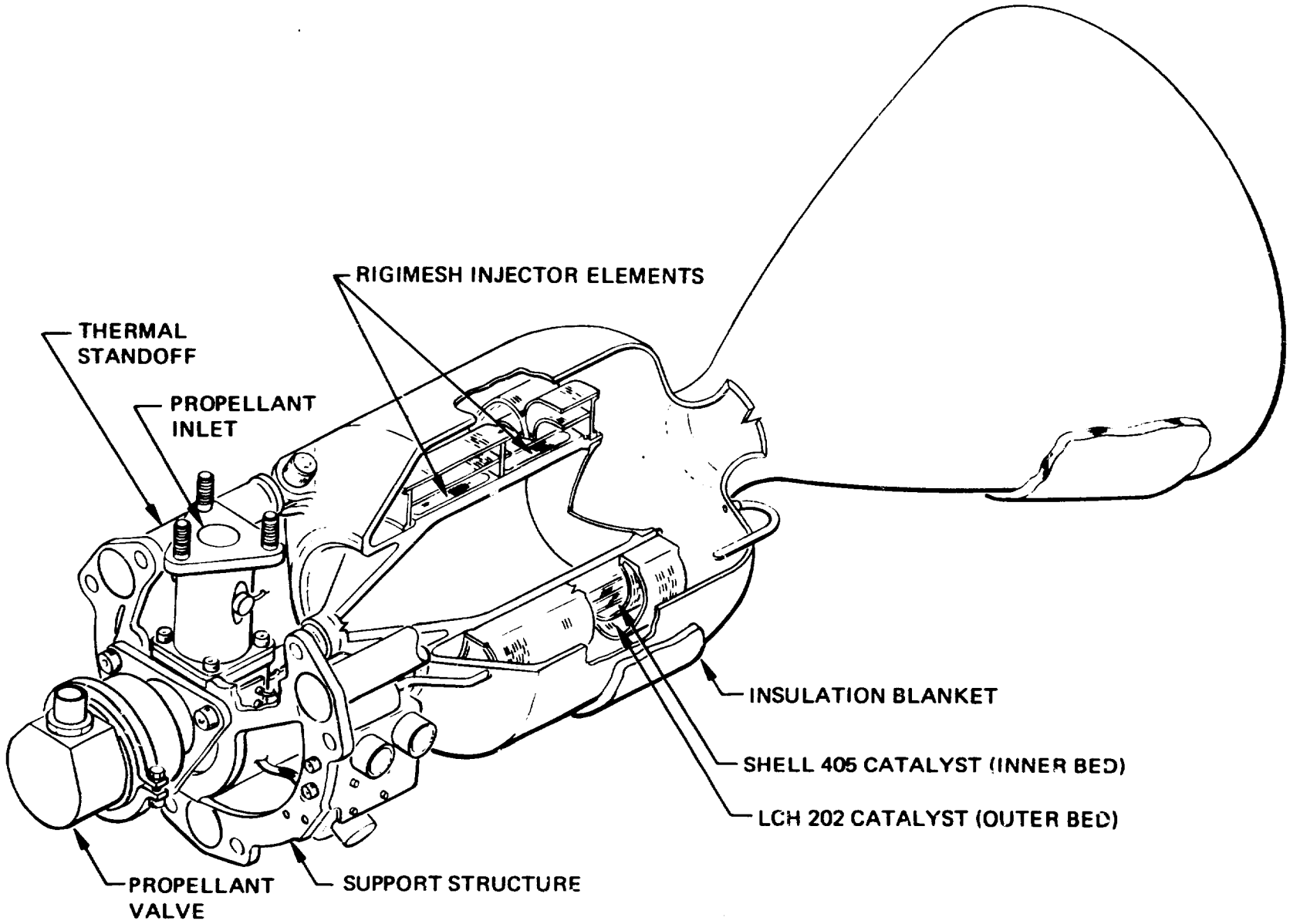

Figure 2-1

Table 2-1
RCS ENGINE DESIGN SUMMARY

THRUST LEVEL	–	485 lbf
FEED PRESSURE	–	300 psia
CHAMBER PRESSURE	–	153 psia
BED LOADING	–	0.045 lbm/in.^{2}sec
BED PRESSURE DROP	–	35 psi
HARDNESS RATIO	–	0.66
AMMONIA DISSOCIATION	–	50%
SPECIFIC IMPULSE	–	230 lbf-sec/lbm
BED GEOMETRY		
• INNER BED DIAMETER	–	3.2 inches
• OUTER BED DIAMETER	–	4.8 inches
• AXIAL LENGTH	–	4.0 inches
THROAT DIAMETER	–	1.53 inches
EXIT DIAMETER	–	8.38 inches
TOTAL LENGTH	–	24.6 inches
THRUST/EXIT AREA	–	8.8 lbf/in.^{2}

V01048 R1

INJECTOR BODY SUBASSEMBLY

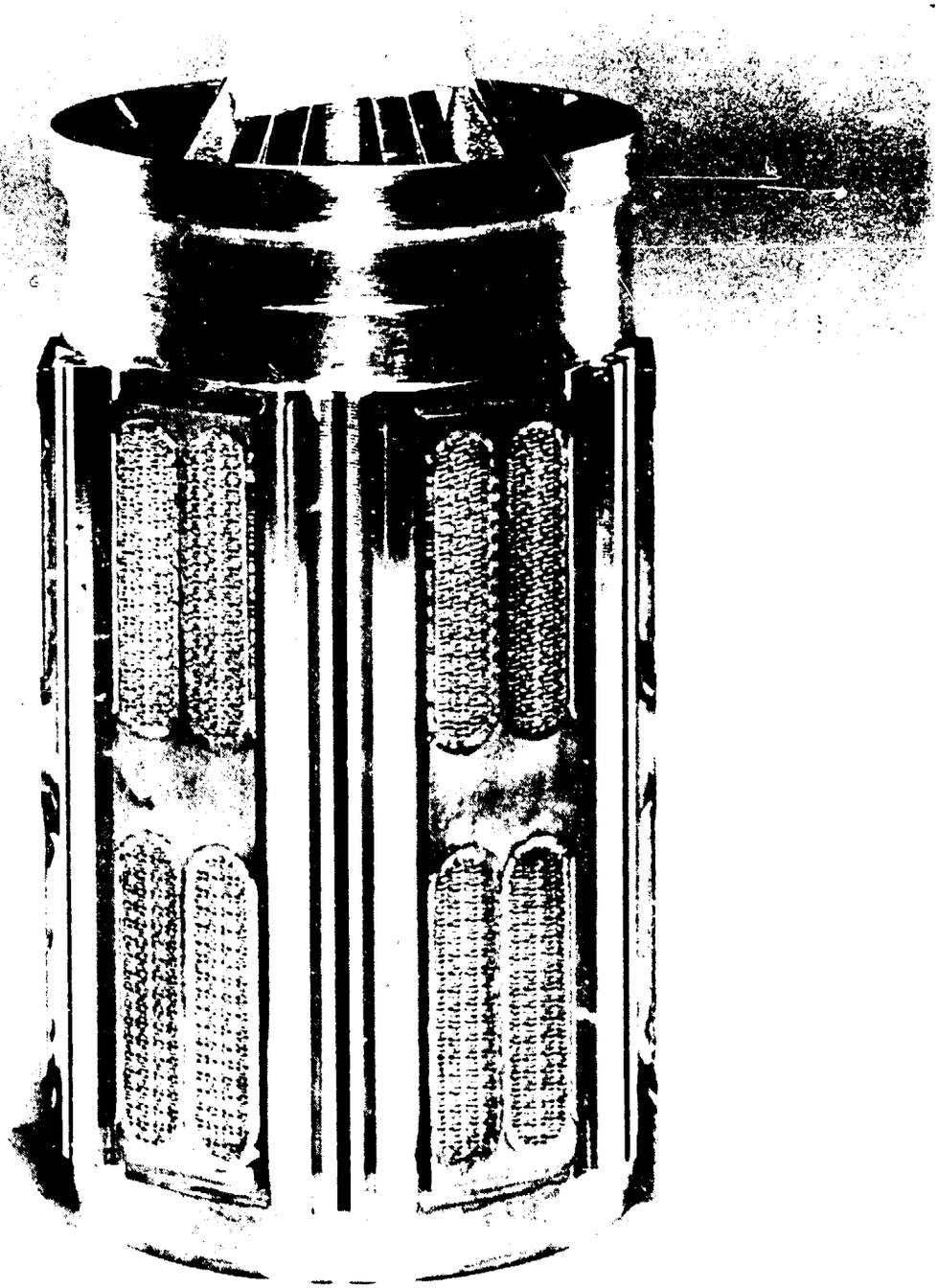

11070-21

Figure 2-2

INJECTOR/CATALYST BED ASSEMBLY

11070-31

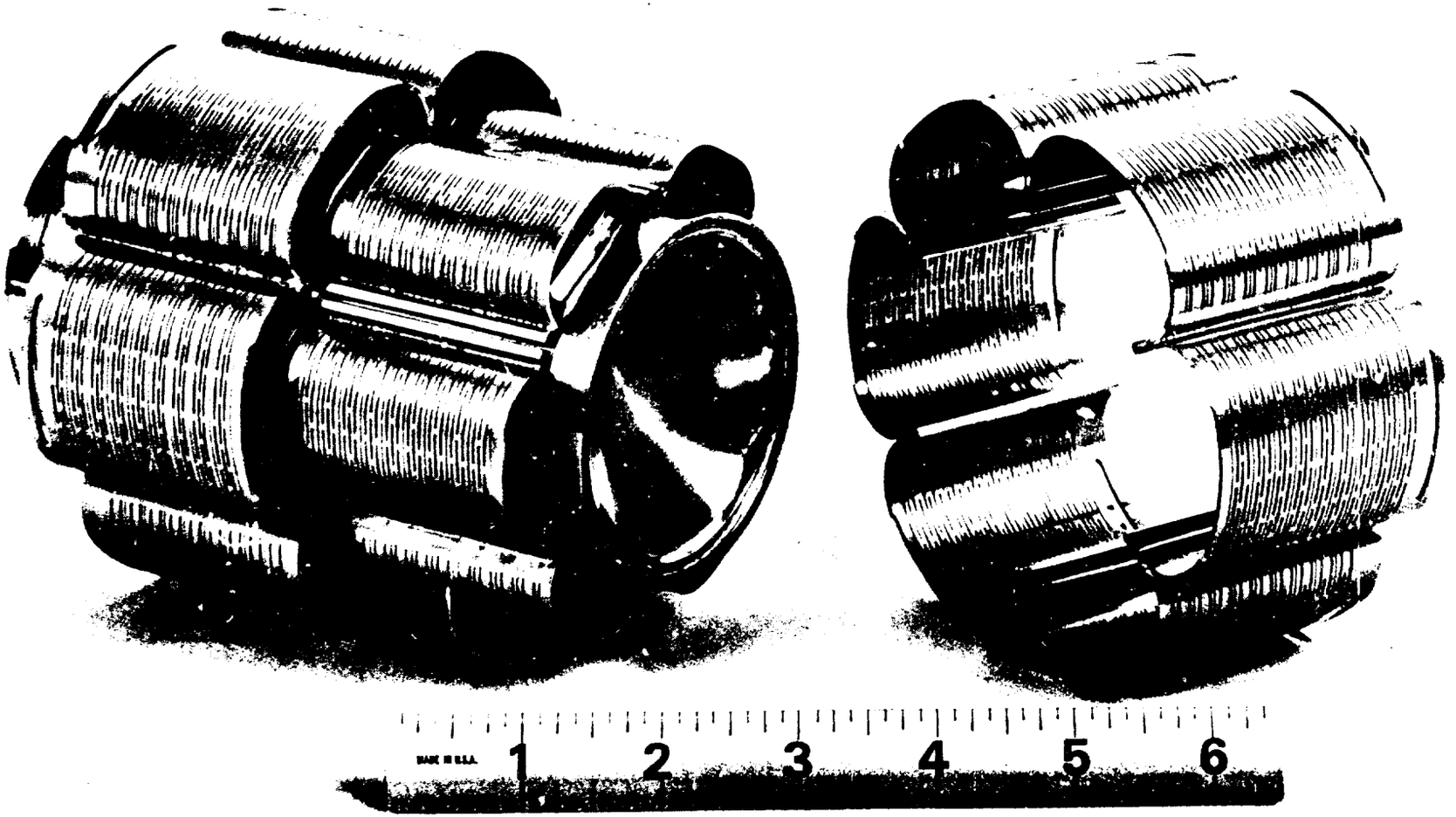

Figure 2.3

CHAMBER/NOZZLE SUBASSEMBLY

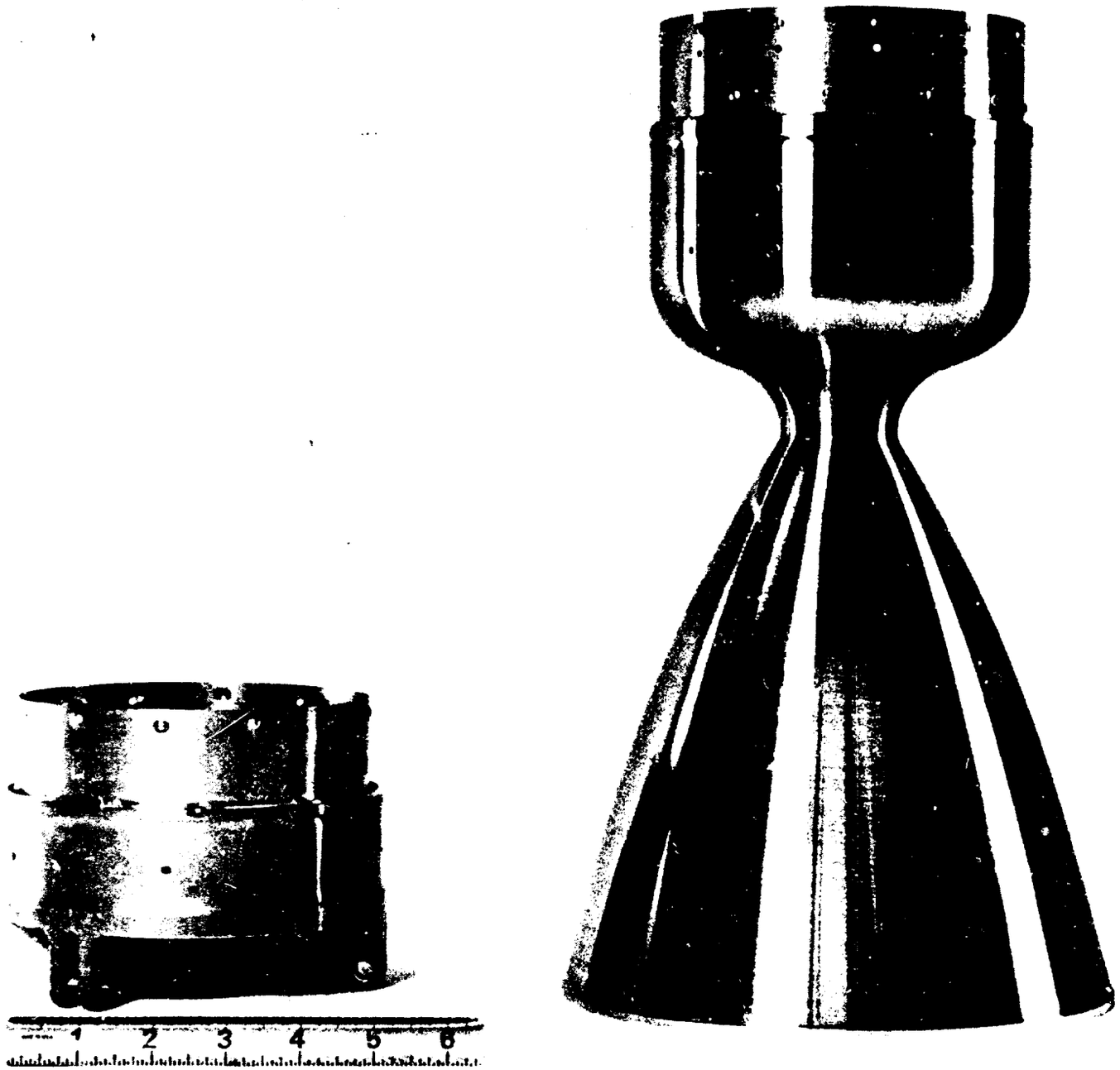

11070-32

Figure 2-4

CHAMBER SUBASSEMBLY

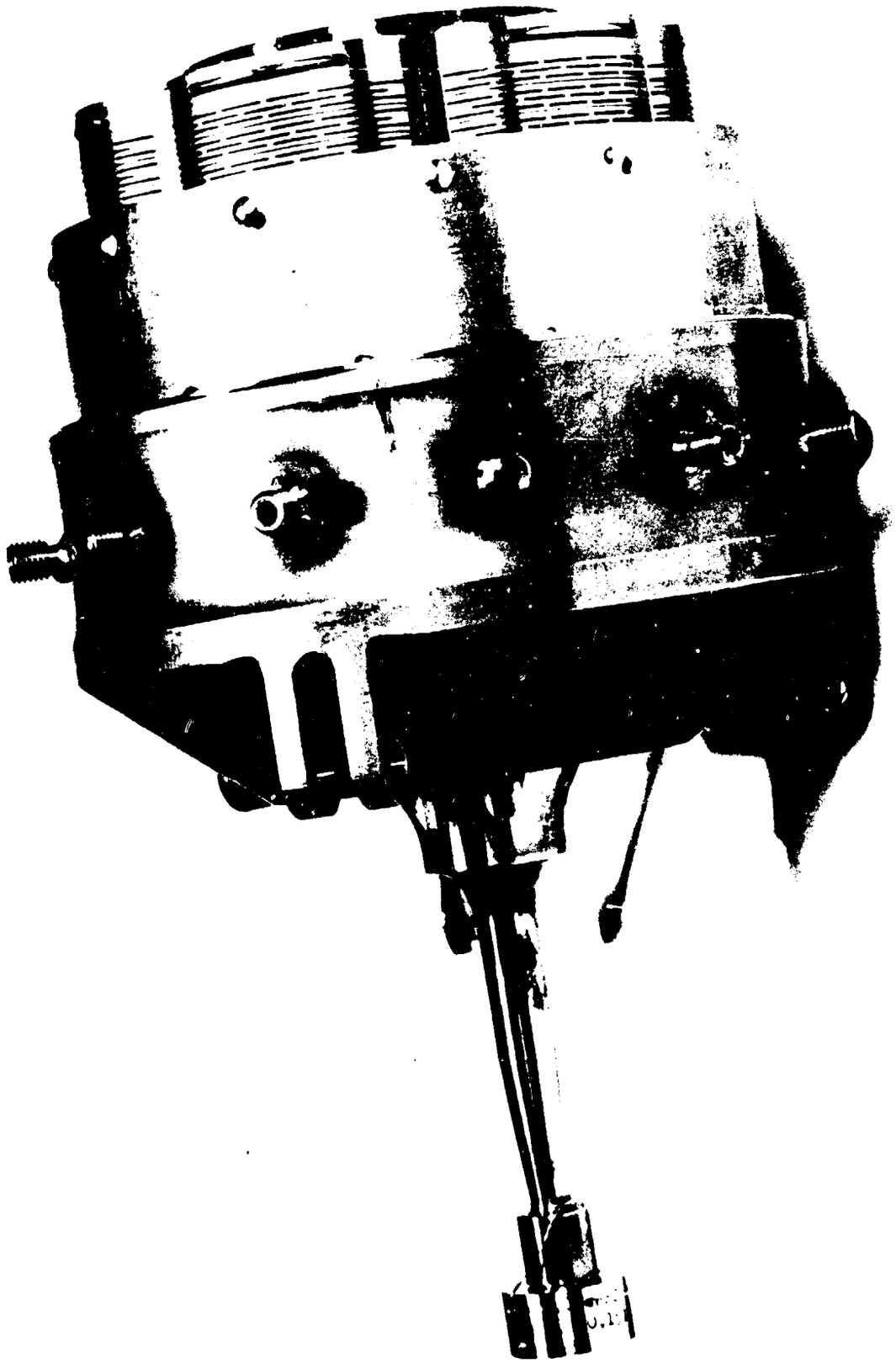

11070-23

Figure 2-5

2.3 TASK III – HARDWARE FABRICATION, TEST, AND EVALUATION

Following assembly of the engine, a test program was initiated consisting of a sea level acceptance test firing and performance mapping firings conducted under simulated altitude conditions.

The acceptance test firing consisted of a 10-second steady-state firing, followed by a 30-minute down time, and a final series of 10 pulses at 250 msec ON/250 msec OFF. The engine successfully completed the acceptance test with excellent performance during both steady-state and pulse-mode operation. Table 2-2 presents a comparison of the design and measured performance values obtained during the steady-state firing. The delivered values for characteristic velocity and bed pressure drop were within 1% of predicted values.

Table 2-2
STEADY-STATE ACCEPTANCE TEST RESULTS

Parameter	Design Goal	Acceptance Test
Characteristic velocity	4,350 ft/sec	4,361 ft/sec
Chamber pressure	153.3 psia	153.7 psia
P_{cu} roughness	–	±3.0 psid
P_{cd} roughness	–	±1.5 psid
Flow rate	2.108 lbm/sec	2.108 lbm/sec
Bed drop	41.5 psid	41.7 psid
Response time (cold bed)	700 msec	425 msec
Tailoff time	–	52 msec

Pulse-mode data also showed excellent agreement with predicted values. Maximum peak pressure was 162 psia (8 psi overshoot) and the integrated pressure-time values varied less than 1.1% for the final six pulses.

Uniform gas temperature was achieved around the circumference of the catalyst bed. Thermocouples monitoring gas temperature at the exit of the catalyst bed at each angular 30° recorded a nominal gradient of only 40°F.

Following the acceptance test the engine was removed from the sea level test stand and stored for approximately 1 week while the altitude facility was prepared for the performance mapping tests. The first altitude test consisted of a single pulse to check out the propellant system. All systems functioned normally; however, no chamber pressure rise was observed in the engine. Subsequently, the engine temperature increased reaching a value of 800°F. The engine was then allowed to cool and a second pulse initiated. This pulse exhibited normal pressure rise and thermal response with transient times similar to the acceptance test values. It was postulated that residual hydrazine in the engine following the acceptance firing had poisoned the catalyst, and that the high temperature achieved by the bed following the first pulse in the performance mapping test, restored the catalyst to near original activity.

The performance mapping tests were then continued with four successive 100-second steady-state firings. Each of the four steady-state firings had performance characteristics similar to those obtained during the acceptance test firing. Some anomalies were noted, however, in temperature distribution and bed pressure drop.

Pulse-mode testing was then initiated with satisfactory performance obtained during the first two sequences (0.1 sec ON/9.9 sec OFF and 0.1 sec ON/99.9 sec OFF). Some pulse distortion was noted during the initial three pulses for the second sequence. During the third pulse sequence (0.1 sec ON/999.9 sec OFF), pulse shape distortion was observed and the sequence was terminated after accumulating six pulses. It was postulated that the pulse distortion was due to operation in a marginal thermal regime. The next duty cycle in the sequence was then initiated (0.1 sec ON/0.99 sec OFF), at which time a pressure spike occurred with subsequent loss in performance. The only visual damage to the engine following shutdown was loss of one catalyst bed end closure. Subsequent inspection of the engine, however, indicated that the pressure spike caused a structural failure of the injector body assembly and subsequent loss of catalyst from the bed.

A detailed teardown and failure analysis was then conducted to determine the cause of the structural failure. Based on an extensive investigation, including subscale testing, it was concluded that the failure was due to insufficient injector thermal margins for low duty cycle operation, which resulted in propellant boiling and decomposition within the injector manifold. This conclusion was verified using heated injector elements which were pulsed at conditions similar to those encountered during the RCS tests. From these tests, as well as analysis of the RCS test data, it was determined that the RCS injector encountered a worst-case thermal condition when the injector temperature was in the range 700 to 1,100°F.

Recommended design changes to increase the injector thermal margin included: 1) provide smooth transition from the circular feed passage to the Rigimesh manifold, 2) reduce injector holdup volume, and 3) reduce mass of metal in the injector at the juncture of the 12 feed passages.

Unfortunately, as a result of funding limitations and NASA redirection to emphasize the Space Shuttle APU application over the RCS, the above design modifications were not subsequently incorporated and tested. However, sufficient analytical studies, subscale testing, and APU GG testing over extreme duty cycle conditions were conducted to provide assurance that a 900-lbf RCS thruster can be built and operated with no duty cycle limitations over Space Shuttle thermal environmental extremes.

3.0 TASK I – PRELIMINARY DESIGN INVESTIGATION

The basic approach adopted for the Task I studies is shown in Figure 3-1. The baseline design approach selected for the initial design studies was the Viking 600-lbf REA, which was under development by RRC for the Viking Lander. Using this engine as a starting point, studies were conducted of the major problem areas anticipated in developing the Space Shuttle RCS engine, with design refinements then made to the baseline engine on the basis of results of the problem area investigations. Results of the various studies are presented in the ensuing paragraphs.

3.1 PRELIMINARY ENGINE DESIGN STUDIES

On the basis of preliminary analyses of engine size, weight, and life, a radial bed was baselined as the optimum design approach for engines in the 400- to 1,100-lbf thrust range. To meet the life requirements, it was further postulated that the catalyst bed should be divided into a number of small compartments. An isometric view of the preliminary baseline design is shown in Figure 3-2. This engine was identical to the Viking engine except for compartmentation of the catalyst bed. The thrust chamber assembly consisted of an injector for distributing propellant to the catalyst bed, a catalyst bed of granular catalyst to initiate spontaneous decomposition of the monopropellant hydrazine, a catalyst bed support system consisting of perforated cylinders and plates to retain the catalyst, and an outer case assembly to contain pressure and direct flow of the reaction products to the nozzle. The catalyst bed was divided into an inner bed containing fine mesh Shell 405 catalyst and an outer bed containing a less active (and low cost) catalyst fabricated by RRC and designated LCH-101. Screen wires were attached to the bed cylinders to retain the catalyst. The injector consisted of six Rigimesh injection elements oriented longitudinally along the chamber axis.

One of the goals of the preliminary design investigation was to establish the optimum size of the catalyst bed compartments and the optimum method of propellant injection. Two fundamentally different methods of injection and bed compartmentation were studied (Figures 3-3 and 3-4). The technique used for the Viking engine, shown in Figure 3-3, has injection elements located longitudinally along the axis of the engine. Radial compartment dividers are equally spaced between the injection elements, resulting in the same number of compartments as injection elements. Axial compartment members can be used to further compartment the bed as shown in the lower left-hand figure.

Shown in Figure 3-4 is the other injection technique evaluated which incorporated the use of circumferential injection elements. Compartmentation of the bed is similar to that shown for the longitudinal injector design.

Design studies were undertaken for both the circumferential and longitudinal injector design approaches with the goal of selecting the optimum approach to be used in the Task II studies. Preliminary analyses were conducted to determine the thermal, structural, and performance

11064-21

TASK I PRELIMINARY DESIGN FLOW DIAGRAM

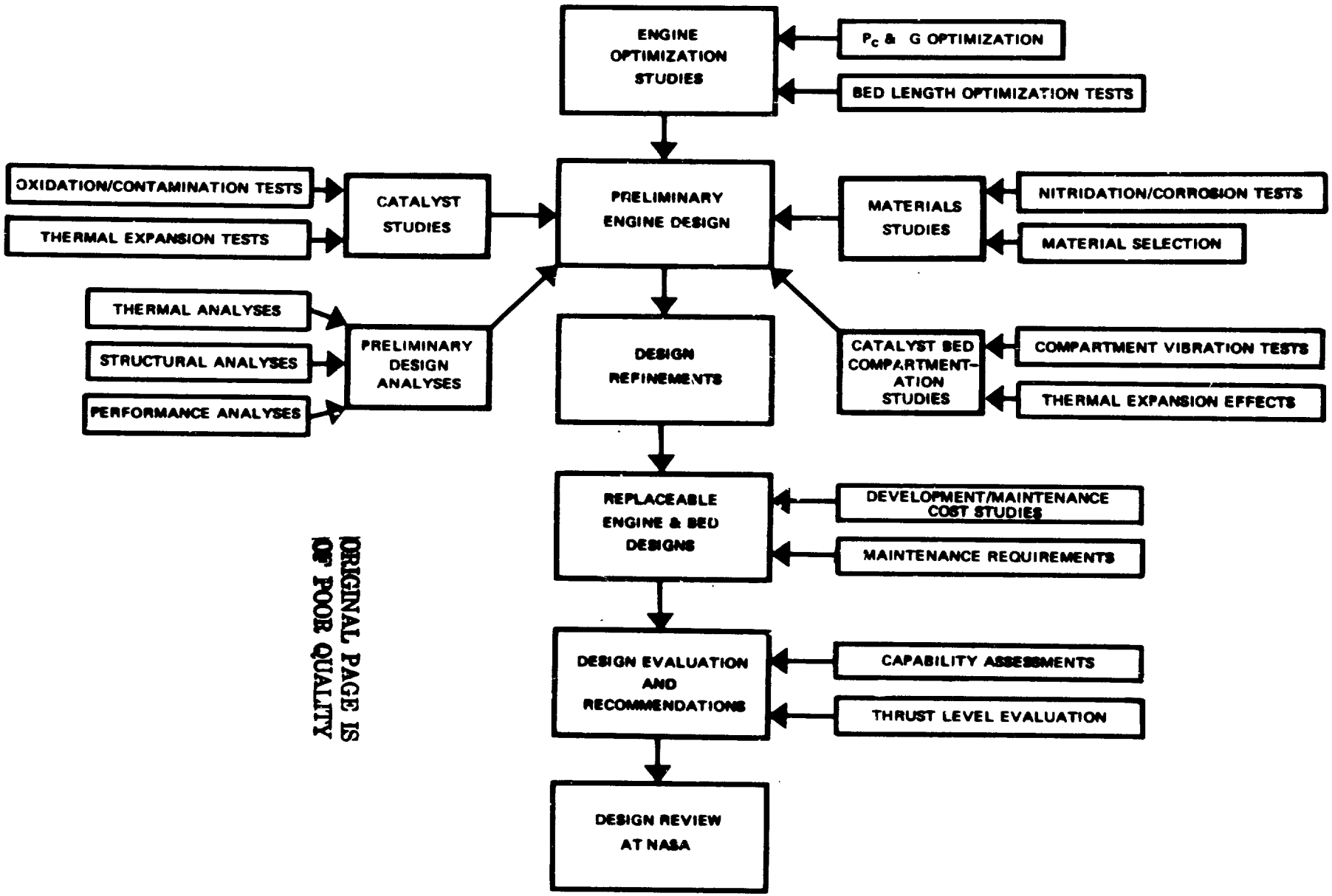

Figure 3-1

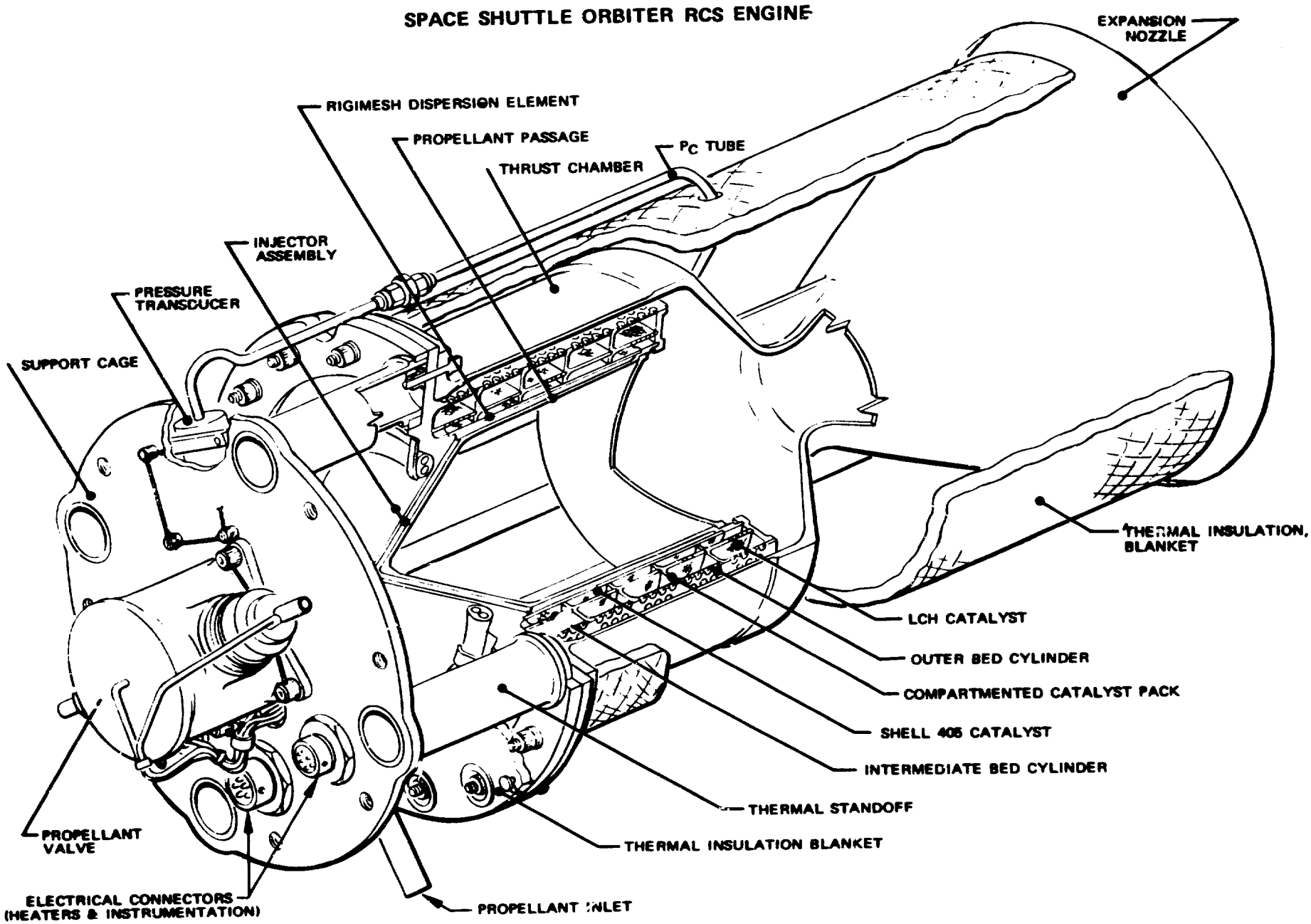
SPACE SHUTTLE ORBITER RCS ENGINE
EXPANSION NOZZLE
RIGIMESH DISPERSION ELEMENT
PROPELLANT PASSAGE
PC TUBE
THRUST CHAMBER
INJECTOR ASSEMBLY
PRESSURE TRANSDUCER
SUPPORT CAGE
THERMAL INSULATION, BLANKET
LCH CATALYST
OUTER BED CYLINDER
COMPARTMENTED CATALYST PACK
SHELL 405 CATALYST
INTERMEDIATE BED CYLINDER
THERMAL STANDOFF
THERMAL INSULATION BLANKET
PROPELLANT VALVE
ELECTRICAL CONNECTORS (HEATERS & INSTRUMENTATION)
PROPELLANT INLET

Figure 3-2

VIKING RADIAL INJECTOR CATALYST BED ASSEMBLY

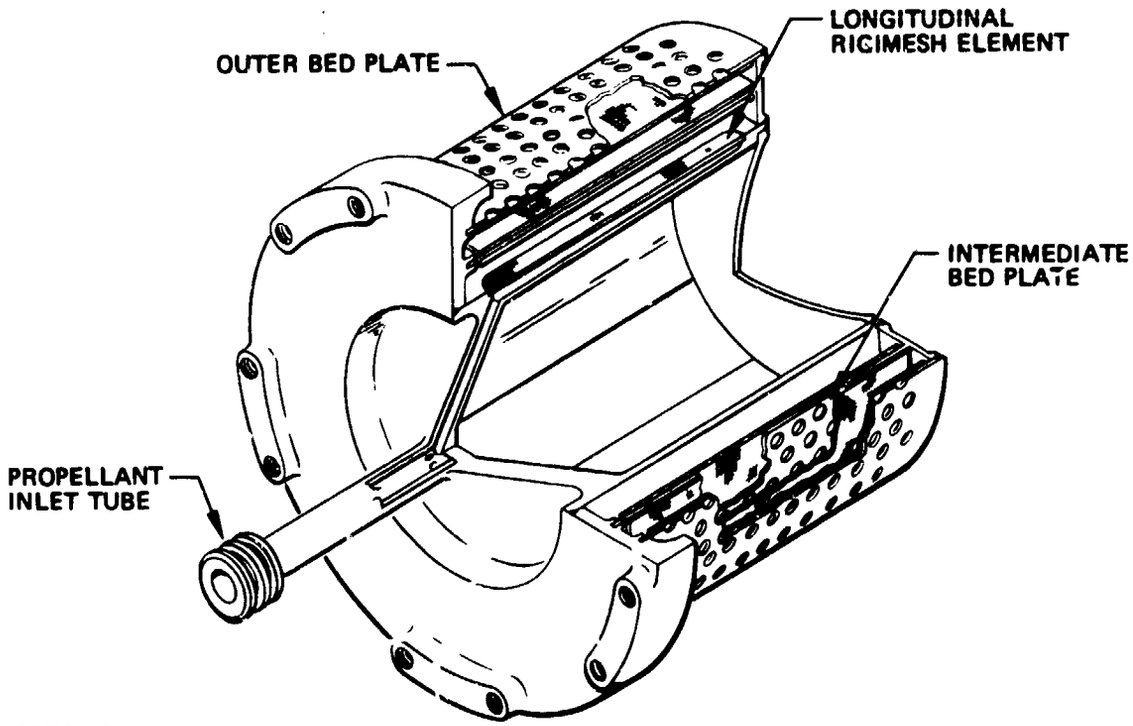

11054-16

RADIAL AND AXIAL CATALYST BED COMPARTMENTATION
LONGITUDINAL INJECTOR ELEMENT

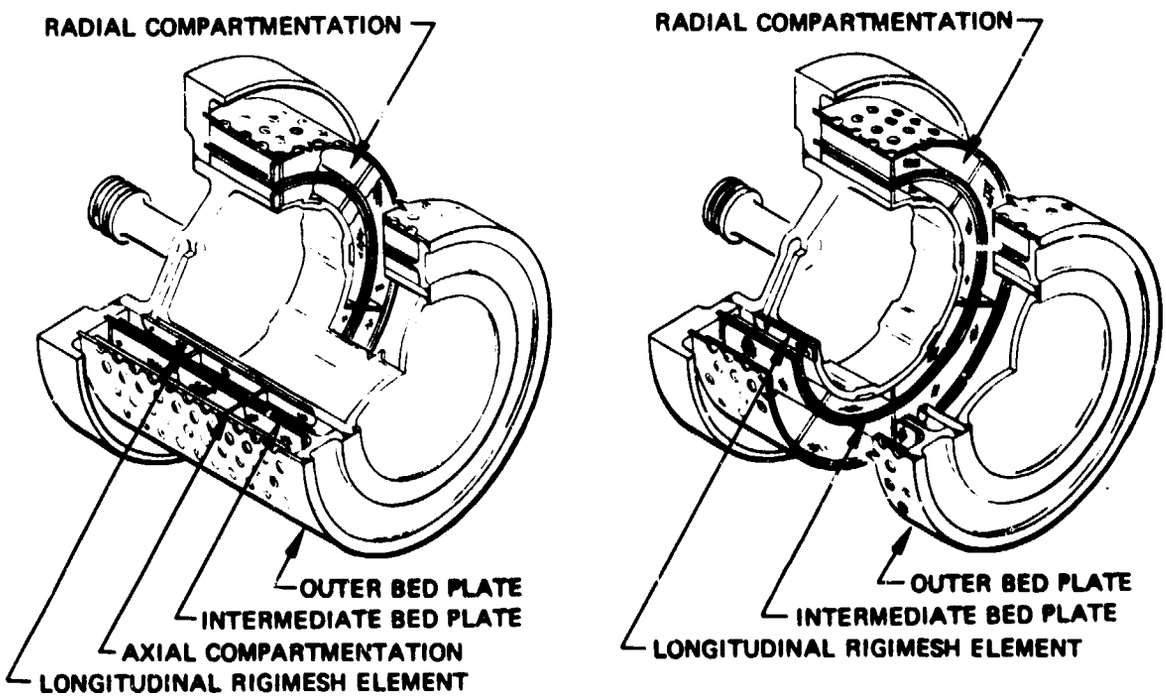

RADIAL AND AXIAL CATALYST BED COMPARTMENTATION
CIRCUMFERENTIAL INJECTOR ELEMENT

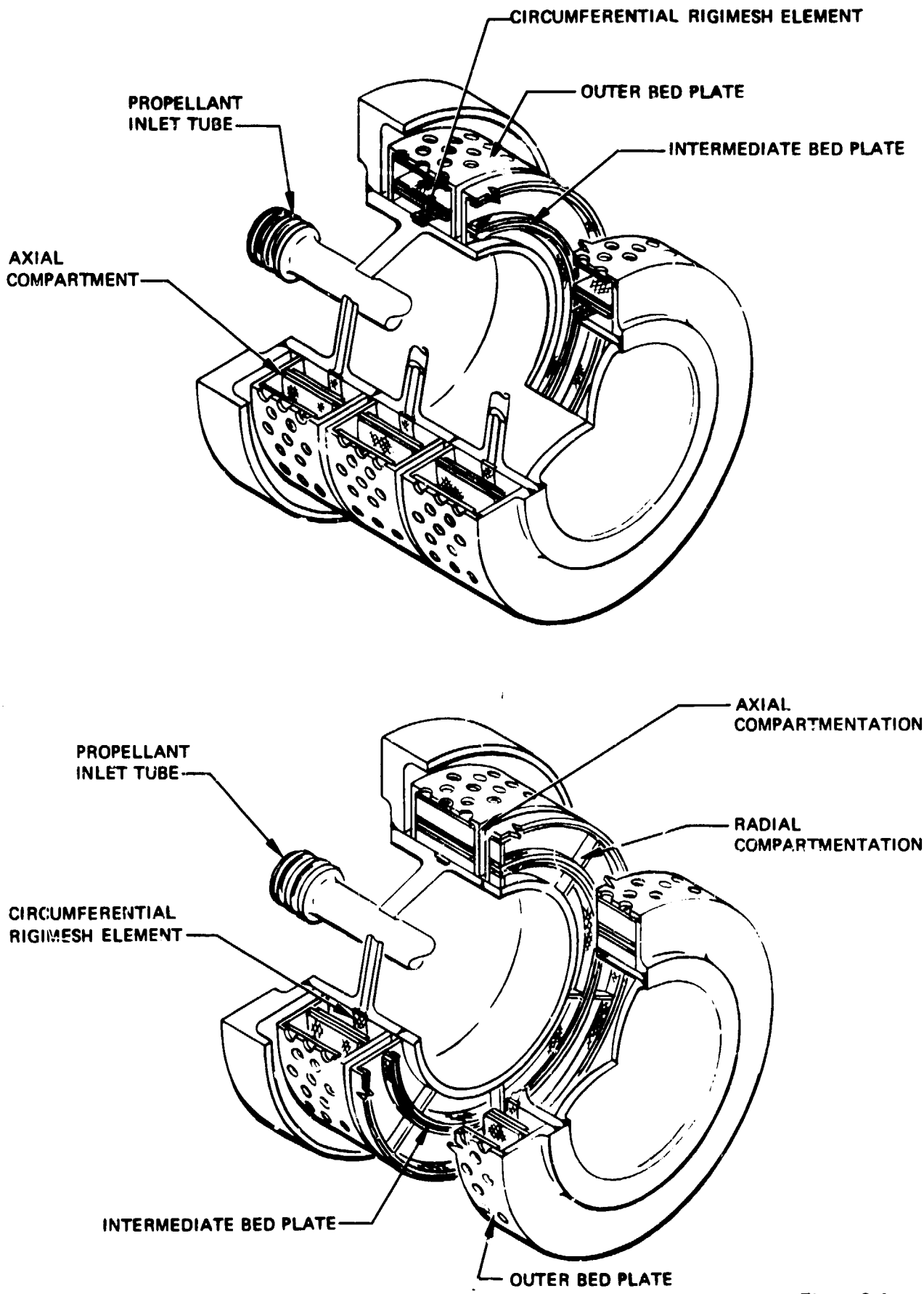

characteristics associated with each approach. In order to maximize catalyst life, it was a design goal to incorporate as many injection elements as possible consistent with thermal restraints. The primary problem encountered in distributing the propellant more uniformly to the catalyst bed is that of propellant boiling in the injector manifold. Consequently, analyses were conducted on a preliminary basis to determine the propellant thermal margin for the various design approaches.

Shown in Figures 3-5 and 3-6 are various designs for the longitudinal and circumferential injection approaches, respectively. From a design viewpoint, the primary problems with the longitudinal injector design were twofold: 1) providing axial compartmentation, and 2) propellant manifolding. In relation to the latter, a problem exists at the junction where the propellant branches from the single inlet tube to the multiple tubes leading to the injection elements. The problem becomes more severe as the number of branch passages increases.

The primary problems associated with the circumferential injector designs were: 1) more complex injector manifold, 2) relatively high propellant holdup volume, 3) higher engine weight, 4) larger size, and 5) more costly to fabricate. Because of the many problems associated with the circumferential injection approach, the conventional longitudinal injector was selected for further study.

Thermal analyses were then conducted to determine propellant thermal margins for longitudinal injectors having 6, 8, 10, and 12 injection elements. Thermal margin was defined as the difference between the propellant saturation temperature and the calculated fluid temperature at the point of injection into the catalyst bed. Results of the calculations are presented below:

No. of Injection Elements	Injector ΔP (psid)	$\Delta T = T_{sat} - T_b$ (^oF)
6	18.7	112
8	21.3	103
10	23.6	95
12	25.0	86

These results indicate that the 12-element injector, although having significantly less thermal margin than the 6-element injector, has sufficient margin to warrant its implementation for the Task II detailed design.

3.2 BED RETENTION STUDIES

The primary objective of these studies was to optimize the catalyst bed design for maximum life. On the basis of in-house catalyst attrition studies, it was concluded that the primary design variables affecting catalyst life related to 1) the technique used for catalyst retention and 2) propellant injection momentum. A review of the life capability of existing catalytic thrusters revealed that smaller thrusters generally had substantially longer demonstrated life than that of large thrusters, indicating that retention of the catalyst in small volumes may be an instrumental factor in achieving long life. In support of this hypothesis, calculations were performed to determine void volume

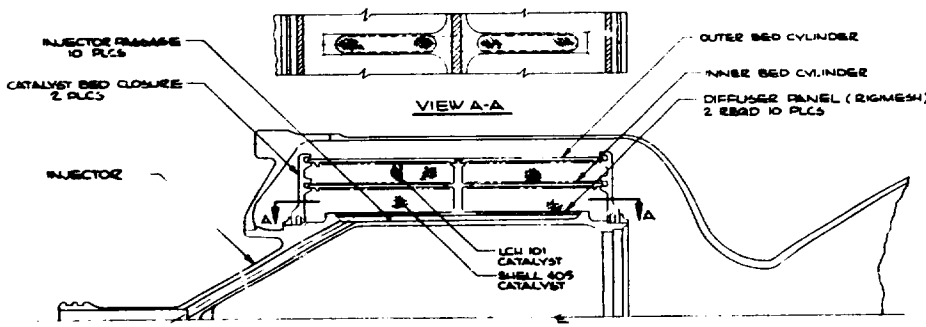

SECTION C-C

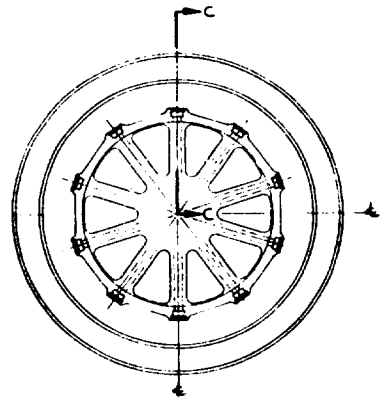

INJECTOR SECTION VIEW
10 FEED PASSAGES

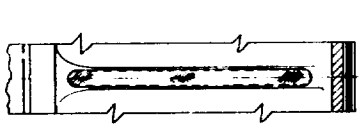

VIEW B-B

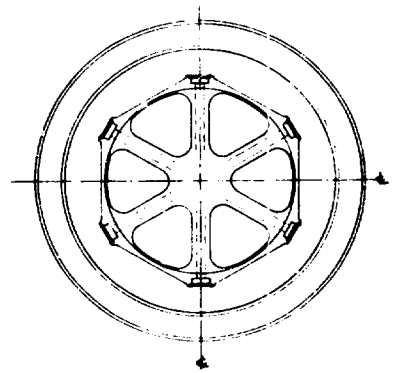

INJECTOR SECTION VIEW
6 FEED PASSAGES

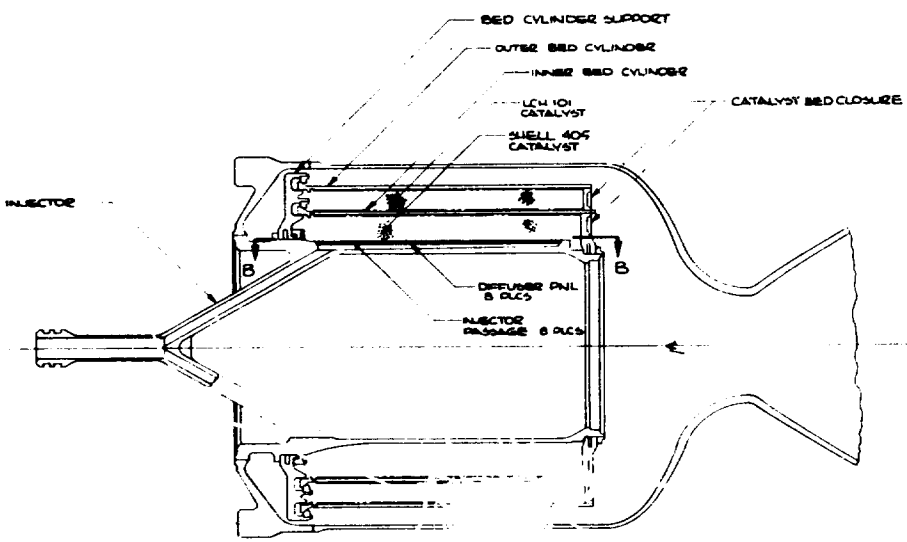

SECTION D-D

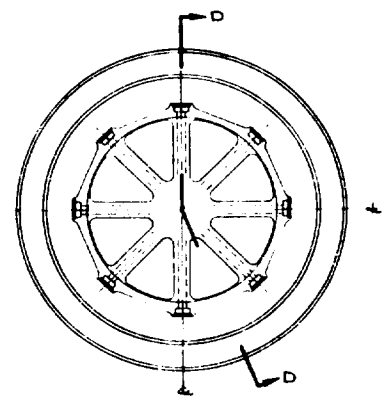

INJECTOR SECTION VIEW
8 FEED PASSAGES

ROCKET RESEARCH CORPORATION REDMOND, WASHINGTON	
TRW INJECTOR STUDIES LONGITUDINAL ELEMENT	SK 5111

Figure 3-5

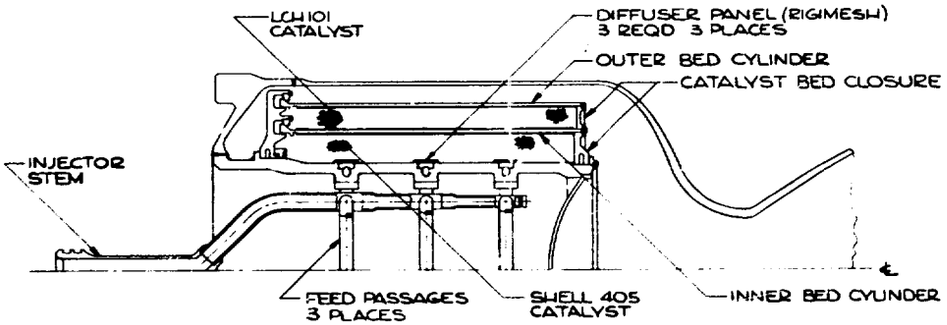

SECTION A-A
NON-SEGMENTED, CIRCUMFERENTIAL INJECTOR

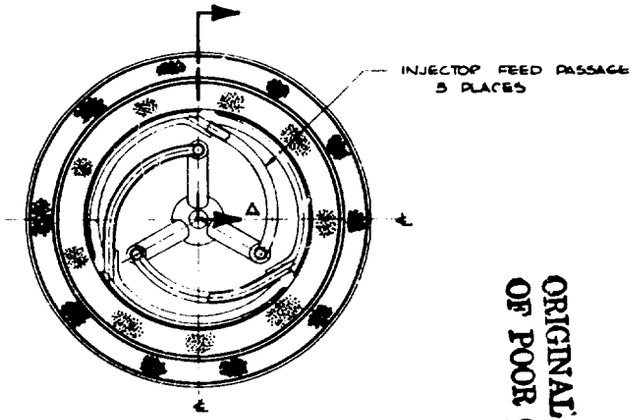

SECTION INJECTOR CIRCUMFERENTIAL PASSAGES

ORIGINAL PAGE IS
OF POOR QUALITY

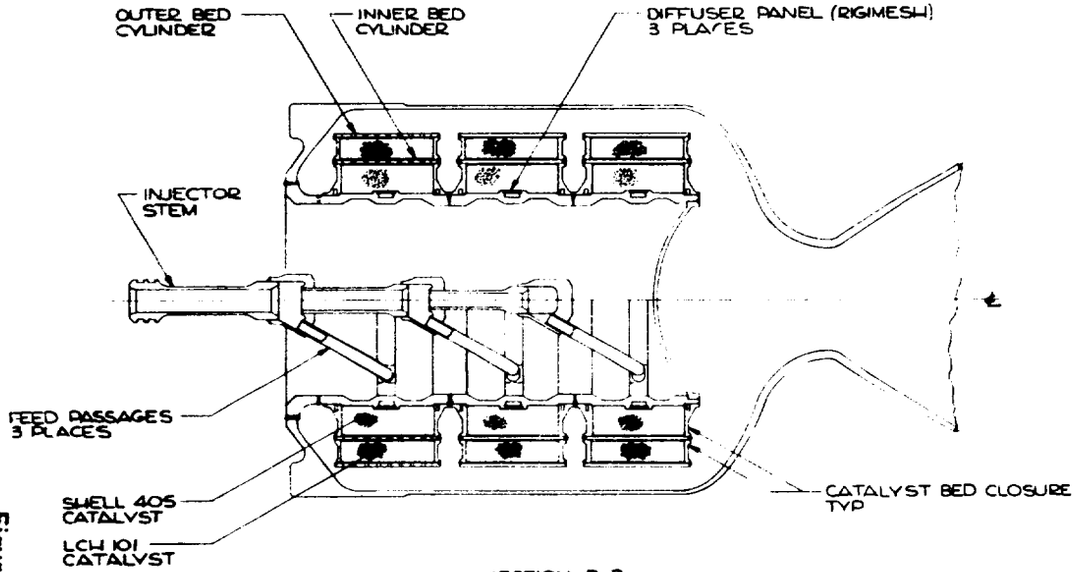

SECTION B-B
3 SEGMENT, CIRCUMFERENTIAL INJECTOR

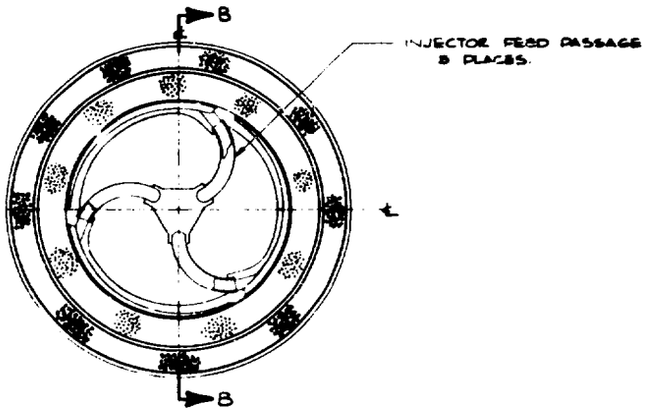

INJECTOR SEGMENT SECTION
(8 CIRCUMFERENTIAL PASSAGES)

ROCKET RESEARCH CORPORATION
REDMOND, WASHINGTON
INJECTOR STUDIES
SK 5112

Figure 3-6

growth in the catalyst bed of various size thrusters resulting from differences in thermal expansion of the catalyst and the bed retaining walls. These calculations showed that rather large void volumes occur in large catalyst beds as a result of differential thermal expansion during a firing. It was postulated that these voids lead to catalyst attrition due to relative movement between particles induced by vehicle vibration and/or injection of propellant into the bed. Consequently, a variety of design approaches was investigated with the goal of minimizing differential thermal expansion effects. On the basis of results of these design studies, it was concluded that dividing the catalyst bed into small compartments offered the simplest and most practical solution to the problem. Although compartmentation of a given design does not reduce the total void volume introduced by thermal expansion, it does prevent the accumulation of the total void in one location.

In conjunction with the above analyses, studies were also undertaken to establish the effect of random vibration on breakup of catalyst granules. Two catalyst containers (Figure 3-7), one simulating a radial bed design and the other an axial bed design, were fabricated and subjected to vibration (29 *g* rms input) in each of the three orthogonal axes for a total duration of 300 minutes. The objective of these tests was to determine the effect on catalyst breakup of 1) catalyst compartment size, 2) packing density, and 3) particle size. The effect of voids in the catalyst bed was investigated by preloading the bed with initial voids of 5 and 10 percent.

Results of the 25- to 30-mesh catalyst vibration tests are presented in Figure 3-8, where catalyst fines are defined to include all catalysts smaller than the specified minimum mesh size. Maximum breakup was 6 percent for 100 missions at 3 minutes of vibration per mission. The results show that an initial void in the bed has negligible effect on catalyst breakup. Tests were also conducted with longer beds with no difference detected in breakup rates. Screen wires attached to the inside walls of the bed also showed no measurable difference on the breakup rate envelope shown in Figure 3-8. Tests conducted with 14- to 18-mesh catalyst for 50 missions with an initial 10 percent void resulted in breakup of 1.8 percent, which was only slightly less than that experienced with the 25- to 30-mesh catalyst. Tests conducted with used catalyst (25- to 30-mesh) had a breakup of 5.5 percent after 50 missions, which was slightly higher than that of the new catalyst.

In summary, the results of the catalyst vibration tests showed that generation of catalyst fines occurred at a maximum rate of 0.02 percent per minute of random vibration at 29 *g* rms and was independent of compartment size and/or voids. On the basis of these results, it was concluded that the effect of vehicle vibration on catalyst attrition was probably not a serious problem.

Differential thermal expansion effects were also studied to determine the extent of catalyst breakup resulting from "cold starts" where the catalyst heats up faster than the retaining walls. A quartz tube, 2 inches in length, was loaded with catalyst and heated to 1,800°F. The quartz had a volumetric expansion ten times less than the catalyst, causing a theoretical catalyst compression of 0.037 inches. Breakup of the Shell 405 25- to 30-mesh catalyst was 2.1 percent (particles smaller than 30 mesh). The corresponding breakup for the LCH-101 14- to 18-mesh catalyst was 0.65 percent. Based on the results of these tests, it was concluded that thermal expansion effects resulting from cold starts would have only a secondary effect on catalyst loss.

CATALYST COMPARTMENTS FOR VIBRATION STUDIES

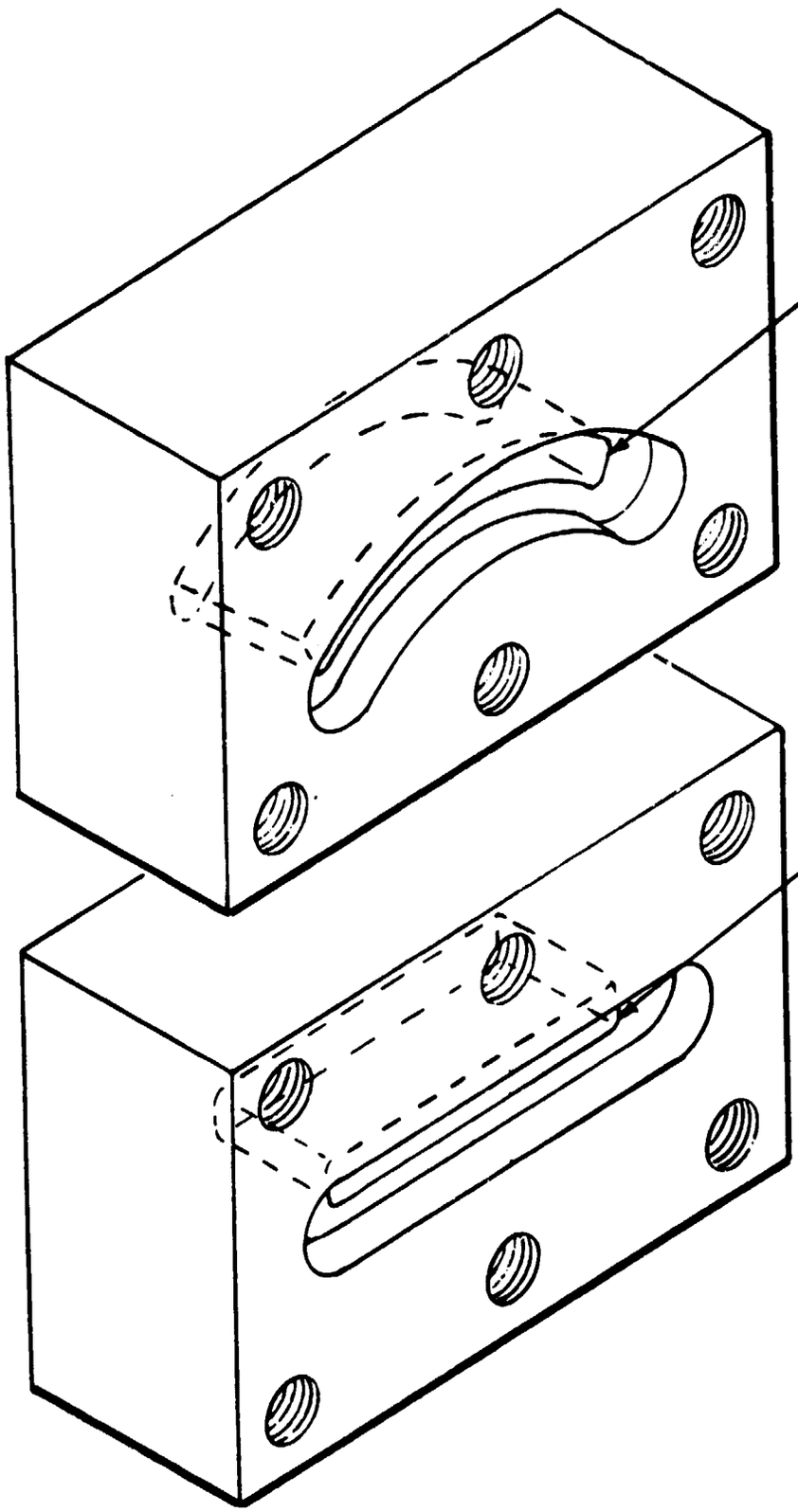

Figure 3-7

CATALYST VIBRATION RESULTS

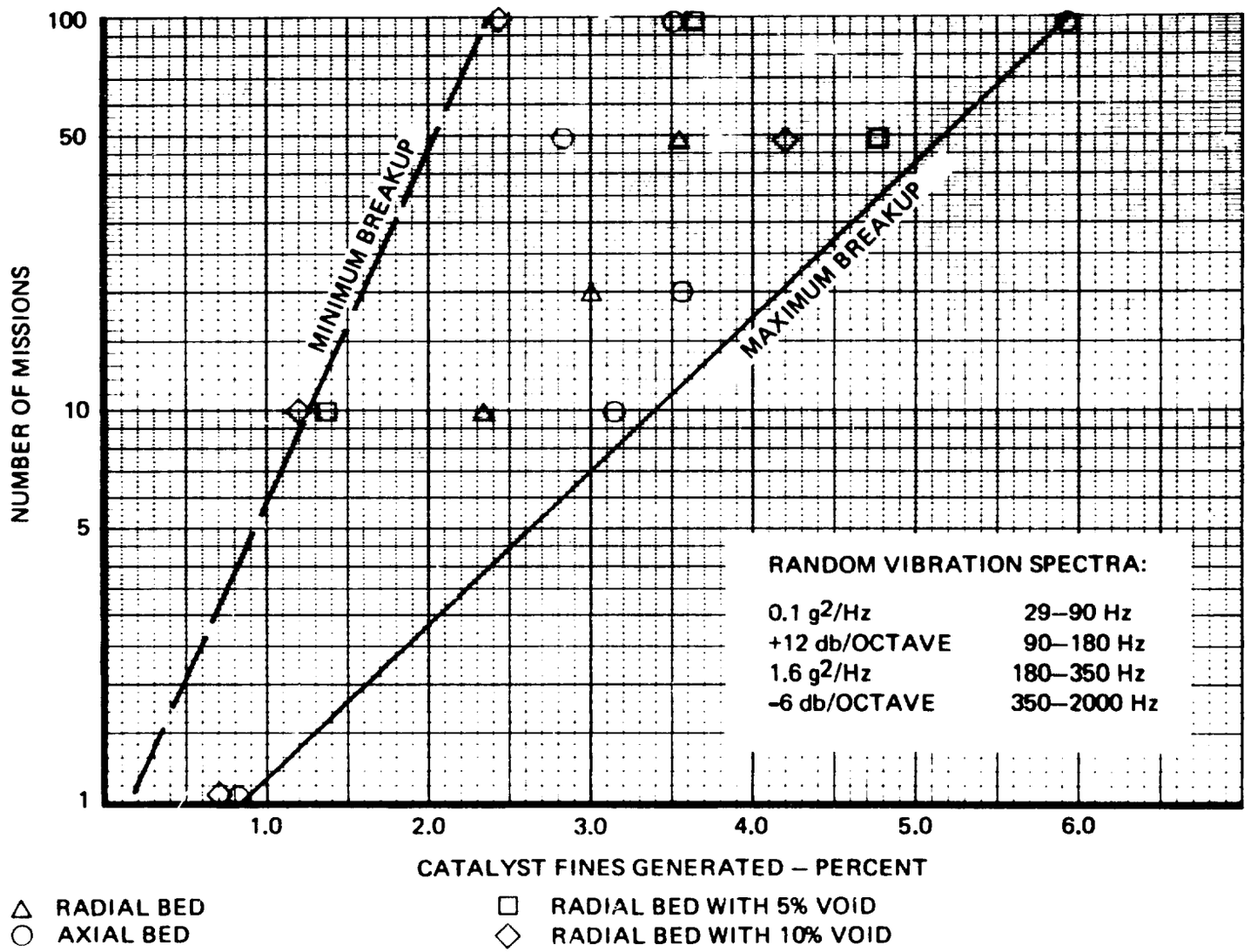

Figure 3-8

3.3 ENGINE OTPIMIZATION STUDIES

The primary goal of the engine optimization studies was to select an engine configuration based on optimization of life, weight, cost, performance, and size. The primary variables used in the optimization included chamber pressure, bed loading, catalyst bed geometry and composition, bed pressure drop, and system hardness ratio defined as the ratio of the liquid pressure drop to downstream chamber pressure. The intent of these studies was to determine only the relative effects of the pertinent variables on the parameters to be optimized. Consequently, proportionality type equations were introduced and computations made for variations in size, weight, and cost of a bseline engine as a function of the primary variables. The baseline engine selected for these studies was a 1,050-lbf thruster for which detailed design data was available. Perturbation of this design was accomplished using basic design equations with weight calculations based on scaling from the detailed weight analyses for the baseline engine.

Shown in Figure 3-9 is a schematic of an RCS engine and feed system showing the nomenclature used in the study. The basic design equations for the engine are as follows:

$$\text{Bed loading} = \frac{\dot{w}}{\pi D_{Bi} L_B}$$

$$\text{Aspect ratio} = L_B D_{Bi}$$

$$\text{Bed radial length} = K_1 \frac{G^{0.554}}{P_{cd}^{0.306}}$$

$$\text{Bed pressure drop} = K_2 \frac{G^{1.8} l_B}{P_{cd}}$$

$$\text{Hardness ratio} = \frac{P_F - P_{cd} - \Delta P_B}{P_{cd}}$$

$$\text{Flow ratio} = F/I_{sp}$$

The parameters K_1 and K_2 are proportionality constants used to scale from the baseline engine design.

An ammonia dissociation of 45 percent was sele. early in the study as the optimum for performance. Although higher performance can be achiev d at lower ammonia dissociation, it was decided that lower values would adversely affect life due to the correspondingly higher temperatures. Additionally, designing for low ammonia dissociation results in short beds which are more susceptible to washout. For these reasons, engine performance for the optimization studies was assumed to be consistent with an ammonia dissociation of 45 percent.

VARIABLES FOR ENGINE OPTIMIZATION STUDIES

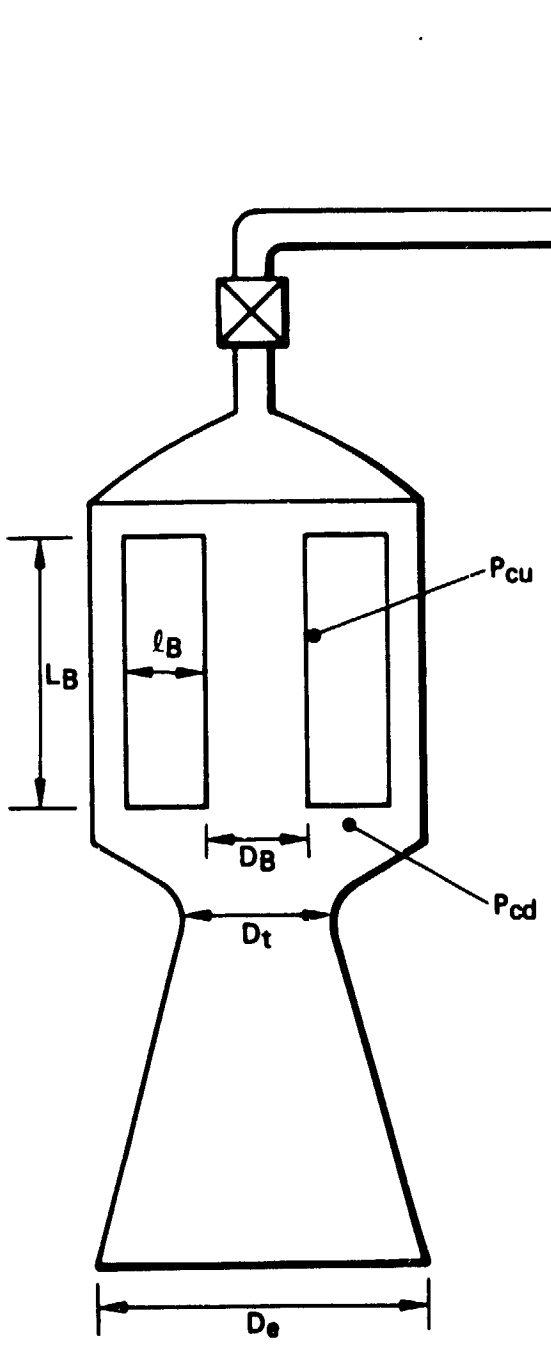

P_F	=	FEED PRESSURE
F	=	THRUST LEVEL
P_{cd}	=	DOWNSTREAM CHAMBER PRESSURE
ΔP_B	=	BED PRESSURE DROP
ΔP_{LIQ}	=	LIQUID PRESSURE DROP
D_{Bi}	=	BED DIAMETER (INNER)
L_B	=	BED AXIAL LENGTH
ℓ_B	=	BED RADIAL LENGTH
ϵ	=	NOZZLE AREA RATIO

In order to solve the above set of design equations, it was necessary to specify values for four of the variables. Values were accordingly selected for bed loading, chamber pressure, L/D ratio, and thrust. A computer program was used to compute the engine design variables, as well as weight, for a wide range of input values.

Results of engine weight computations are presented in Figure 3-10 showing the effects of bed loading, bed pressure drop, and system hardness ratio. Based on chamber pressure stability considerations, a minimum hardness ratio of 0.5 was selected. Bed pressure drop was limited to 70 psi based on life considerations. Consequently, a region bordered by the pressure drop and hardness ratio limits was identified for acceptable operation of an optimized engine. For minimum engine weight, the optimum bed loading and chamber pressure are located at the point where the bed pressure drop and hardness ratio limit curves intersect. As can be seen, the optimum bed loading and chamber pressure for minimum engine weight are 0.045 lbm/in.^{2}-sec and 153 psid, respectively.

It should be noted that the results presented in Figure 3-10 are for a bed length-to-diameter ratio of 2.0. The effect of this parameter on engine weight is shown in Figure 3-11 for the conditions noted. As can be seen, engine weight decreases very rapidly with increasing L/D up to approximately 2.0. For higher L/D values, the engine weight reductions are less pronounced. Catalyst weight, however, increases with increasing L/D ratio. Since catalyst cost is a factor in optimizing the design, it is desirable from a cost viewpoint to design for lower L/D ratios. Consequently, a trade exists between engine weight and catalyst weight (cost) versus L/D ratio. Other factors used to optimize the L/D ratio were envelope limitations and injector thermal margin, both of which generally favor lower L/D ratios. Consequently, an L/D of 2.0 was selected as optimum based on the available data and past design experience.

The effect of bed loading on the maximum diameter of the chamber is shown in Figure 3-12 for various bed pressure drop values. The limiting hardness ratio line is also shown.

Relative production cost as a function of bed loading is presented in Figure 3-13. The relative costs of engines at various thrust levels and chamber pressures are also shown. Production costs are seen to be lower for engines operating at higher bed loadings, which is due to the smaller size of the various engine components and quantity of catalyst.

Presented in Figure 3-14 is a comparison of the relative engine cost, weight, and size as a function of bed loading. Since it is desirable to minimize all these parameters, it is apparent that the optimum design is toward higher bed loading. However, as already noted, bed pressure drop and hardness ratio limitations result in a maximum allowable bed loading of 0.045 lbm/in.^{2}-sec. Additionally, it has also been established that higher bed loadings adversely affect catalyst life. Since the exact relationship between life and bed loading was unknown, it was decided to limit bed loading due to pressure drop and hardness ratio considerations at 0.045 lbm/in.^{2}-sec.

In summary, the design conditions for an optimum engine configuration were established to be as follows:

ENGINE WEIGHT TRADE STUDY RESULTS FOR SPACE SHUTTLE RCS

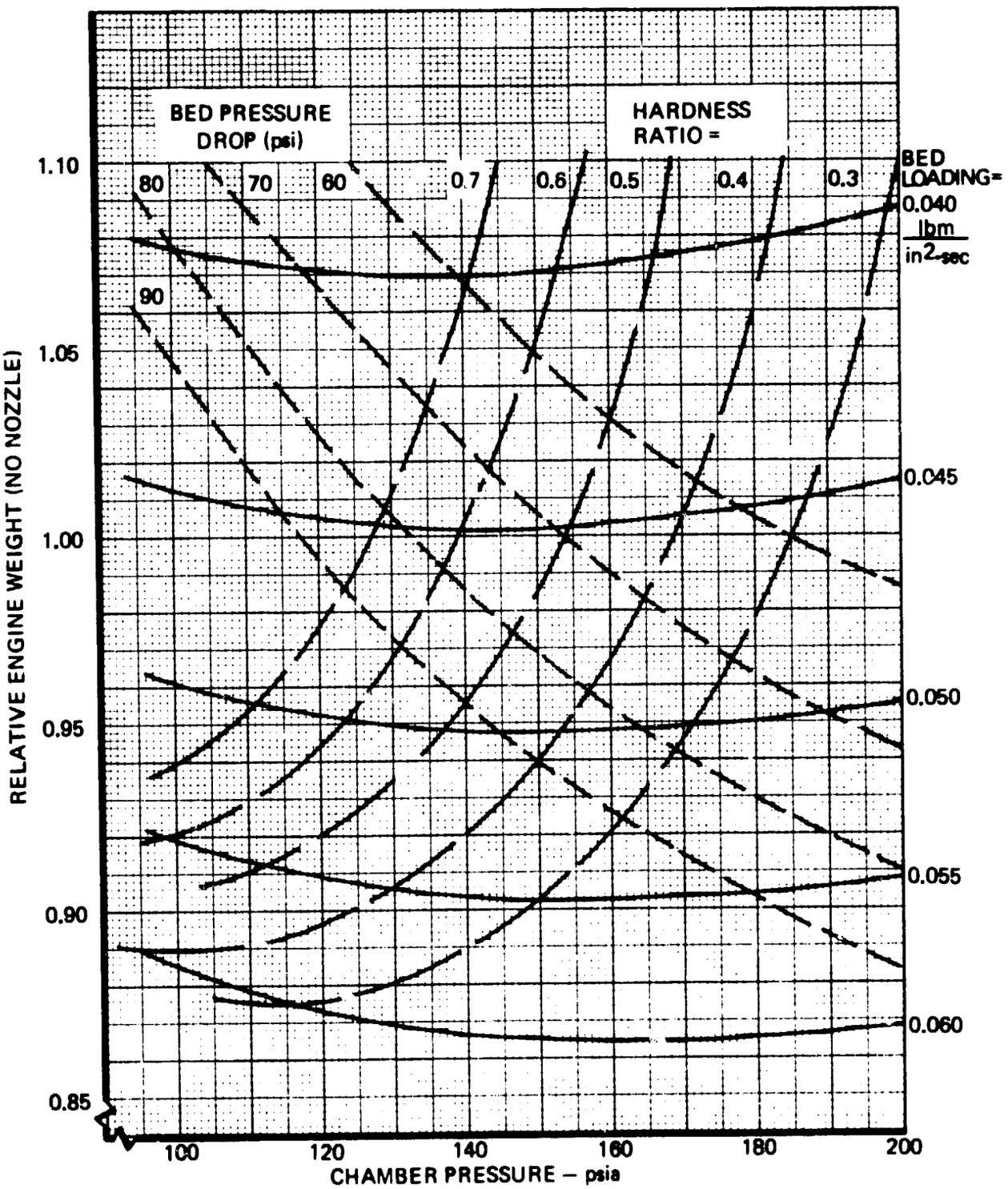

X = 45% P_F = 300 psia
L/D = 2.0

EFFECT OF BED LENGTH TO INJECTOR DIAMETER RATIO ON RCS WEIGHT

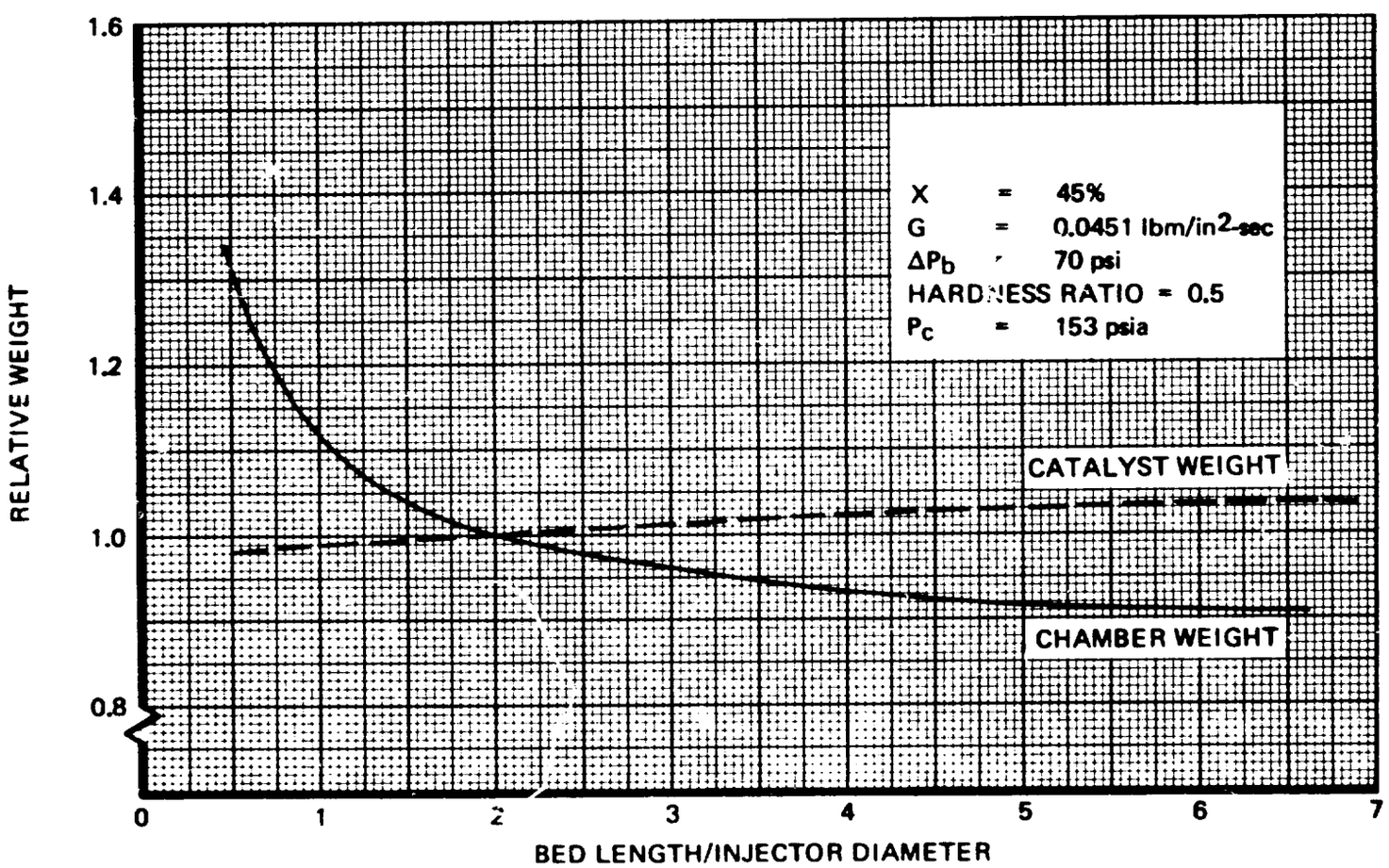

Figure 3-11

NORMALIZED MAXIMUM ENGINE DIAMETER AS A FUNCTION OF BED LOADING

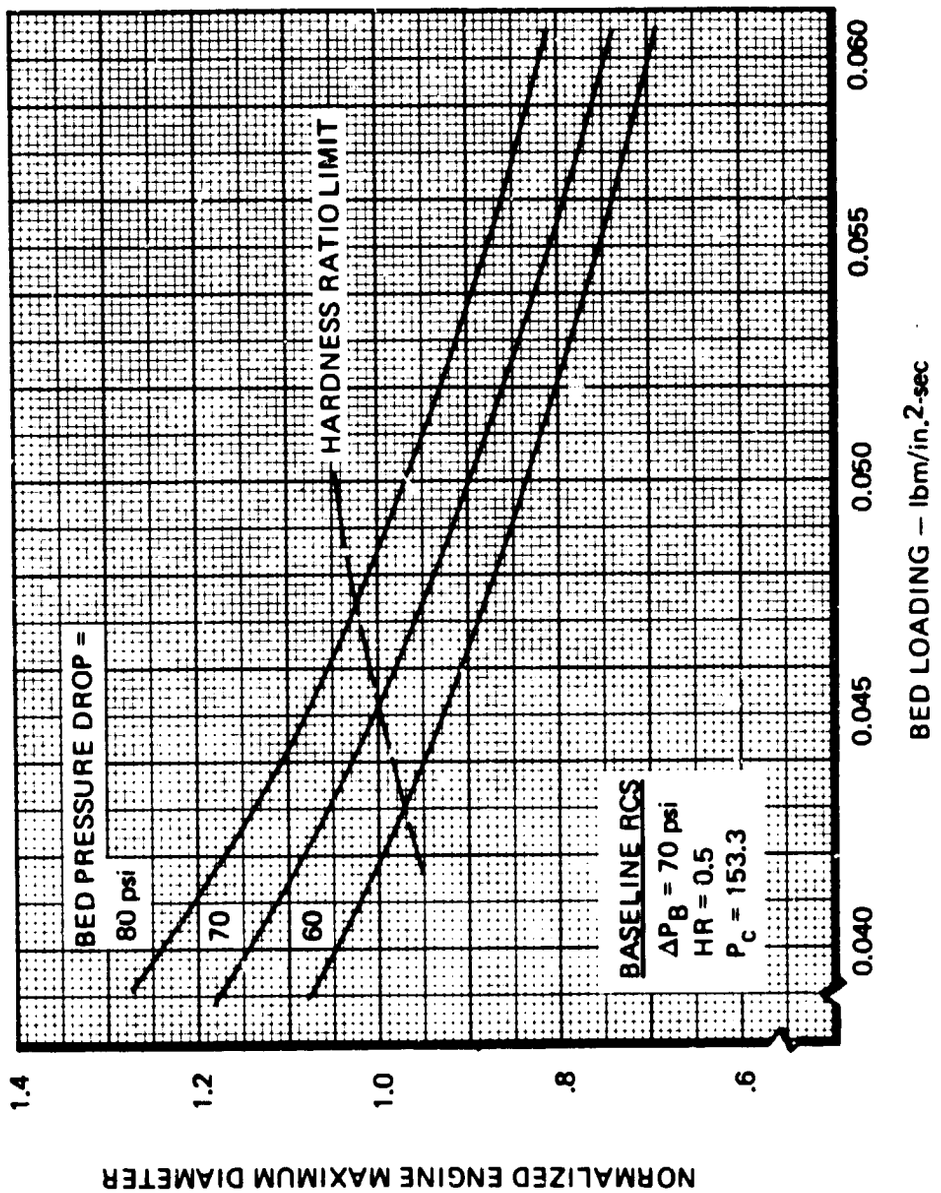

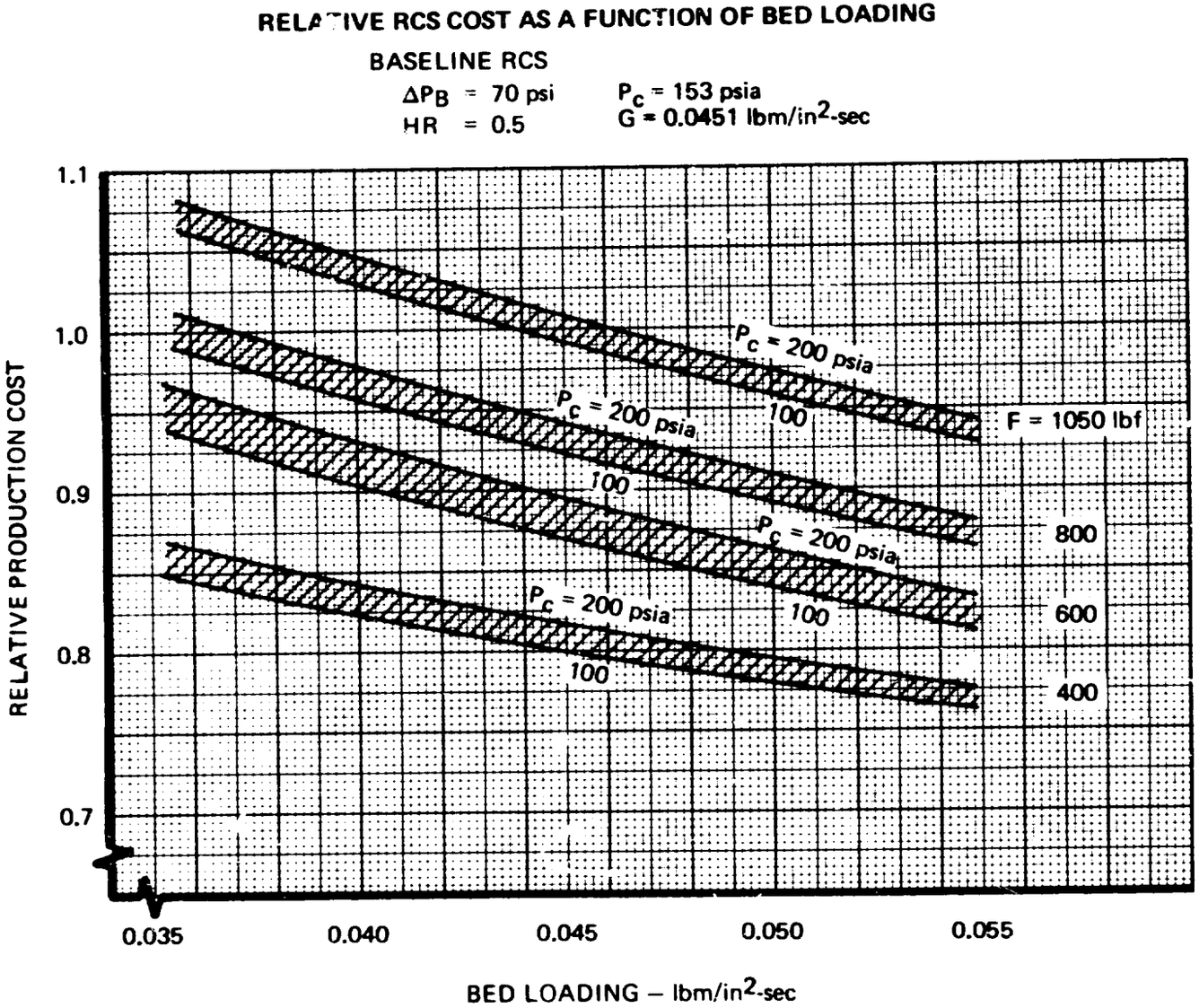
RELATIVE RCS COST AS A FUNCTION OF BED LOADING
BASELINE RCS
ΔPB = 70 psi
HR = 0.5
Pc = 153 psia
G = 0.0451 lbm/in2-sec
RELATIVE PRODUCTION COST
1.1
1.0
0.9
0.8
0.7
Pc = 200 psia
100
F = 1050 lbf
800
600
400
0.035
0.040
0.045
0.050
0.055
BED LOADING – lbm/in2-sec

Figure 3-13

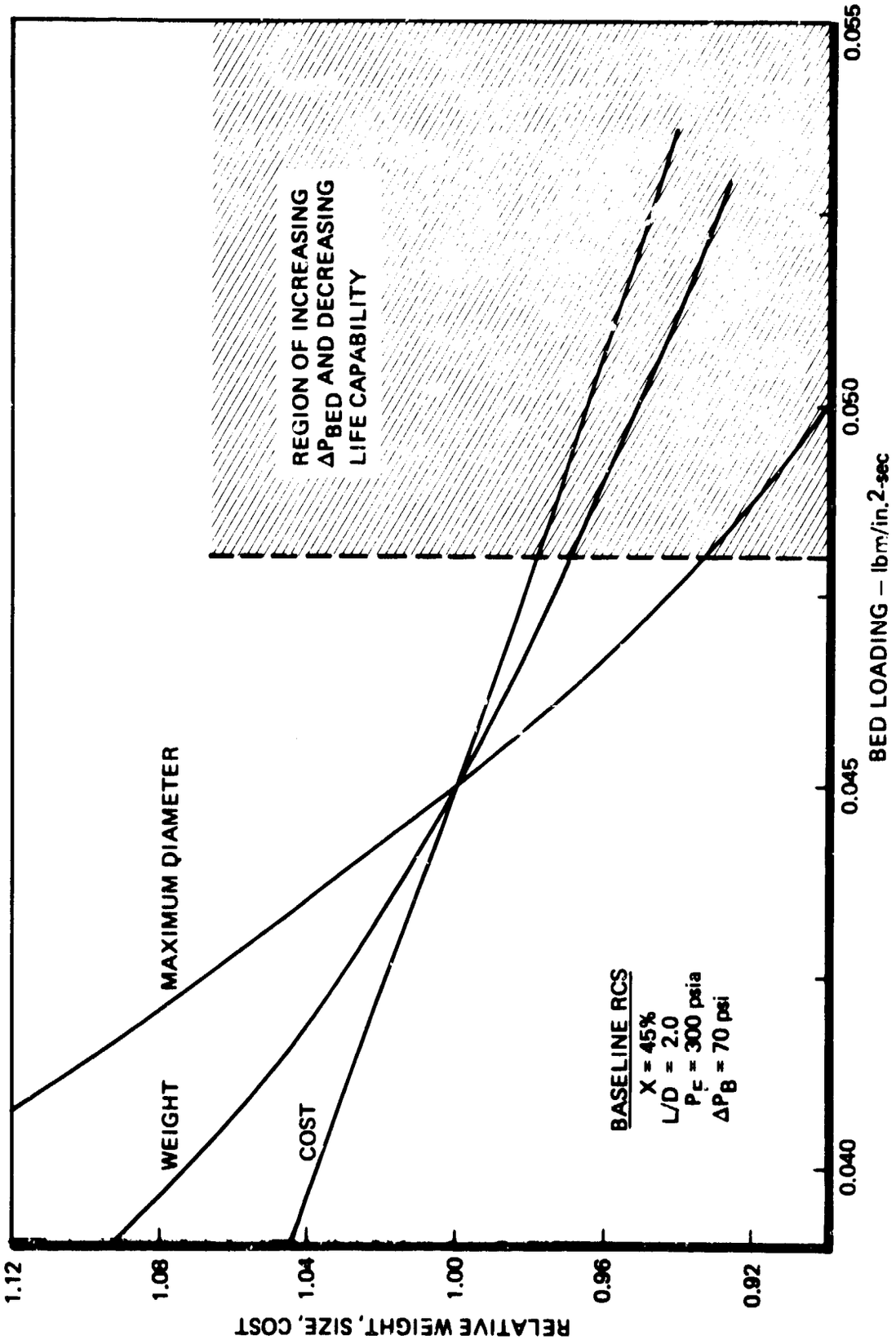
BED LOADING OPTIMIZATION FOR SPACE SHUTTLE RCS
REGION OF INCREASING ΔP_{BED} AND DECREASING LIFE CAPABILITY
MAXIMUM DIAMETER
WEIGHT
COST
BASELINE RCS
X = 45%
L/D = 2.0
P_c = 300 psia
ΔP_B = 70 psi
RELATIVE WEIGHT, SIZE, COST
1.12
1.08
1.04
1.00
0.96
0.92
BED LOADING – lbm/in.^{2}-sec
0.040
0.045
0.050
0.055

G	=	0.045 lbm/in.^{2}-sec
P_C	=	153 psia
X	=	45 percent
L_B/Di	=	2.0
HR	=	0.5
ΔP_B	=	70 psi
P_F	=	300 psia

The above conditions are valid for thrust levels within the specified 400- to 1,100-lbf range.

3.4 MATERIALS STUDIES

An extensive materials investigation was undertaken to provide the necessary data for selection of satisfactory materials for fabrication of the RCS engine components. Presented in the following paragraphs is a summary of the results obtained from the material studies. A detailed discussion of the results is presented in Reference 3-1. Tests were conducted on several candidate materials for oxidation, corrosion, and nitriding resistance. The material nitriding tests were conducted for a 30-hour duration using a synthetic gas mixture at 1,800°F. Tests were also conducted for the same duration with the nitriding environment at 1,650 and 1,900°F. These tests consisted of exposing sample materials to a gas mixture of ammonia and nitrogen. The sample materials were centrally located in a quartz tube (2-3/8 inches in diameter by 36 inches in length) which was inserted in a tube furnace. The material samples were 0.5 inch wide by 3.0 inches long with a thickness of 0.005 inch. The gas mixture was forced through the quartz tube at a flow rate of approximately 2,800 ml/min. Gas samples were frequently taken at the tube exit and the gas composition determined by use of a gas chromatograph. The ammonia dissociation was nominally 50 percent. Hastelloy B, as well as most materials evaluated, showed excellent nitridation resistance.

After exposure to the nitriding environment for the predetermined time interval, the samples were removed from the furnace and tested for weight change, hardness, ductility, and depth of nitriding. Results of the weight measurements, bend tests, and nitride layer depth measurements are summarized in Tables 3-1 and 3-2 and Figure 3-15, respectively. The bend test was a simple free bend with measurement made of the bend angle at fracture, or the radius formed at 180 degrees of bend. The depth of nitriding was determined from photomicrographs and a Tukon hardness traverse. The nitride depth, as measured from the photomicrographs, was taken as the maximum distance where any structural change could be observed. The Tukon hardness results correlated well with the photomicrograph results, although generally yielding slightly greater nitrided depths.

Oxidation and salt corrosion tests were also conducted using nitrided samples. The oxidation tests were performed by cyclically exposing the sample material to an air atmosphere at 1,600°F for a total of five cycles. Each cycle was 30 minutes in duration followed by a rapid air quench. Weight gain or loss was measured for the first, second, and fifth cycles with the results shown in Table 3-3. The results show that the majority of the materials exhibit excellent resistance to high-temperature

Table 3-1

WEIGHT CHANGE DATA FROM NITRIDING IN AMMONIA ATMOSPHERE

Material	Weight Change $gm/cm^2 \times 10^{-4}$				
	6 Hour 1,800°F	18 Hour 1,800°F	30 Hour 1,800°F	30 Hour 1,650°F	30 Hour 1,900°F
Hastelloy B	5.8×10^{-4}	7.88	8.93	6.23	10.28
Hastelloy C276	12.6	17.47	21.93	14.29	17.98
Hastelloy X	22.0	30.8	34.69	21.19	23.46
Haynes 625	12.5	17.72	21.48	12.78	18.06
Haynes 188	17.2	23.4	28.57	21.42	19.71
Rene 41	13.7	23.0	28.20	18.80	25.93
Waspalloy	11.1	20.0	23.45	16.27	22.27
Duranickel 301	-1.94	-7.9			
Inconel 600	8.55	11.4	12.91	9.18	9.64
601	12.0	20.16	24.80	15.11	24.12
617	10.4	17.65	22.69	16.26	18.28
625	11.7	21.0	25.32	13.29	21.71
718	16.7	26.6	30.59	32.97	39.73
706	30.8	40.5	41.98	17.52	39.37
Incolov 825	28.2	40.6	47.66	31.71	44.59
L-605	20.6	26.6	28.76	20.43	17.64
Unitemp AF 2' DA	8.05	13.6	18.47	13.18	19.43
Fansteel 85	8.35	12.15			
Fansteel 291	7.60	11.3	12.91	7.50	18.32

Table 3-2
BEND TEST RESULTS

Material	Bend Radius or Angle (inches or ^{o})				Comments
	As Received	6-Hours at 1,800°F	18-Hours at 1,800°F	30-Hours at 1,800°F	
Hastelloy B	.04	.07	.125	.19	Hardened
Hastelloy C276	.03	.25	.25	180°	Hardened
Hastelloy X	.06	.50	150°	90°	Hardened
Haynes 188	.01	.25	.44	10°	Hardened
Haynes 625	.04	.12	.06	.25	Hardened
Rene 41	.015	90°	80° *	20°	Transition
Waspalloy	.015	.18	.12	.19	Hardened
Duranickel 600	.08	.04	.09	.05	Ductile
Duranickel 601	.09	.06	.12	.06	Ductile
Duranickel 617	.09	.12	.08	.19	Ductile
Duranickel 625	.06	.12	.12	.19	Ductile
Duranickel 706	.12	.15	60° *	.19	Hardened
Inconel 718	.12	.12	60° *	180°	Hardened
Incoloy 825	.015	.25	45° *	90°	Hardened
Incoloy L605	.015	60°	15° *	5°	Hardened
Unitemp AF 21DA	20°	45°	90° *	60°	Softened
Fansteel 85	.01	5°	5° *	NA	
Fansteel 291B	.01	5°	5° *	NA	Hardened

*Indicates material failure

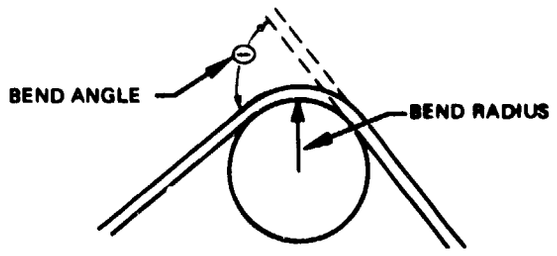

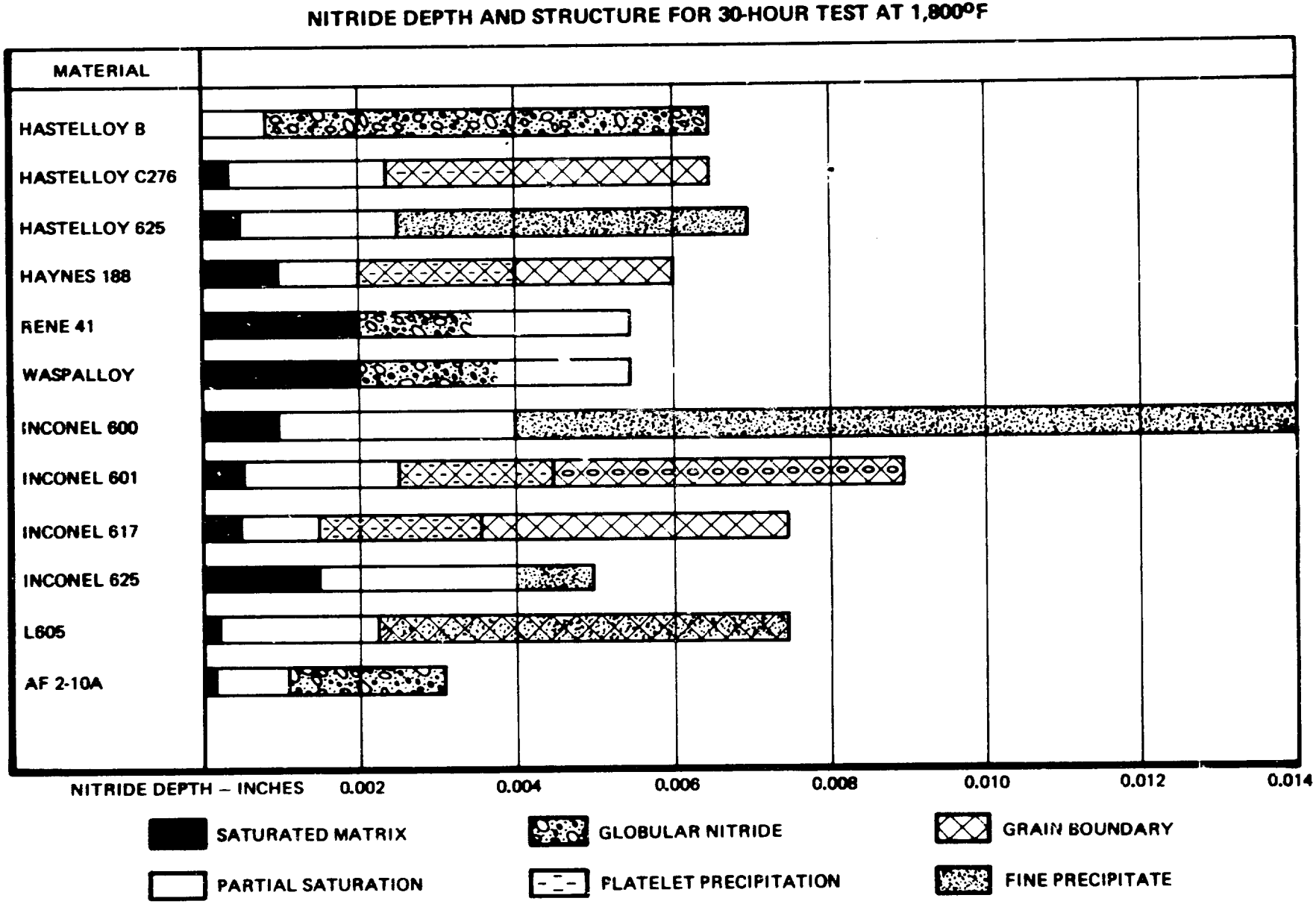
NITRIDE DEPTH AND STRUCTURE FOR 30-HOUR TEST AT 1,800°F
MATERIAL
HASTELLOY B
HASTELLOY C276
HASTELLOY 625
HAYNES 188
RENE 41
WASPALLOY
INCONEL 600
INCONEL 601
INCONEL 617
INCONEL 625
L605
AF 2-10A
NITRIDE DEPTH – INCHES
0.002
0.004
0.006
0.008
0.010
0.012
0.014
SATURATED MATRIX
PARTIAL SATURATION
GLOBULAR NITRIDE
PLATELET PRECIPITATION
GRAIN BOUNDARY
FINE PRECIPITATE

Figure 3-15

Table 3-3
OXIDATION EVALUATION

Material	Weight Change, $gm/cm^2 \times 10^{-4}$			Remarks
	1st Cycle	2nd Cycle	5th Cycle	
Hastelloy B	9.16	-4.41	-17.40	Spalled
C276	5.55	0.056	-3.48	Spalled
X	4.13	0.690	1.26	Flaking
625	2.31	-0.230	0.115	
Haynes 188	1.33	-0.290	0.115	
Rene 41	2.37	0.057	1.040	
Waspalloy	1.79	0.000	0.460	
Duranickel				
Inconel 600	2.13	-0.280	0.167	
601	2.20	-0.282	0.056	
617	2.48	0.000	0.562	
625	3.37	-0.392	0.112	
718	2.97	0.335	1.120	
706	4.37	-1.400	0.279	Scaling with evidence of rust beneath scale
Incoloy 825	1.90	0.335	0.503	
L605	2.64	-0.056	0.393	
Unitemp	1.00	-0.233	0.175	

*Sample material previously nitrided for 30 hours at 1,800°F exposed to air atmosphere at 1,600°F for five cycles for 1/2 hour each followed by rapid air cooled.

oxidation. Hastelloy B, however, which consists of 30 percent Mo, shows rather pronounced effects of oxidation. Molybdenum in alloys oxidizes at temperatures greater than 1,400°F with subsequent spalling of the molybdenum oxide. A rhodium-coated sample of Hastelloy B was subjected to the same tests and showed no effects of oxidation.

The salt corrosion tests (30 days) were conducted per ASTM Specification B117. Samples used for this test were previously nitrided for 6 hours at 1,800°F. Visual observations relating to surface appearance of the exposed samples is presented in Table 3-4. The rating for the various samples ranges from 1 to 19 with the higher numbers corresponding to less observed corrosion. In general, those materials with iron in their composition showed less resistance to corrosion. It is postulated that nitriding reduced the corrosion resistance of all the samples evaluated.

On the basis of results of the above studies, as well as a consideration of material physical properties, Hastelloy B was selected for fabrication of the engine components. Its high strength at elevated temperature and low coefficient of thermal expansion were significant factors in the selection. Although the oxidation resistance of Hastelloy B is relatively low, it was considered a minor problem which, if encountered, could be resolved by coating the critical parts with rhodium.

3.5 CATALYST OXIDATION STUDIES

Oxidation of catalyst resulting from operation within the atmosphere was considered a potential problem especially in view of the multiple mission requirements. Several past studies have indicated that the reaction of the Shell 405 catalyst active metal (iridium) and oxygen sometimes occurs with the formation of stable, inert compounds rendering the catalyst inactive. Studies were therefore undertaken to quantitatively determine the effect of an oxidizing environment on catalyst activity under various temperature conditions. Presented in the ensuing paragraphs is a summary of the catalyst oxidation studies. A detailed discussion of the studies is presented in Reference 3-2.

Laboratory experiments were conducted wherein Shell 405 catalyst was exposed to flowing air for 30 minutes at temperatures ranging from 200 to 1,700°F. Tests were also conducted with an ozone/air mixture (15 ppm O_3) typical of the upper atmosphere. Following exposure, the catalyst sample was tested for ignition delay and hydrogen chemisorption. Ignition delay was measured with a specially designed apparatus capable of measuring the time interval between contact of a hydrazine droplet with the catalyst sample and the initiation of decomposition.

The results presented in Figure 3-16 show that a marked change occurs in both ignition delay and hydrogen chemisorption at a temperature of approximately 1,200°F. the ignition delay characteristics indicated no oxygen damage at exposure temperatures below 1,200°F, whereas, hydrogen chemisorption indicated a continual decrease in surface area with increasing temperature. The results obtained with the ozone/air mixture have the same trend, although showing somewhat more degradation than that obtained with atmospheric air.

Several samples of 1,400°F oxidized Shell 405 were placed in a reducing environment (20 minutes in hydrogen at 1,800°F) to determine if oxygen-damaged catalyst could be reactivated. The results indicated a minor improvement in ignition delay with no measurable improvement in hydrogen chemisorption.

IGNITION DELAY AND H_2 CHEMISORPTION RESULTS FOR OXIDIZED SHELL 405 CATALYST

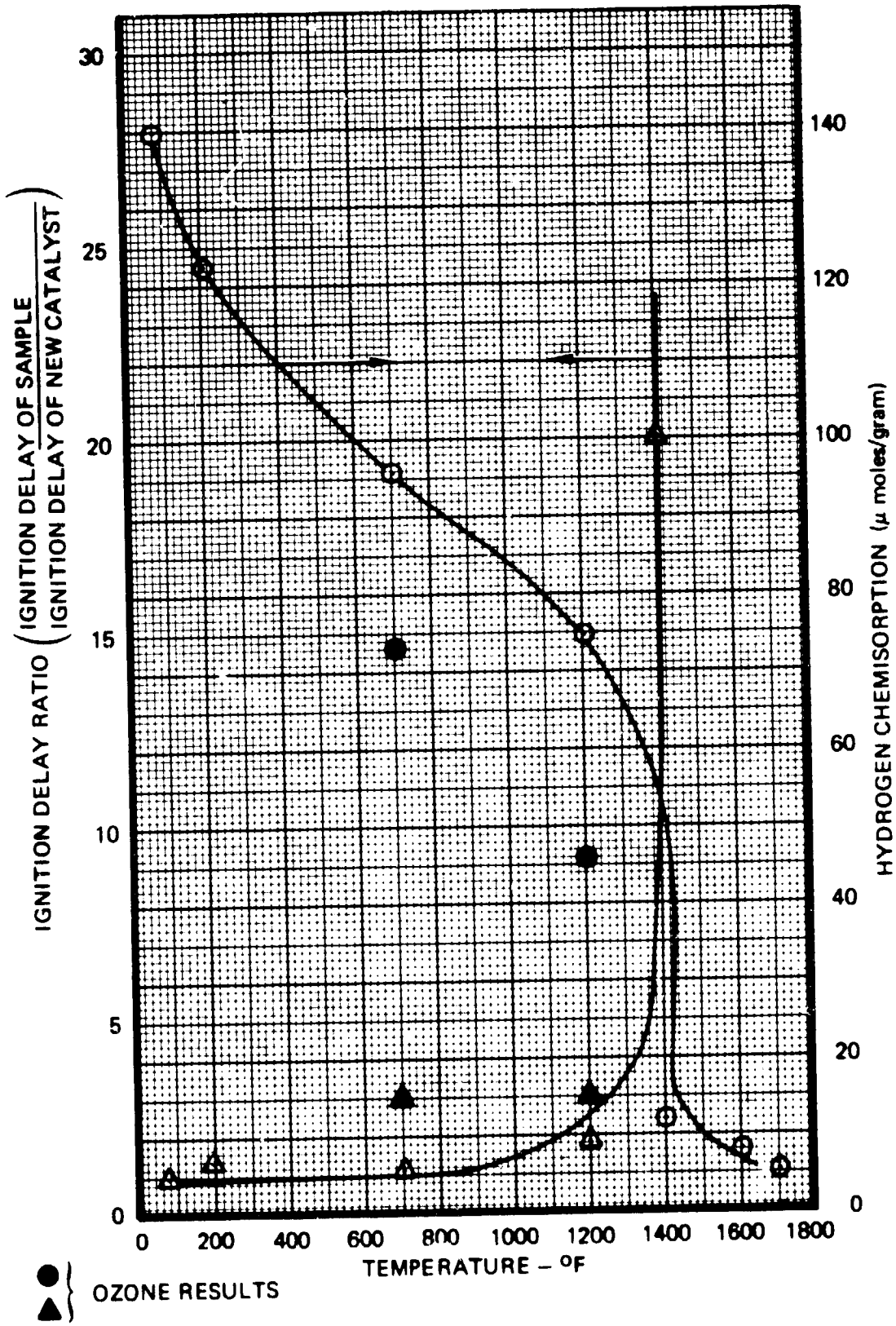

11057-69A

Figure 3-16

Table 3-4
SALT SPRAY CORROSION TEST

Material	% Cr	% FE	Visual Appearance	Rating *
Hastelloy B	1	5	Tarnished – green yellow film	15
Hastelloy C276	15	5	Tarnished – green yellow film	16
Hastelloy X	22	19	Rusted – red orange coating	7
Hastelloy 625			Tarnished lightly – blue film	14
Haynes 188	22	3	Tarnished – green yellow film	5
Rene 41	19		Tarnished – green orange film	9
Waspalloy	20		Tarnished – green film	10
Duranickel 301	0.3		No change	17
Inconel 600	16	8	Lighdy rusted	8
Inconel 601	23	14	Rusted	4
Inconel 617	22		Tarnished – dark green film	11
Inconel 625	22	3	Tarnished lightly	13
Inconel 706	16	40	Heavily rusted	1
Inconel 718	19	19	Rusted	6
Incoloy 825	22	30	Heavily rusted	2
L605	20	3	Rusted – yellow orange coating	3
Unitemp	12	0.3	Tarnished – light green film	12
Fansteel 85			No change	18
Fansteel 291B			No change	19

*Numbers indicate most severe corrosion condition starting with No. 1.

To further establish the effects of oxidation, a series of tests was conducted using oxygen-exposed catalyst in a 0.5-lbf thruster. Five test firings were conducted (100 seconds each) with three oxidized catalyst samples and compared to a baseline test with unoxidized catalyst. The first firing was with 700°F oxidized catalyst. Ignition delay and operation were normal, although there was a weak ignition pressure spike. The reactor was allowed to cool to ambient temperature following the firing and a second firing made. No anomaly was noted on the second startup. The first test with the 1,200°F oxidized sample resulted in an ignition pressure spike (200 psia) with an ignition delay

four times longer than that obtained with the unoxidized catalyst. The second firing showed no improvement. A test attempted with a 1,400°F sample was terminated when no ignition occurred after several seconds of operation.

On the basis of the above results, it was concluded that unfired Shell 405 catalyst could be permanently damaged by air at temperatures above 1,200°F. It was postulated, however, that fired catalyst would be somewhat more difficult to oxidize than the unfired catalyst evaluated in the laboratory tests. It is well known that ammonia and hydrogen are absorbed by the catalyst during a firing, subsequently providing a protective layer preventing oxygen reaction with the active metal. Outgassing of catalyst, even in vacuum, continues for several hours following a firing, during which time the catalyst cools to ambient temperature. Consequently, it was postulated that in a practical application, oxidation would not occur.

This hypothesis was verified in tests conducted both at NASA-JSC and RRC wherein air was directed into the chamber of thrusters following a firing. In the NASA tests, jets of air were directed into the nozzle of the Transtage 27-lbf thruster following each of several separate firings. No anomalies were observed on subsequent restarts. Post-test analysis of the catalyst revealed that only the downstream layer of catalyst showed evidence of catalyst damage.

In the RRC test, a wedge reactor was purged following a firing with air through a pressure tap for a duration of 8 minutes with the catalyst above 1,200°F. No abnormal engine behavior was detected upon startup, and subsequent examination of the catalyst revealed no oxidation damage.

Several test firings have been conducted to date with subscale and full-scale hardware with no purge or other preventive measures taken to avoid oxidation of the catalyst. No damage was observed during testing or in post-test examination of the catalyst. On the basis of these results, it was concluded that outgassing provides sufficient protection to prevent any catalyst oxidation damage for the Space Shuttle application.

3.6 SUBSCALE TESTING

In order to evaluate the effects of replacing substantial quantities of Shell 405 catalyst with a low cost catalyst, a test program was initiated with a subscale reactor (wedge) that simulated the operating characteristics of the full-scale RCS. The subscale reactors were simple segments of a conceptual design for the RCS injector. The reactor consisted of a 60-degree segment of the RCS engine with an axial length equal to one-half that of the full-scale engine. The flow rate was 1/12 that of the RCS with a throat sized to provide the same chamber pressure as the RCS engine. An isometric of the subscale concept is shown in Figure 3-17.

The first three wedge reactors fabricated and tested were specifically for catalyst bed optimization. The results of the wedge testing, however, indicated that the subscale technique could be used to evaluate new catalyst bed retention techniques and thus, additional wedges were fabricated and tested for life capability. Most of this testing was conducted during Task II but is discussed in this section of the report. The following paragraphs summarize the design and results of each wedge test.

SUBSCALE WEDGE CHA ER

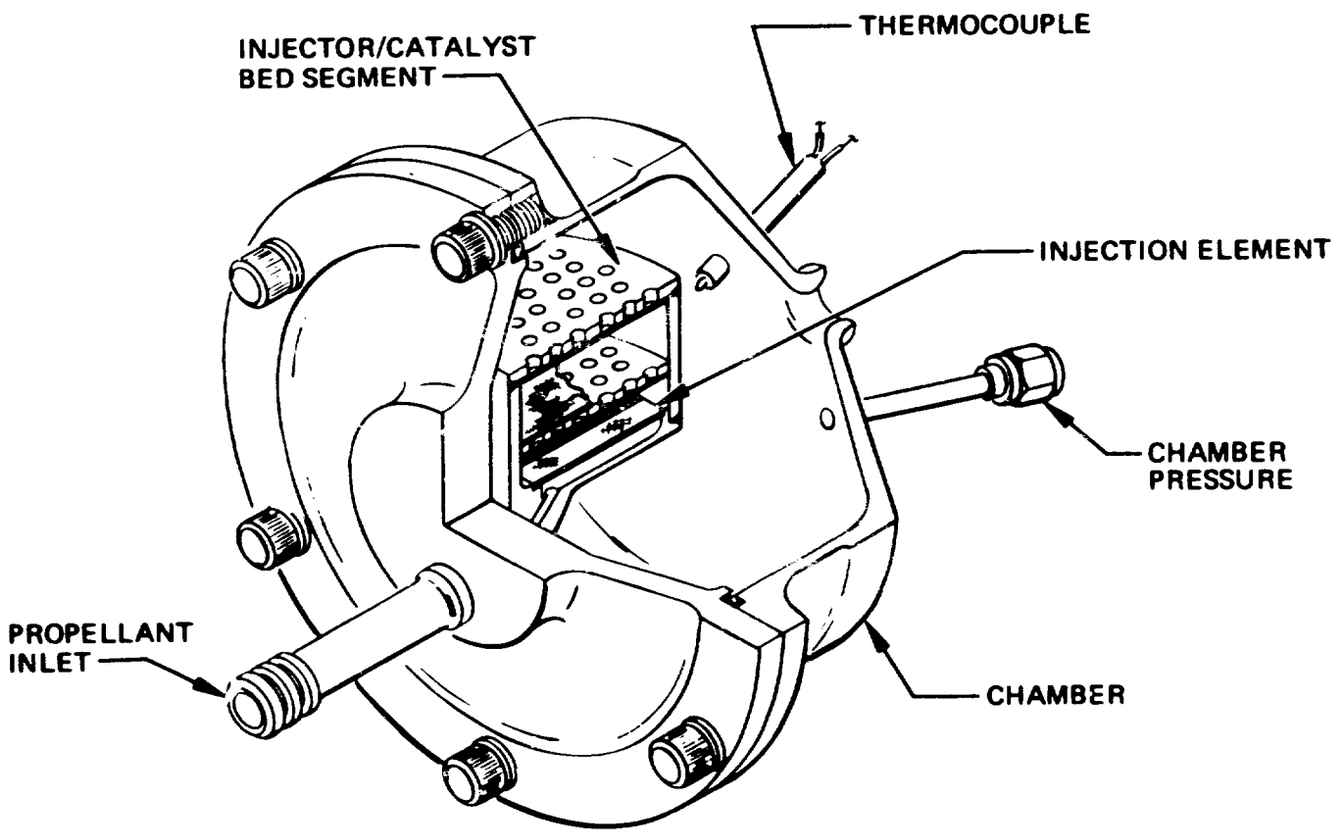

Figure 3-17

Subscale Reactor S/N 001 – A photograph of the first wedge is shown in Figure 3-18 and the pressure vessel is shown in Figure 3-19. The injector incorporated a single laminated wire mesh element, 0.3 inch in width and 2.0 inches in length, which simulated an RCS injector having six elements, 4.0 inches long. The flow rate was controlled so that the local bed loading was identical to the RCS design. The catalyst bed consisted of 50 percent Shell 405/50 percent LCH 101 which is identical to the combination employed by the Viking 600-lbf flight-qualified engine. The test conditions and results are tabulated in Table 3-5. The goal of this initial test series was to establish baseline performance during start transient and 600-second steady-state burns.

A secondary test was conducted on the first wedge to evaluate the effect of exposing the catalyst to hot air immediately upon shutdown. After start 5, 600°F air was forced through the P_c tap for approximately 8 minutes while the bedplates cooled to 1,200°F. Start number 6 was conducted with no anomalous behavior, indicating no damage to the catalyst caused by oxidation damage.

Subscale Reactor S/N 002 – This subscale engine was identical to S/N 001 except that the inner bed length was decreased approximately 0.040 inch, so that the overall catalyst composition changed to 40 percent Shell 405, 60 percent LCH 101. The primary goal of this test was to observe performance characteristics and possible washout tendencies (due to decreased Shell 405 catalyst) during 60- and 600-second steady-state runs. The test results for S/N 002 are tabulated in Table 3-5. The data shows a substantial increase in outer bedplate temperature with a decrease in inner bedplate temperature. Since the outer bed temperature was higher than the inner bed, it appeared that the "decomposition flame front" had moved to the outer bed – a marginal condition for long-life reactors. This unit also had increased roughness at comparable life.

Subscale Reactor S/N 003 – A detailed evaluation of the S/N 002 data indicated that further reduction of Shell 405 catalyst on the baseline injector would create only a more marginal design. At this time it was decided that wedge S/N 003 should be designed to simulate a 12-element injector instead of the baseline 6-element design. This decreased the total flow rate per element to one-half the previous value, reducing the local bed loading by 50%. S/N 003 wedge remained as a single element but the side walls were moved inward so that the wedge consisted of a 30-degree arc insteady of 60 degrees as used in the previous wedges. The inner bed length was also decreased so that the catalyst bed ratio was 25 percent Shell 405/75 percent LCH 101. The test results are shown in Table 3-5. Performance parameters were similar to the S/N 001 unit even though only half the quantity of Shell 405 was used, which indicated that an injector providing increased propellant distribution should be utilized for the RCS.

Subscale Reactor S/N 004 – Due to the success of S/N 003 wedge, a fourth subscale reactor was fabricated with two laminated wire mesh elements in a 60-degree arc to more fully simulate the 12-element injector. The reactor was assembled with a catalyst ratio of 30 percent Shell 405/70 percent LCH 101. Since this reactor design was considered to be the probable baseline for the RCS engine, an extensive test sequence was planned with this unit. A sketch of the wedge cross-section is shown below along with instrumentation location.

11058-68

Figure 3-18

WEDGE ENGINE CHAMBER

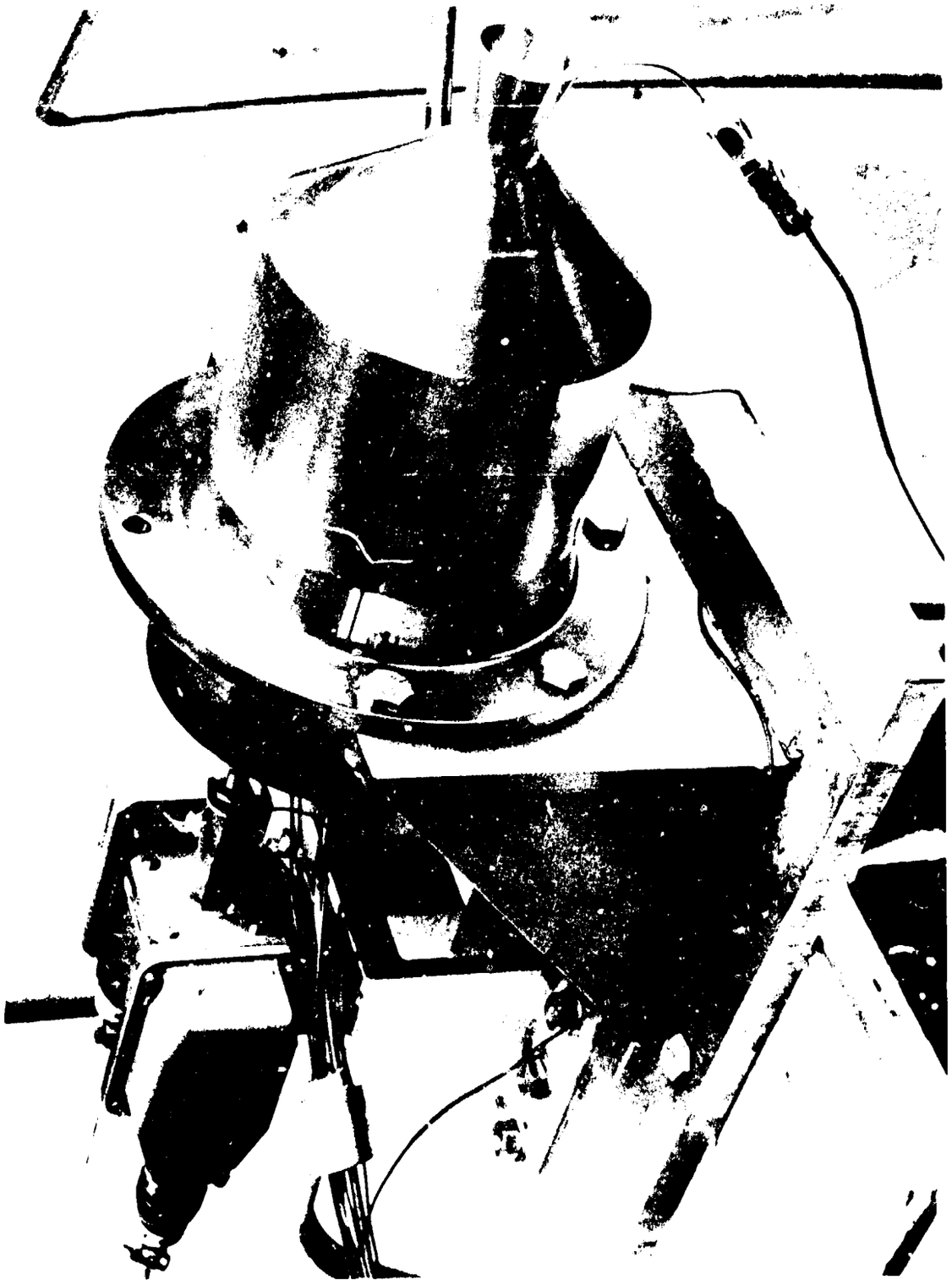

11058-67

Figure 3-19

Table 3-5
SUBSCALE ENGINE DATA FOR S/N 001, 002, AND 003

Parameter \ Test	001							002				003	
	1-1	1-2	1-3	1-4	1-5	1-6*	1-7	2-1	2-2	2-3	2-4	1-1	1-2
Run time, secs	60	600	60	60	100	33	90	60	600	100	60	60	600
Feed pressure, psia	366	382	379	369	366	377	364	365	364	128	362	223	226
Chamber pressure, upstream, psia	195	194	199	190	184	–	187	186	180	87	177	178	180
Chamber pressure, downstream, psia	153	159	164	156	156	147	155	157	157	70	160	158	158
Temperature fuel, °F	66	65	66	66	61	60	61	54	54	50	51	51	51
Flow rate, lbm/sec	0.1791	0.1849	0.1908	0.1807	0.1853	0.1839	0.1833	0.1834	0.1839	0.0840	0.1873	0.0928	0.0934
Throat area (cold), $in.^2$	0.1514	0.1514	0.1514	0.1514	0.1514	0.1514	0.1514	0.1514	0.1514	0.1514	0.1514	0.07451	0.07451
Ignition delay (0 to 10% P_{cd}), msec	50	40	40	45	–	37	36	46	36	75	38	70	73
P_{cu} roughness, ±psi	3	4.0	3.5	3.5	3.0	4.0	3.5	3.0	2.0	1.5	2.0	1.5	2.0
P_{cd} roughness, ±psi	1.5	2.0	2.0	2.5	6.5	6.5	2.5	1.5	1.5	1.5	3.0	0.6	1.5
T_1 initial, °F	70	70	125	125	70	185	235	75	65	70	135	60	120
T_1, °F	1,570	1,580	1,590	1,590	–	1,570	1,530	–	1,560	1,475	1,630	1,570	1,460
T_2, °F	1,710	1,800	1,800	1,780	1,810	1,710	1,780	–	1,860	1,700	1,930	1,680	1,635
T_3, °F	1,715	1,780	1,780	1,770	1,800	1,705	1,750	–	1,930	1,750	1,910	1,800	1,750
T_4, °F	1,890	1,880	1,860	1,850	1,855	1,845	1,845	–	1,850	1,800	1,790	–	–
T_5, °F	1,900	1,880	1,870	1,860	1,860	1,825	1,840	–	1,845	1,800	1,810	1,820	1,860
T_6, °F	1,620	1,610	1,680	1,660	1,640	1,660	1,630	–	1,660	1,495	1,595	1,840	1,860
T_{gas}, °F	1,520	–	1,600	1,590	1,610	1,530	1,595	–	1,640	1,460	1,660	1,500	1,570

*Did not achieve equilibrium

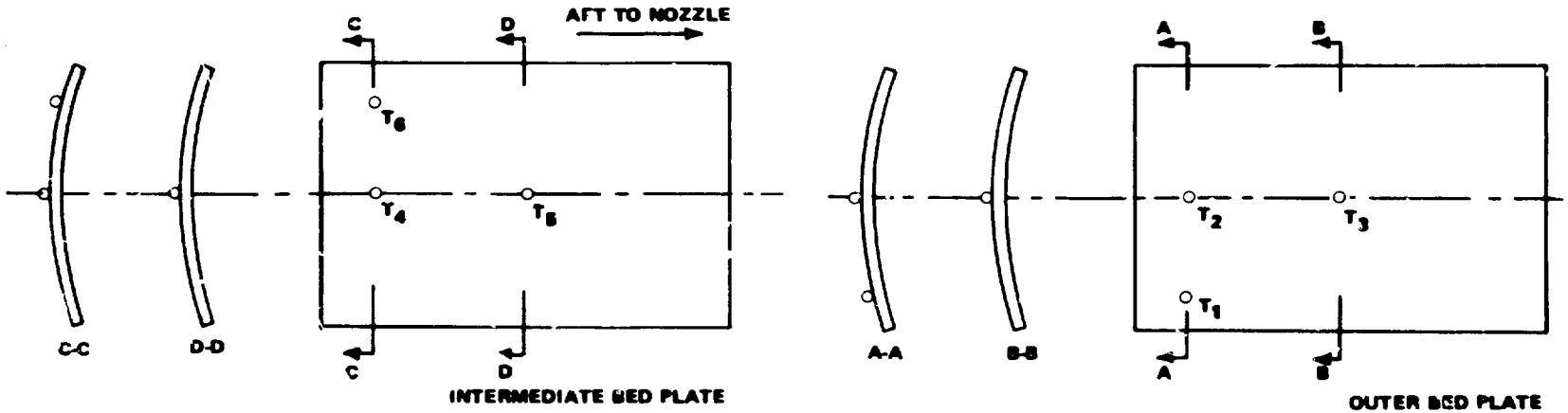

01060

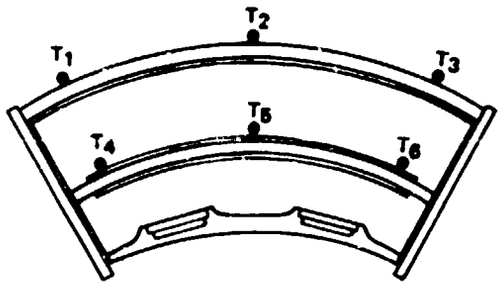

A total of 3,400 seconds total burn time was accumulated (2,400 seconds at 1/3 nominal flow), with 10 ambient starts. Several start-up transient spikes were noted, and were attributed to propellant wicking to the walls and/or accumulation on the outer bed. Gas temperatures began at 1,755°F and decreased to 1,710°F at completion of the test. Bed pressure drop also increased 20 psi during the test sequence, and roughness was a nominal ±4 psi at test completion. Table 3-6 lists the basic performance of S/N 004.

Table 3-6
SUBSCALE ENGINE DATA FOR S/N 004

Parameter \ Test	LCH 101*	LCH 201* (1st Refurbishment)	LCH 202* (2nd Refurbishment)
Total run time, sec	3,400	3,060	3,000
Chamber pressure, upstream, psia	222	197	183
Chamber pressure, downstream, psia	172	159	147
Initial temperature, °F	46	68	67
Flow rate	0.193	0.179	0.181
Throat area (cold), $in.^2$	0.1514	0.1514	0.1514
P_{cd} roughness, ± psi	±2	±4	±4
Bed temperatures – °F			
T_1	1,645	1,830	1,850
T_2	1,635	1,775	1,740
T_3	1,710	1,815	1,820
T_4	–	1,940	1,830
T_5	1,875	1,810	1,730
T_6	1,910	1,955	1,820

*Performance data from last run.

After completion of this test sequence, a teardown analysis was conducted to determine any damage incurred to the catalyst bed. The catalyst retention system (bedplates and screens) appeared to be in excellent condition; the only anomaly was a slight dimpling of the inner-most screen into

the bedplate holes. The inner catalyst bed (Shell 405) had sustained a catalyst loss of 8 8 percent while the outer bed (LCH) lost only 0.5percent. Additional data are shown in Table 3-7.

Examination of the outer bed LCH 101 catalyst (from this test series, as well as that from previous tests) revealed a small loss of active metal which potentially could become significant for the long-life requirements of the Space Shuttle. The LCH catalyst from several tests was thoroughly analyzed using a scanning electron microscope (SEM) and electron microprobe. Based on the results of these studies, processing techniques for improving the LCH 101 were implemented. In addition, other LCH catalysts were developed and subjected to extensive in-house testing. The goal of these studies was to develop an LCH catalyst having improved characteristics in the following areas: 1) improve the cold start characteristics by increasing the low temperature catalytic activity; 2) provide higher steady-state performance by retarding ammonia dissociation; and 3) provide substantially longer life capability (see paragraph 3.5). To evaluate the capability of new low cost catalysts, it was decided to refurbish wedge S/N 004 with LCH 201 and LCH 202 catalyst and compare life capability over similar life demonstrations.

S/N 004 was then refurbished with new Shell 405 catalyst on the inner bed and LCH 201 catalyst on the outer bed. To improve the life potential of the outer bed, a low-cost catalyst using a lower active metal content was produced and tested under similar conditions as the LCH 101. The refurbishment unit was tested for a total run time of 3,060 seconds with 5 starts. Table 3-7 lists the performance parameters at the conclusion of testing the refurbished unit. The unit was removed from the test stand and a teardown analysis conducted to determine catalyst attrition rates. The results of the catalyst analysis are shown in Table 3-7.

At this point, S/N 004 wedge had accumulated 6,400 seconds of total firing time with no evidence of degradation of the bedplates, screens, or injector elements. This unit was refurbished a second time with new Shell 405 in the inner bed and LCH 202 catalyst in the outer bed. Additional thermocouple instrumentation was inserted into the bed in order to investigate cook-off spikes encountered during startup which was attributed to propellant wicking. Based on the test results, the injector was modified so that the injector penetrated further into the bed. A total of 3,000 seconds firing time was accumulated with 5 ambient starts. Figure 3-20 plots the various bed temperatures versus run times during the test. It is interesting to note from this plot that stable temperatures exist on the inner bedplate, indicating constant gas composition, and a low temperature on the injector face indicating continuous exposure to liquid hydrazine (node 2). The wedge appeared to be in excellent shape at the conclusion of this test sequence. The catalyst teardown results are shown in Table 3-7.

Based on the S/N 004 test results, LCH 202 catalyst was selected for the outer bed of the RCS engine. However, inner bed catalyst loss rates exhibited in the S/N 004 design were approximately 7 percent per hour of run time, which was considered too high for Space Shuttle applications. Therefore, the next series of tests was conducted to evaluate one of two alternate design concepts for the baseline Space Shuttle RCS. Both alternate design concepts were aimed at providing maximum retention of the catalyst bed with the goal of minimizing catalyst loss. The two approaches, denoted "composite" and "scalloped" designs, provide different techniques for compartmenting the catalyst. The composite design had been under study on in-house funds for application in low thrust engines.

Table 3-7
DUAL ELEMENT TEST (S/N 004)
CATALYST SUMMARY

	LCH 101 Test Series	LCH 201 Test Series	LCH 202 Test Series
Firing time (sec)	3,400	3,060	3,000
9 Starts	10	5	5
Spikes	Yes	Yes	No
Shell 405 loaded (g)	24.04	24.90	25.54
% Loss	8.8%	5.6%	7.7%
% Fines > 30 mesh	23.6%	15.6%	14.3%
> 35 mesh	13.5%	8.1%	6.7%
Outer bed catalyst	LCH 101	LCH 201	LCH 202
Loaded weight (g)	34.85	30.54	31.50
% Loss	0.5%	2.3%	1.7%
% Fines	2.6%	6.5%	4.9%
H_2 chemisorption μmoles/g			
Prior to firing	3.5	6.3	42
After firing	6.7	2.5	33.3

11063-81

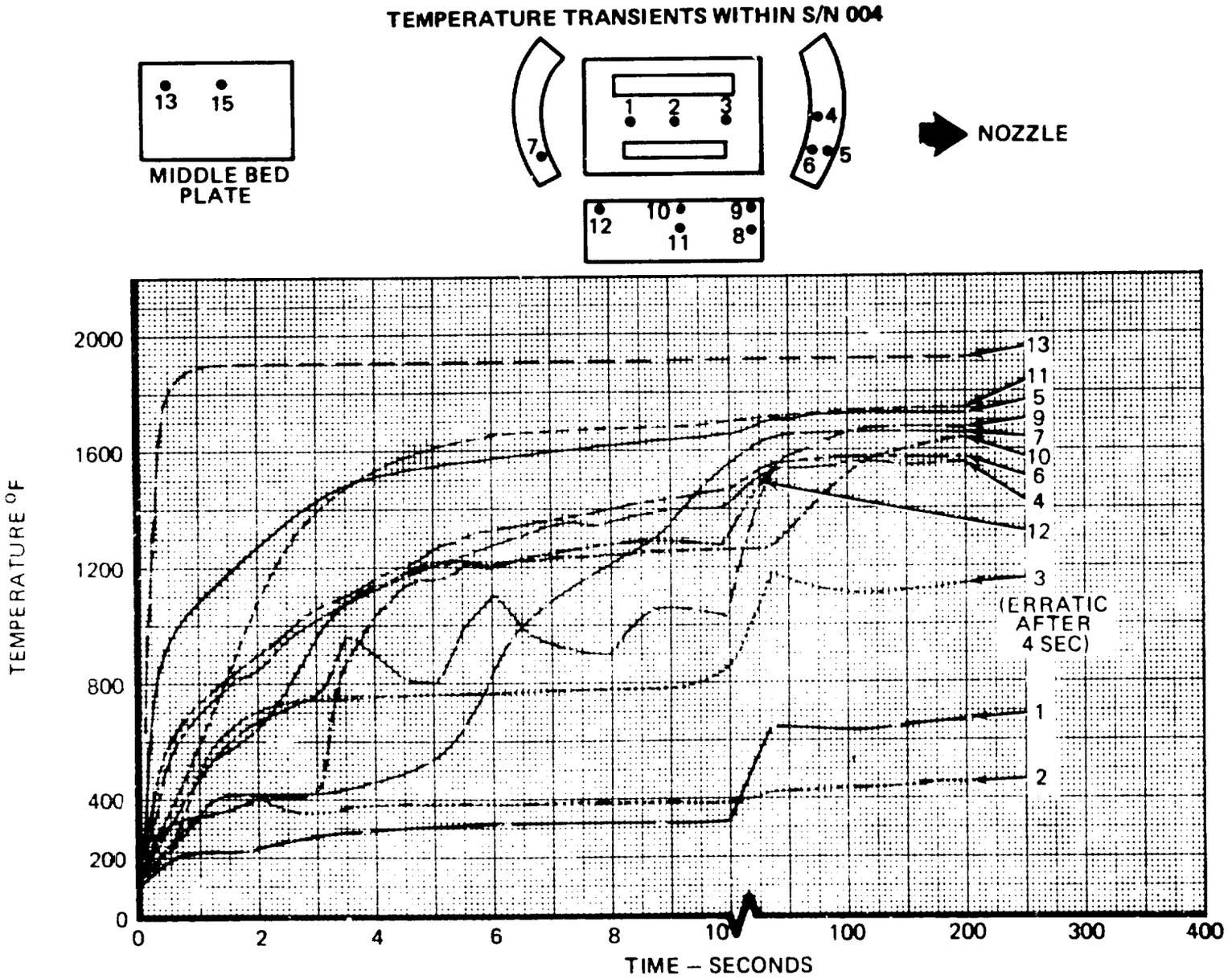

Figure 3-20

The scalloped design approach resulted from studies aimed at providing a technique to minimize differential thermal expansion effects. A design which provided negligible differential thermal growth between the inner bed catalyst and bedplate was fabricated with a nominal bed composition of 25 percent Shell and 75 percent LCH 101 and designated as S/N 005. The design incorporated slotted bedplates with the slots sufficiently small to permit elimination of screen wires.

Subscale Reactor S/N 005 – A photo of the scalloped wedge is shown in Figure 3-21. This initial scallop design was fabricated with the thought of encapsulating single injector elements inside inner bedplates, as shown in the photo. Since this unit had only one injection element, total flow rate and chamber pressure were 50 percent of S/N 004 tests. The test duration on this unit was 3,000 seconds in order to evaluate the potential increased life capability of the design. The unit performed similarly to S/N 004 at comparable periods of life. Table 3-8 compares the inner bed catalyst loss data to that of the S/N 004 design. As seen in this table, the scalloped design provided approximately 3 times increased life over the S/N 004 design. To fully assess this potential, S/N 005 was refurbished with LCH 202 catalyst and the plenum chamber nozzle was reconfigured to provide 155 psia at 0.090 lbm/sec flow rate. The goal of this test was to accumulate 12,000 seconds total firing time, to be accumulated during twenty 600-second steady-state firings in addition to 20,000 pulses ranging in duty cycle from 10 to 50 percent. The results of the test are summarized below.

The twenty 600-second steady-state firings were accomplished with excellent performance of the reactor. No abnormal start up transients occurred, roughness remained below ±3.0 psi and the outer bedplate temperature remained essentially constant at 1,760°F. Figure 3-22 shows the reproducibility of temperatures within the wedge for each firing, and Figure 3-23 shows the chamber pressure roughness and bed pressure drop versus life. Four additional ambient starts were conducted to provide the 20,000 pulses. Typical pulses are shown in Figure 3-24. At the conclusion of the pulses, an additional 110 second steady-state firing was conducted. At this point (14,000 seconds accumulated burn time) the roughness was ±3.5 psi, the outer bed temperature was 1,720°F and all other parameters appeared excellent. A detailed teardown analysis was then conducted.

The subscale engine hardware, after accumulating 14,000 seconds on the catalyst bed (17,000 seconds on the engine), was in excellent shape. Deformation of the inner bedplate was 0.002 inch while the outer bedplate was limited to a slight bowing of approximately 0.020 inch. A nominal catalyst loss of 14.7 percent occured in the inner bed and only 2.9 percent in the outer bed. The hydrogen chemisorption for the Shell 405 and LCH catalysts were 113 μ moles/grams and 40 μ moles/grams, respectively.

The life capability demonstrated by the S/N 005 reactor was extremely encouraging, but comparative data on the scalloped concept versus conventional concept was limited due to the differing test conditions. A test series was formulated to demonstrate the life capability of the two design concepts (conventional - designated as S/N 006 and scalloped – designated as S/N 007) using simulated mission firings and multiple vibrations. Propellant flow rates, chamber pressures, and effective bed loadings were identical between subscale engines.

Subscale Reactor – S/N 006 – The conventional subscale engine was fabricated with a catalyst bed ratio of 35 percent Shell 405 and 65 percent LCH 202 to provide a slight margin over the bed

S/N 005 SUBSCALE ENGINE (SCALLOPED WEDGE) LOOKING INTO CATALYST COMPARTMENTS

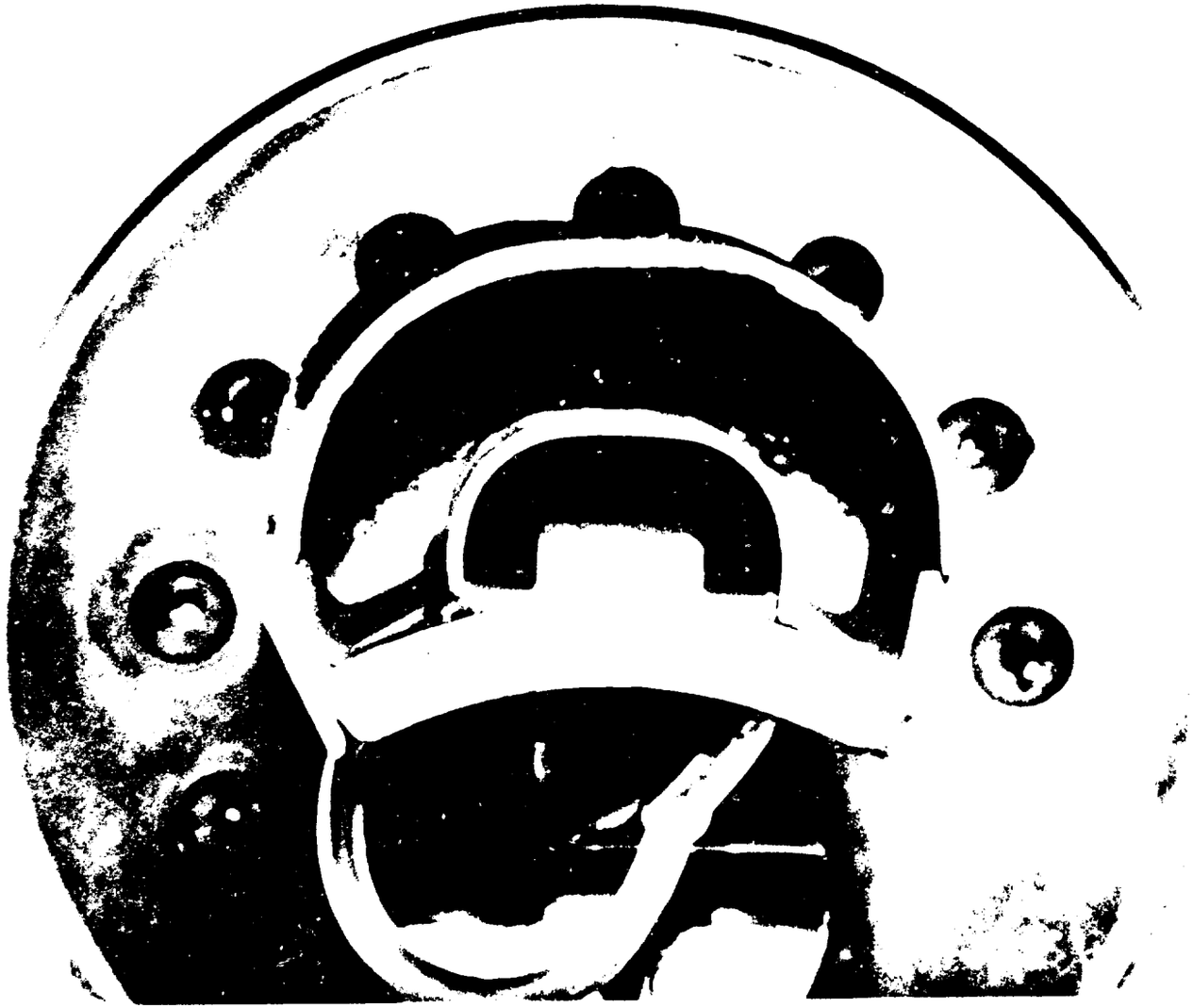

11063-14

Figure 3.21

Table 3-8
SCALLOPED WEDGE CATALYST DATA

	S/N 004 TEST 3	S/N 005 SCALLOPED
FIRING TIME, SECONDS	3,000	3,060
NUMBER OF STARTS	5	6
SPIKES	NO	NO
SHELL 405 LOADED, g	25.54	10.01
% LOSS	7.7%	2.5%
% FINE, >30 MESH	14.3%	10.5%
>35 MESH	6.7%	3.7%
OUTER BED CATALYST	LCH 202	LCH 101
LOADED WT, g	31.50	29.27
% LOSS	1.7%	(0.56g INCREASE)
% FINES	4.9%	1.9%

STEADY-STATE ENGINE TEMPERATURES VERSUS RUN TIME
TEST SERIES EIGHT
SCALLOPED ENGINE (S/N 005)

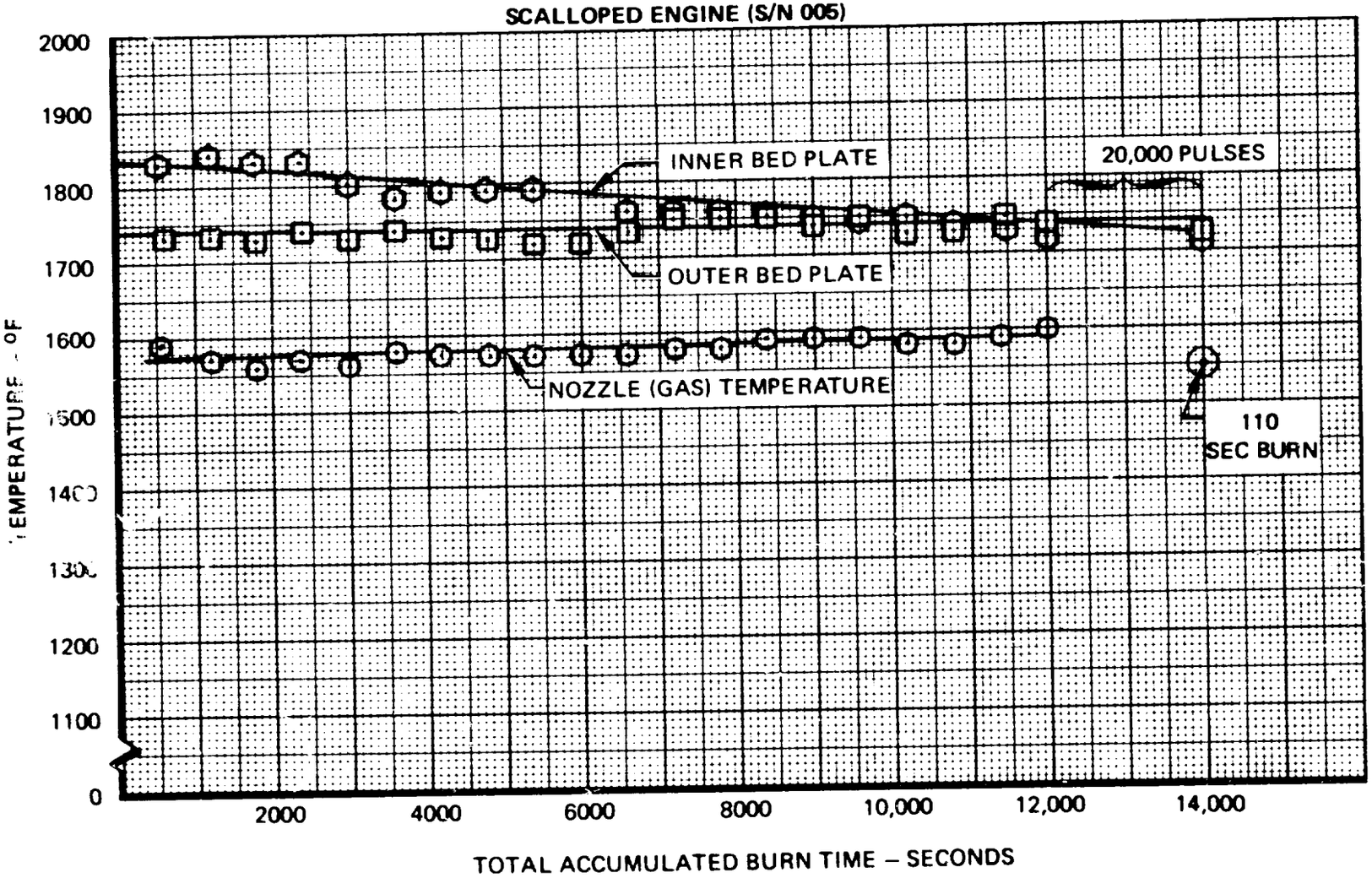

Figure 3-22

SCALLOPED ENGINE (S/N 005) TEST SERIES EIGHT
CATALYST BED PRESSURE DROP VS. RUN TIME
CHAMBER PRESSURE ROUGHNESS VS. RUN TIME

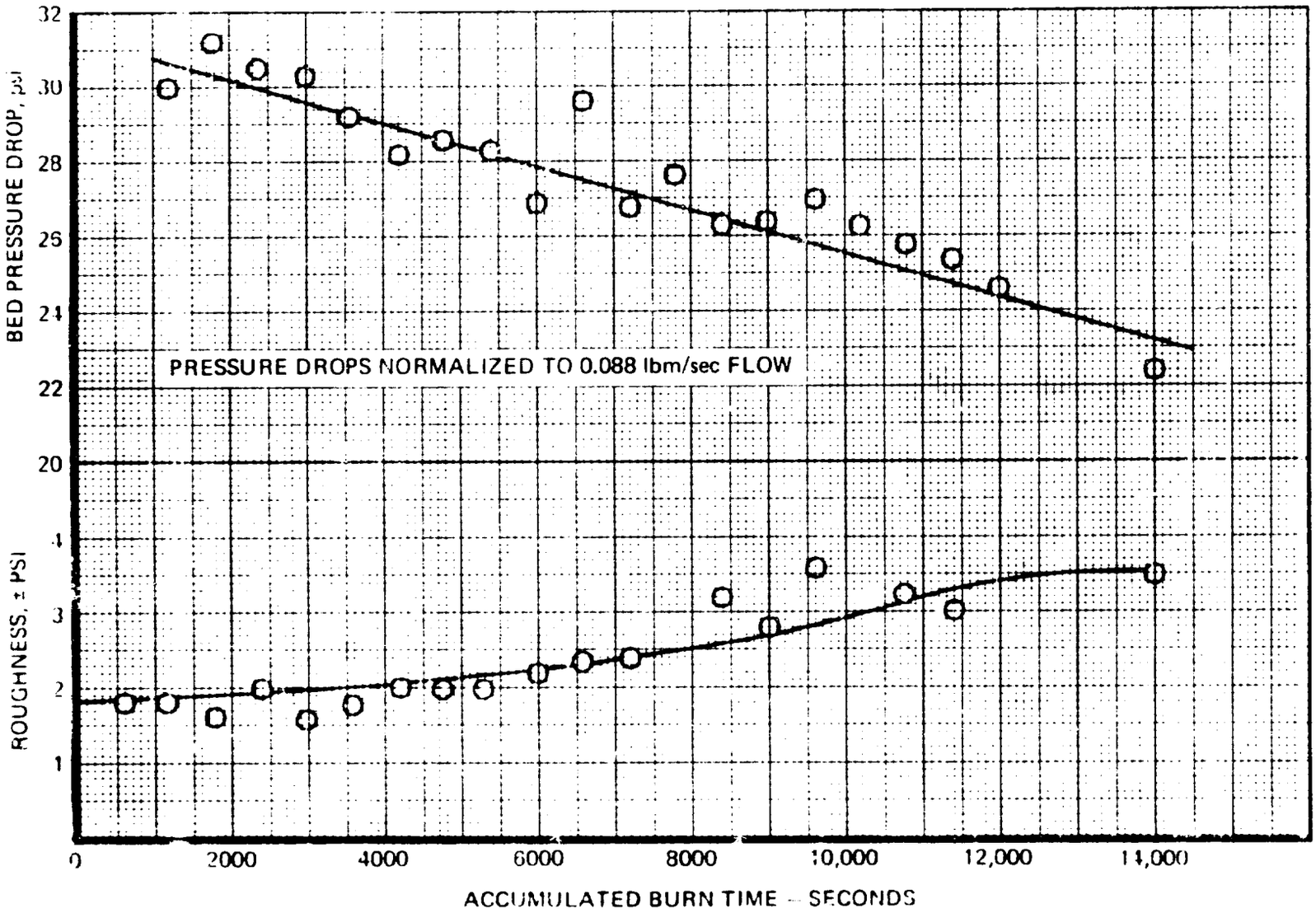

Figure 3-23

TEST SERIES EIGHT PULSE TRACES
100-MILLISECOND PULSES

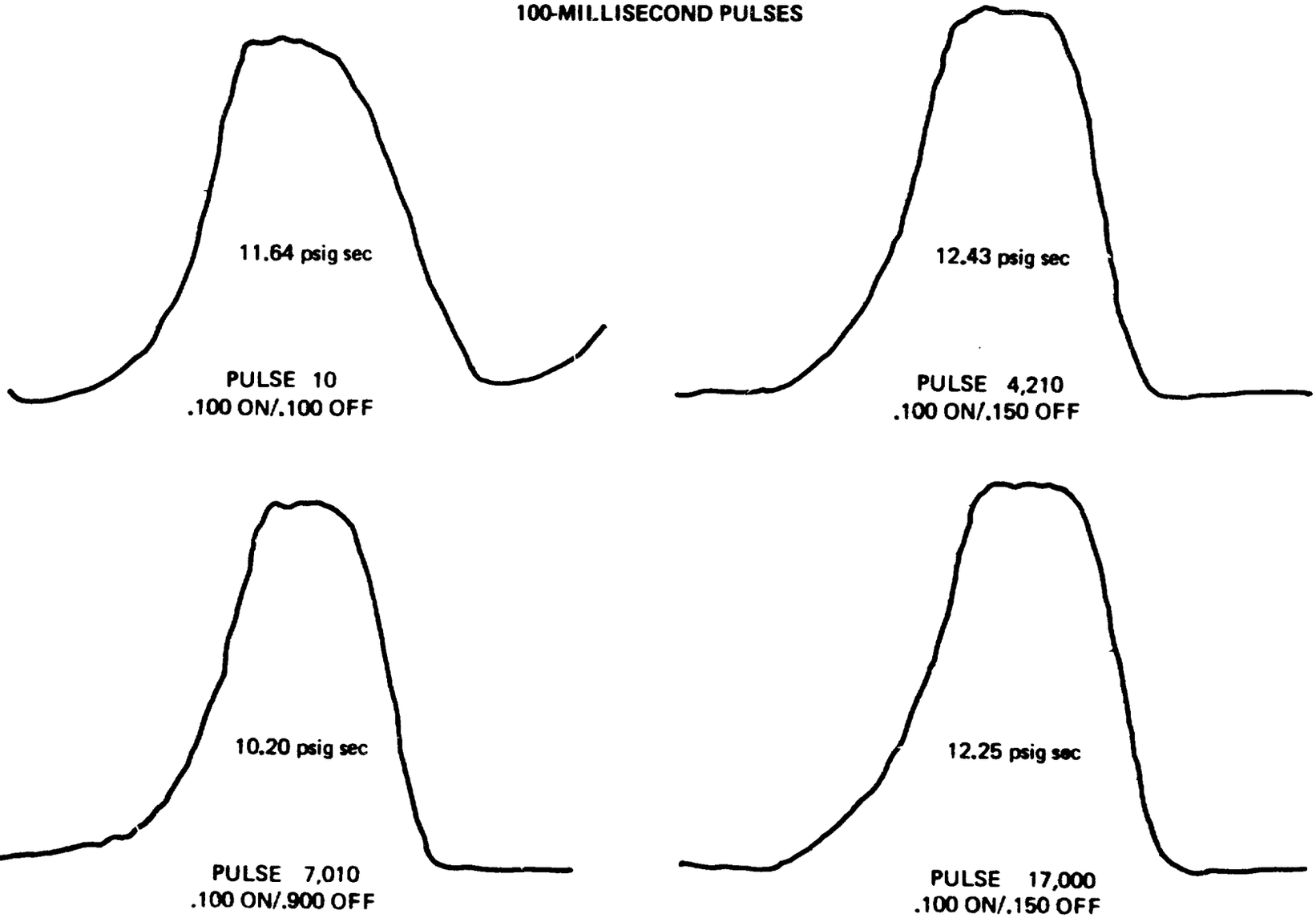

Figure 3-24

configuration established previously. Dual element injectors were also used; the distance between elements was reduced from that used in S/N 004 to prevent start transient cook-off spikes. The testing of the conventional subscale engine is described below.

Ten 600-second steady-state runs were successfully tested on S/N 006. Performance data for the first and tenth runs are shown in Table 3-9. After 2 firings (1,200 seconds) a 3-minute vibration of the reactor (11.7 g's rms) was conducted. Approximately 1 milligram of catalyst was recovered after vibration. No spikes or perks occurred during the first nine tests; tests 9 and 10 had a 20 psi perk at approximately 0.7 seconds into the run. Chamber pressure roughness and bed pressure drop had slowly increasing values as shown in Figures 3-25 and 3-26.

Table 3-9
TEST DATA SUMMARY FOR CONVENTIONAL SUBSCALE ENGINE LIFE TESTS (S/N 006)

	Initial Steady-State Firing, 9–1	Final Steady-State Firing, 9–10
Burn time	600 seconds	600 seconds
Accumulated burn time	600 seconds	6,000 seconds
Initial catalyst bed temperature	110°F	195°F
Propellant flow rate	0.175 lbm/sec	0.172 lbm/sec
Chamber pressure	167 psia	163 psia
Outer bedplate temperature	1,730°F	1,710°F
P_c roughness	±4 psi	±6 psi
Characteristic velocity	4,290 ft/sec	4,260 ft/sec

A series of 4,100 pulses was then conducted with intermittent 10-second steady-state firings. Chamber pressure roughness continued to increase to approximately ±10 psi after 4,100 pulses (roughness obtained during a 10-second steady-state run). After the 4,100 pulses, a 1 percent duty cycle with 0.050 pulse widths was attempted on the hot engine. On the third pulse of the series, a high pressure excursion occurred in the propellant inlet tube after valve shutdown. The pressure surge that occurred in the injector was determined to be a result of exceeding the thermal design capability of the subscale hardware. The chamber of the subscale engine is an all-welded structure, but quite massive to allow a large number of refurbishments. The end closure of the chamber is a very large heat sink which in turn required the propellant inlet tube to be longer than normal to minimize valve soakback. The combination of the large heat sink (end closure) surrounding the feed tube with a long hold-up volume (nominally 20 msec) constrained the subscale hardware to limited duty cycles.

CONVENTIONAL AND SCALLOPED SUBSCALE ENGINE LIFE TESTS
CHAMBER PRESSURE ROUGHNESS VS. RUN TIME

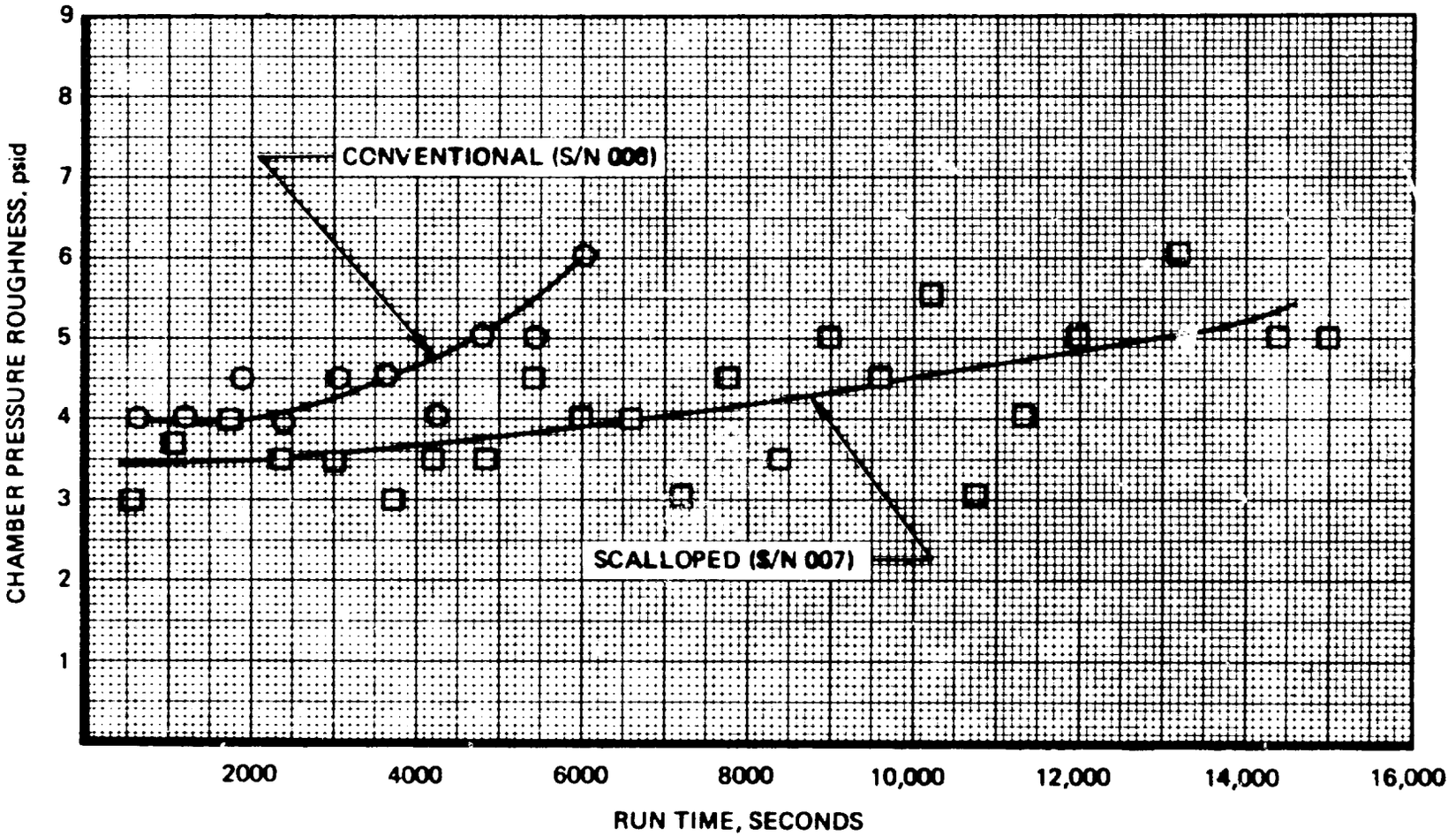

Figure 3-26

11064-56A

CONVENTIONAL AND SCALLOPED SUBSCALE ENGINE LIFE TESTS
CATALYST BED PRESSURE DROP VS. RUN TIME

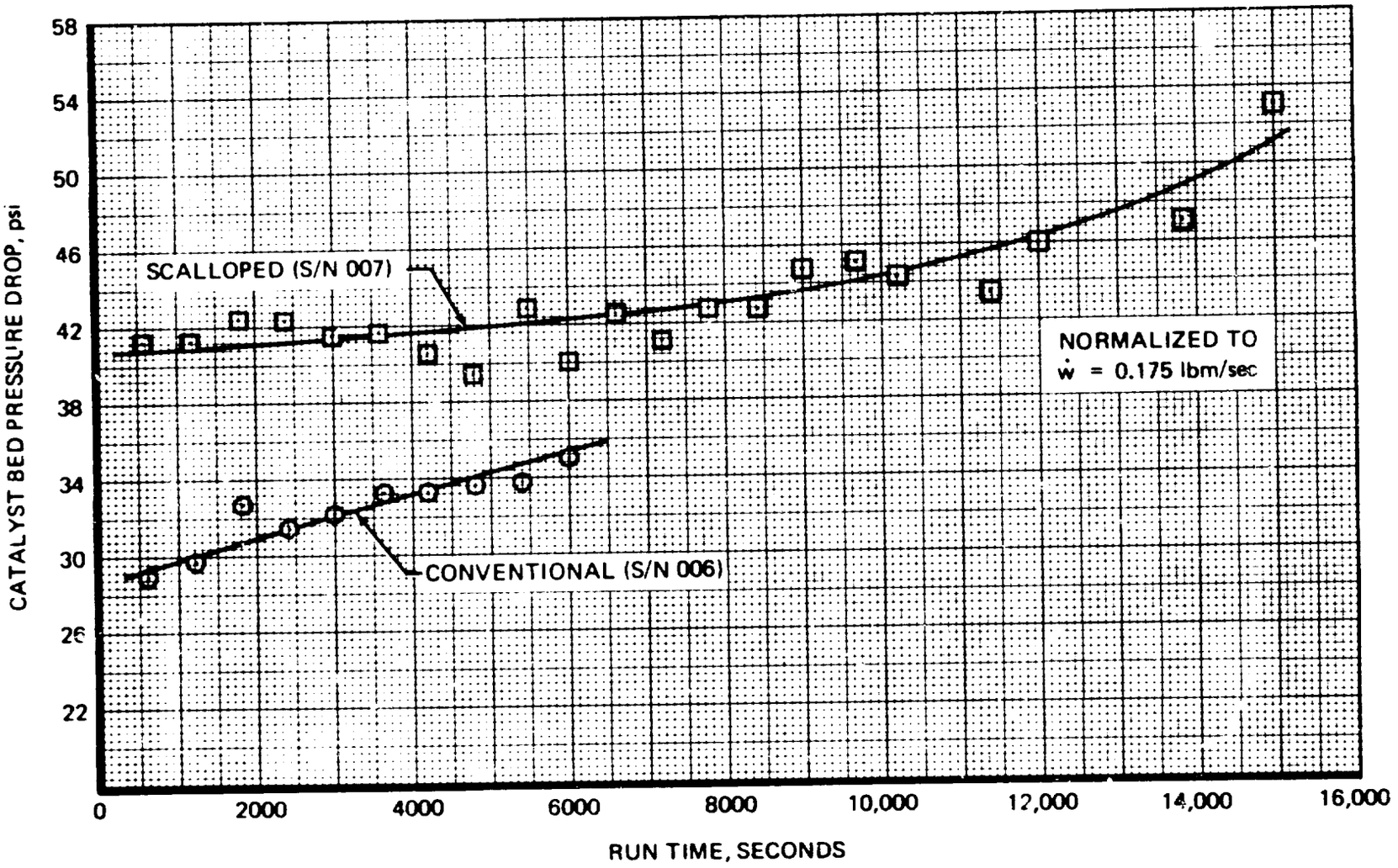

Figure 3-26

Subscale Reactor S/N 007 – A subscale engine using the scalloped concept was fabricated with a dual element injector. The injector feed tube was cooled to prevent tailoff pulses as observed in the previous tests. This test series was conducted to determine life capability of the scalloped concept and compare performance data with that obtained with the conventional design. The radial bed lengths were similar to the conventional design; however, the scallop design provided a net reduction of 35 percent Shell 405 and 17% LCH 202 over that required for the conventional engine design. Test results are described below.

Twenty 600-second steady-state runs were conducted. Performance data for these runs are shown in Table 3-10.

Table 3-10

DATA SUMMARY FOR THE SCALLOPED SUBSCALE LIFE TESTS – S/N 007

	Initial Steady-State Firing, 10–1	Steady-State Firing Prior to Pulsing, 10–20	Final Steady-State Firing After 32,000 pulses
Burn time	600 seconds	600 seconds	600 seconds
Accumulated burn time	600 seconds	12,000 seconds	18,000 seconds
Initial catalyst bed temperature	150°F	150°F	190°F
Propellant flow rate	0.168 lbm/sec	0.171 lbm/sec	0.175 lbm/sec
Chamber pressure	161 psia	164 psia	168 psia
Outer bedplate temperature	1,750°F	1,760°F	*(1,800°F)
P_c roughness	±3.0 psid	±5.0 psid	±8.0 psid
Characteristic velocity	4,260 ft/sec	4,264 ft/sec	4,279 ft/sec

*Approximated from inner bed measurement

As with the conventional subscale engine (S/N 006), a 3-minute vibration at 11.7 g's rms was conducted at 1,200 seconds and 0.068 grams was recovered after vibration.

A total run time of 18,000 seconds, ten ambient starts, 32,000 pulses and intermittent steady-state runs was accumulated following the 20 steady-state burns. Chamber pressure roughness increased to ±8 psi, and catalyst bed pressure drop decreased to 25 psi while characteristic velocity showed a slight increase at the end of 18,000 seconds. Figures 3-25 and 3-26 show the effect of life on roughness and bed pressure drop.

Three additional 3-minute vibration tests were conducted during the test sequence. Table 3-11 tabulates the catalyst recovered from the engine after each vibration.

At 18,000 seconds, sufficient time had been accumulated to demonstrate the capability of the scalloped engine design, thus, no further testing was conducted. To provide further design information for the 490-lbf RCS, a detailed teardown was conducted with results as discussed below.

Table 3-11
CATALYST LOSS FROM SCALLOPED ENGINE (S/N 007) DURING VIBRATION

Vibration Sequence	Accumulated Run Time	Accumulated Pulses/Starts	Catalyst Recovered From Engine
1	1,200 sec	2	0.068 grams
2	15,000 sec	23,000	0.439 grams
3	16,200 sec	26,000	0.040 grams
4	17,400 sec	30,000	0.023 grams

Bedplates – No cracking or significant deformation was observed in either bedplate assembly. The physical appearance of the bedplates after subscale testing indicated that the 490-lbf engine would be structurally capable of meeting the 100-mission goal.

Injector Body – Preliminary observations indicated that the injector body was fully capable of meeting the 100-mission goal/requirement. No deterioration of the injector propellant passage or injector element was evident under 10X magnification.

Catalyst Bed – Examination of the catalyst beds following testing indicated that the scallop engine bed retention system was capable of providing a minimum of 50 Space Shuttle missions prior to refurbishment. The inner catalyst bed, composed of 25- to 30-mesh Shell 405, lost 29 percent of the original loaded weight. The LCH 202 outer bed catalyst lost only 3.3 percent. Hydrogen chemisorption values of the pre- and post-fired samples are listed below.

	Pretest Catalyst μ Moles/Gram	Post-Test Catalyst (18,000 Seconds Accumulated Firing Time) μ Moles/Gram
Shell 405	140	119
LCH-202	65	32

3.7 SUBSCALE TEST CONCLUSIONS

The initial purpose of the subscale reactor testing was to establish an optimal mixture of Shell 405 catalyst with a low-cost catalyst. As testing proceeded, the flexibility and potential of wedge reactors proved much more extensive than originally contemplated. Thus, the subscale reactor became a tool to develop an improved low-cost catalyst, optimized the mixture ratio of the two types of catalyst, developed a new catalyst retention technique that increased life over the standard catalyst retention system, and finally verified the increased life capability of an injector having increased propellant distribution. The ability of subscale reactors to serve as a tool that simulates all aspects of reactor environment and life offers a technique for providing significant cost savings on materials, catalyst, and propellant during development of large hydrazine engines.

3.8 SELECTED DESIGN APPROACH

Results of the various subtasks of the Task I investigation were used to arrive at a baseline design for the Task II detailed analyses and design effort. Based on the injector studies (paragraph 3.1), a 12-element longitudinal injector was baselined. Design studies of an all-welded engine and a flanged engine were conducted with the goal of determining which design offered the most cost-effective approach for replacing the catalyst bed. The primary disadvantages of the flanged engine (Figure 3-27) are: 1) a high temperature gas seal is required and 2) heavier weight. These disadvantages are partially offset, however, by the higher cost associated with refurbishment of the all-welded engine. Cost studies conducted for both approaches revealed that the all-welded design was more economical if the number of missions between refurbishment of the bed exceeded 13. Since 25 missions between refurbishment were projected, and because of the flanged engine heavier weight and gas seal requirement, an all-welded design was baselined for the Task II studies.

The RCS preliminary design, which evolved during Task I, is shown in Figure 3-28. A design summary is presented in Table 3-12. As noted previously, subscale testing was continued during Task II, which was aimed at further exploring the scalloped bed design approach. This approach was subsequently adopted during Task II as the baseline design approach for the RCS engine.

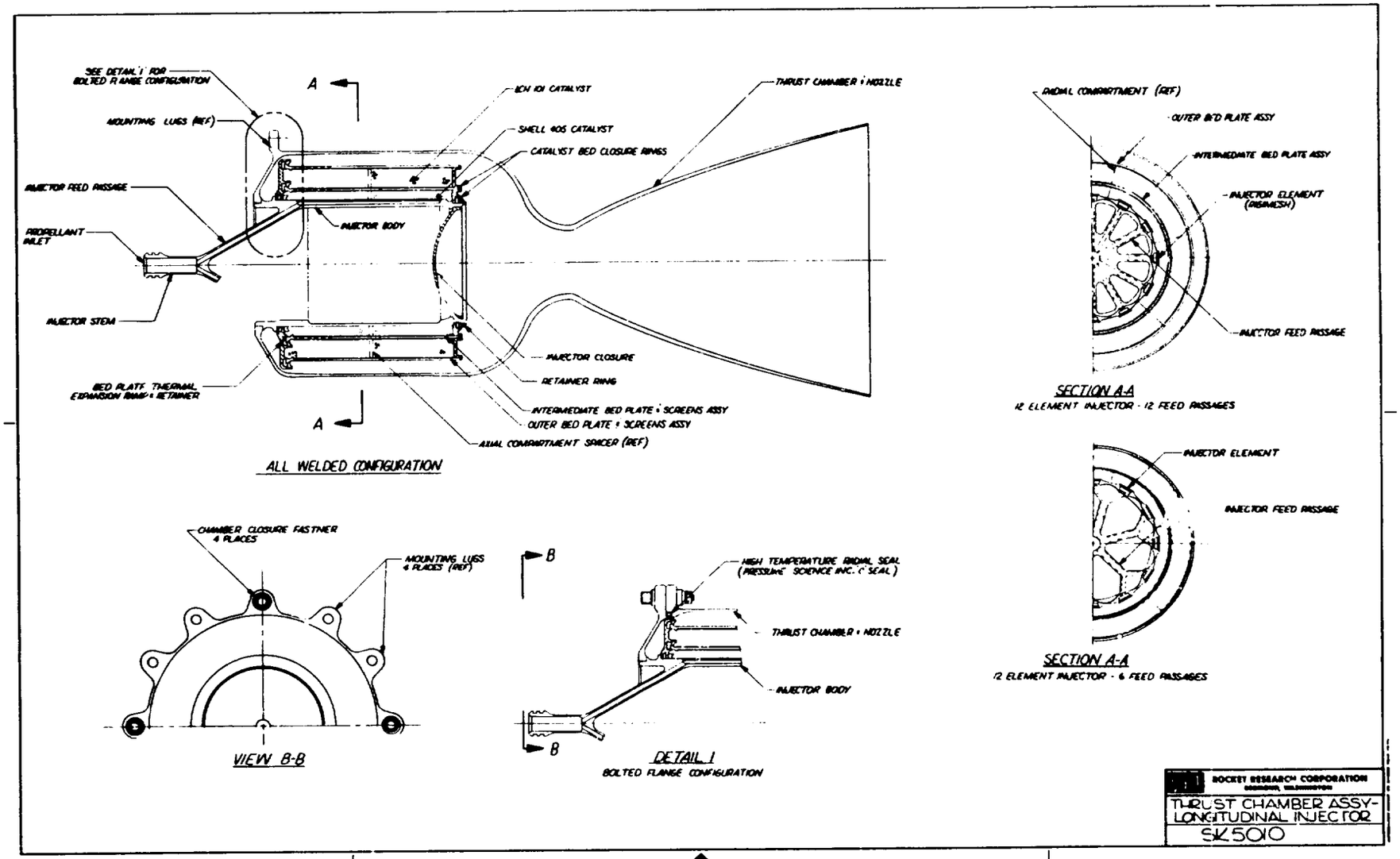

Figure 3-27

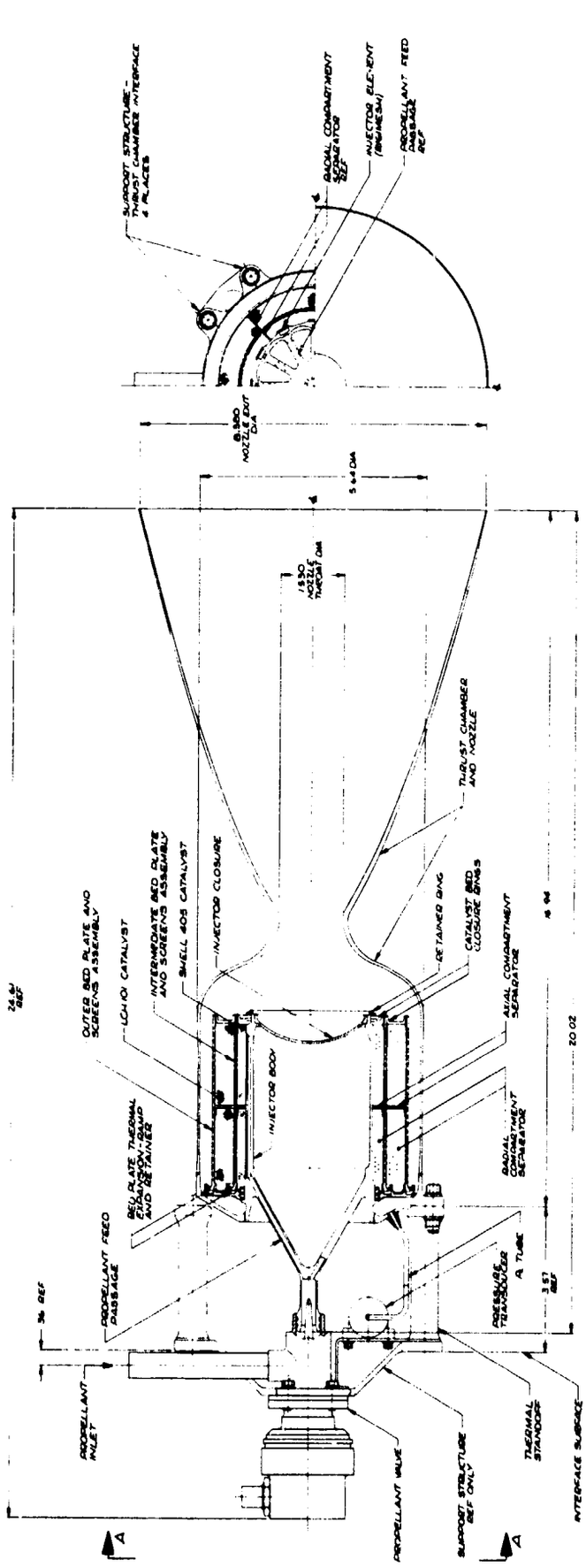

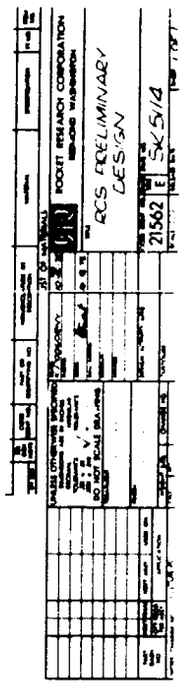

ORIGINAL PAGE IS
OF POOR QUALITY

Figure 3-28

Table 3-12

TASK I

RCS ENGINE DESIGN SUMMARY

THRUST LEVEL	–	490 lbf
FEED PRESSURE	–	300 psia
CHAMBER PRESSURE	–	153 psia
BED LOADING	–	0.045 lbm/in.^{2}-sec
BED PRESSURE DROP	–	70 psi
HARDNESS RATIO	–	0.55
AMMONIA DISSOCIATION	–	45%
SPECIFIC IMPULSE	–	233 lbf-sec/lbm
BED GEOMETRY		
• INNER BED DIAMETER	–	3.2 inches
• OUTER BED DIAMETER	–	4.8 inches
• AXIAL LENGTH	–	4.0 inches
THROAT DIAMETER	–	1.53 inches
EXIT DIAMETER	–	8.38 inches
TOTAL LENGTH	–	24.6 inches
THRUST/EXIT AREA	–	8.9 lbf/in.^{2}

V01048 R2

4.0 ENGINE DETAILED DESIGN AND ANALYSIS

4.1 DESIGN SUMMARY

Presented in this section are the results of the analytical and design studies that were conducted to support the final engine design. At the outset of this task, design analyses were initiated using the preliminary engine design obtained from Task I as a starting point. Design iterations were then made to the preliminary design to arrive at the final optimized design. Final design analyses were then conducted of the thermal, performance, and stress characteristics of the engine. The objective and scope of the Task II effort is shown in Figure 4-1. A summary of the Task II accomplishments is presented in Figure 4-2.

Additional subscale testing was conducted to: 1) determine the optimum quantities of Shell 405 and LCH catalysts, 2) evaluate an alternate LCH catalyst, and 3) evaluate various compartmentation techniques. Based on the results of extensive testing it was concluded that the life capability of the LCH-101 catalyst was limited and that the RRC proprietary catalyst, LCH-202, should be used for the RCS outer bed. The optimum ratios of Shell 405 and LCH-202 were subsequently determined to be 35 and 65%, respectively.

Various techniques for compartmenting the catalyst bed were evaluated analytically and experimentally. Based on earlier studies during Task I, it was concluded that differential thermal expansion between the catalyst and retaining walls was instrumental in catalyst attrition. Consequently, design studies were conducted to arrive at an approach which minimized void volume growth resulting from differential thermal expansion. Results of calculations for two appreaches are shown in Figure 4-3. The scalloped design provides a technique wherein each pair of injection elements and catalyst retention system function as separate small engines with corresponding small void volume growth.

Based on encouraging subscale test results obtained with scalloped subscale engines, it was decided to adopt this approach for the Task II detailed RCS design. An isometric of the engine is shown in Figure 4-4. The RCS design summary is presented in Table 4-1.

4.2 THERMAL ANALYSIS

This section includes significant aspects of the RCS thermal design approach including thermal requirements, assumptions, analytical models, predicted thermal characteristics, and correlation of experimental results.

4.2.1 Thermal Design Objectives

The basic thermal design objectives of the Task II analysis were as follows:

TASK II – ENGINE DETAILED DESIGN AND ANALYSIS

- OBJECTIVE
  - TO ESTABLISH DETAILED ENGINE DESIGN SUPPORTED BY THOROUGH ANALYSIS
- DESIGN ANALYSIS
  - PERFORMANCE
  - THERMAL
  - STRUCTURAL
  - MATERIALS
  - SCALABILITY
- ASSESS POST–FLIGHT SERVICE, MAINTAINABILITY, AND CHECKOUT REQUIREMENTS
- DESIGN SAFETY ASSESSMENT
- RELIABILITY ASSESSMENT
- DETAILED OPERATING CHARACTERISTICS PREDICTION
- EFFECTS OF DIFFERENCE IN TEST ENGINE WEIGHT AND PREDICTED FLIGHT ENGINE WEIGHT
- RECOMMENDED PROPELLANT SPECIFICATION
- DETAILED TEST PLAN
- DETAILED DRAWINGS AND MANUFACTURING PLANS
- IDENTIFY CRITICAL TECHNOLOGY AREAS

Figure 4-1

TASK II SUMMARY

SUBTASK	ACCOMPLISHMENT
• SUBSCALE ENGINE TESTS	• ESTABLISHED OPTIMUM SHELL 405/LCH RATIO • EVALUATED LCH CATALYSTS • EVALUATED 3 COMPARTMENTATION TECHNIQUES • CONDUCTED LIFE TESTS
• DETAILED ANALYSES	• PERFORMANCE, THERMAL, AND STRESS PREDICTIONS COMPLETED
• DETAILED DESIGN	• DESIGN LAYOUT COMPLETED AND DETAIL DRAWINGS OF MOUNTING STRUCTURE AND CHAMBER/NOZZLE PREPARED – ALL DRAWINGS COMPLETED
• MATERIALS STUDIES	• TESTS COMPLETED AND MATERIALS SELECTED
• DESIGN SAFETY AND RELIABILITY ASSESSMENT	• ASSESSMENTS COMPLETED
• MAINTENANCE REQUIREMENTS	• POST-FLIGHT SERVICE, MAINTENANCE AND PREFLIGHT CHECKOUT REQUIREMENTS ESTABLISHED
• SCALABILITY ANALYSIS	• TECHNOLOGY ESTABLISHED TO BE APPLICABLE OVER 400–1,100 THRUST RANGE
• WEIGHT DIFFERENCE EFFECTS	• EFFECT OF Δ WEIGHT BETWEEN TECHNOLOGY ENGINE AND FLIGHTWEIGHT ENGINE ASSESSED
• CRITICAL TECHNOLOGY	• AREAS CRITICAL TO APPLICATION OF N_2H_4 TO SPACE SHUTTLE IDENTIFIED

Figure 4-2

01227

11086-93

THERMAL EXPANSION EFFECTS

CONVENTIONAL DESIGN

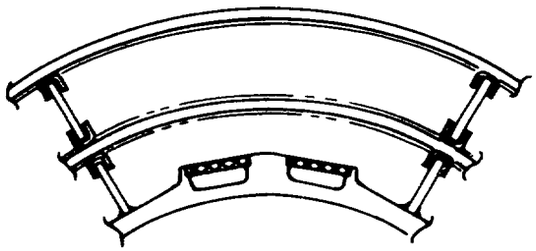

- VOID VOLUME PER COMPARTMENT
  - INNER BED = 0.067 IN^3
  - OUTER BED = 0.035 IN^3

SCALLOPED DESIGN

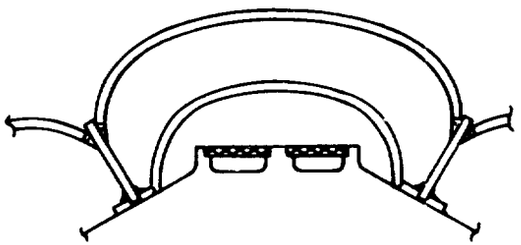

- VOID VOLUME PER COMPARTMENT
  - INNER BED = 0.004 IN^3
  - OUTER BED = 0 IN^3

Figure 4-3

11064-37A

4-5

SPACE SHUTTLE RCS TECHNOLOGY ENGINE

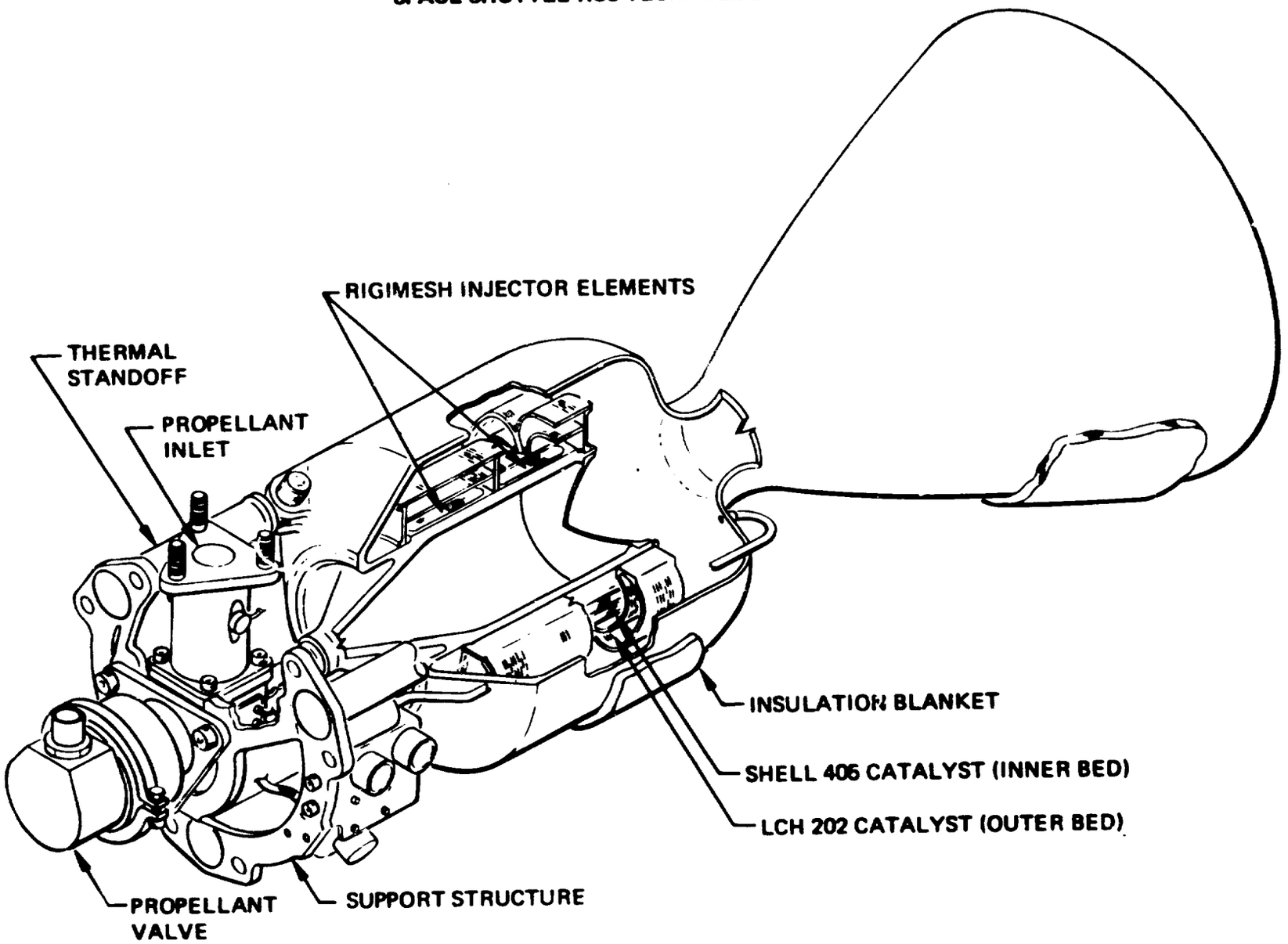

Figure 4-4

Table 4-1
TASK II
RCS ENGINE DESIGN SUMMARY

THRUST LEVEL	–	485 lbf
FEED PRESSURE	–	300 psia
CHAMBER PRESSURE	–	153 psia
BED LOADING	–	0.045 lbm/in.^{2}-sec
BED PRESSURE DROP	–	35 psi
HARDNESS RATIO	–	0.66
AMMONIA DISSOCIATION	–	50%
SPECIFIC IMPULSE	–	230 lbf-sec/lbm
BED GEOMETRY		
• INNER BED DIAMETER	–	3.2 inches
• OUTER BED DIAMETER	–	4.8 inches
• AXIAL LENGTH	–	4.0 inches
THROAT DIAMETER	–	1.53 inches
EXIT DIAMETER	–	8.38 inches
TOTAL LENGTH	–	24.6 inches
THRUST/EXIT AREA	–	8.8 lbf/in.^{2}

V01048 R1

a. Demonstrate engine thermal characteristics as a function of duty cycle
b. Provide estimate of worst-case heating duty cycle
c. Display thermal soakback characteristics
d. Design injector with hot restart thermal margin
e. Define heater requirements
f. Analyze worst-case aerodynamic entry temperatures
g. Limit reactor surface temperature to 800°F
h. Minimize conduction heat input to vehicle

The worst-case combinations of environmental and vehicular conditions used in the analysis are listed in Table 4-2.

4.2.2 Design Goals and Analytical Results

Table 4-2 summarizes basic thermal design goals and analytical results. The last item in Table 4-3 was found to be invalid under certain engine operational modes and will be discussed in more detail in paragraph 4.2.4.2.

4.2.3 Analytical Model

Thermal networks relate the simultaneous iteraction of conduction, convection, and radiation heat transfer. The convection network is given in Figure 4-5. Convection resistances were calculated from the following relation:

$$R = \frac{1}{hA}\left(\frac{hr\ ^{o}F}{Btu}\right)$$

where h is the value of the unit surface conductance, in units of Btu/hr-ft^{2}-^{o}F, and A is surface area in square feet. Similar networks were used for the radiative and conductive analyses.

4.2.4 Analytical Results

This section discusses analytical results concerning basic engine thermal characteristics with respect to duty cycle and time, injector soak temperatures and thermal margin, engine heater requirement studies, and re-entry temperatures.

4.2.4.1 Engine Transient and Pulsing Operation

Inner and outer catalyst bed maximum local temperatures versus duty cycle are presented in Figure 4-6. An inner bed ammonia dissociation of 39% was assumed in order to establish the 2,000°F maximum temperature with 110°F propellant from Table 4-1. Catalyst bed structural design was based on this maximum local temperature, which was established based upon experimental findings in the development of the Viking Lander radial bed engine.

Figure 4-7 presents an average catalyst bed temperature versus time at various duty cycles. Such data can be used to estimate the number of pulses required to reach equilibrium for a given pulse width.

Table 4-2

SPACE SHUTTLE THERMAL ENVIRONMENT ASSUMPTIONS

PARAMETER	HOT BIAS	COLD BIAS
PROPELLANT	110°F	40°F
VEHICLE ENVIRONMENT	200°F	-20°F
NOZZLE VIEW	SOLAR CONSTANT	-460°F
VOLTAGE SUPPLY	32 vdc	24 vdc
AERODYNAMIC HEATING AT NOZZLE EXIT	5 MIN @ 2,000°F	N/A
AERODYNAMIC HEATING AT NOZZLE THROAT	5 MIN @ 1,500°F	N/A
VEHICLE INTERIOR TEMP RESPONSE TO AERO HEATING	15 MIN @ >300°F	N/A

Table 4-3

SPACE SHUTTLE THERMAL DESIGN GOALS AND SUMMARY

DESIGN PARAMETER	GOAL	INTENT OF GOAL	LIMITS	PREDICTED VALUES AND COMMENTS	
Catalyst bed minimum temperature	150°F	Provide smooth starts and promote catalyst life	40°F	161°F	Worst-case cold environment, reactor heater 20 watts @ 24 vdc. Other variations considered.
Propellant valve minimum temperature	50°F	Prevent propellant freezing	35.6°F	51°F	Worst-case cold environment, valve heater 2.98 watts @ 24 vdc.
Propellant valve maximum temperature	<280°F	Avoid valve seat overheat damage	300°F	112°F 254°F 280°F	During operation Post-firing soak transient Aerodynamic entry firing soak
Feed tube O-ring	<350°F	Avoid EPR-rubber overheat damage	350°F Continuous	112°F 328°F 351°F	During operation Post-firing soak transient Aerodynamic entry firing soak exceeds 350°F for less than 10 minutes
Insulation surface	<800°F	Customer requirement	800°F	768°F	Worst-case hot environment
Conductive heat dissipation	Minimize	Diminish REA impact on vehicle thermal control	TBD	26.8 watts	Worst-case hot environment
Propellant hot restart thermal margin $\Delta T = T_{sat} - T_b$	$\Delta T > 50°F$	Provide unlimited duty cycle operation	44°F	82°F	Worst-case hot environment

SPACE SHUTTLE THERMAL MODEL (CONVECTION NETWORK DETAILS)

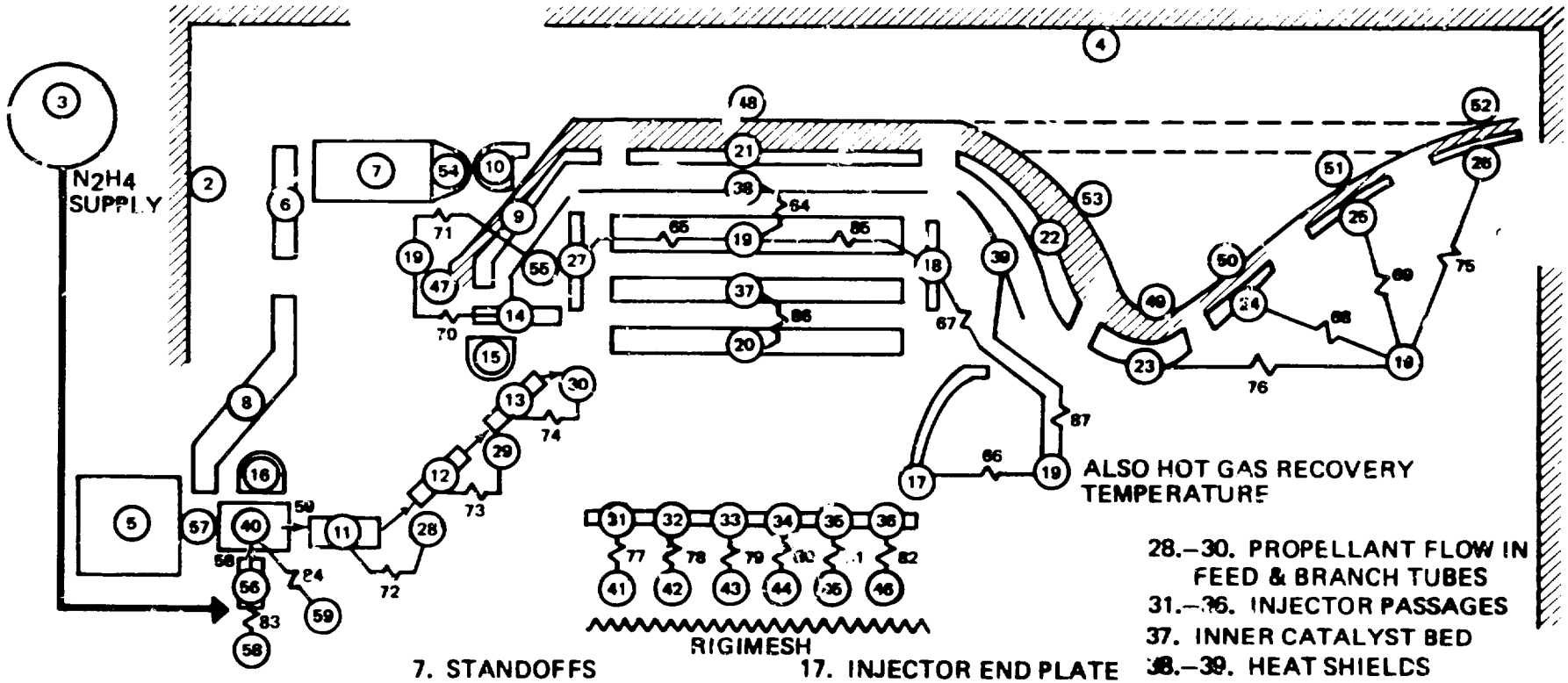

NODE DESCRIPTIONS

1. SPACE
2. VEHICLE CONDUCTIVE INTERFACE
3. HYDRAZINE SUPPLY
4. VEHICLE RADIATIVE INTERFACE SECTION
5. VALVE ACTUATOR HOUSING
6. SUPPORT STRUCTURE RING
7. STANDOFFS
8. SUPPORT STRUCTURE ARMS
9. UPPER INJECTOR CLOSURE
10. PIN ENDED MOUNT BRACKET
11. FEED TUBE
12. UPPER HALF OF BRANCH TUBES
13. LOWER HALF OF BRANCH TUBES
14. TOP INJECTOR FLANGE
15. REACTOR HEATER
16. VALVE HEATER
17. INJECTOR END PLATE
18. LOWER CATALYST CLOSURE
19. OUTER CATALYST BED
20. INJECTOR WEBS
21. REACTOR WALL
22. NOZZLE CONVERGENT
23. NOZZLE THROAT
24.–26. NOZZLE DIVERGENT
27. UPPER CATALYST CLOSURE
28.–30. PROPELLANT FLOW IN FEED & BRANCH TUBES
31.–36. INJECTOR PASSAGES
37. INNER CATALYST BED
38.–39. HEAT SHIELDS
40. VALVE SEAT ZONE
41.–46. PROPELLANT FLOW IN INJECTOR PASSAGES
47.–53. INSULATION
54. STANDOFF PIN END
55. HEAT SHIELD
56. FILTER
57. JUNCTION NODE
58.–59. FILTER & VALVE PROPELLANT FLOW

Figure 4-5

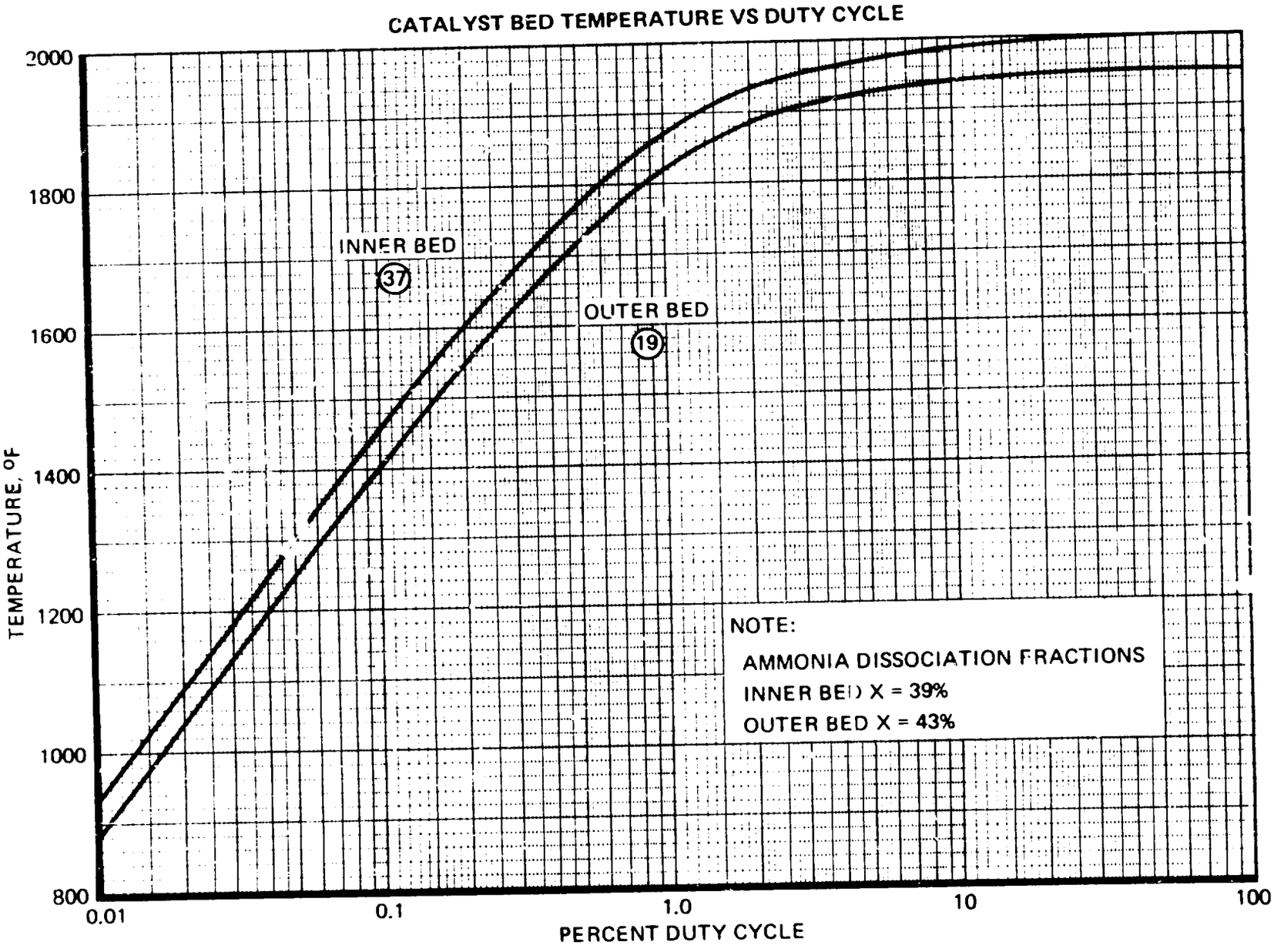

11063-16A

Figure 4-6

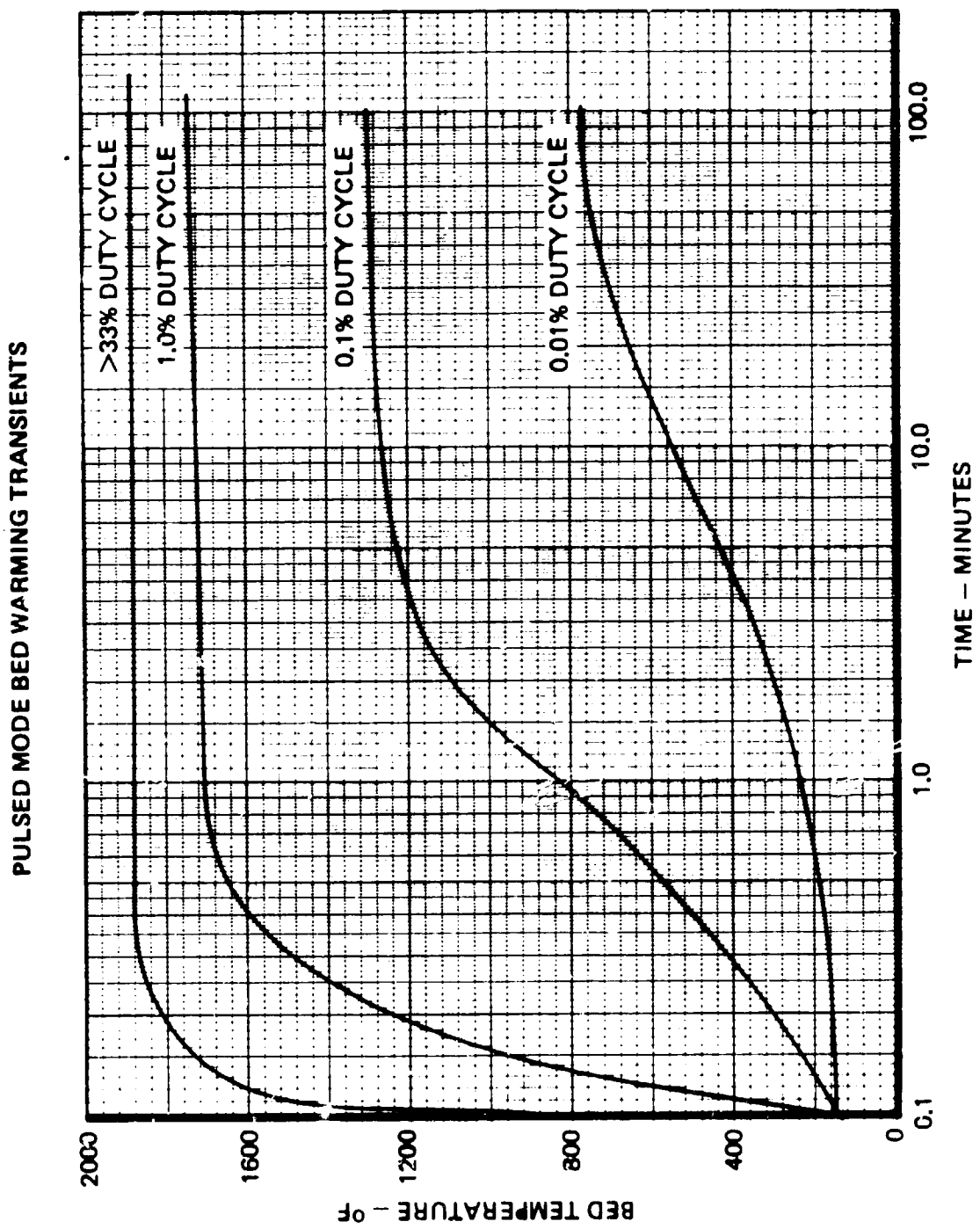

11064-52

Figure 4-7

Figure 4-8 shows the effect of internal convection heat shields on the transient thermal characteristics of basic pressure vessel walls. The heat shields have the potential to greatly reduce the total time the reactor walls will spend at high temperature for pulse-mode operation. For long steady-state firings the heat shields would become effective only if the outer wall Min-K insulation blanket were not required.

4.2.4.2 Injector Soakback and Thermal Margin

Figure 4-9 shows that the valve/injector interface O-ring seal will not be damaged due to heat. The EPR O-ring is capable of continuous operation under 350°F.

Figure 4-10 shows that maximum injector soakback temperatures occur after a steady-state firing in hot orbit. The data shown in Figure 4-9 also apply to this condition. Figure 4-11 shows maximum injector soakback temperature versus duty cycle.

Figure 4-12 shows the results of the thermal margin calculations that were subsequently found to be invalid under certain engine operational modes. Bulk propellant temperatures were calculated by the methods described in paragraph 4.2.4. Thermal margin, the difference between maximum bulk propellant temperature and local saturation, was found to be minimum when the injector cooled for 1.9 hours after a steady-state firing. According to the method discussed in paragraph 4.2.4, only then would the majority of the wetted injector walls be within the nucleate boiling region (10 to 90°F above saturation). As shown in Figure 4-12 the positive thermal margin of 393 minus 311 or 82°F is predicted.

The other case shown in Figure 4-12 has a higher thermal margin, 393 minus 186 or 207°F, because film boiling heat flux is not as severe as nucleate. Positive thermal margin is desirable, and a hydrazine engine having this characteristic will usually not be duty-cycle limited under a mode of operation where pulse widths are of sufficient length to cool critical locations within the injector below decomposition temperatures during flow.

Obviously, for a mode of operation with 100-millisecond pulse widths, the positive thermal margin prediction is invalid as was found in testing. Had the pulse widths been longer, it is felt that there would not have been any problems.

4.2.4.3 Engine Heater Power Requirements

As shown in Table 4-3, minimum valve heater power required to maintain trapped propellant above freezing with a comfortable margin is 2.98 watts. At 2.98 watts in the cold environment the valve temperature will be above 50°F.

A similar calculation was made to determine reactor heater power required to maintain the catalyst bed above 150°F to ensure catalyst life and smooth engine starts. Basic results are presented in Figure 4-13 which shows the inner and outer catalyst bed temperatures versus heater power for cold and nominal environments. As shown, slightly over 20 watts is the minimum requirement. At 20 watts the inner bed is above 150°F; thus, this value was listed in Table 4-3.

11062-15

INTERNAL HEAT SHIELD/COMPONENT TRANSIENT RESPONSE COMPARISON

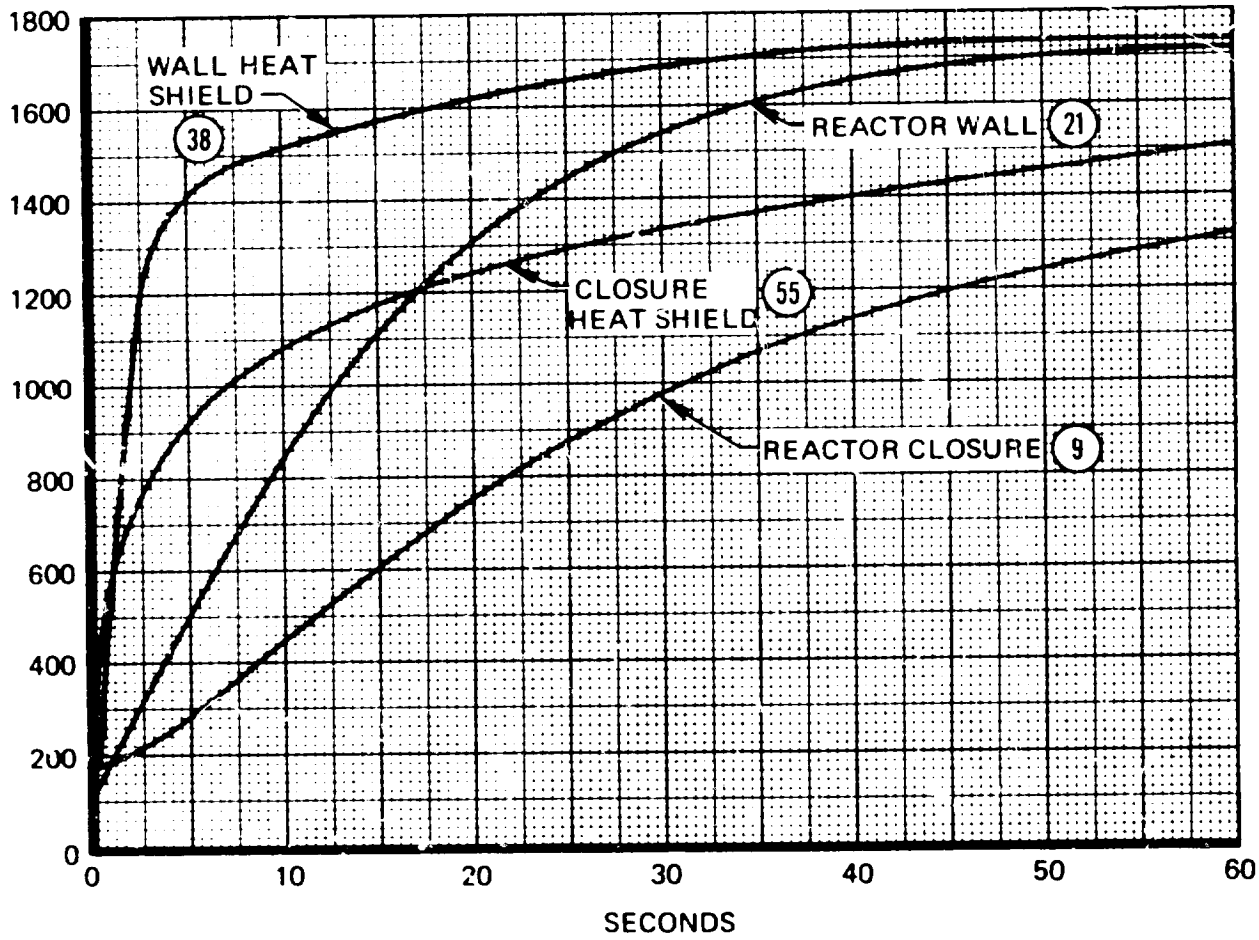

Figure 4-8

STEADY-STATE POST-FIRING SOAK PERIOD
(HOT BIAS ENVIRONMENT)

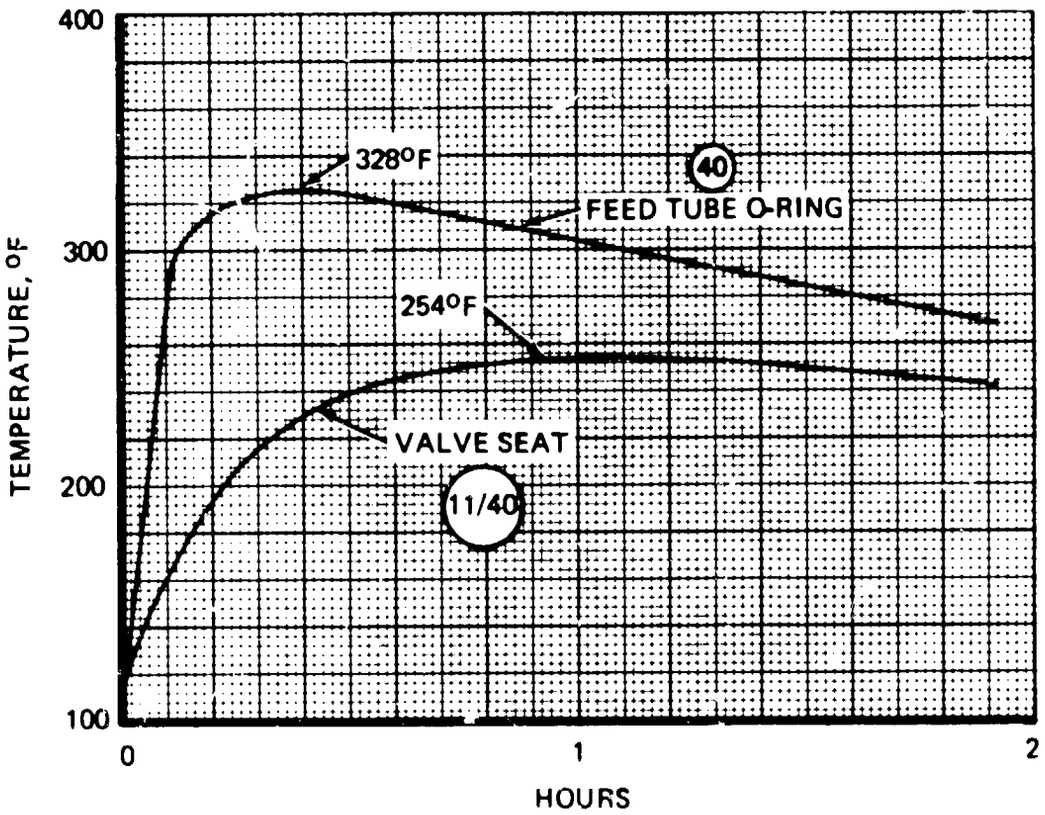

11064-51

INJECTOR PASSAGE
SOAK TEMPERATURES VS DUTY CYCLE

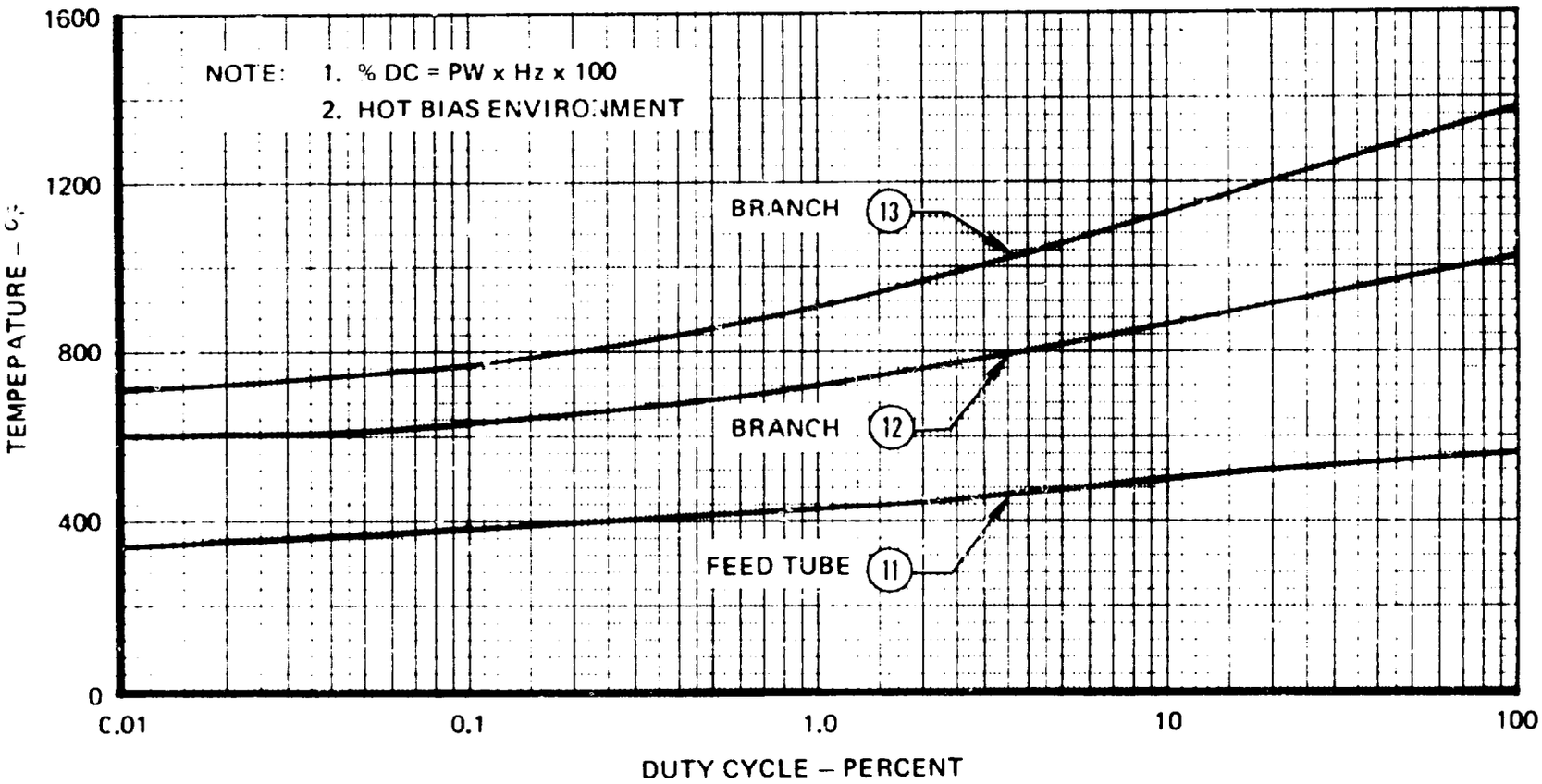

Figure 4-10

MAXIMUM INJECTOR SOAK TEMPERATURES
(HOT BIAS ENVIRONMENT)

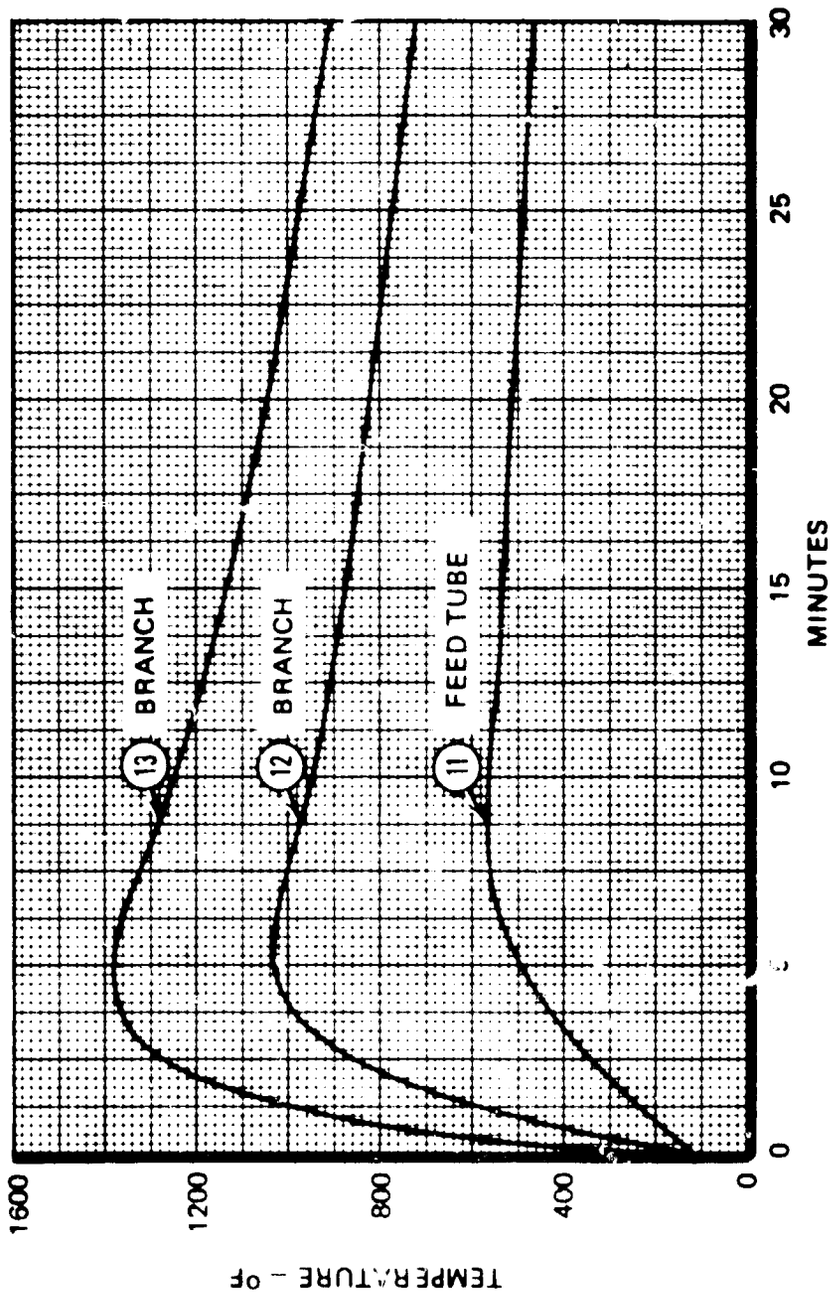

11064-50

Figure 4.11

MAXIMUM PROPELLANT TEMPERATURES DURING HOT RESTART

CASE A
1-MINUTE SOAK

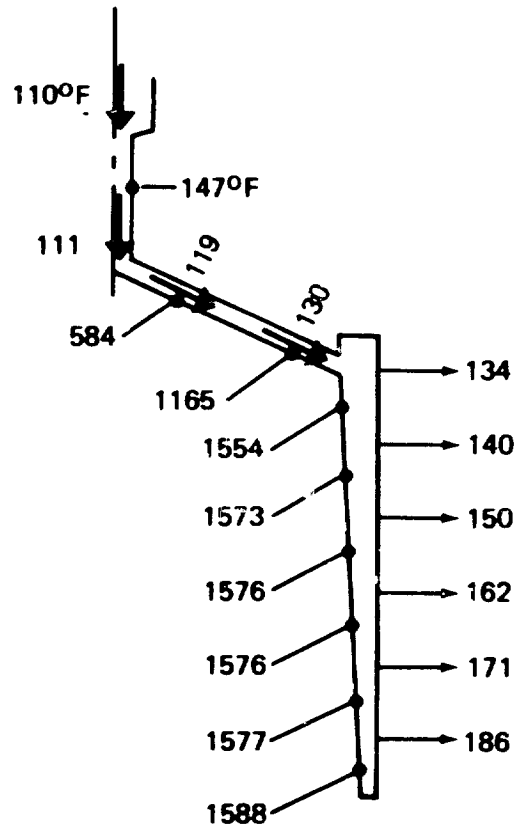

P_{SAT} = 179 psia
T_{SAT} = 393°F

CASE B
1.9-HOUR SOAK

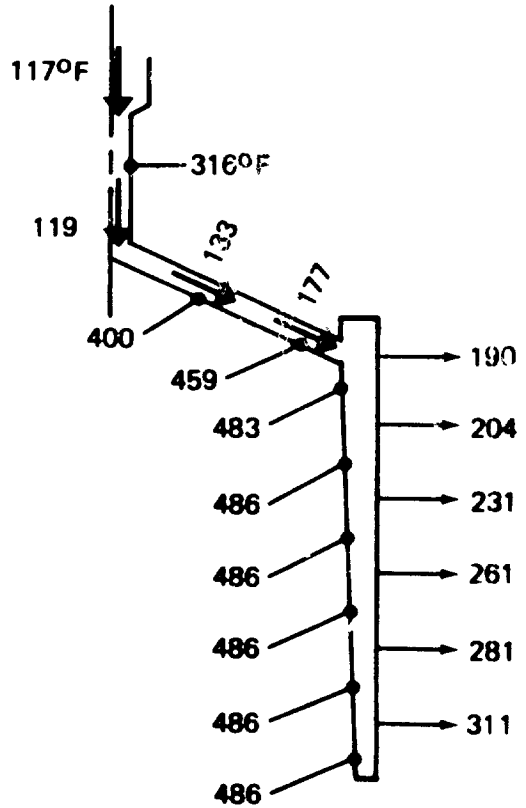

P_{SAT} = 179 psia
T_{SAT} = 393°F

Figure 4-12

EQUILIBRIUM HEATER POWER VARIATIONS

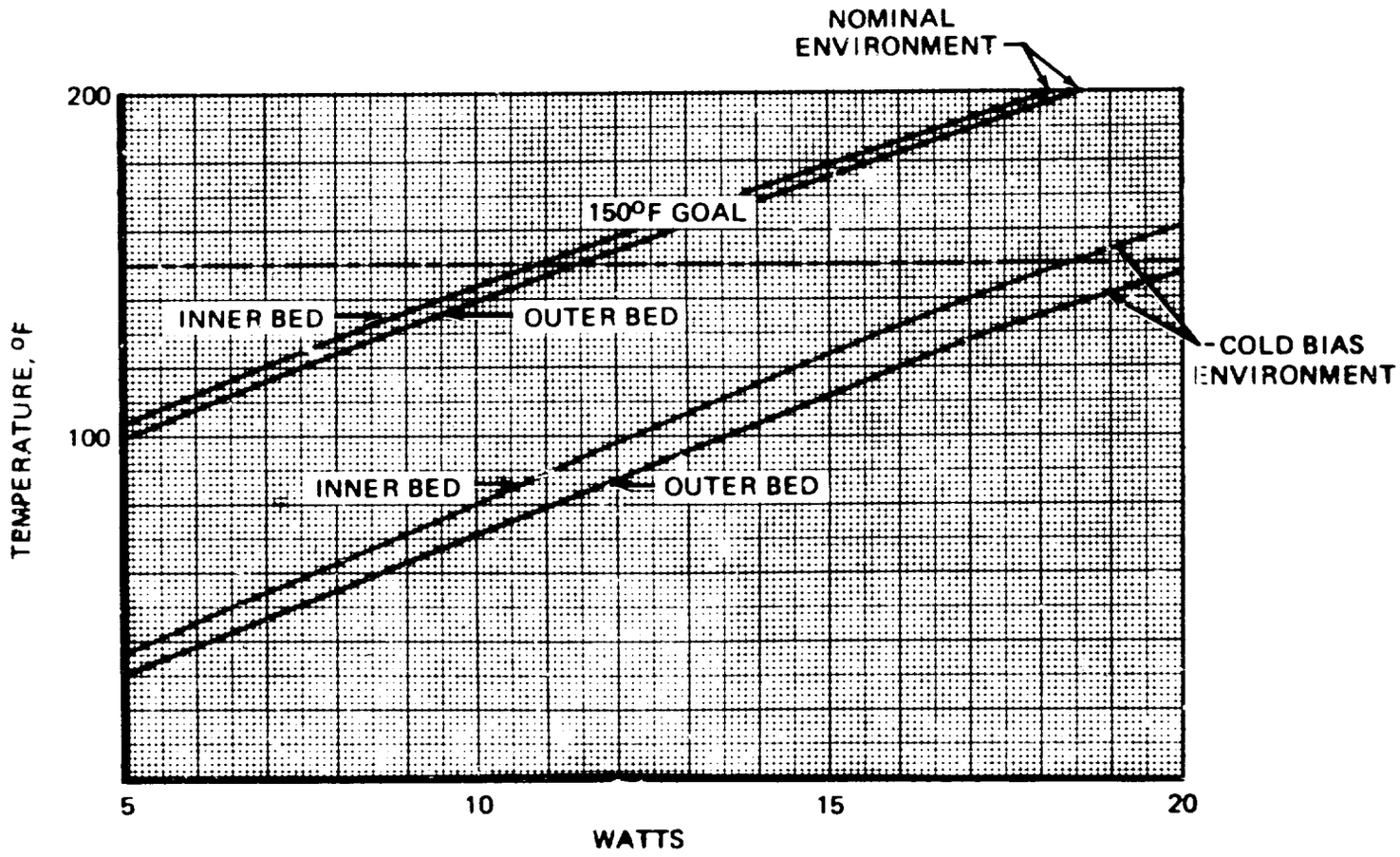

Figure 4-13

4.2.4.4 Re-entry Thermal Considerations

In support of catalyst bed oxidation studies, and in support of basic thermal/structural design studies, the effects of the re-entry profiles presented in Figure 4-14 on catalyst bed and propellant valve temperatures were determined. Two cases were analyzed. One considered stabilized nonfiring conditions prior to re-entry and the other considered re-entry after a firing.

The results of the nonfiring case prior to re-entry are presented in Figure 4-15. No problems are indicated. The results of the firing case prior to re-entry are presented in Figure 4-16. At touchdown, valve seat and O-ring temperatures are 280 and 351°F respectively. These values are higher than the previously calculated values of 254 and 328°F. Thus, the re-entry values were used for design.

4.3 STRUCTURAL ANALYSIS

Structural analyses were conducted using results obtained from the thermal analyses. Both static and dynamic analyses were undertaken. The primary objectives of these studies were to: 1) provide guidance for the final design and 2) verify integrity of the final RCS engine. Definitions used in the structural analysis are shown in Table 4-4.

Results of the steady-state analyses shown in Table 4-5 indicate large margins of safety.

Results for cyclic loading are shown in Table 4-6 which indicate satisfactory capability of the RCS to accommodate the required number of cycles.

Margins on creep rupture and predicted deformations due to creep are presented in Table 4-7 showing satisfactory capability.

Results of a dynamic analysis showing component random vibration levels resulting from an input vibration of 28.2 g rms is shown in Table 4-8.

Margins of safety for three-sigma random dynamic stresses are shown in Table 4-9. The only component of concern was the injector feed tube which had a relatively low (although adequate) margin of safety for lateral random vibration.

Based on the results of the structural analyses, it was concluded that the RCS design was conservatively designed for structural considerations.

4.4 PERFORMANCE ANALYSIS

Detailed analyses were conducted to predict the performance and operating characteristics of the RCS. Performance losses due to nozzle divergence, nozzle drag, heat losses, and boundary layer effects were determined for nominal operation at an ammonia dissociation of 50%. The predicted specific impulse efficiency was 96.27% resulting in a delivered specific impulse of 230.0 lbf-sec/lbm. Predicted performance at off-nominal conditions is presented in Table 4-10.

HOT BIAS REENTRY PROFILES

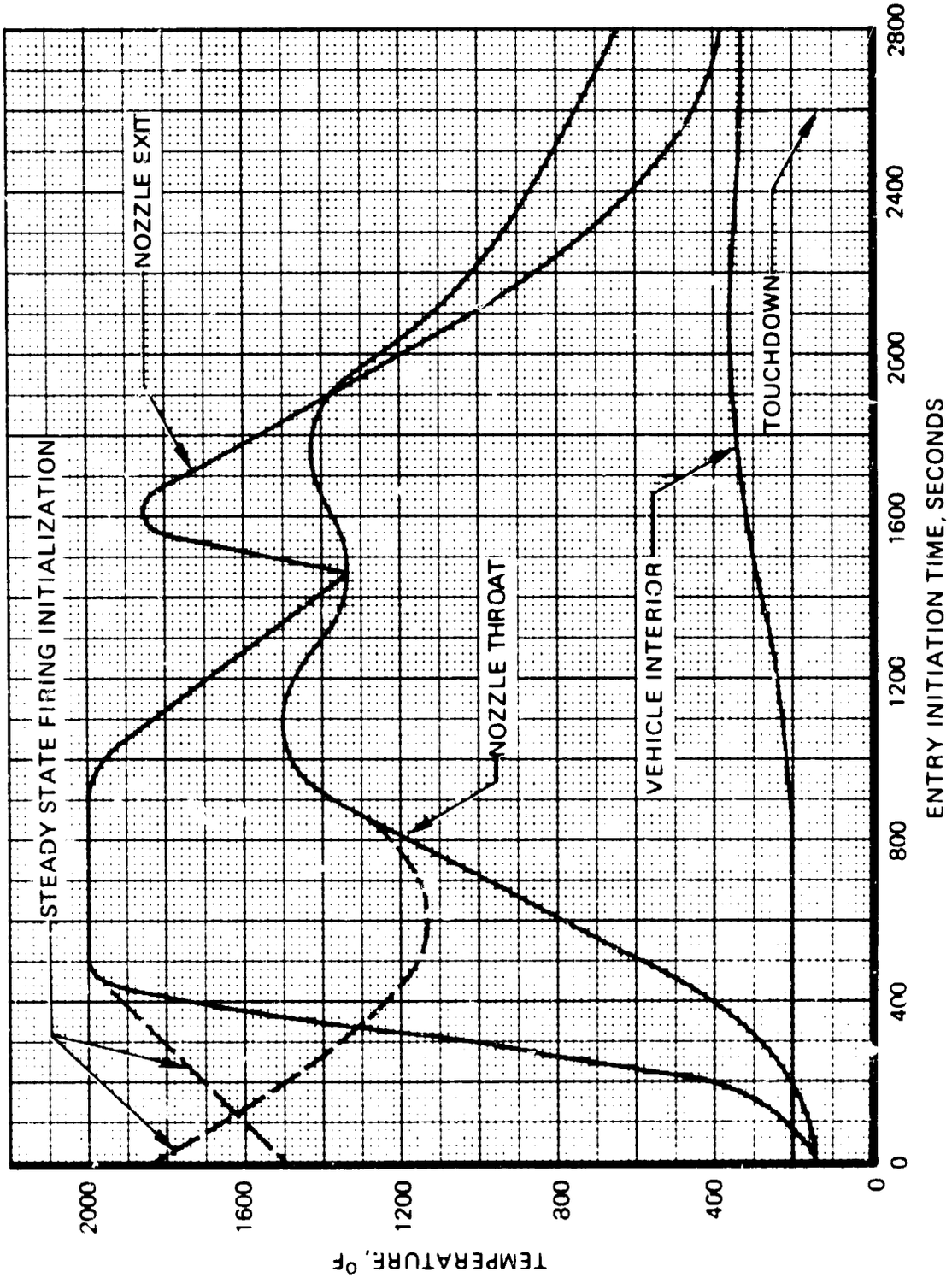

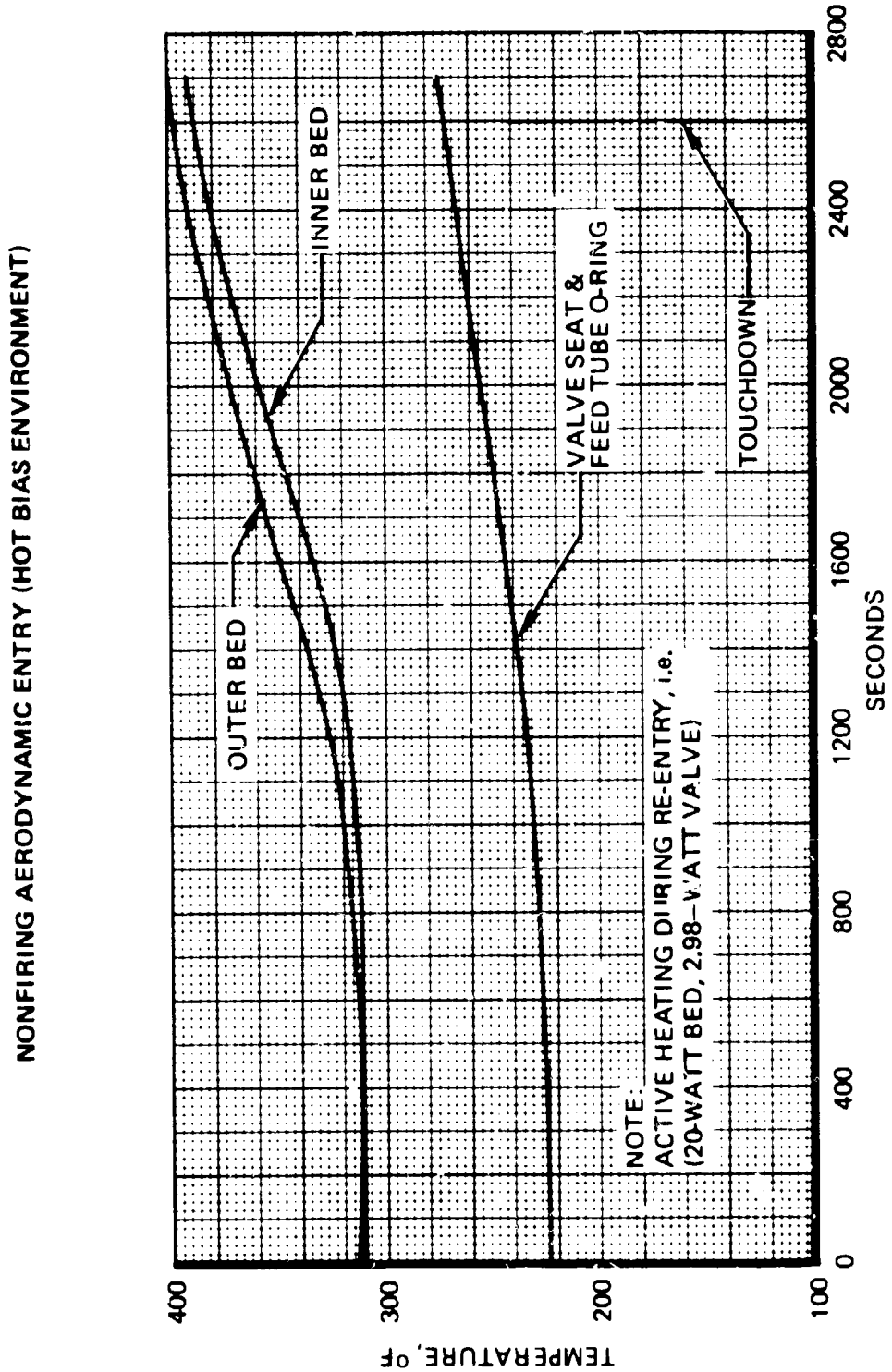
NONFIRING AERODYNAMIC ENTRY (HOT BIAS ENVIRONMENT)
TEMPERATURE, °F
400
300
200
100
0
400
800
1200
1600
2000
2400
2800
SECONDS
OUTER BED
INNER BED
VALVE SEAT &
FEED TUBE O-RING
TOUCHDOWN
NOTE:
ACTIVE HEATING DURING RE-ENTRY, i.e.
(20-WATT BED, 2.98-WATT VALVE)

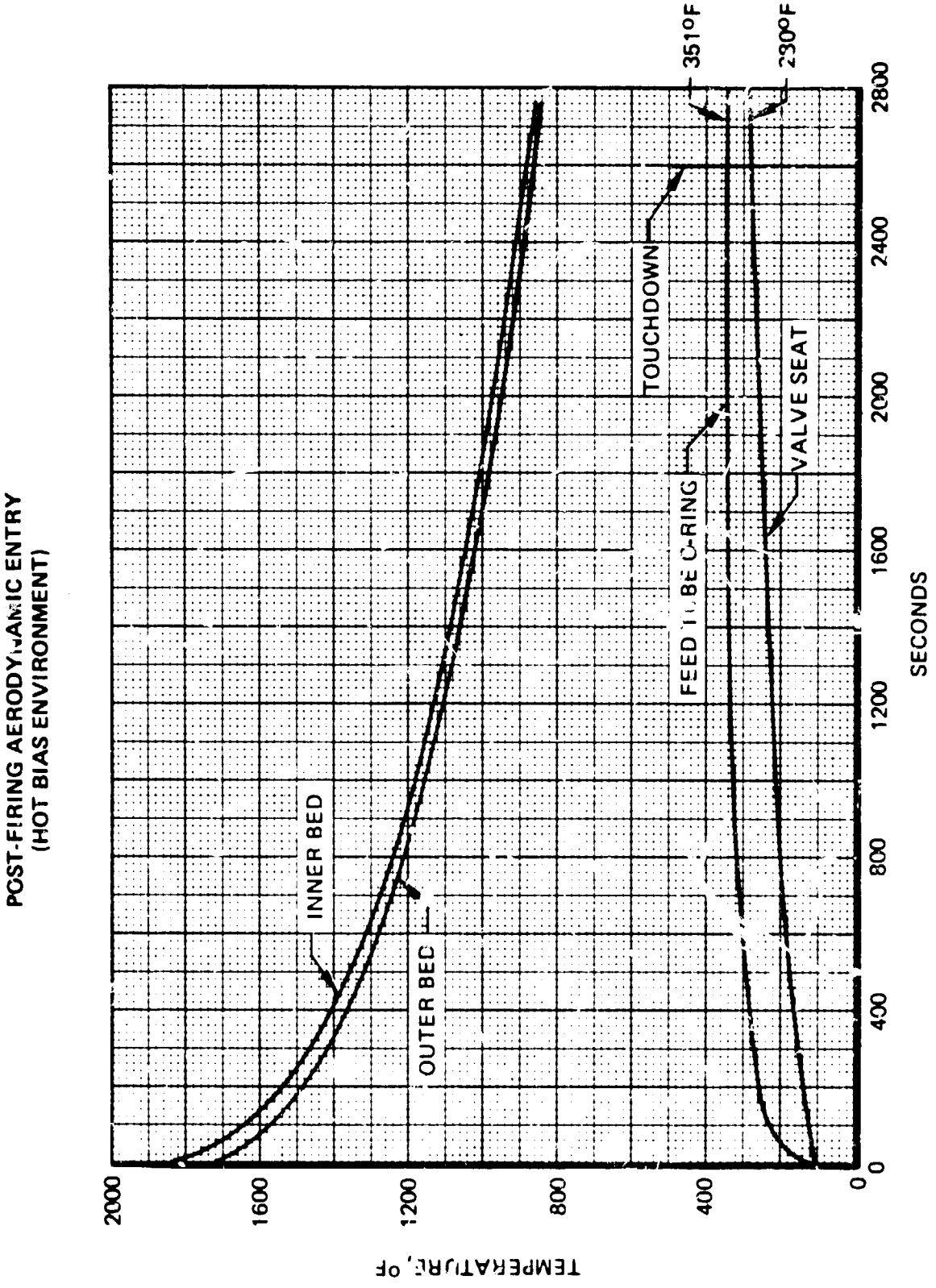

11062-82

Figure 4-16

Table 4-4

DEFINITIONS

MARGIN OF SAFETY AND SAFETY FACTOR

- GENERAL $MS = \left(\frac{S_a}{S_D \times SF} - 1\right)$

- MS ON BURST PRESSURE; SAFETY FACTOR = 2.0

$$MS = \left(\frac{S_{ULT}}{S_p \times SF} - 1\right)$$

- MS ON PROOF PRESSURE; SAFETY FACTOR = 1.5

$$MS = \left(\frac{S_{YP}}{S_p \times SF} - 1\right)$$

- MS ON OPERATING LIMIT LOADS; SF = 1.0

$$MS = \left(\frac{S_{YP}}{S_p + S_T + S_{DYN}} - 1\right)$$

- MS ON ULTIMATE FATIGUE LOADS; SAFETY FACTOR = 1.25

$$MS = \left(\frac{S_{ULT}}{S_p \times SF + S_T} + \frac{S_{af}}{S_{DYN} \times SF} - 1\right)$$

- MS ON CREEP RUPTURE; SAFETY FACTOR = 1.25

$$MS = \left(\frac{S_R}{S_p \times SF} - 1\right)$$

- NOTATION MS – MARGIN OF SAFETY

S_a	ALLOWABLE STRESS
S_D	DESIGN STRESS AT OPERATING CONDITIONS
S_{DYN}	3σ DYNAMIC STRESS
SF	SAFETY FACTOR
S_p	STRESS DUE TO MAXIMUM OPERATING
S_R	CREEP RUPTURE STRESS
S_{ULT}	ULTIMATE STRESS
S_{YP}	YIELD POINT STRESS

V01426

Table 4-5

MARGIN OF SAFETY TABLE ON STATIC STRESSES

	Margin on Proof Pressure SF = 1.5	Margin on Burst Pressure SF = 2.0	Margin on Operating Pressure + Maximum Thermal SF = 1.0	Margin on Creep Rupture Strain SF = 1.25
Thrust chamber	2.61	1.71	0.271	3.20
Nozzle dome	1.47	0.855	0.478	5.32
Forward closure	2.07	1.30	0.293	4.84
Injector body and dome	3.42	2.60	0.102	Large
Feed tube and branches	Large	Large	0.303	Large
Catalyst bed assembly	Large	Large	0.667	Large
Mounting structure	Large	Large	5.341	Large
Internal heat shield	Large	Large	1.770	Large

Margin of safety:

$$MS = \left(\frac{S_{ALLOWABLE}}{S_{DESIGN} \times SF} - 1 \right)$$

Table 4-6

STRENGTH UNDER CYCLIC LOADINGS

FATIGUE STRENGTH DATA
HASTELLOY ALLOY B BAR

Loading	Temperature	Time to Failure (Hours)	Strength (psi)	N, Number of Cycles
Alternating bending stress, 120 cps	1,200	231	66,000	1.0×10^8
	1,200	579	64,000	2.5×10^8
	1,500	231	34,000	1.0×10^8

LIMIT CYCLIC LOADING – SPACE SHUTTLE RCS REA

Condition	N, Number of Cycles	Location/ Temperature (°F)	Stress (ksi)	Syp (ksi)	MS for Safety Factor = 1.0
Cold start to transient assumes 70°F initial 240°F injector	1,700 for 100 missions at 30 seconds per cycle	Injector closure 650	20.2	34.5	0.708
		Injector closure 1,100	25.3	33.5	0.324
		Thrust chamber 1,650	14.7	30.4	1.068
Cold start to steady state 70°F initial 240°F injector	3,400 for 100 missions at 60 seconds per cycle	Injector closure 800	30.1	34.0	0.129
		Injector closure 1,640	28.3	30.7	0.085
		Thrust chamber 1,800	7.9	23.0	1.911

Table 4-7

MARGINS ON CREEP RUPTURE

Location	Average Temperature Steady-State (°F)	Pressure Stress (KSI)	Time* At Temperature (Hours)	Rupture Stress @ Time @ Temperature (KSI)	M.S. On Rupture Stress SF = 1.25	(Reference) 30-Hour Rupture Stress (KSI)
Injector closure	1,620	7.9	9.5	24.0	1.43	18.5
Thrust chamber wall	1,788	5.6	12.5	9.5	0.357	7.6
Thrust chamber weld	1,788	4.6	12.5	9.5	0.650	7.6

*Based on 1,000 seconds/mission, 100 missions, average of 15 burns per mission at 67 seconds per burn

DEFORMATION DUE TO CREEP

	Thrust Chamber Wall – Bi-Axial Stress				
Stress (KSI)	Time (Hours)	Strain (in./in.)	Radial Growth (inches)	Strain At Rupture (in./in.)	M.S. on Strain SF = 1.25
5.6 hoop 2.8 axial	12.5	0.012	0.036	0.063+	3.20+

Table 4-8
SPACE SHUTTLE RCS ENGINE
COMPONENT RANDOM VIBRATION LEVELS

DESCRIPTION	LATERAL OVERALL GRMS (RANDOM X)	LONGTIDUINAL OVERALL GRMS (RANDOM Z)
INPUT	28.2	28.2
VALVE	56.6	59.3
STANDOFF TO THRUST CHAMBER ATTACHMENT	39.1	45.3
FORWARD END OF CATALYST BEDS	38.1	61.0
AFT END OF CATALYST BEDS	52.0	63.0
NOZZLE THROAT	57.4	47.0
NOZZLE EXIT	145.6	48.6

Table 4-9

MARGIN OF SAFETY TABULATION FOR THREE SIGMA RANDOM DYNAMIC STRESSES

Component	Material	Minimum Yield Strength (ksi)	Margin of Safety	
			Lateral Random Vibration	Longitudinal (Thrust Axis) Random Vibration
Standoff to vehicle attachment lugs	TI-6AI-4V	120	0.633	2.093
Standoffs	TI-6AI-4V	120	0.944	7.275
Valve standoffs	TI-6AI-4V	120	1.069	Large
Thrust chamber mounting lugs	Hastelloy B	46	0.523	2.571
Injector feed tube	Hastelloy B	46	0.034	Large
Injector feed tube branches	Hastelloy B	46	1.238	Large
Injector	Hastelloy B	46	Large	Large
Forward end of thrust chamber	Hastelloy B	46	0.79	1.968
Thrust chamber	Hastelloy B	46	8.58	Large
Nozzle Throat	Hastelloy B	46	1.421	Large

Table 4-10
PREDICTED STEADY-STATE PERFORMANCE

Valve Inlet Pressure, psia	300	290			280
Propellant temperature, °F	110	110	75	40	40
Valve pressure drop, psi	83.8	77.9	77.8	78.2	72.6
Injector pressure drop, psi	24.7	24.0	24.0	24.0	23.2
Bed pressure drop, psi	35.1	34.6	34.9	35.2	34.6
Chamber pressure, psia	156.4	153.5	153.3	152.6	149.6
Thrust, lbf	495.5	485.7	484.9	482.4	472.7
Characteristic velocity, ft/sec	4384.	4373.	4350.	4323.	4315.
Thrust coefficient	1.7039	1.7023	1.7013	1.7001	1.6993
Specific impulse, lbf-sec/lbm	232.2	231.4	230.0	228.5	227.9
Flow rate, lbm/sec	2.134	2.059	2.108	2.111	2.074

Early predictions for bed pressure drop indicated a value of 70 psi would be obtained. However, values measured during subscale testing indicated much lower values. Consequently, the analytical model was reviewed and modified to more accurately describe the flow through the catalyst bed. Shown in Figure 4-17 is the improved analytical model used for predicting bed pressure drop, which considers flow from only one injector element. This model was successfully used to correlate test data obtained during subscale testing as well as the Viking engine. Predictions were then made for the RCS engine resulting in a value of 34.9 psi.

The predicted start response characteristics of the engine are presented in Figure 4-18 for various initial engine temperatures. The time required to achieve 90% of the steady-state thrust is less than 700 milliseconds with the bed initially at 150°F.

Predicted pulse-mode specific impulse characteristics are shown in Figure 4-19 for various pulse widths. The results shown are applicable for all duty cycles ranging from 5 to 50%. Performance at lower duty cycles is shown in Figures 4-20 and 4-21. The results show that under equilibrium pulsing conditions, pulse-mode performance approaches the steady-state value. Transient performance, characteristic of monopropellant engines, occurs as a result of energy being expended to heat the catalyst during the initial pulses. The number of pulses required for the catalyst to reach thermal equilibrium (and constant performance) is a function primarily of the pulse width as shown in Figure 4-19.

Predicted impulse bit characteristics of the engine are presented in Figures 4-22 and 4-23. During equilibrium pulsing conditions, a minimum impulse bit of approximately 7 lbf-sec can be delivered with a 15-millisecond pulse width. Substantially smaller impulse bits can be delivered during the initial few pulses starting with the engine at 150°F as shown in Figure 4-22. For example, the impulse bit for a 20-millisecond pulse is less than 5 lbf-sec for the first pulse, increasing to about 6 lbf-sec following 10 pulses.

4.5 DESIGN SAFETY AND RELIABILITY ASSESSMENT

A design safety and reliability analysis was conducted with the details and results of the analysis presented in Appendix A. The results of the reliability prediction, based on a single engine, are as follows:

1 mission	(7 days)	0.999
25 missions	(Refurbishment cycle)	0.975
100 missions	(Life cycle)	0.903

4.6 MAINTENANCE ASSESSMENT

A preliminary analysis was conducted to determine the preflight checkout, maintenance, and post-flight service requirements of the RCS engine. Details of the analysis are presented in Reference 4-1. A summary of the study is presented in the following paragraphs.

The following assumptions were made to establish a baseline for the maintenance analysis:

ANALYTICAL MODEL FOR BED PRESSURE DROP

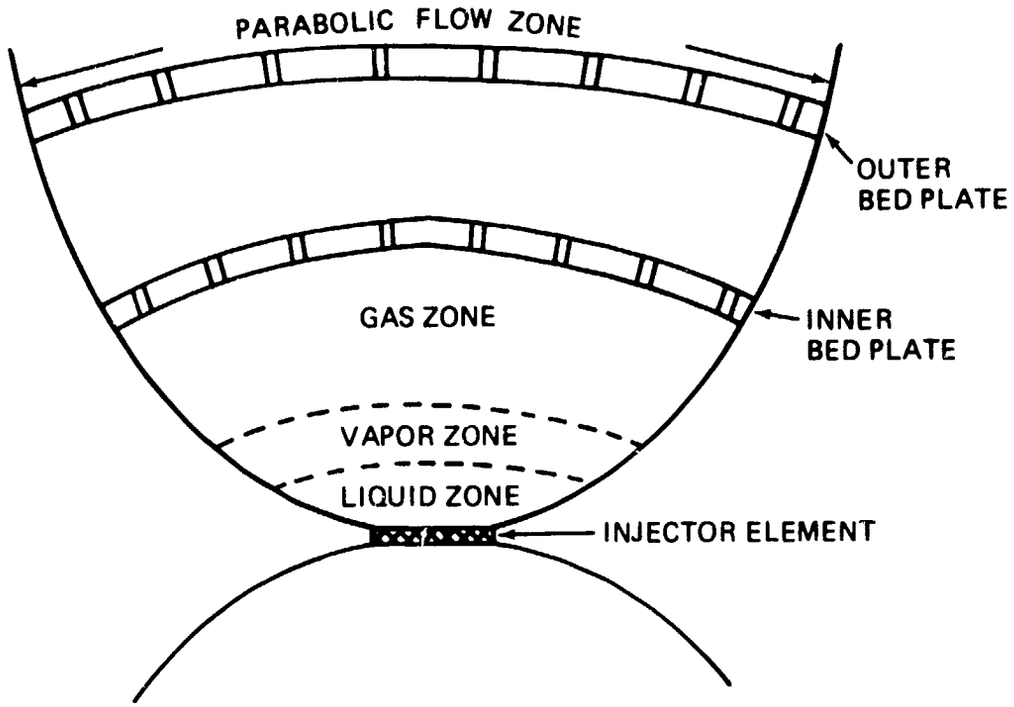

VARIABLES:

- LIQUID ZONE LENGTH
- VAPOR ZONE LENGTH
- GAS ZONE LENGTH
- CATALYST BED POROSITY
- PARABOLIC FLOW ZONE WIDTH

PREDICTED RCS ENGINE START RESPONSE CHARACTERISTICS

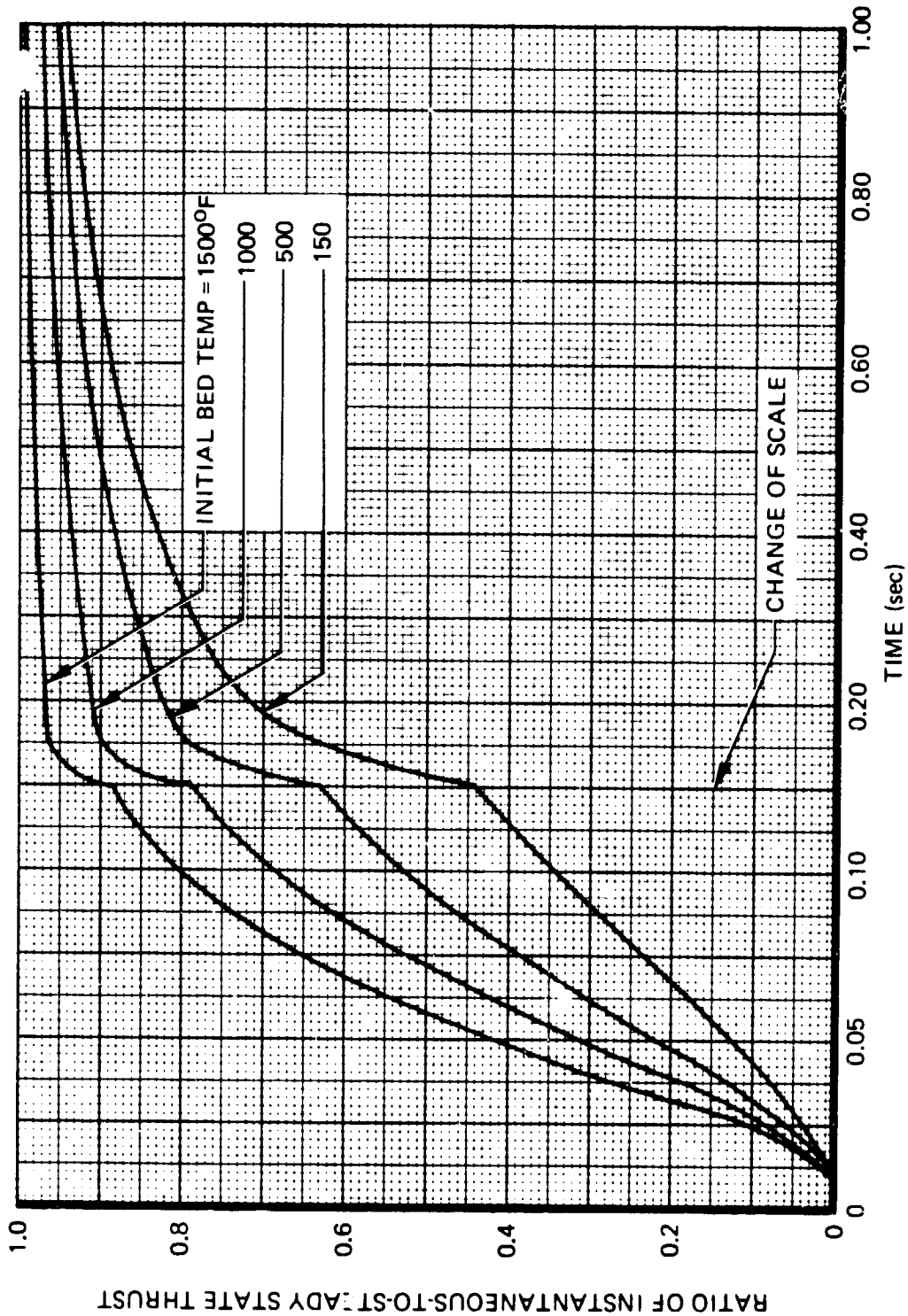

TRANSIENT PULSE MODE SPECIFIC IMPULSE

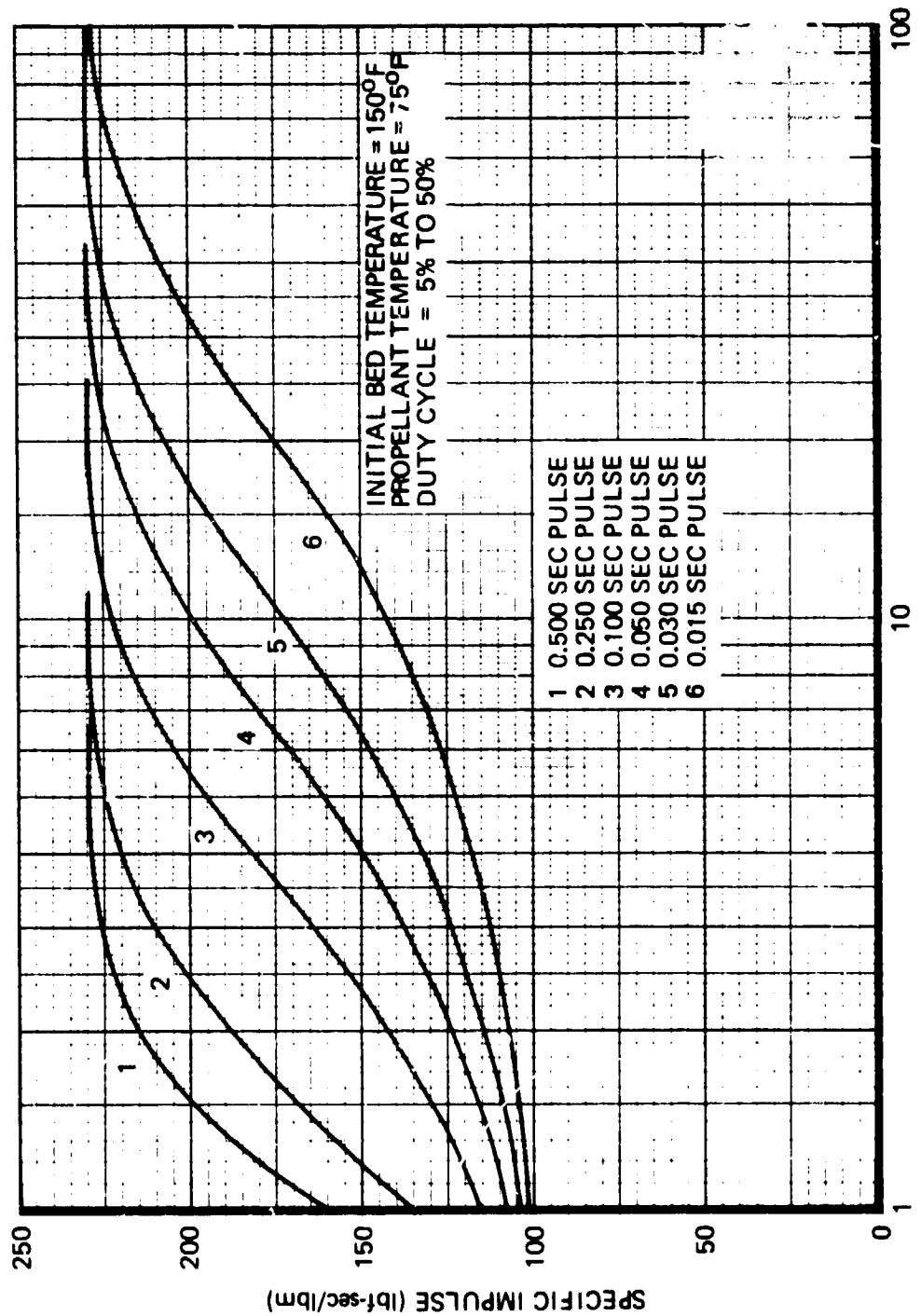

TRANSIENT PULSE MODE SPECIFIC IMPULSE
– 0.1% DUTY CYCLE –

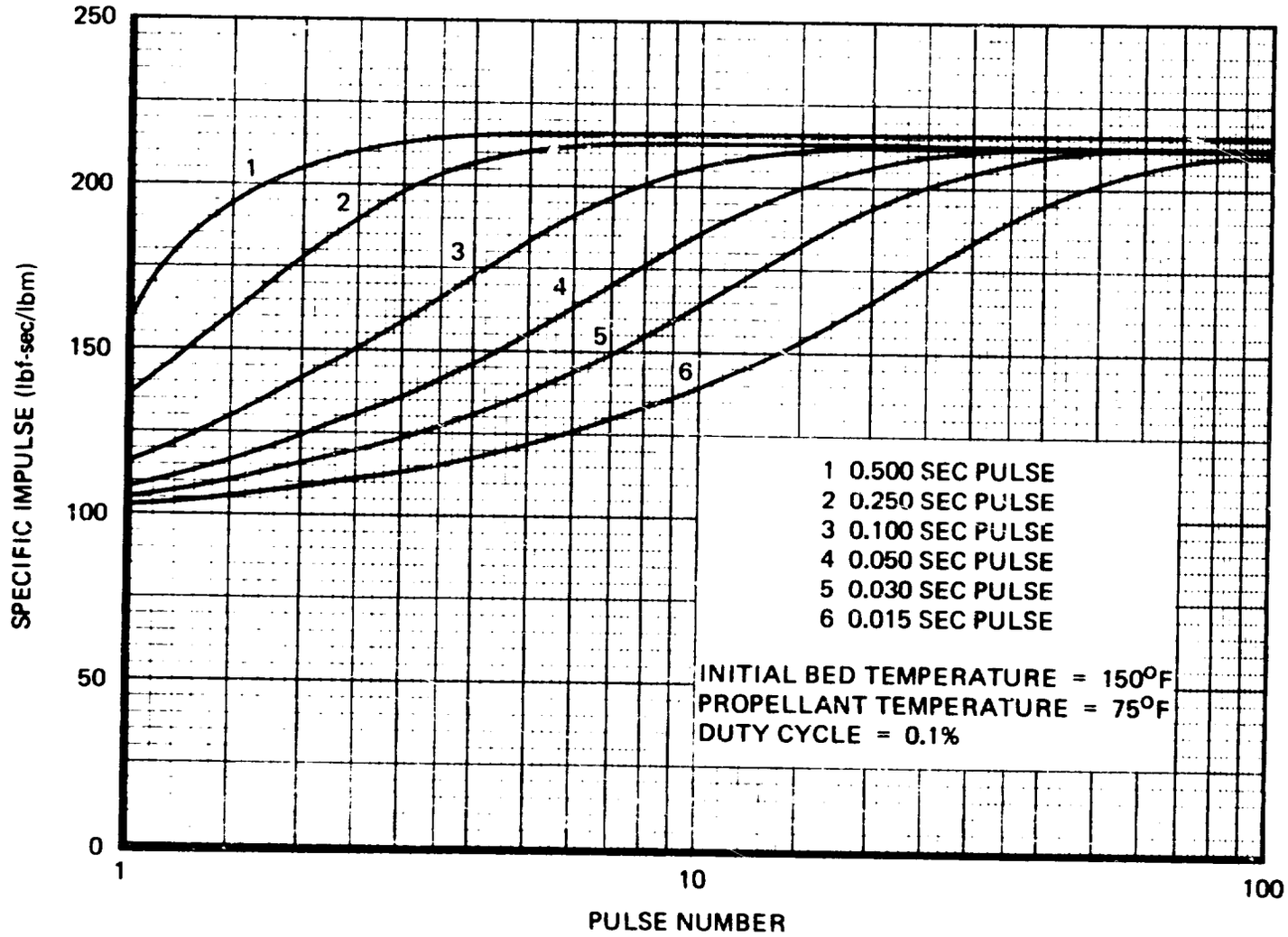

Figure 4-20

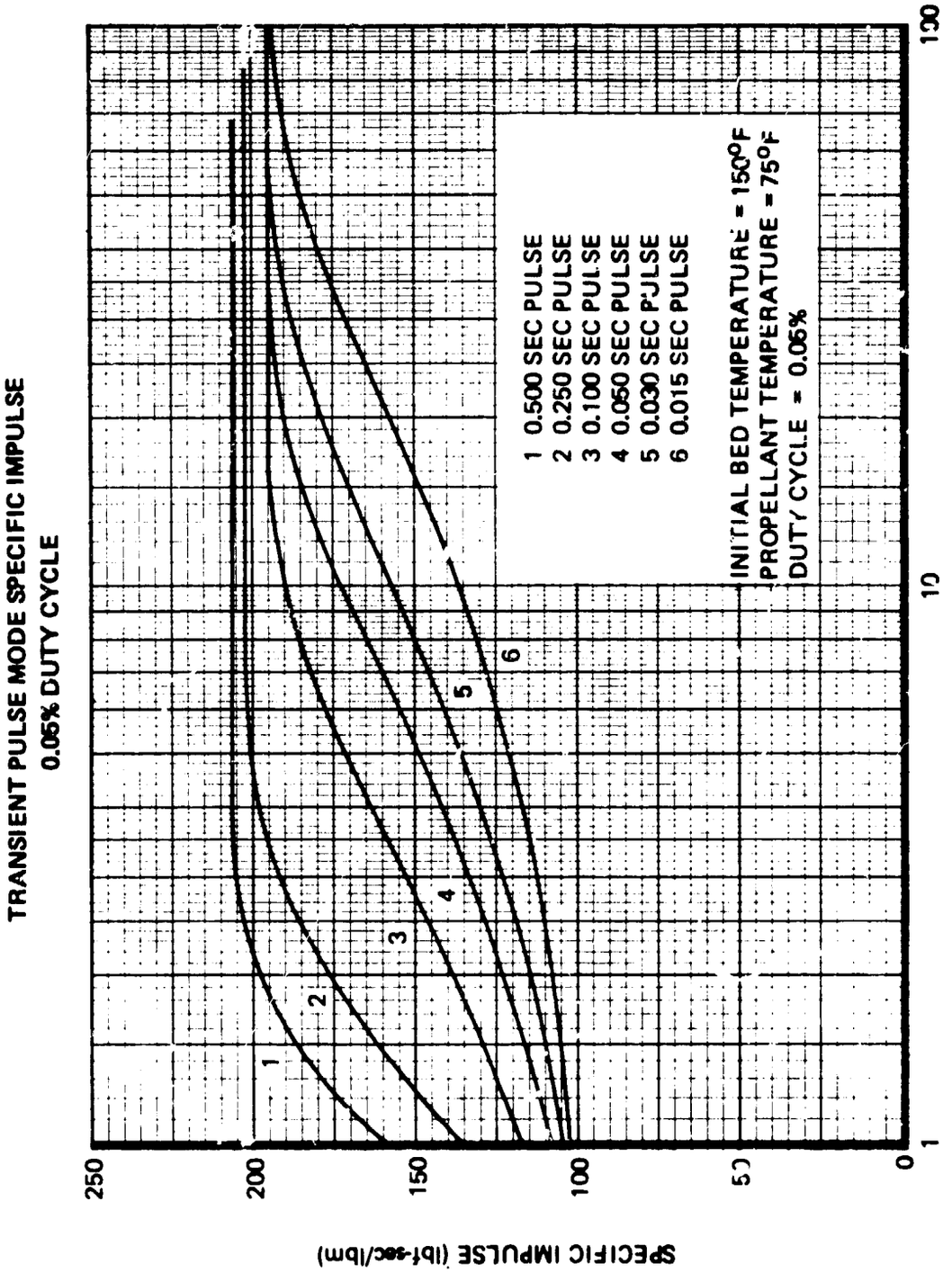
TRANSIENT PULSE MODE SPECIFIC IMPULSE
0.05% DUTY CYCLE
1 0.500 SEC PULSE
2 0.250 SEC PULSE
3 0.100 SEC PULSE
4 0.050 SEC PULSE
5 0.030 SEC PULSE
6 0.015 SEC PULSE
INITIAL BED TEMPERATURE = 150°F
PROPELLANT TEMPERATURE = 75°F
DUTY CYCLE = 0.05%
SPECIFIC IMPULSE (lbf-sec/lbm)
250
200
150
100
50
0
1
10
100
PULSE NUMBER

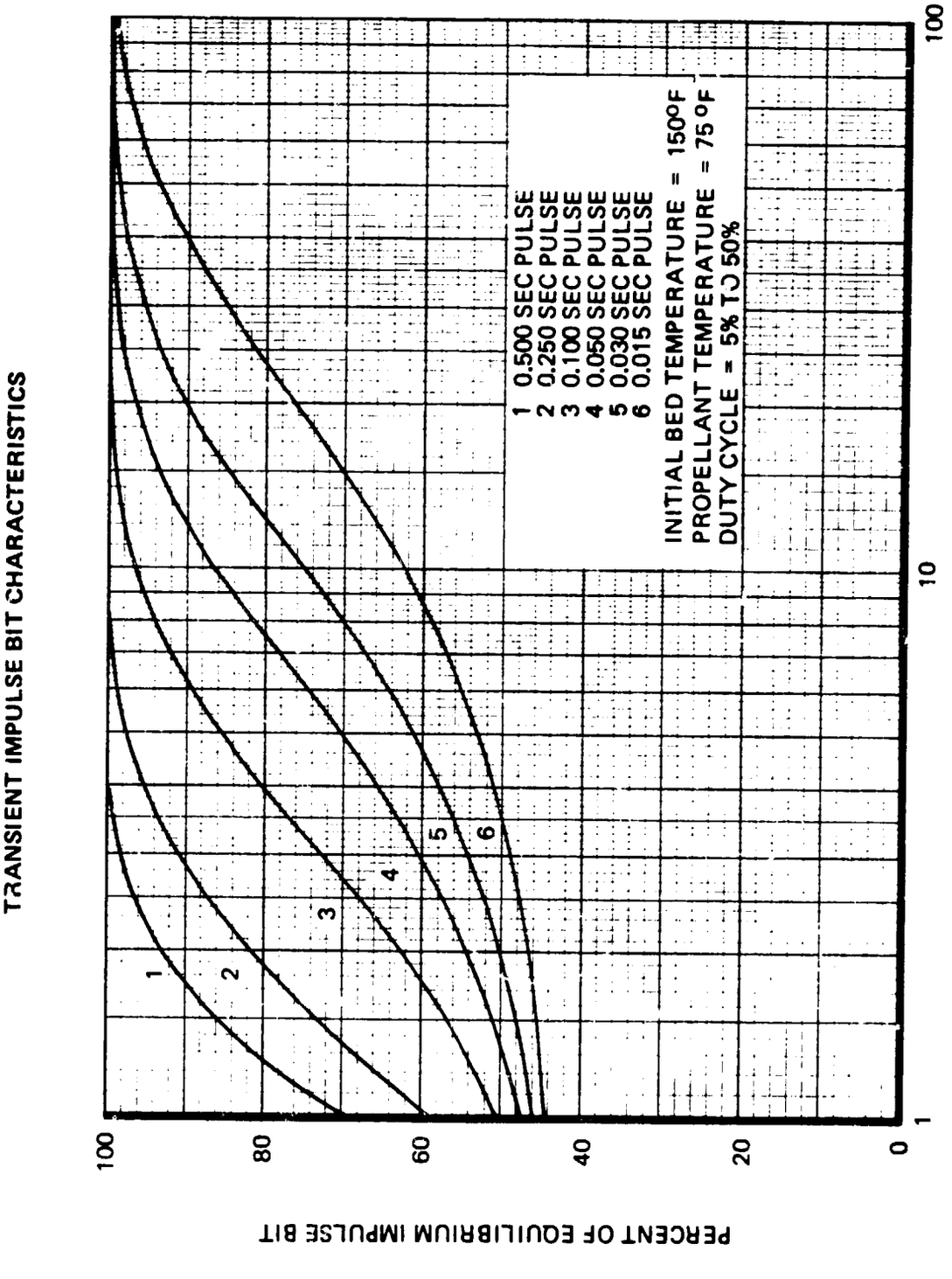
TRANSIENT IMPULSE BIT CHARACTERISTICS
PERCENT OF EQUILIBRIUM IMPULSE BIT
100
80
60
40
20
0
1
10
100
PULSE NUMBER
1 0.500 SEC PULSE
2 0.250 SEC PULSE
3 0.100 SEC PULSE
4 0.050 SEC PULSE
5 0.030 SEC PULSE
6 0.015 SEC PULSE
INITIAL BED TEMPERATURE = 150°F
PROPELLANT TEMPERATURE = 75°F
DUTY CYCLE = 5% TO 50%
1
2
3
4
5
6

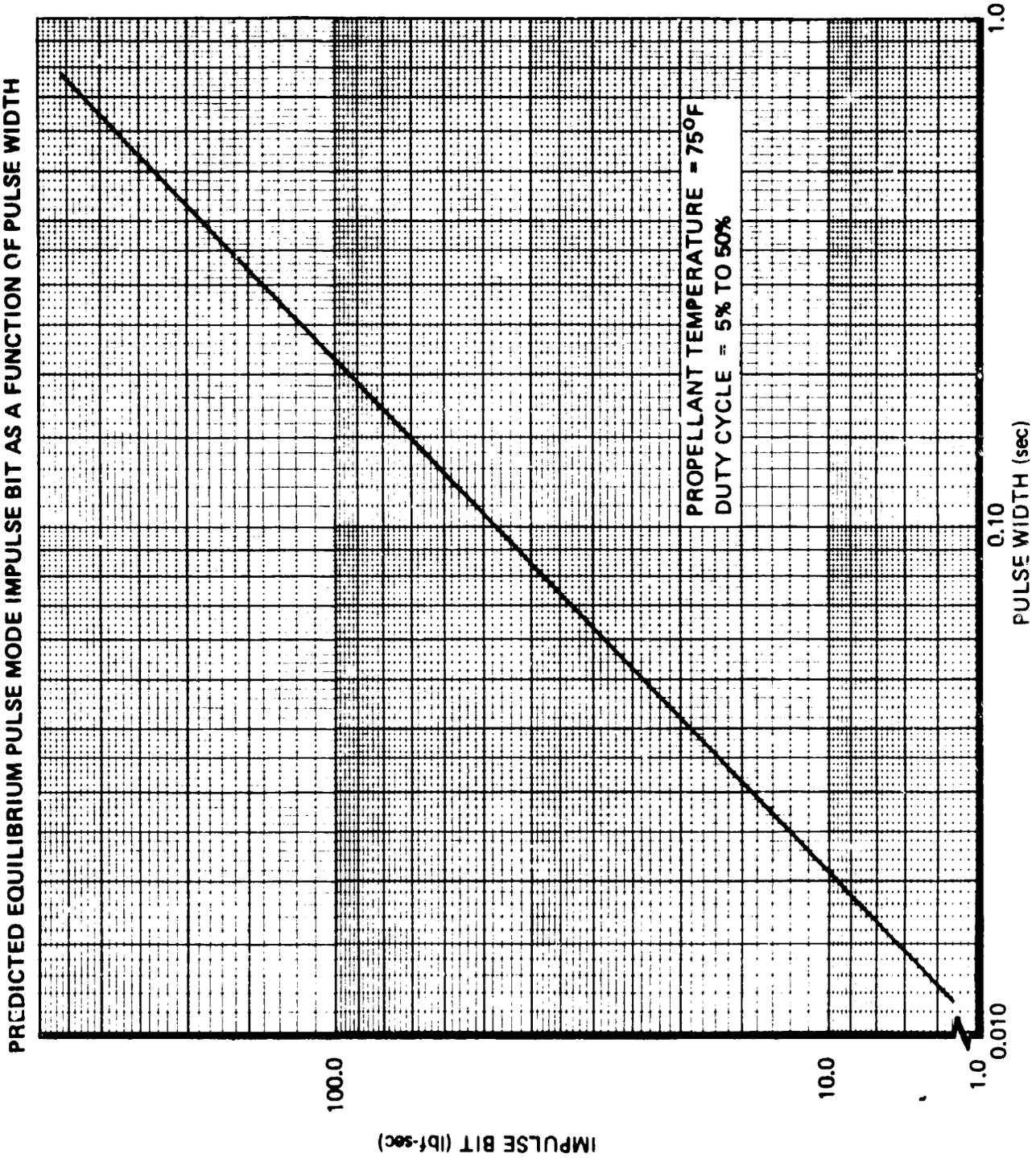
PREDICTED EQUILIBRIUM PULSE MODE IMPULSE BIT AS A FUNCTION OF PULSE WIDTH
PROPELLANT TEMPERATURE = 75°F
DUTY CYCLE = 5% TO 50%
IMPULSE BIT (lbf-sec)
100.0
10.0
1.0
PULSE WIDTH (sec)
1.0
0.10
0.010

a. The RCS engine design is adequate to allow 25 equivalent Space Shuttle orbiter missions without major scheduled maintenance.

b. The Shuttle orbiter vehicle will have on-board recording or telemeter transmitting capability to continuously monitor the chamber pressure on any RCS engine that is firing. This engine chamber pressure data would then be analyzed to verify operational readiness for the next scheduled flight of each RCS engine.

c. The flight crew will have the capability to monitor the following RCS engine parameters on at least a go/no-go basis:

   1. Valve temperature: above 36°F -- below TBS.
   2. Thrust chamber temperature: above 150°F.
   3. Engine chamber pressure (P_{cd}): indication of pressure response subsequent to firing command; average chamber pressure (indicative of thrust); and chamber pressure roughness.

d. Each RCS engine would be readily accessible for inspection, fault isolation, maintenance, repair, and replacement.

e. Post-flight servicing is limited to faulty line replaceable unit (LRU) replacement.

f. RCS engines will return from the flight mission with low-pressure propellant locked up by the RCS engine propellant valve. RCS engines would not be purged prior to landing.

Figure 4-24 presents a schematic of the RCS engine showing the major components.

The RCS engine assembly is attached to the Shuttle orbiter by bolting at the mounting structure interface. The thrust chamber assembly is attached to the mounting structure by three pinned joints (or bolted joints) on titanium standoffs. The propellant valve is also bolted to the mounting structure.

A pressure transducer is "soft" mounted to the mounting structure assembly for monitoring the downstream chamber pressure (P_{cd}). A tap is provided to allow upstream chamber pressure measurement (P_{cu}) during engine acceptance and fault isolation firing sequences. The P_{cu} tap will be capped for flight.

A thrust chamber assembly heater is located at the injector end of the TCA, and a thermocouple is provided on the TCA to monitor TCA temperature. This thermocouple could be used to provide logic signals to control the TCA heater in the event that heater power is limited and the heater cannot be energized continuously. The TCA will be insulated with a preformed insulation blanket.

A thermostatically controlled heater is provided on the propellant valve to prevent propellant valve freezing during cold engine-off sequences. Temperature monitoring of the propellant valve is provided by a thermistor mounted to the valve. A position indicator is also provided on the propellant valve to allow remote monitoring of valve open or valve closed status.

RCS ENGINE SCHEMATIC

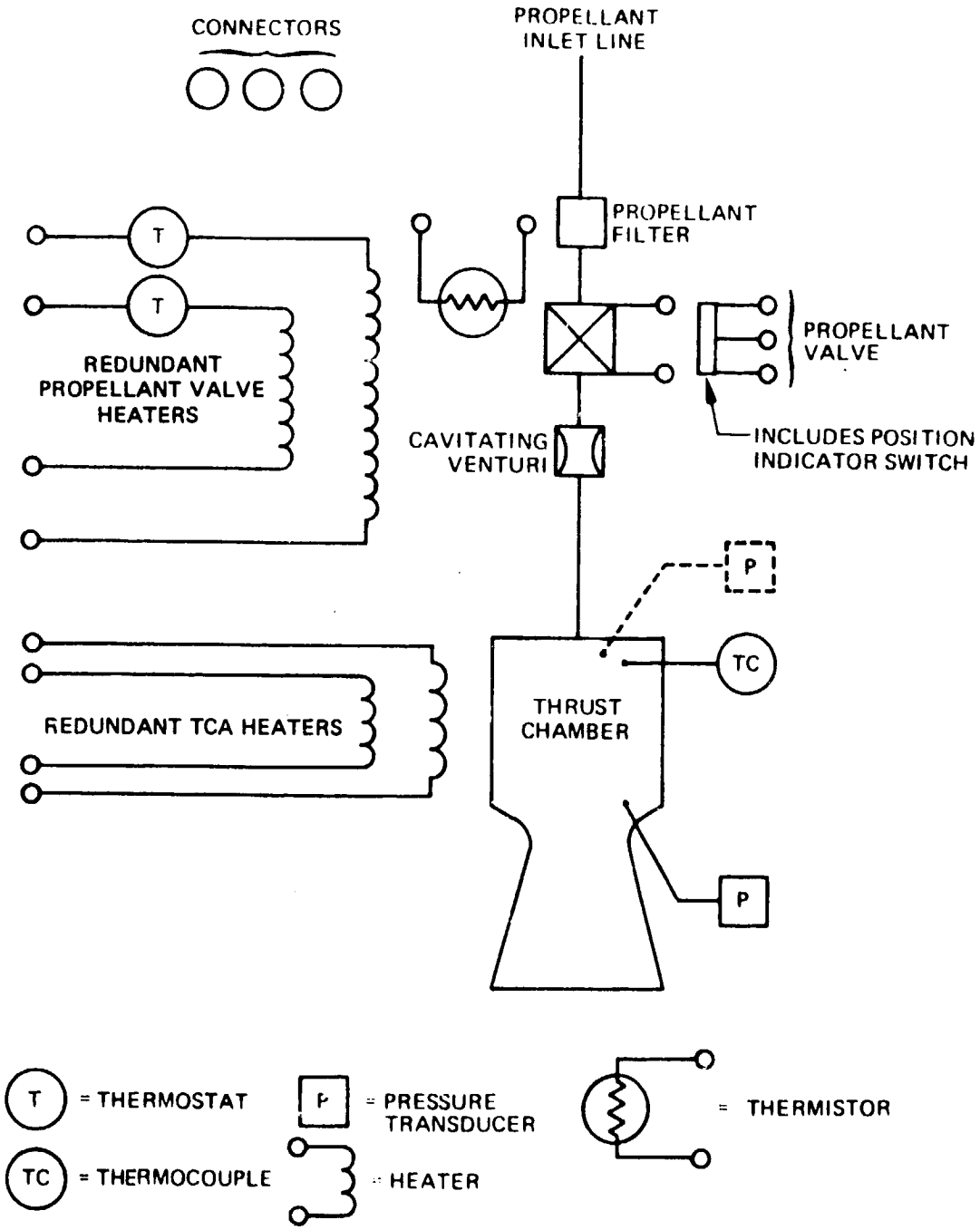

Propellant filtration is provided at the inlet side of the propellant valve to protect the valve seat and the TCA injector from contamination; it should be noted, however, that system filtration is provided upstream of the RCS engine assembly and the aforementioned valve filter represents a final/protection filter for the RCS engine itself.

A cavitating venturi located in the TCA injector inlet stem, immediately below the propellant valve outlet, is provided to decouple the engine propellant flow from small perturbations due to engine chamber pressure roughness or minor changes in the catalyst bed pressure drop due to catalyst packing and thermal considerations.

For the purpose of the analysis, the following terminology was assigned to maintenance tasks:

Level I – (On-Vehicle Maintenance)

- Repair limited to LUR replacement
- Scheduled maintenance performance
- Post-flight/preflight checkout and/or fault isolation testing.

Level II – (On-Site Repair of LRU's)

- On-site repair of LRU (limited to repair by replacement of subassemblies)
- Periodic calibrations or adjustments

Level III – (Off-Site Repair of LRU's) by Supplier

- Major repair of LRU's or subassemblies
- Overhaul
- Major retrofits
- Acceptance verification tests

The most rapid turnaround of the Shuttle orbiter would be accomplished by limiting all vehicle maintenance to Level I activities; this approach is consistent with the current plan for engine pod turnaround within 40 hours.

A flow diagram of the maintenance plan is shown in Figure 4-25. The Space Shuttle flight and turnaround activities are shown in five phases as follows:

Flight mission	–	Phase I
Shuttle lands	–	Phase II
Post-flight checkout	–	Phase III
Post-flight service	–	Phase IV
Preflight checkout	–	Phase V

A brief discussion of each phase, from a maintainability standpoint, is presented below.

RCS SUBSYSTEM MAINTENANCE PLAN FLOW DIAGRAM

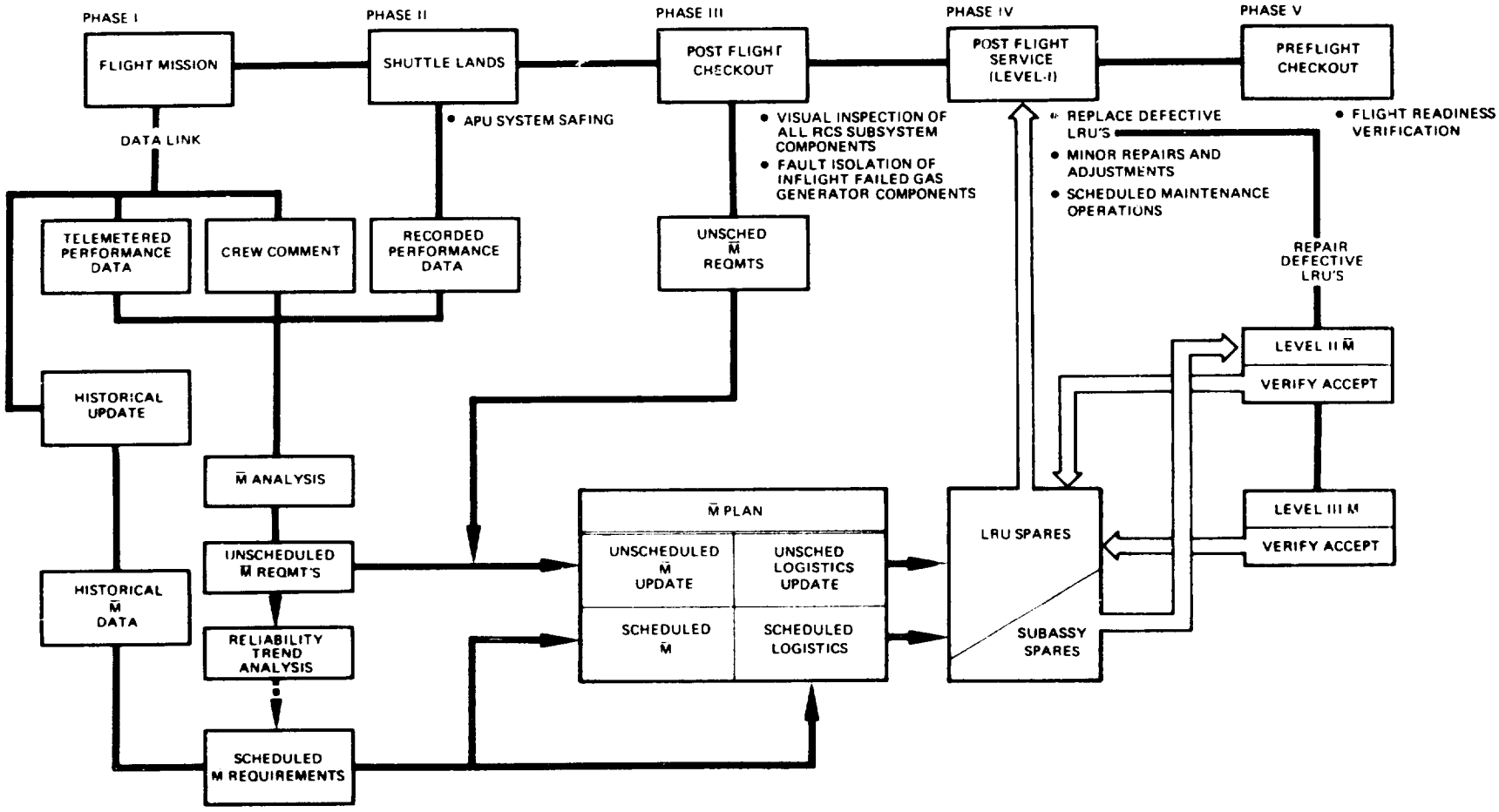

NOTE M INDICATES "MAINTENANCE"

Figure 4-25

Phase I – Flight Mission – The performance of the hydrazine monopropellant RCS engine can be characterized by analysis of the TCA chamber pressure (P_{cd}) data recordings. In particular, catalyst bed degradation can be detected by analysis of one or more of the following parameters:

- Average chamber pressure (thrust)
- Chamber pressure roughness
- Chamber pressure spiking
- Ignition delay (valve command open to 90% P_{cd})
- Tailoff time (valve command shut to 10% P_{cd})

This parameter (P_{cd}) should be continuously recorded during all engine firings. This data could be recorded and stored on board the Shuttle orbiter for analysis subsequent to Phase II (landing) or telemetered to the landing site for analysis to determine the acceptability of RCS engine performance. Analysis of this data will highlight unscheduled maintenance requirements during the turnaround period.

Crew comments on the overall performance of the RCS engines would also be used as inputs for analysis to determine unscheduled maintenance requirements during turnaround.

The data link with the Shuttle orbiter would also be used to provide historical data updating the scheduled maintenance requirements relative to the 25 equivalent mission life limit (minimum) for the RCS engine components.

The Phase I data link will allow rapid planning updates to the maintenance plan to ensure LRU availability and to highlight manpower requirements during turnaround.

Phase II – Shuttle Lands – There will be no RCS engine maintenance activities associated with the landing of the Shuttle, with the possible exception of the retrieval of recorded engine performance data and the analysis of same.

There will undoubtedly be safing operations associated with the RCS propellant system, and it is RRC's understanding that the RCS engine pods may be removed from the Shuttle orbiter; however, based on studies to date, there is no specific scheduled maintenance task required for the RCS engine assemblies during Phase II.

Phase III – Post-Flight Checkout – During Phase III, a visual inspection of each RCS engine would be conducted as part of the verification for reuse process. Any visual anomalies noted would trigger an unscheduled maintenance action item for Phase IV servicing.

Fault isolation testing would be accomplished on any RCS engine that has been identified as marginal or faulty during Phase I or II.

At the conclusion of the Phase III checkout, all faulty LRU's will have been verified and identified, including those components that have accumulated 25 equivalent missions and are therefore due for replacement.

Phase IV – Post-Flight Service (Level I) – All faulty or life-limited RCS engines or LRU engine components will be removed; new or refurbished spare components will be installed. Those RCS engines or engine components which have been removed will be properly identified and routed to Level II or Level III repair facilities for repair, rework, verification acceptance testing, and eventual return to spares inventory.

Phase V – Preflight Checkout – Subsequent to the conclusion of Phase IV, each RCS engine assembly is assumed flight ready. The Phase V task is to verify flight readiness which will include the following tasks:

- Final visual inspection to each TCA
- Electrical checks to ensure that power and control signals as supplied at the RCS engine interface are proper and within specification limits
- Crew indication of proper valve temperature, proper TCA temperature, and proper valve position indication.

5.0 TASK III – HARDWARE FABRICATION, TEST, AND EVALUATION

5.1 ENGINE FABRICATION AND ASSEMBLY

Following completion of the Task II design analyses, and upon approval of the detailed design, fabrication of the engine was initiated.

Photographs of the engine components in various stages of fabrication and assembly are shown in Figures 5-1 through 5-5. The injector assembly, shown in Figure 5-1, incorporated 24 injection elements with each pair of longitudinal elements connected with a common manifold. The injector was fabricated from Hastelloy B. The Rigimesh elements were fabricated from Haynes 25.

The catalyst bedplate assembly, shown in Figure 5-2, consisted of inner and outer bedplates, end closures, and the injector subassembly. Slots were EDM machined in the bedplates to provide for passage of the decomposition gases while simultaneously retaining the catalyst. End closures were assembled at both upstream and downstream ends of the catalyst bed and welded at the injector. The outer edges of the end closures were inserted into bedplate slots and were free to expand radially outward. A separator similar to the end closures was inserted at the midpoint of the injector, thereby dividing the assembly into 12 separate bed assemblies with 2 injection elements in each bed. The inner bedplates were welded to the injector while the outer bedplate assembly was held in place by grooves milled into the injector body.

A photograph of the catalyst bed assembly packed with catalyst is shown in Figure 5-3. The inner bed catalyst was Shell 405 (25–30 mesh) and the outer bed catalyst was LCH-202 (14–18 mesh).

A photograph of the outer chamber and nozzle assembly is shown in Figure 5-4. An internal liner was used, as shown, to reduce thermal heat fluxes during start transients. Also shown in the photograph are holes for inserting thermocouples into the chamber at various angular and axial locations for monitoring gas temperature. A total of 26 thermocouple ports was provided in the thrust chamber.

Shown in Figure 5-5 is the assembled engine on the thrust stand. Insulation was installed on the chamber to reduce heat loss. The engine, which had a nozzle with a ratio of 30:1, was operated overexpanded during seal level testing.

The propellant valve was fabricated by E-Systems, Inc. The valve was a modified throttling valve (developed for the Viking Lander engine) and thus was not fully optimized for minimum opening and closing response. The valve incorporated a cavitating venturi in the outlet port to control propellant flow rate. The valve employed a torque motor geared through a ball screw for displacing the pintle. Operating characteristics of the valve are presented in Table 5-1.

INJECTOR BODY SUBASSEMBLY

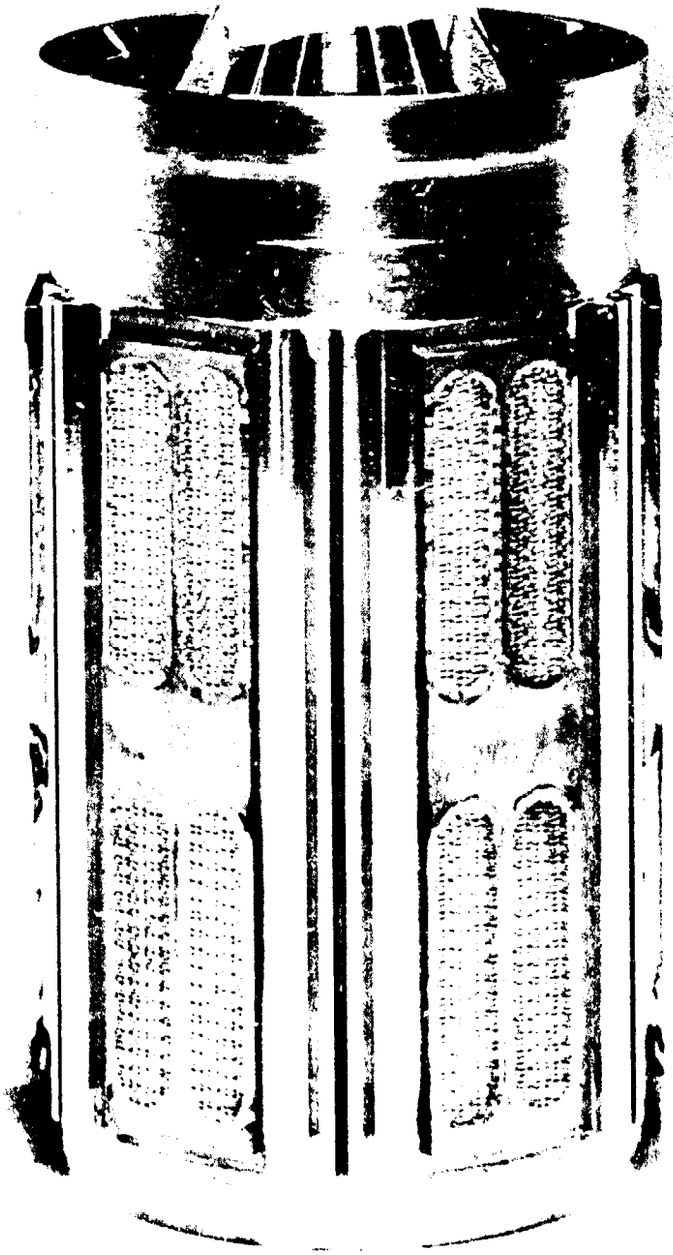

11070-21

Figure 5-1

INJECTOR/CATALYST BED ASSEMBLY

11070-31

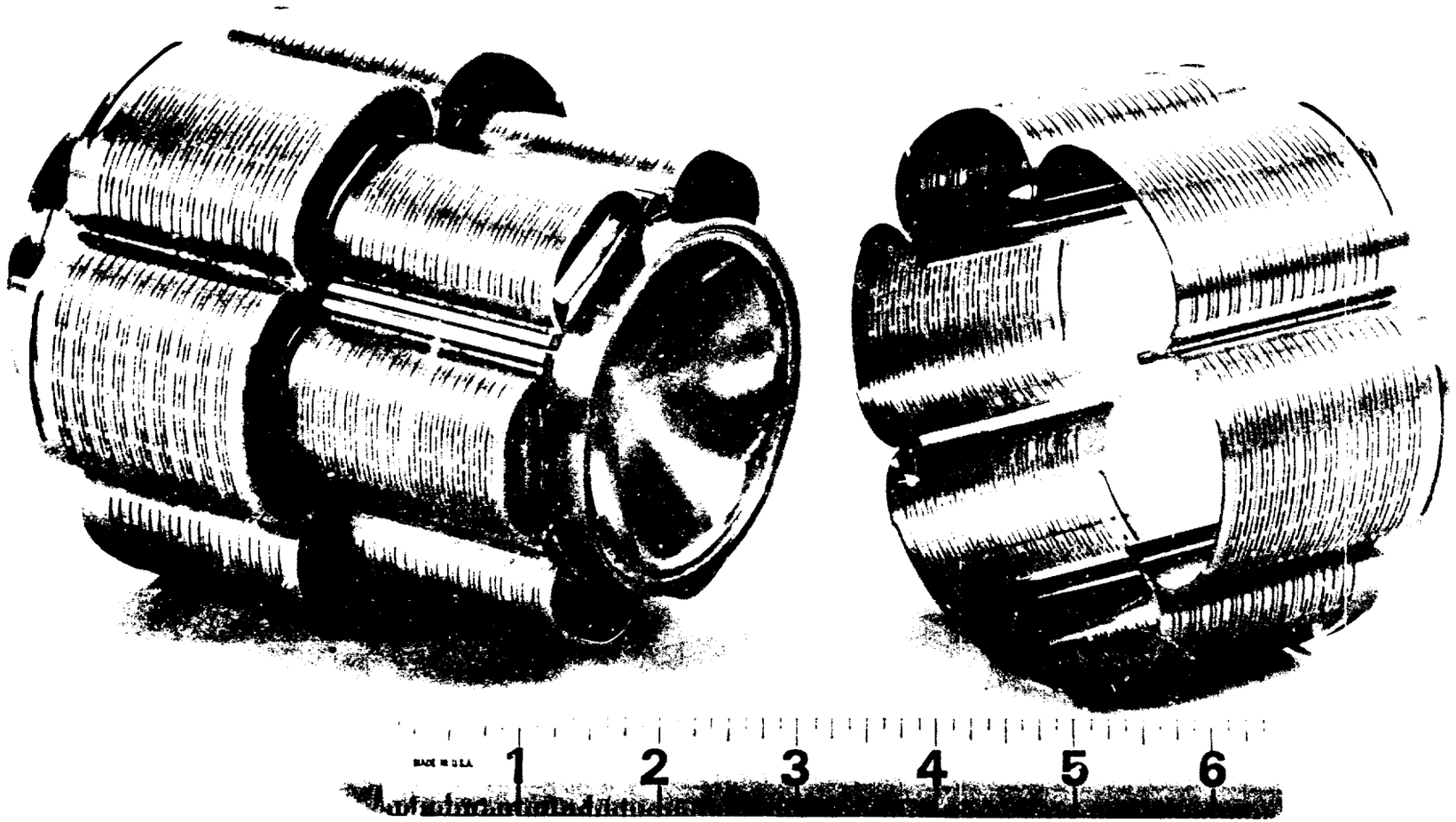

Figure 5-2

INJECTOR/CATALYST BED ASSEMBLY

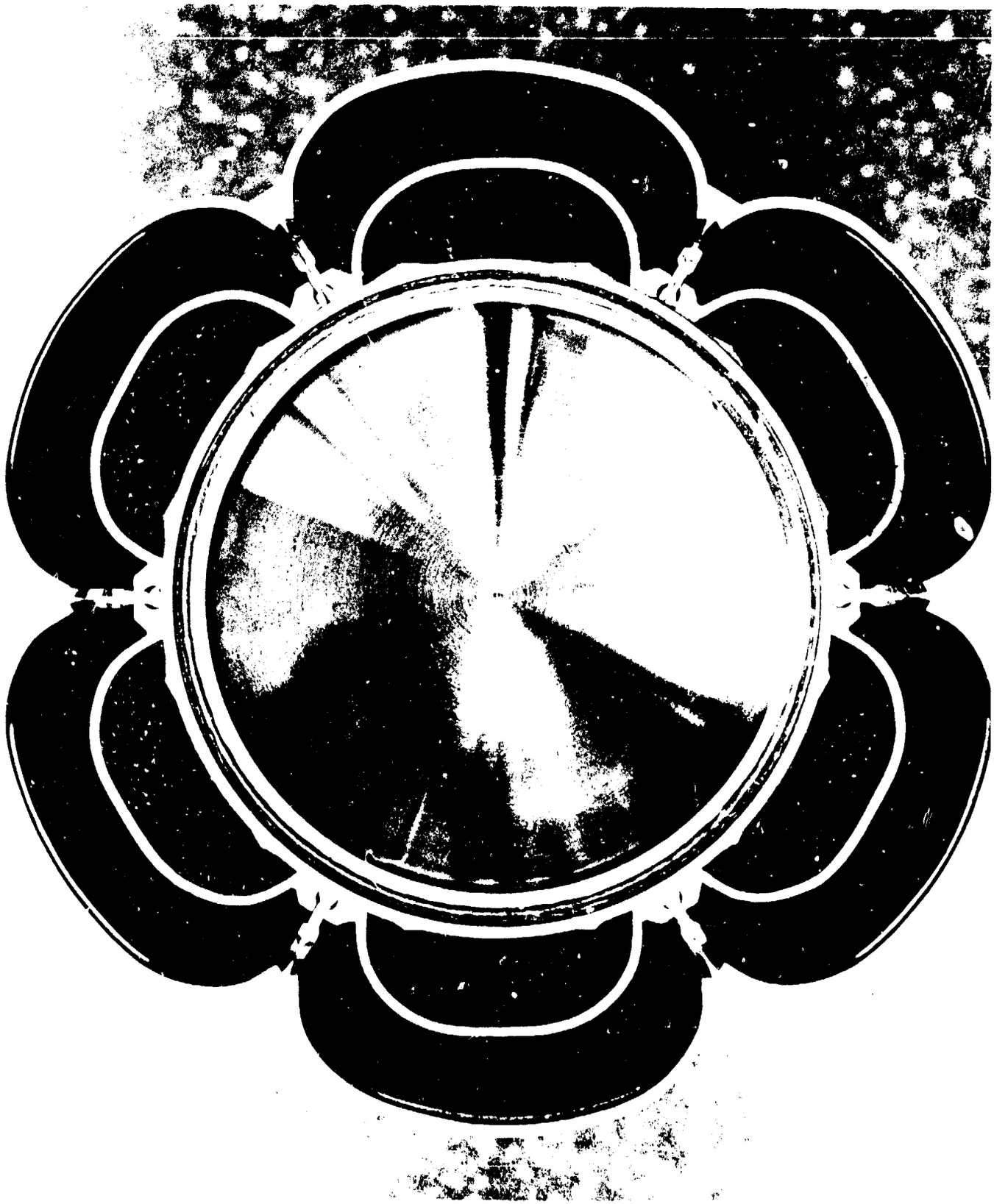

11070-19

Figure 5-3

CHAMBER/NOZZLE SUBASSEMBLY

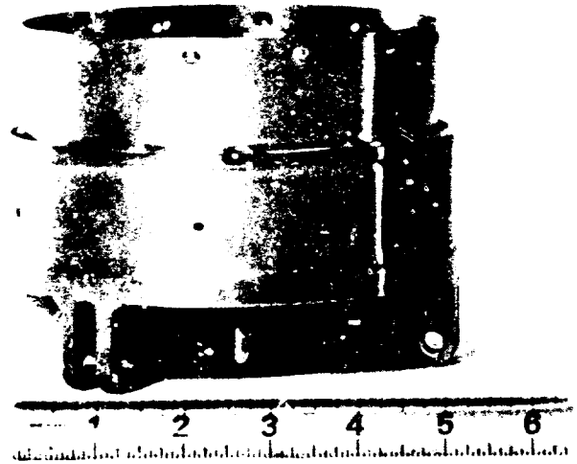

11070-32

Figure 5-4

RCS MOUNTED ON THRUST STAND

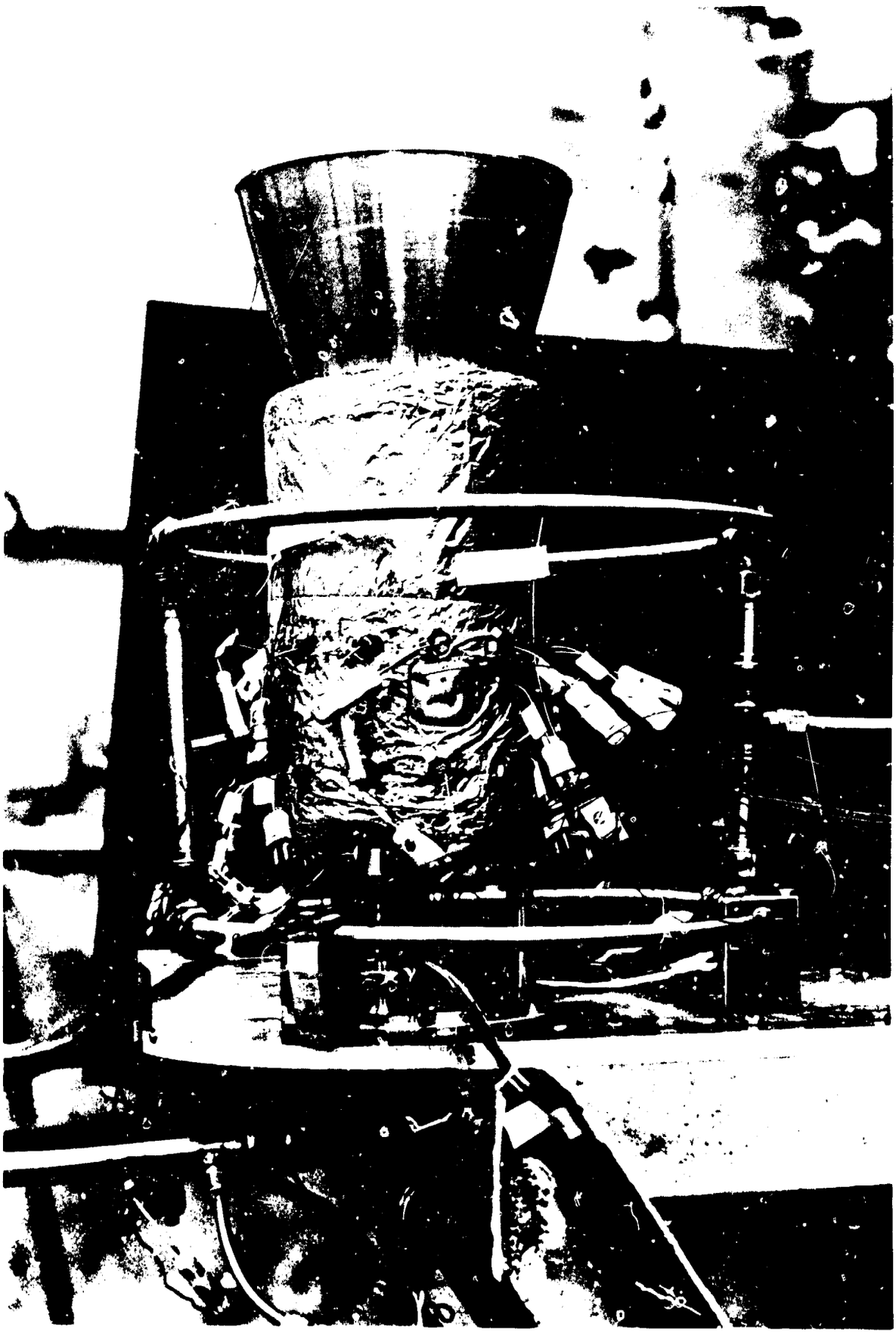

11070-30

Figure 5-5

Table 5-1
SPACE SHUTTLE MONOPROPELLANT
490-lbf ENGINE THRUST
CHAMBER VALVE

Pull-in voltage	28 volts
Drop-out voltage	1? volts
Opening response*	22 msec
Closing response*	34 msec
Flow rate	2.108 lbm/sec at 310 psia
Leakage	<10 scc/hr

*Transient times were determined at operating pressure with a linear voltage differential transducer monitoring ball gear location.

The final assembled weight of the engine was 19.0 lbm excluding instrumentation. Total catalyst weight was 1.16 lbm.

5.2 ENGINE TEST PROGRAM

5.2.1 Test Plan

Following assembly of the engine, a test program was initiated consisting of a series of sea level and simulated altitude firings. The planned test sequence, shown in Figure 5-6, consisted of an acceptance test firing, performance mapping, mission firings, and vibration of the engine.

The acceptance test firing consisted of a 10-second steady-state sea level firing, followed by a 30 minute downtime, and a final series of ten pulses at 250 msec ON/250 msec OFF.

The performance mapping test matrix is shown in Table 5-2. Thrust was measured only during the performance mapping test firings.

The mission duty cycle consisted of 490 seconds total on-time, 1,006 hot pulses/starts and 4 ambient temperature (150°F) starts.

5.2.2 Test Facilities

The sea level test firings were conducted in the RRC high energy test cell. Altitude firings were conducted in the Boeing Tulalip altitude test facility. A description of both test facilities is presented in Appendix 7.2.

5.2.3 Instrumentation and Data Acquisition

The engine was well instrumented with thermocouples to measure gas temperature at various locations within the chamber. A total of 26 immersion thermocouple ports was provided in the chamber. A total of 30 external thermocouples was also provided to measure outer wall temperatures on the thrust chamber.

Instrumentation for the sea level and altitude firings is presented in Table 5-3 Thrust was not measured during the sea level firings. Location of the catalyst bed exit temperatures is shown in Figure 5-7. Because of recorder limitations only 18 of the thermocouples were monitored during the firings – 6 uniformly spaced at the longitudinal mid-point of the bed and 12 at the downstream end of the bed. The thermocouples were centrally located in the annular space between the outer bedplate and thrust chamber wall. All temperature measurements were taken with chromel-alumel, sheathed, immersion-type thermocouples with the exception of the external wall temperatures, which were taken with bare-wire thermocouples.

SPACE SHUTTLE ENGINE TEST FLOW PLAN

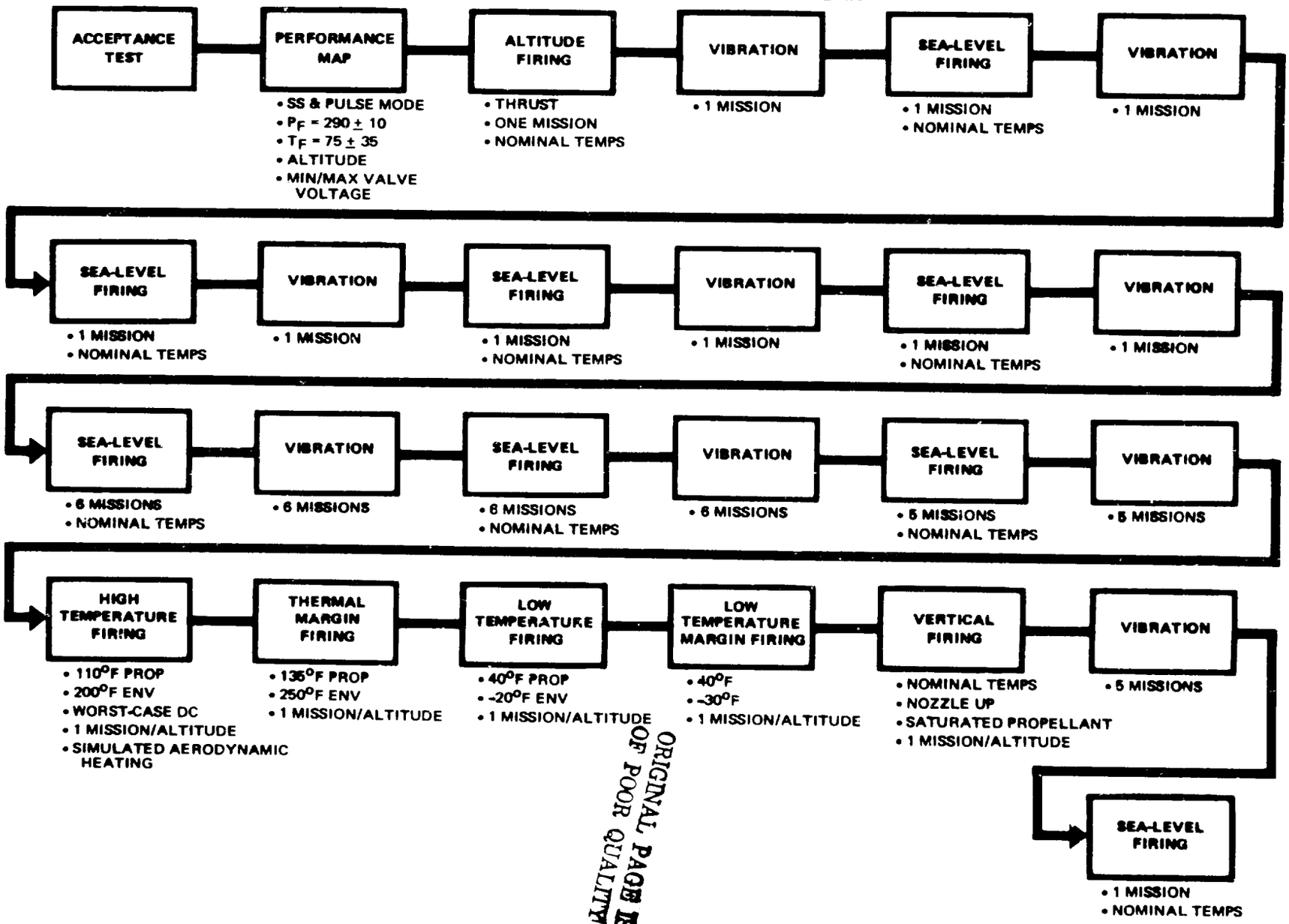

Figure 5-6

Table 5-2

PERFORMANCE MAPPING DUTY CYCLE

Sequence	No. of Firings	On Time (secs)	Off Time (secs)	% Duty Cycle	Accumulated On Time (secs)	Accumulated Pulses/Starts	Accumulated Time/Seq (secs)	Information Retrieval	Test Condition
A-1	1	100	600	100	100	1	700	• Steady-state C_F	Nominal test conditions
-2	1	100	600	100	200	2	1,400		
-3	1	100	600	100	300	3	2,100	• Steady-state C_F	Max. test cond.
-4	1	100	600	100	400	4	2,800	• Steady-state C_F	Min. test cond.
			Cool to 150°F				5 hrs		
B-1	25	0.100	9.90	1.0	402.5	29	250	• Full transient to equilibrium	Nominal test conditions
			Cool to 800°F				~600		
-2	25	0.100	99.90	0.10	405.0	54	3,350	• Partial transient to equilibrium	
			Cool to 800°F				~600		
-3	15	0.100	999.90	0.01	406.5	69	18,950		
-4	25	0.100	0.90	10	409.0	94	18,975		
			Cool to 150°F				5 hrs		
C-1	50	0.030	29.97	0.10	410.5	144	1,500	• Full transient to equilibrium	Nominal test conditions
			Cool to 800°F				~600		
-2	25	0.030	299.97	0.01	411.25	169	9,600	• Equilibrium	
-3	25	0.030	2.97	1.0	412.0	194	9,675	• Partial transient to equilibrium	
			Cool to 800°F				~600		
-4	25	0.030	0.27	10.0	412.75	219	10,282.5	• Partial transient to equilibrium	
			Cool to 800°F				~600		
D-1	25	0.030	29.97	0.10	413.50	244	1,250	• Partial transient to equilibrium	Max. test conditions
-2	25	0.030	2.97	1.0	414.25	269	1,375	• Equilibrium	
-3	25	0.030	0.27	10.0	415.0	294	13,825	• Equilibrium	
			Cool to 800°F				~600		
E-1	25	0.030	29.97	0.10	415.75	319	1,250	• Partial transient to equilibrium	Min. test conditions
-2	25	0.030	2.97	1.0	416.50	344	1,375	• Equilibrium	
-3	25	0.030	0.27	10.0	417.25	369	1382.5	• Equilibrium	
Totals					**417.25**	**369**	**20 hrs**		

THERMOCOUPLE LOCATIONS

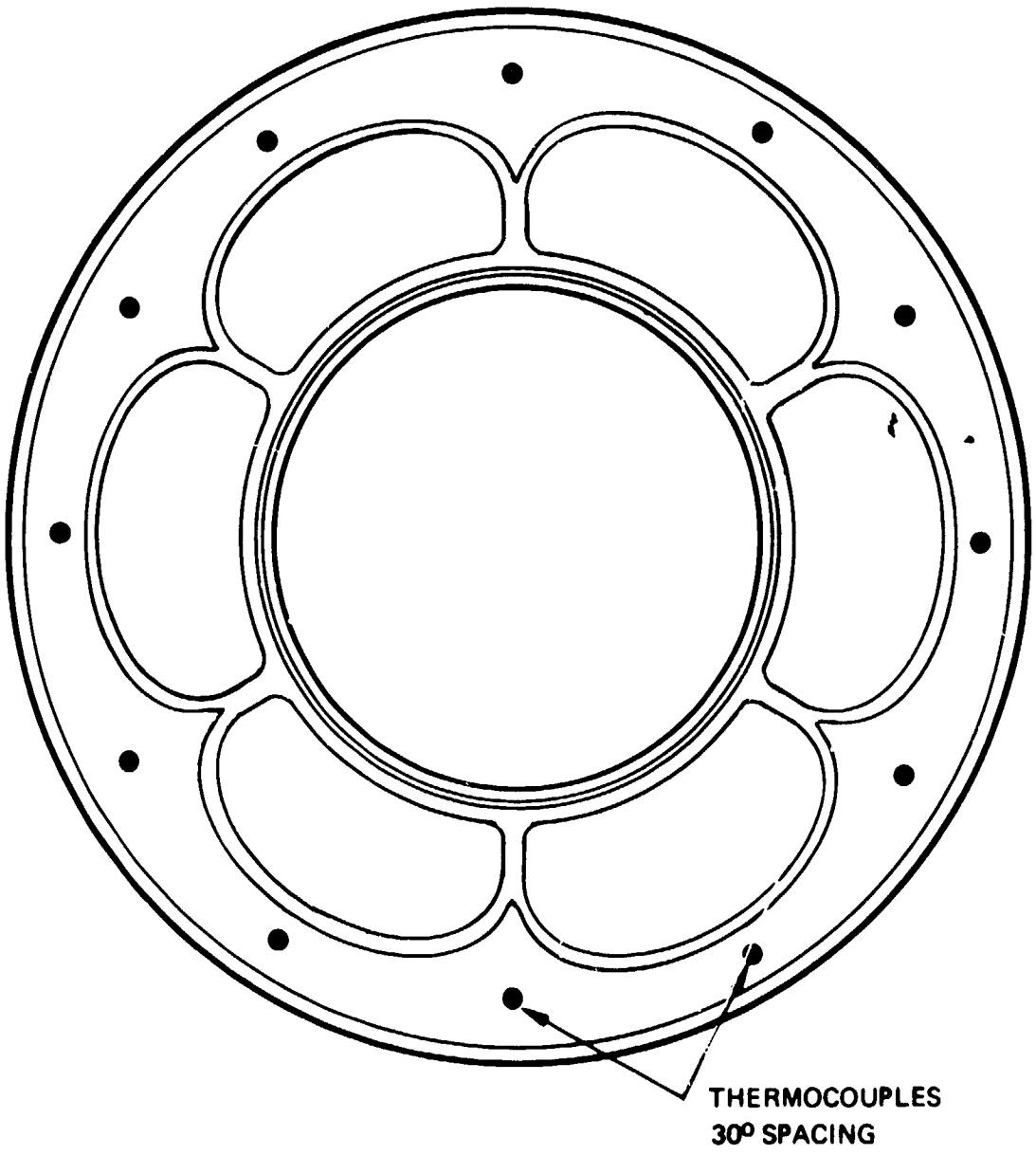

NOTE: THERMOCOUPLES LOCATED AT AXIAL MIDPOINT OF BED AND AT DOWNSTREAM END OF BED.

Table 5-3
INSTRUMENTATION FOR RCS FIRINGS

Symbol	Parameter	Range	Recorders	
			Strip Chart Recorder	O-Graph
F	Thrust	0 – 600 lbf	X	X
P_F	Propellant inlet pressure	0 – 500 psig	X	X
P_{cu}	Upper chamber pressure	0 – 250 psig	X	X
P_{cd}	Lower chamber pressure	0 – 250 psig	X	X
W_1	Propellant flow rate	0 – 3 lb/sec		X
W_2	Propellant flow rate	0 – 3 lb/sec		X
i_{TCV}	Valve current	0 – 4 amps		X
v_{TCV}	Valve voltage	0 – 50 vdc		X
T_p	Propellant inlet temperature	32 – 250°F	X	
T_v	Valve temperature (2)	32 – 500°F	X	
T_i	Injector temperature (7)	32 – 2,250°F	X	
T_g	Catalyst bed exit temperature (24)	32 – 2,250°F	X	
T_w	Chamber wall temperature (14)	32 – 2,250°F	X	
T_G	Exhaust gas temperature (2)	32 – 2,250°F	X	
T_N	Nozzle temperature (2)	32 – 2,250°F	X	
T_{IB}	Insulation blanket	32 – 2,250°F	X	
$\int P_{cd}$	P_c integral	Variable		X

All test data were recorded on 12-inch Honeywell oscillographs and/or Hewlett-Packard Mosely two-channel strip chart recorders. For altitude test firings, data were also recorded on magnetic tape with a high-speed digital data system.

5.2.4 Test Procedures

5.2.4.1 Propellant Sampling

Prior to each test a hydrazine sample was taken and analyzed to determine if the propellant met Military Specification MIL-P-26536C. All propellant analyzed during the program was found to be within the specified impurity limits.

5.2.4.2 Test Firing Procedure

The engine was heated to 150 to 170°F prior to commencing a firing using an electrical resistance heater attached to the engine. Heater power was then removed and the engine test firing initiated.

The planned test firing duty cycle was stored on punched paper tape, which was used in conjunction with a Tally tape system to control the propellant valve as well as other time-dependent test support equipment.

Upon completion of the test firings, the engine was allowed to cool without purging through the engine. No attempts were made to prevent ambient air from entering the nozzle subsequent to sea level firings.

When the engine was removed from the test stand, precautions were taken to ensure that the system and/or propellant valve would not become contaminated. The valve was removed from the engine and purged with 190°F nitrogen for a period of one hour to remove residual hydrazine. The engine inlet was covered to prevent contamination.

5.3 TEST RESULTS AND DISCUSSION

5.3.1 Acceptance Tests

Upon completion of the RCS assembly, the thrust chamber valve and the catalyst bed heater were subjected to individual acceptance tests. The engine acceptance test included proof and leak tests, and a sea level firing.

5.3.1.1 Thrust Chamber Valve Acceptance Test

The Space Shuttle 490-lbf monopropellant engine valve was fabricated by E-Systems, Inc. The valve was a modified throttling valve (developed for the Viking Lander engine), and thus was not fully optimized for minimum opening and closing response. The valve incorporated a cavitating venturi in the outlet port to control flow. The venturi was slightly undersized, requiring a feed pressure of 310 psia to obtain the designated flow rate. Table 5-4 lists the valve operating characteristics.

Table 5-4
SPACE SHUTTLE MONOPROPELLANT
490-lbf ENGINE THRUST CHAMBER VALVE

Pull-in voltage	28 volts
Drop-out voltage	12 volts
Opening response*	22 msec
Closing response*	34 msec
Flow rate	2.108 lbm/sec at 310 psia
Leakage	<10 scc/hr

*Transient times were determined at operating pressure with a linear voltage differential transducer monitoring ball gear location.

5.3.1.2 Catalyst Bed Heater

The catalyst bed heaters were designed to provide 30 watts of power (15 watts/element) to maintain the catalyst bed at a minimum temperature of 150°F. The heaters, fabricated by Clayborn Laboratories, had operational characteristics, as shown in Table 5-5.

Table 5-5

SPACE SHUTTLE MONOPROPELLANT
490-lbf ENGINE CATALYST BED HEATER

Voltage	28 vdc
Current	0.6 amps/element
Resistance	42.9 ohms
Insulation resistance	
Circuit to circuit	1 megohm
Circuit to case	100 megohms

5.3.1.3 Engine Acceptance Test

An engine proof test at 300 psig and an engine leak test at 200 psig were conducted with no anomalies. Following these tests the engine was installed in the sea level high-thrust test cell for an acceptance test firing. Table 5-6 presents the test conditions during acceptance test firing.

Table 5-6

ACCEPTANCE TEST CONDITIONS

Environment temperature	Ambient
Ambient pressure	Sea level
Catalyst bed temperature	160°F
Propellant inlet temperature	65°F
Propellant inlet pressure	310 psia

The firing sequence was controlled by a Tally tape control system. The duty cycle consisted of a 10-second steady-state firing, followed by a 30-minute downtime, and a final series of ten pulses 250 msec on/250 msec off. Table 5-7 lists the designed operating performance characteristics of the 490-lbf engine and the measured values obtained during the steady-state tests. As can be seen, the measured performance characteristics are nearly identical to the predicted values.

Table 5-7

SPACE SHUTTLE 490-lbf MONOPROPELLANT
STEADY-STATE PERFORMANCE CHARACTERISTICS

	Design Goal	Acceptance Test Results
Characteristic velocity	4,350 ft/sec	4,361 ft/sec
Chamber pressure	153.3 psia	153.7 psia
Chamber pressure roughness		
Upstream	---	±3.0 psid
Downstream	---	±1.5 psid

Table 5-7 (Concluded)

SPACE SHUTTLE 490-lbf MONOPROPELLANT STEADY-STATE PERFORMANCE CHARACTERISTICS

	Design Goal	Acceptance Test Results
Flow rate	2.108 lbm/sec	2.108 lbm/sec
Catalyst bed pressure drop	41.5 psid	41.7 psid
Response time (valve signal to 90% P_c)	700 msec	425 msec
Tailoff time (valve signal to 10% P_c)	–	55 msec

Pulse-mode data also appeared to be in excellent agreement with predicted pulse performance. Maximum peak pressure was 162 psia (8 psi overshoot) and $\int P_c dt$ values varied by less than 1.1% from nominal for the last six pulses. A trace of pulse 10 is shown in Figure 5-8.

Uniform gas temperature was achieved around the circumference of the radial bed. Thermocouples monitoring gas temperature exiting the catalyst bed at every 30° recorded a nominal gradient of only 40°F, indicating uniform propellant distribution. Figure 5-9 is a plot of the radial temperature distribution of gases exiting the outer bed.

At completion of testing the engine was removed from the sea level test facility and stored for a short time prior to being transported to the Boeing Tulalip test facility for altitude firings. No purging or decontamination operations were conducted on the engine following ATP, since purging was not considered a nominal Space Shuttle maintenance procedure.

5.3.1.4 RCS Altitude Firings

After completing all installation and instrumentation hook-ups, and just prior to initiation of performance mapping, a short pulse was manually signaled to the valve for final check out of system operation. All feed system functions and instrumentation appeared to operate normally; however, there was no indication of propellant reaction within the engine. Instrumentation was monitored for a short period following the pulse with no indication of decomposition. Test cell vacuum was then terminated and the cell opened to visually inspect the engine, at which time hydrazine vapor began exiting the nozzle. Altitude pressure was then reinstated as the accumulated hydrazine began to react with the warming catalyst bed. Following this incident, a second pulse was manually signaled to the valve and a normal pulse (160 msec long) was achieved. After assessment of the data, it was decided to initiate the performance mapping tests. The performance mapping test sequence consisted of the duty cycle shown below.

A-1	100-second steady-state, 150°F initial catalyst bed temperature
A-2	100-second steady-state, hot restart
A-3	100-second steady-state, increase P_f 10 psi, hot restart
A-4	100-second steady-state, decrease P_f 10 psi, hot restart
B-1	Twenty-five 100-msec pulses at 1% duty cycle

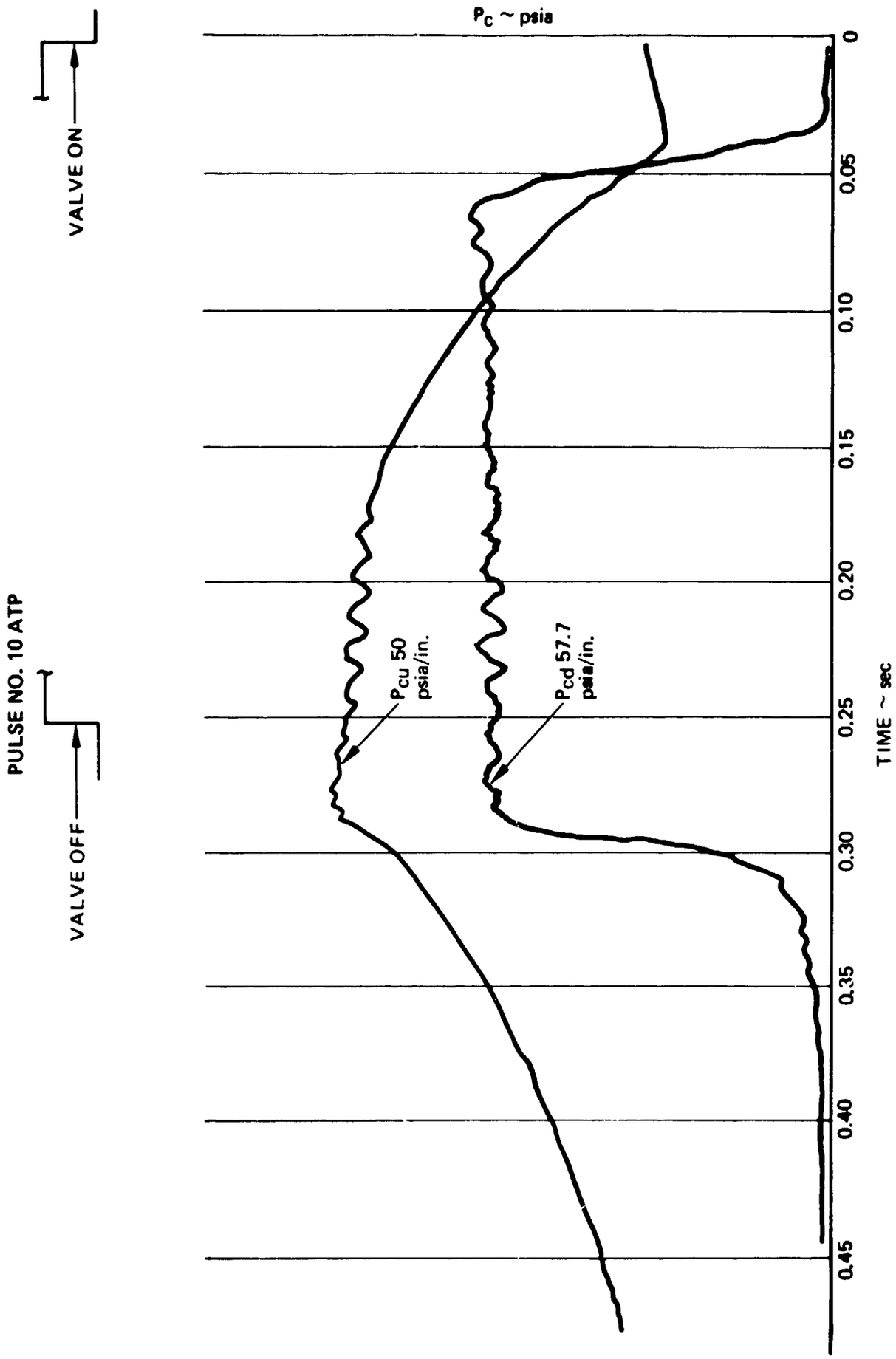
P_C ~ psia
VALVE ON
PULSE NO. 10 ATP
VALVE OFF
P_{cu} 50 psia/in.
P_{cd} 57.7 psia/in.
0
0.05
0.10
0.15
0.20
0.25
0.30
0.35
0.40
0.45
TIME ~ sec

Figure 5-8

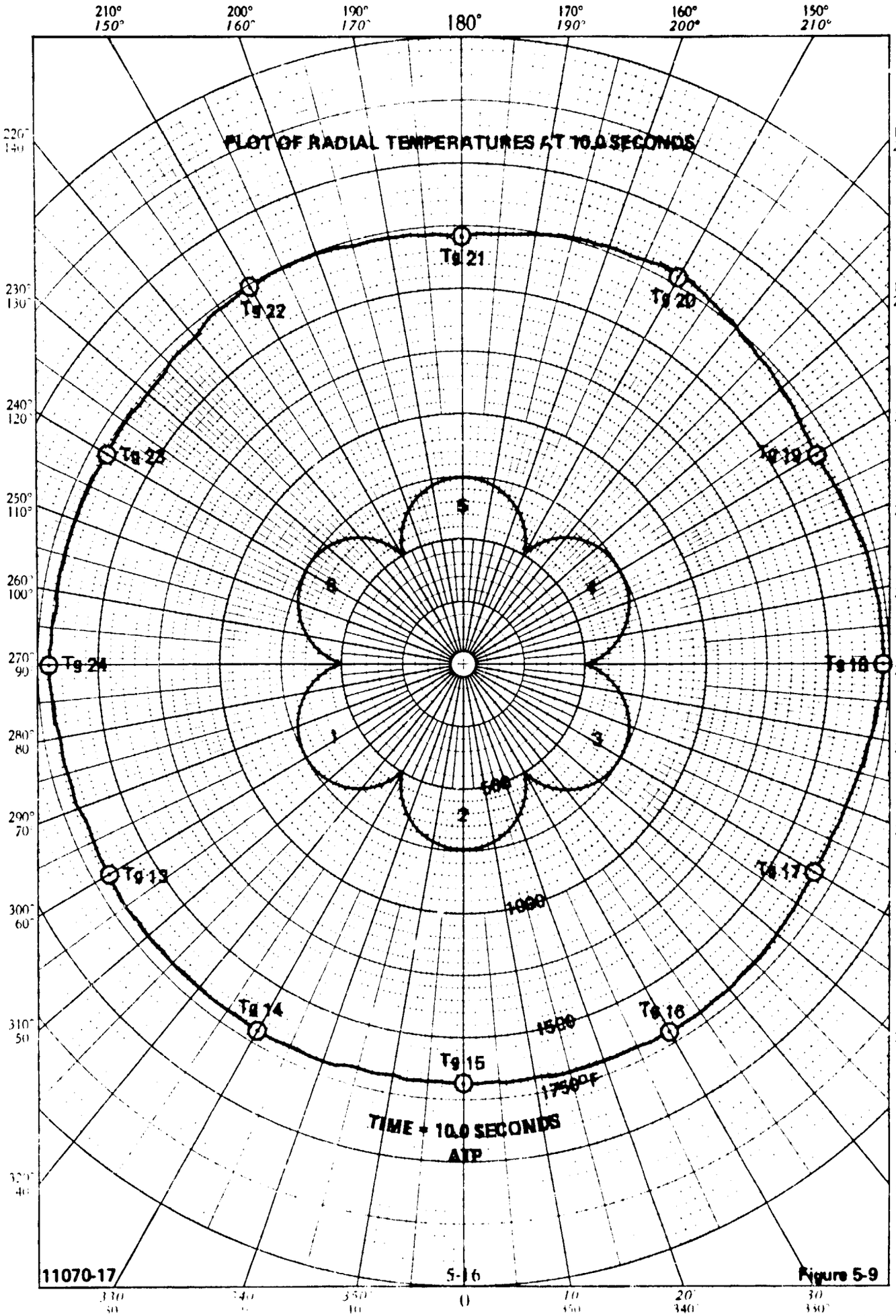
PLOT OF RADIAL TEMPERATURES AT 10.0 SECONDS
Tg 21
Tg 20
Tg 19
Tg 18
Tg 17
Tg 16
Tg 15
Tg 14
Tg 13
Tg 24
Tg 23
Tg 22
1
2
3
4
5
6
1000
1500
1750°F
TIME = 10.0 SECONDS
AIP

B-2 Twenty-five 100-msec pulses at 0.1% duty cycle
B-3 Fifteen 100-msec pulses at 0.01% duty cycle
B-4 Twenty-five 100-msec pulses at 10% duty cycle

Preliminary data obtained during the steady-state firings indicated the engine operational characteristics were the same as during ATP. However, gas temperature was slightly higher and not as uniform as the ATP values, and the bed pressure drop decreased to 10 to 14 psi during the 100-second firing. Each of the steady-state firings had similar performance characteristics. A summary of the results for the steady-state firings is presented in Table 5-8. Visual inspection of the engine following the steady-state firings revealed no structural anomalies.

Pulse-mode testing was then initiated with no significant anomalies during the first two sequences (B-1 and B-2). Performance as a function of pulse number is shown in Figure 5-10. Testing of the B-3 sequence was terminated after the sixth pulse due to pulse shape distortion which was postulated to have been due to operation in a marginal thermal regime. Sequence B-4 was then initiated at which time a pressure spike occurred with subsequent loss of performance. Inspection of the engine indicated that a pressure spike (or spikes) caused a structural failure of the injector body assembly and subsequent loss of catalyst from the bed retention system.

A detailed investigation of the initial misfire and subsequent engine failure revealed the following.

5.3.2 Misfire Incident

Incomplete hydrazine decomposition occurred on the first pulse of the performance mapping test due to a large quantity of ammonia residing on the catalyst surface acting as a temporary catalyst poison. The ammonia poisoning occurred as a result of the relatively short acceptance firing and inadequate engine securing techniques following the acceptance testing. A review of the ATP procedures determined that liquid hydrazine was trapped in the engine injector. Slow drainage of the hydrazine from the injector during storage (the engine was stored in the vertical nozzle down position) and subsequent slow decomposition allowed the cold catalyst to be blanketed by ammonia and hydrogen. After exposure to the trapped gases, the catalyst adsorbed sufficient ammonia to poison the catalyst and cause total washout on the first pulse. Subsequent decomposition of the residual propellant sufficiently heated the catalyst to desorb the ammonia poison restoring catalyst activity. Post-test measurement of catalyst activity revealed it to be lower than that of new catalyst. However, it is noted that the high bed temperatures encountered subsequent to the misfire caused catalyst sintering with a resultant loss in surface area.

Subscale engine testing was conducted to simulate catalyst poisoning by exposure to hydrazine vapors. The bolt-up engine was loaded with a new catalyst bed, tested at the RCS engine ATP duty cycle. After cooling to 100°F, 1/4 cc of liquid hydrazine was inserted into the engine inlet tube so that slow vaporization of hydrazine would occur. The catalyst bed was exposed to these conditions for periods of four and twenty-four hours prior to retesting. The ignition delays following each of these exposure tests were very long (160 to 200 msec) indicating substantial catalyst poisoning had occurred.

Table 5-8
STEADY STATE ENGINE CHARACTERISTICS
AT 100 SECONDS

	A-1	A-2	A-3	A-4
P_{cu}, psia	165	169	167	162
P_{cd}, psia	153	155	156	152
ΔP_{BED}, psid	12	14	11	10
$\dot{w}$, lbm/sec	2.135	2.146	2.163	2.115
c*, ft/sec	4,320	4,372	4,366	4,335
P_{cu} ROUGHNESS, ± psia	±2.0	±1.5	±1.5	±1.0
P_{cd} ROUGHNESS, ± psia	±2.0	±1.5	±1.5	±1.5
F VACUUM, lbf	503	513	517	501
I_{sp}, lbf-sec/lbm	235	239	235	237

01688

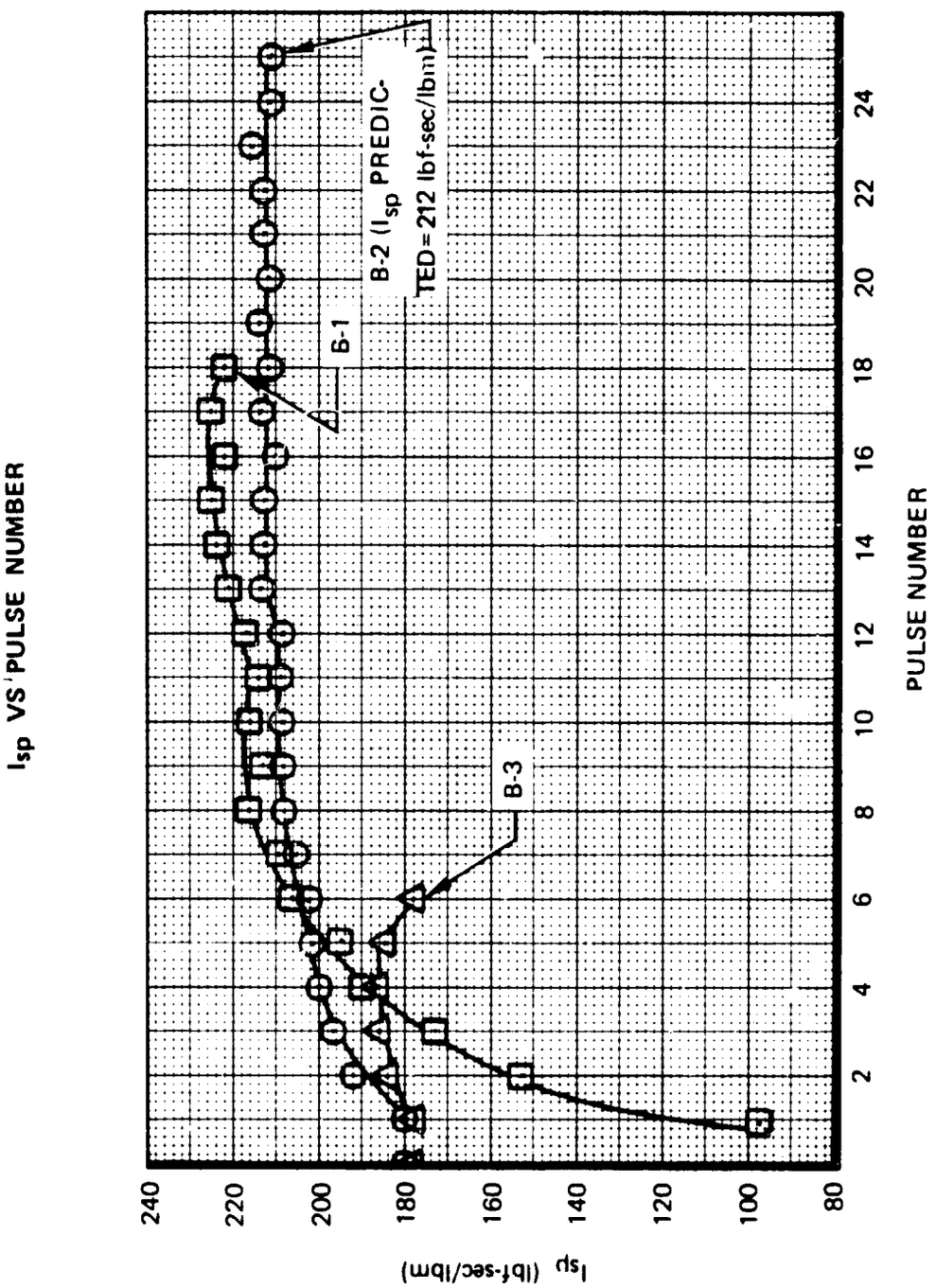
I_{sp} VS PULSE NUMBER
B-1
B-2 (I_{sp} PREDIC-TED = 212 lbf-sec/lbm)
B-3
I_{sp} (lbf-sec/lbm)
PULSE NUMBER
240
220
200
180
160
140
120
100
80
2
4
6
8
10
12
14
16
18
20
22
24

To obtain a "self-poisoned" catalyst bed is a phenomena requiring environmental conditions not normally experienced in engine testing. Catalyst bed temperatures must be relatively cold and exposed to ammonia vapors for a considerably long period of time. Laboratory data has demonstrated that by maintaining a catalyst bed at 200°F – or heating a bed to 200°F prior to operation – will prevent the heavy adsorption of ammonia or drive off the species from the surface if they are already present.

5.3.3 Engine Structural Failure

Engine testing was terminated following loss of compartment 4 bed closure plate (Figure 5-11). Subsequent teardown analysis indicated that rapid decomposition of hydrazine occurred in the propellant passages causing a high pressure spike in the injector body assembly (Figure 5-12). The spike occurred during low duty cycle operation (0.01%) indicating insufficient thermal margin to handle the large heat soakback.

Analysis of the data indicated that pulse distortion was encountered during operation at a specific thermal regime of the injector. Shown in Figure 5-9 is a plot of injector temeprature versus pulse number for the three test sequences. Also noted are comments concerning the observed pulse shapes. As can be seen, pulse distortion was observed when the injector temperature was in the range of 750 to 1,100°F. During sequence B-3 the temperature was nearly stable at 850°F. It was therefore postulated that the pressure spike was due to inadequate thermal margin of the injector.

Tests to verify the thermal anomaly in the injector were conducted in the following manner. An individual injector element was fabricated and externally heated to simulate engine thermal environment (Figure 5-13). The initial tests were conducted by pulsing the hot element at 1,600 and 1,100°F (Figure 5-14). No thermal problems were encountered at these temperatures. However, pulsing the hot injector at 800°F showed evidence of spiking and roughness at 650°F injector body temperature, a significant pressure spike occurred in the injector similar to the failure experienced on the 490-lbf engine.

Based on the results of the failure analysis, it was concluded that the pressure spike was caused by inadequate injector thermal margin. As a result of a detailed review of the injector design, the following design changes were recommended to correct the thermal deficiencies noted in the initial test series.

a. Decrease injector holdup volume
b. Provide smooth transition from circular passage to Rigimesh manifold
c. Improve Rigimesh weld
d. Alter passage dimensions consistent with thermal analysis.

Unfortunately, as a result of funding limitations and NASA redirection to emphasize the Space Shuttle APU application, the above RCS design modifications were not incorporated and tested. However, sufficient analytical and experimental studies were conducted over extreme duty cycles to provide assurance that the engine could be built and operated with no duty cycle restraints over the Space Shuttle thermal environment extremes. The gas generator, designed and tested during Task IVA and reported on in Volume II, successfully completed hot restarts and a wide range of duty cycles were conducted.

CHAMBER SUBASSEMBLY

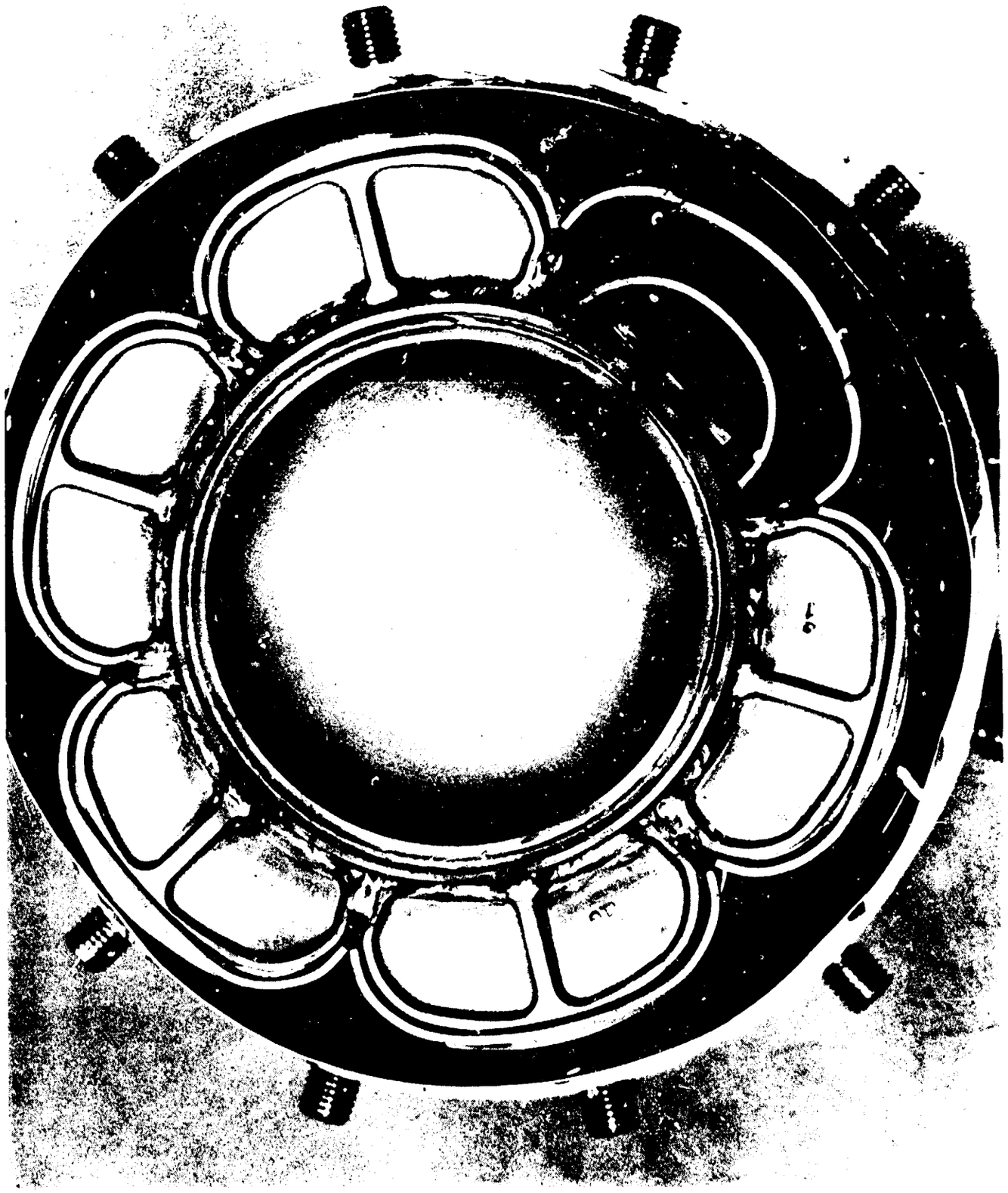

11070-36

Figure 5-11

INJECTOR ASSEMBLY

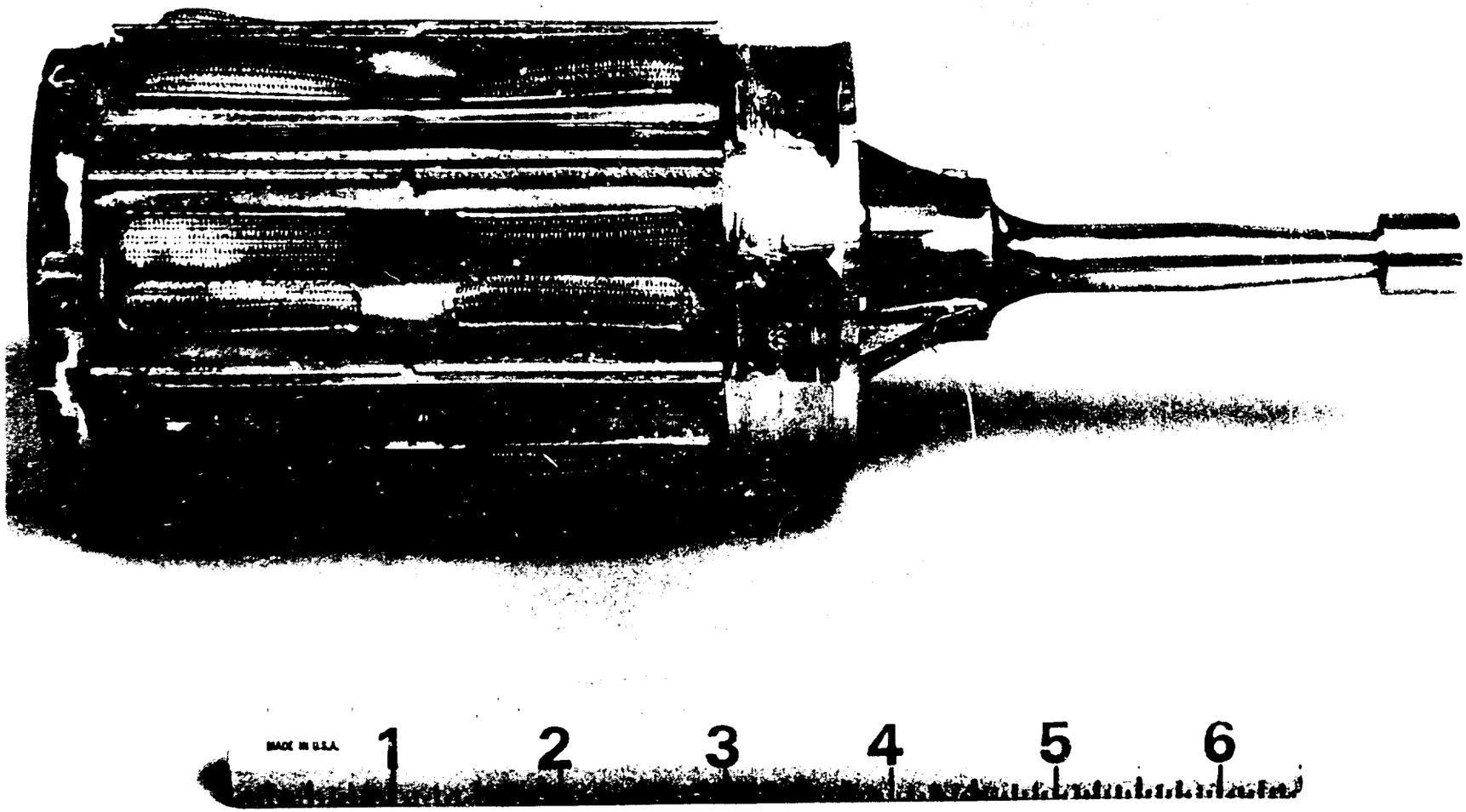

11070-24

Figure 5-12

HOT RESTART TEST INJECTOR ELEMENT

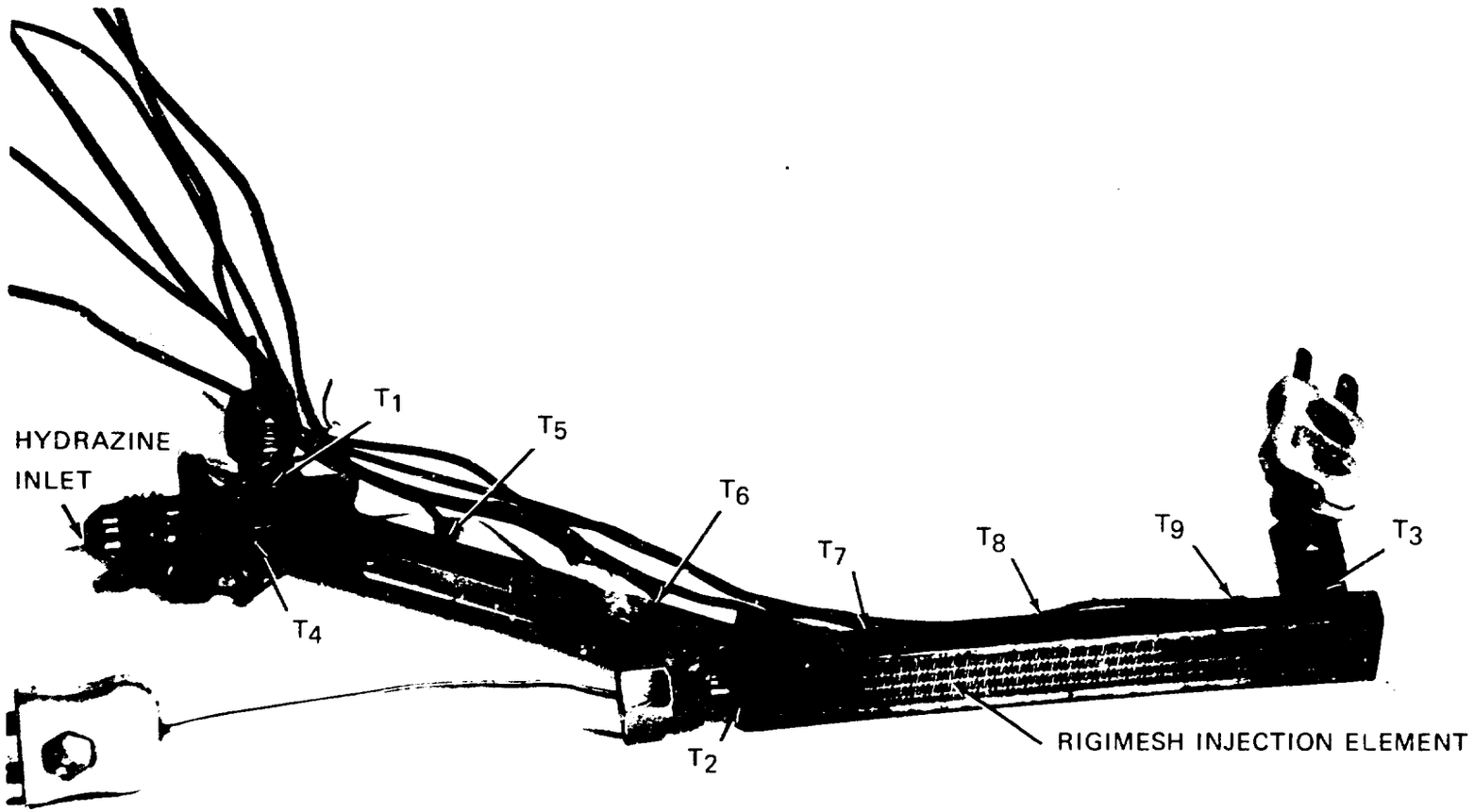

- INITIAL VACUUM AND SEA LEVEL HOT RESTARTS
- HOT RESTARTS AT MAXIMUM EXPECTED TEMPERATURES (>1,375°F) AND AT PREDICTED WORST-CASE CONDITIONS (10 TO 100°F ABOVE SATURATION)
- $T_1 - T_3$ ~ HIGH RESPONSE LIQUID MEASUREMENTS
- $T_4 - T_9$ ~SLOWER RESPONSE METAL TEMPERATURES
- PRESSURE MEASUREMENTS NOT SHOWN
- TEST SPECIMEN MOUNTED BETWEEN COPPER BLOCKS TO SIMULATE TOTAL INJECTOR ENVIRONMENT

11059-30

Figure 5-13

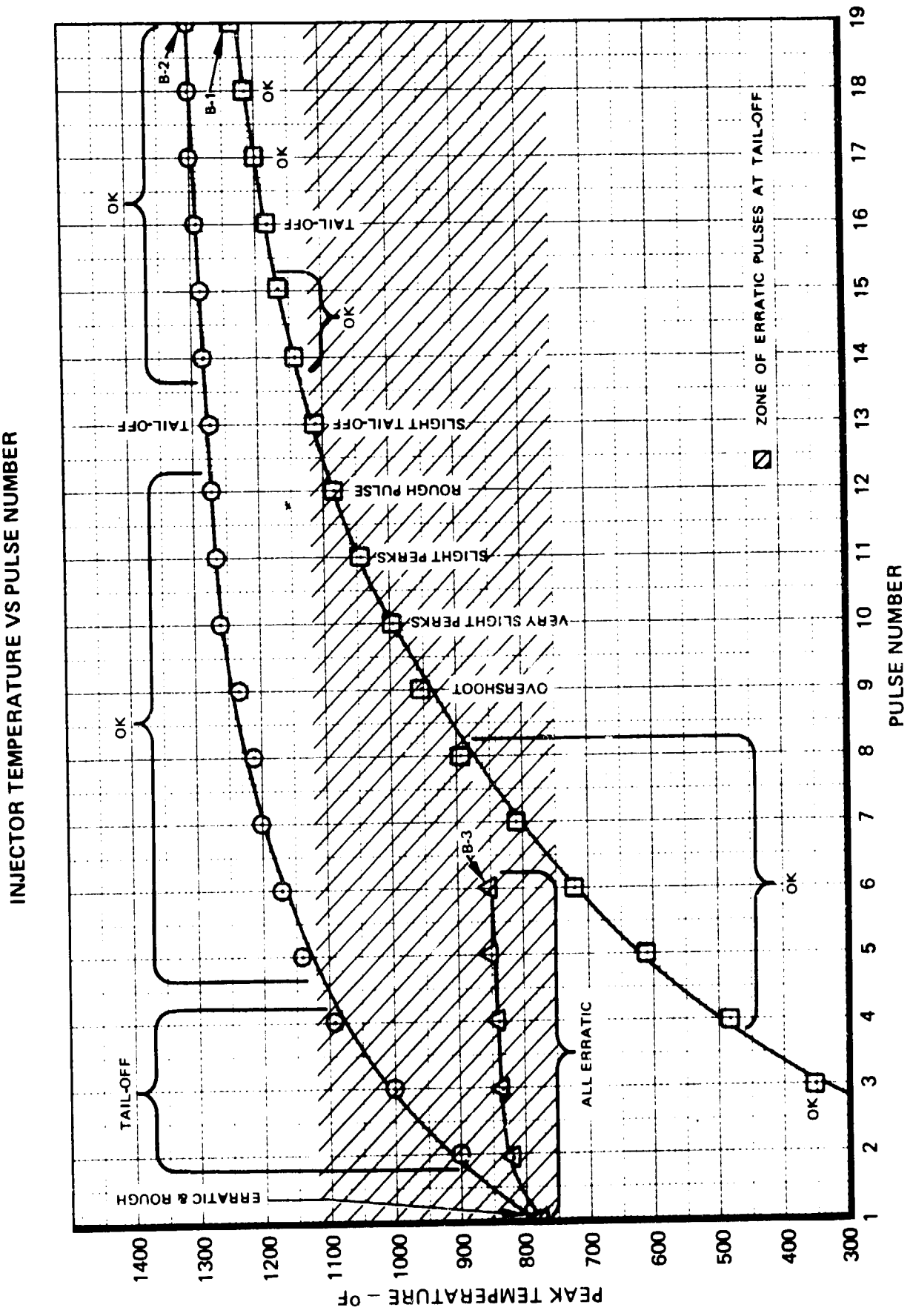
INJECTOR TEMPERATURE VS PULSE NUMBER
PEAK TEMPERATURE – °F
PULSE NUMBER
ZONE OF ERRATIC PULSES AT TAIL-OFF
B-1
B-2
B-3
OK
TAIL-OFF
SLIGHT TAIL-OFF
ROUGH PULSE
SLIGHT PERKS
VERY SLIGHT PERKS
OVERSHOOT
ALL ERRATIC
ERRATIC & ROUGH

Figure 5-14

6.0 CONCLUSIONS AND RECOMMENDATIONS

The major results, conclusions, and recommendations of the Space Shuttle RCS program are as follows:

1. Although it was found that catalyst oxidation damage can occur under certain conditions, it was concluded that catalyst outgassing would prevent any oxidation damage during reentry.
2. Random vibration of catalyst confined in simulated compartments at 29 g rms resulted in negligible breakup rates (0.02 percent/minute). Neither voids nor screen wires inserted in the compartment affected the breakup rate.
3. A subscale test technique was developed which provides a cost effective, scalable approach for parametrically optimizing the design of large monopropellant engines.
4. Catalyst retention was achieved without the use of screen wires with a bedplate design which simultaneously retained the catalyst and minimized thermal expansion.
5. The 490-lbf RCS engine had excellent performance and operating characteristics during acceptance testing with measured performance within 1 percent of the predicted values.
6. The RCS engine misfire incident was due to catalyst poisoning resulting from residual propellant in the injector manifold following the acceptance firing, which was not thoroughly removed prior to storage.
7. The engine structural failure resulted from heat soakback to the injector with subsequent decomposition of propellant in the manifold.
8. It is recommended that additional studies be conducted to establish the effects of injector design variables and heat soakback on hydrazine stability in injector manifolds.
9. The use of foam metal for retention of the inner bed catalyst should be more thoroughly explored for use in large thrust monopropellant engines.

APPENDIX 7.1
RELIABILITY PREDICTION

7.1 RELIABILITY PREDICTION

7.1.1 Introduction and Summary

This analysis covers the reliability prediction for the flight configuration space shuttle orbiter reaction control system (RCS) engine. The results of the prediction, based on a single engine, are as follows:

1 mission	(7 days)	0.999
25 missions	(refurbishment cycle)	0.975
100 missions	(life cycle)	0.903

The mission duty cycles are covered in Section 4.0. Detailed models and calculations are covered in Section 6.0. The basic analysis covers one mission, or flight, of 7 days. From this base, predictions are extended for 25- and 100-mission groups. These extended predictions have been made because a) as now projected by RRC, a complete refurbishment will be accomplished after each cycle of 25 flights and b) the total life cycle is specified as 100 flights.

7.1.2 System Description

The RCS engine is designed to provide a nominal thrust of 490 lbf, using monopropellant hydrazine. Propellant flow to the thruster is controlled by a single-seat, open/closed, motor-operated propellant valve (thrust chamber valve — TCV). The TCV has an integral filter. A cavitating venturi between the valve and the thrust chamber assembly (TCA) maintains a constant propellant flow rate. Redundant heaters will be applied to the TCA to maintain the catalyst bed at the specified 150°F minimum temperature and thus avoid the occurrence of "cold starts." Thermostatically controlled redundant heaters will be applied to the TCV to maintain the valve above the freezing temperature of hydrazine. As now projected, the thermostat of the redundant heater circuit will have a setting a few degrees below that of the primary heater circuit. This will ensure that only the primary circuit is drawing power; and should that circuit fail, the redundant one would be switched into operation automatically. A thermocouple is attached to the TCA to sense temperatures of that unit, but is is assumed that the output of the thermocouple will be fed into a signal conditioning/switching device on the system level that will automatically control the TCA heater operation. Since the control unit is assumed to be a system level component, it is not included in this prediction. The engine thermal control is completed by a thermal shroud (or blanket) around the TCA.

In addition to the thermocouple mentioned above, the flight instrumentation includes a pressure transducer for sensing the TCA pressure and a thermistor for sensing the TCV temperature. This instrumentation is not essential to the mission, inasmuch as the engine will operate and fulfill its mission functions without it. Therefore, these items have not been included in the reliability analysis. The RCS engine is illustrated in Figures 7.1-1 and 7.1-2.

11062-43A

7.1-2

SPACE SHUTTLE ORBITER RCS ENGINE

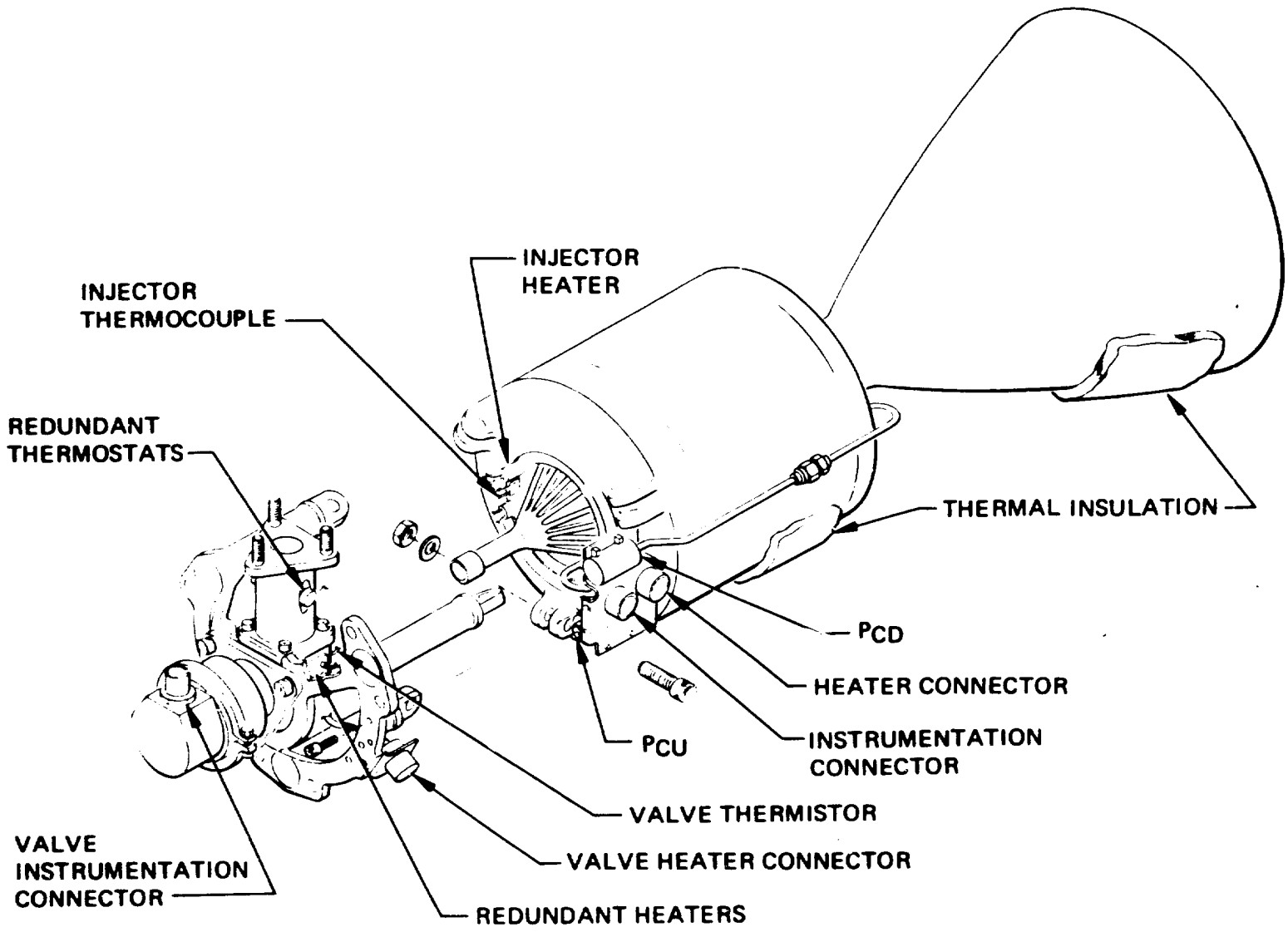

Figure 7.1-1

RCS ENGINE SCHEMATIC

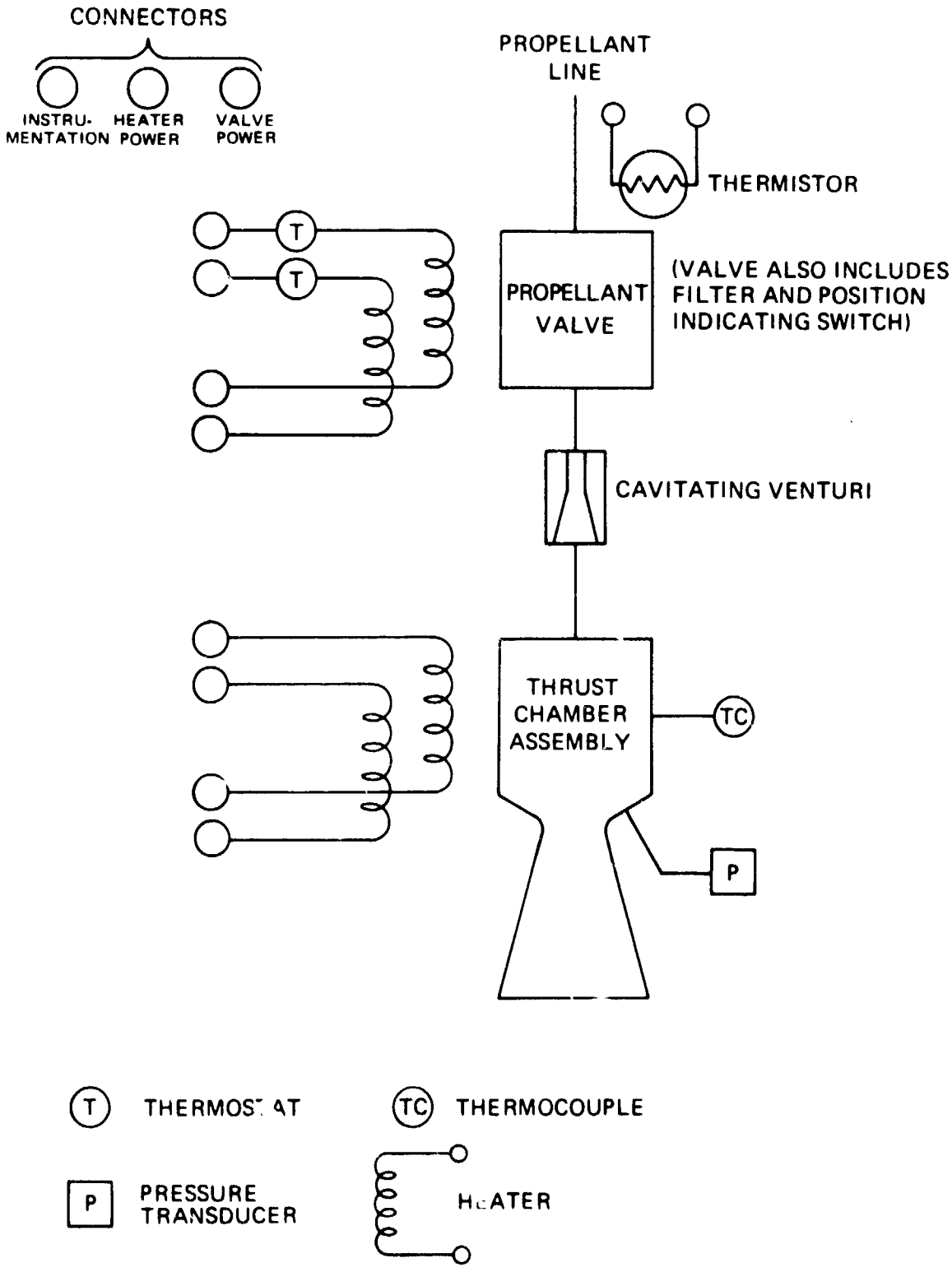

Figure 7.1-2

7.1.3 Reliability Requirement

A numerical reliability goal has not been set by NASA-JSC for the space shuttle orbiter RCS engine. The space shuttle guidelines (per Request No. 1-2-50-23639, Appendix A) include the following statement: "Vehicle subsystems designs should reflect features consistent with a philosophy of high reliability, minimum maintenance and checkout, reuseability, and low cost."

7.1.4 Mission Profile

7.1.4.1 Duty Cycles

The vehicle, engine, and mission life and duty cycles have been specified by Request No. 1-2-50-23639, Appendix A, and by Contract NAS8-28950, Appendix B. Certain operating times and cycles necessary for the prediction were estimated by RRC. The predictions performed herein are based on the time, cycles, and mission frequencies listed below.

Mission duration	7 days
Maximum burn time per mission	1,000 seconds (0.278 hours)
Maximum number of pulses per mission	2,000
On-time for TCV heater per mission	5 hours*
On-time for TCA heater per mission	3 hours*
Boost phase	0.2 hour*
Deorbit and landing phase	0.5 hour*
Total number of missions	100
Number of missions between refurbishment (per RRC proposed program, see paragraph 4.2.4	25

**Estimated*

7.1.4.2 Mission Stress Factors and Assumptions

7.1.4.2.1 Operating Modes

Both time- and cyclic-related failure modes are identified and evaluated in this analysis. Therefore, the propellant valve and the thruster are analyzed with both time- and cyclic-operating failure rates. The propellant valve, in addition to these, is considered subject to a leakage failure mode, which, though a function of a constant pressure stress, is nevertheless considered a non-operating mode. This mode is defined as "leakage nominally in excess of a specified maximum tolerance, causing a parasitic but not a perturbating thrust, with some decrease in length of mission due to gradual loss of propellant." This is contrasted to loss of mission due to fail-to-open or fail-to-close modes of the valve.

7.1.4.2.2 Ambient Starts

Only ambient starts for the engine have been included. The TCA heaters are designed to hold the catalyst bed at the specified 150°F temperature minimum, which is above a "cold start" condition that could cause pressure spikes and possible damage to the catalyst bed. Therefore no "cold starts" are assessed against the TCA in this prediction.

7.1.4.2.3 Mission Phases

A boost phase and a deorbit/landing phase, assumed to be of 0.2-hour and 0.5 hour duration respectively, have been included to account for environmental stresses during those periods that could increase the generic failure rate. A K factor of 900 has been applied as a failure rate modifier to the former and 90 to the latter. A K factor of 1.0 has been applied to the orbiting phase.

7.1.4.2.4 Refurbishment Group

A complete refurbishment will be accomplished after every 25 missions as a major maintenance action on the RCS. This will restore the RCS engines to original condition of performance. It is designed to take place before there can be any out-of-tolerance "wearout" that could result in failure or major performance degradation. This ensures that the component failure rates remain constant.

Redundant O-rings provide a seal where the valve/cavitating venturi inlet tube joins the TCV. This type of joint makes possible the replacement of interfacing subassemblies, if required, during refurbishment. The probability of a leakage failure at this point (during activation of the engine) is extremely remote, but the failure mode is included in "fittings" with the cavitating venturi in this analysis.

7.1.4.2.5 Recycling Unreliability

It is assumed that the additional handling, reconditioning, and checkout involved in recycling the space shuttle after each flight during the turnaround period result in a small, but possible, performance deficiency failure mode. This could result from personnel error, undetected damage or contamination, incomplete inspection, etc., that may arise from normal recycling operations. Further, this is assumed to be cumulative from flight to flight until the major refurbishment after 25 missions. To account for this possibility, each flight (after the first) is assessed a failure rate of 5×10^{-6}, which is additive through the 25th flight. The model for including this is presented in paragraph 7.1.6.2.

7.1.5 Failure Rate Data Sources

Failure rates have been obtained generally from AVCO sources and wherever possible from RRC and RRC supplier test data. The latter two sources apply specifically to the thruster and propellant valve. These data are available in RRC Reliability Bulletin RB-1C, which also covers environmental and application factors (K) used to modify failure rates. The K factor of 90 for deorbit/landing (see paragraph 7.1.4.2.3) has not been included in RRC RB-1C. This value has been derived by assuming it as 1/10 the boost phase factor. (This compares with a K factor of 50 that is applied for aircraft flight stresses.)

7.1.6 Analysis Methods and Mathematical Models

7.1.6.1 Mathematical and Logic Models

The reliability estimate is based on a constant failure rate assumption. Therefore, the exponential distribution is used to estimate the reliability of each functional reliability block defined by the reliability block diagram.

Thus,

$$R = e^{-x_i} \tag{1}$$

in which

R is reliability (probability of no failures)

x_i is failures per mission for the i^{th} reliability block.

Some parts operate in only the time domain, some in only the cyclic domain, and some in both. The appropriate time-related or cyclic-related failure rates have been selected for these parts. It is also necessary to modify the generic failure rates in accordance with the following formula to account for the variables that determine the failure rate of a reliability block.

For time-dependent failure rates:

$$\lambda_t = nK_E K_A \lambda_G \tag{2}$$

Where:

λ_t = Time dependent failure rate (failures/hour)

n = Quantity of items

K_E = Failure rate modifier for environmental stress

K_A = Failure rate modifier for application stress

λ_G = Generic failure rate (failures/hour).

For cyclic-dependent failure rates:

$$\lambda_c = nK_E K_A \lambda_G \tag{3}$$

Where:

λ_c = Cyclic-dependent failure rate (failures/cycle)

λ_G = Generic failure rate (failures/cycle).

Then to estimate the mission failures for a reliability block

$$x_i = \lambda_t t + \lambda_c c \tag{4}$$

Where:

t = The applicable mission time (hours)

c = The applicable number of cycles during mission.

By extension of (1) and (4), the reliability of a group of blocks in series is stated as follows:

$$\prod_{i=1}^{n} R_i = R_1 R_2 \ldots R_n \tag{5}$$

The reliability of a fully redundant pair of blocks (e.g., a and b) is stated as follows:

$$R = 1 - (1 - R_a)(1 - R_b) \tag{6}$$

The alternate form of this is:

$$R = 1 - Q_a Q_b \tag{7}$$

R_1, R_2, R_3 etc. are the reliabilites of the related numbered blocks of the reliability block diagram, Figure 7.1-3. The same identifying notation is used in the reliability block failure rate data, Table 7.1-1, in which the individual mission exponent values, per (4) above, are derived and listed. The mission failure rate, or exponent, values are used in all cases to determine the reliability of each block for one mission.

Incorporating the preceding models, and based on the block diagram of Figure 6-1, the reliability model for the RCS engine for a single mission (flight) may be stated:

$$R_{RCS} = R_1 [1 - (1 - R_2R_3)^2] R_4R_5 [1 - (1 - R_6)^2] R_7R_8R_9R_{10} \tag{8}$$

To account for the possible cumulative effects on RCS performance due to turnaround recycling of the space shuttle system, as discussed under paragraph 7.1.4.2.5, the following terms are assigned:

R_O = Reliability of original countdown = 1.0

Q_F = Unreliability induced by recycling maintenance = 5×10^{-6}

R_R = Reliability of 25th mission (refurbishment group)

R_M = Reliability of 100th mission.

With these terms, the following statements are made:

$$R_R = [R_O (R_O - Q_F)(R_O - 2Q_F)(R_O - 3Q_F) \ldots (R_O - 24Q_F)] R_{RCS}^{25} \tag{9}$$

$$R_M = R_R^4 \tag{10}$$

7.1.6.2 Calculations

7.1.6.2.1 Block Reliability Derivations

The following calculations are made by applying the exponent values for the numbered block from Table 7.1-1:

i	x_i	$R = e^{-x_i}$	Related Calculation
1	0.000305	0.999695	
2	0.0000022	0.999998	$1 - (1 - R_2R_3)^2 = 1 - (1 - .999997)^2$
3	0.0000004	0.999999	$= 1 - (.000003)^2 = 1^{(-)}$
4	0.00000002	$1^{(-)}$	
5	0.0006955	0.999305	

(Continued)

Block Reliability Derivations (Concluded)

i	x_i	$R = e^{-x_i}$	Related Calculation
6	0.0000013	0.999999	$1 - (1 - R_6)^2 = 1 - (.000001)^2 = 1^{(-)}$
7	0.0000002	$1^{(-)}$	
8	0.0000018	0.999998	2 connectors: $R^2 = 0.999996$
9	0.0000018	.999992	
10	0.0000023	0.999998	

7.1.6.2.2 RCS Reliability

The following calculations have been made by substituting the values from the foregoing table in formula (8):

$$R_{RCS}\,(\text{one mission}) = (0.999695)(1.0^{(-)})(1.0^{(-)})(0.999305)(1.0^{(-)})(1.0^{(-)})(0.999998)(0.999992)(0.999998)$$
$$= 0.99899 \approx 0.999$$

$$R_{RCS}\,(25 \text{ missions}) = 0.99899^{25} = 0.975054 \approx 0.975$$

7.1.6.2.3 Mission Reliability (25 and 100)

Substituting in formulas (9) and (10), the following calculations are made:

$$R_R = [1.0\,(1 - 0.000005)(1 - 0.00001)(1 - 0.000015) \ldots (1 - 0.00012)]\,(0.975054)$$
$$= [1.0\,(0.999995)(0.99999)(0.999985) \ldots (0.99988)]\,(0.975054)$$
$$= (0.9997)(0.975054) = 0.974761$$

$$R_M = 0.974761^4 = 0.902804 \approx 0.903$$

7.1.7 Redundancy and Safety Provisions

This prediction covers the currently proposed Task II RCS engine design. Subsequent design analysis or redesign based on the Task III hardware and test program may require a subsequent revision to this analysis.

Redundant TCV and TCA heaters ensure a highly reliable thermal control. To ensure safety for ground crews performing checkout, recycling, or maintenance operations, the use of two-position latching valves upstream of the TCV should be considered. These valves, incorporated at the space shuttle system level, would provide a redundant shut-off capability both in space and on the ground to prevent a possible leakage failure mode (in excess of allowable leakage) of the single-seat TCV. A single LV could shut off a group of manifolded TCV's in a configuration consistent with functional attitude control requirements at the system level.

RCS RELIABILITY BLOCK DIAGRAM

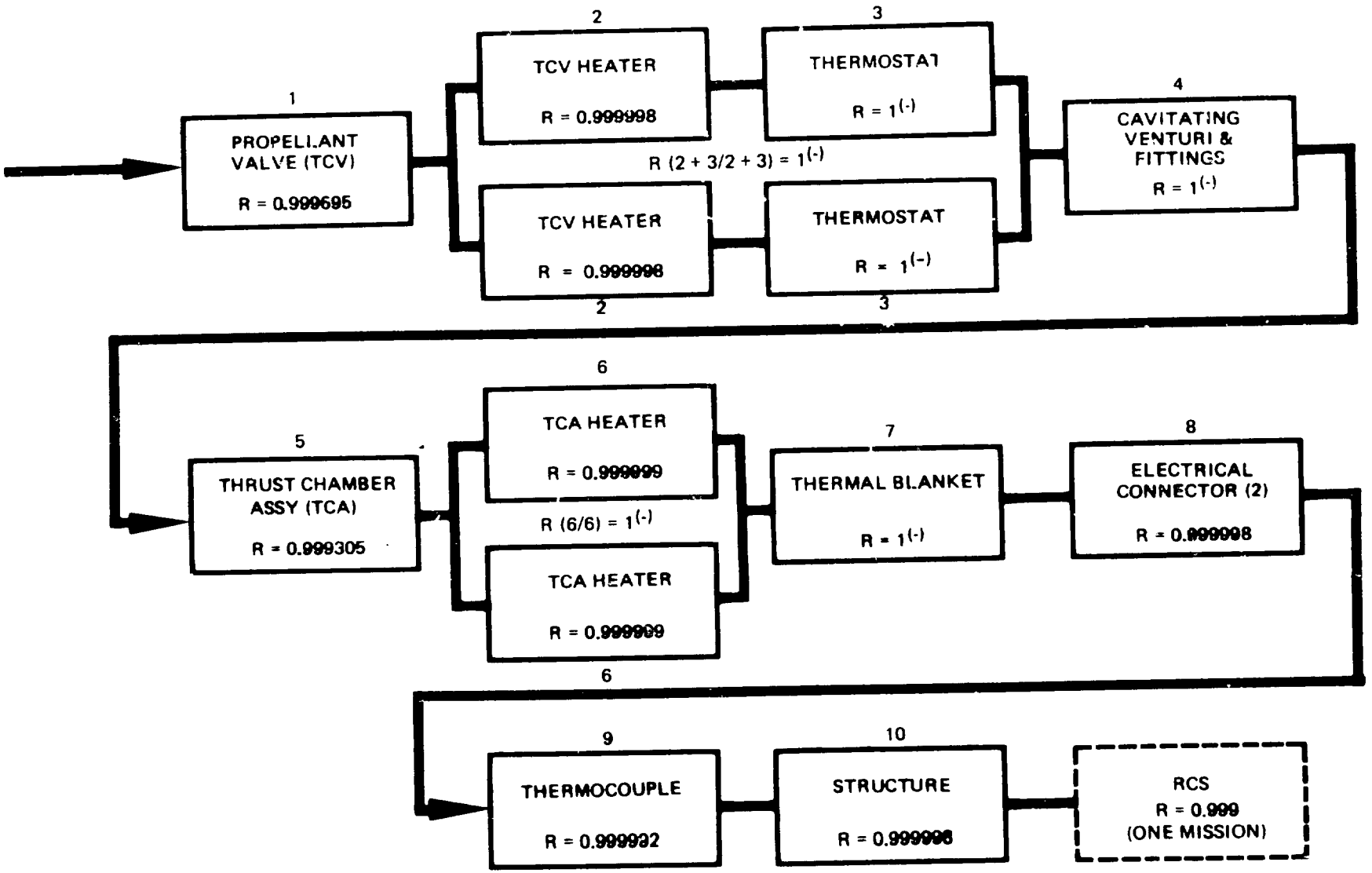

Figure 7.1-3

Table 7.1-1
RELIABILITY BLOCK FAILURE RATE DATA

Index No.	Reliability Block	Qty (n)	Generic Failure Rate ($\lambda_G \times 10^{-6}$)	Mission Phase Code	Modification Factors		$\lambda_o = n\lambda_G K_E K_A$ ($\lambda_o = \lambda_t$ or λ_c) $\times 10^{-6}$	Time (t_i in hrs) or Cycles (C_i)	$\lambda_t t_i$ or $\lambda_c C_i$ $\times 10^{-6}$	Mission Failures $x_i = \lambda_t t_i + \lambda_c C_i$ $\times 10^{-6}$
					K_E	K_A				
1	Propellant valve (TCV)	1	5.0	a)	900	0.001	4.5	0.2 hr.	0.9	
			5.0	b$_1$)	1	0.001	0.005	168 hrs.	0.84	
			0.01*	b$_2$)	1	1	0.01	168 hrs.	1.68	
			5.0	c)	1	1	5.0	0.278 hrs.	1.39	
			0.15	d)	1	1	0.15	2000 cy.	300	305.0
			5.0	e)	90	0.001	0.45	0.5 hr.	0.225	
2	TCV heater	1	0.4	a)	900	0.401	0.36	0.2 hr.	0.072	
			↑	b)	1	0.001	0.0004	163 hr.	0.065	
			↓	c)	1	1	0.4	5 hrs.	2.0	
			0.4	e)	90	0.001	0.036	0.5 hr.	0.018	2.2
3	Thermostat	1	0.07	a)	900	0.001	0.063	0.2 hr.	0.013	
			↑	b)	1	0.001	0.0001	163 hrs.	0.015	
			↓	c)	1	1	0.07	5 hrs.	0.35	
			0.07	e)	90	0.001	0.0063	0.5 hr.	0.003	0.4
4	Cavitating venturi and fittings	1	0.05**	a)	900	0.001	0.0045	0.2 hr.	0.001	
			↑	b)	1	0.001	0.00005	168 hrs.	0.0084	
			↓	c)	1	1	0.05	0.278 hr.	0.0139	
			0.05	e)	90	0.001	0.00045	0.5 hr.	0.0003	0.02
5	Thrust chamber assy (TCA)	1	23.1	a)	900	0.001	20.79	0.2 hr.	4.16	
			23.1	b)	1	0.001	0.023	168 hrs.	3.86	
			23.1	c)	1	1	23.1	0.278 hr.	6.42	
			0.34	d)	1	1	0.34	2000 cy.	680	695.5
			23.1	e)	90	0.001	2.079	0.5 hr.	1.04	
6	TCA heater	1	0.4	a)	900	0.001	0.36	0.2 hr.	0.072	
			↑	b)	1	0.001	0.0004	165 hr.	0.066	
			↓	c)	1	1	0.4	3 hr.	1.2	
			0.4	e)	90	0.001	0.036	0.5 hr.	0.018	1.4

Mission Phase Code: a, launch; b, orbit nonoperating; c, orbit operating time dependent; d, orbit operating cycle dependent; e, deorbit and landing

NOTES: *Leakage failure mode (see paragraph 4.2.1)

**The generic failure rate for a cavitating venturi is 0.005×10^{-6}. An additional failure rate allowance of 0.045×10^{-6} has been included to account for potential leakage of fittings while pressurized.

Table 7.1-1 (Concluded)
RELIABILITY BLOCK FAILURE RATE DATA

Index No.	Reliability Block	Qty (n)	Generic Failure Rate ($\lambda_G \times 10^{-6}$)	Mission Phase Code	Modification Factors		$\lambda_o = n\lambda_G K_E K_A$ ($\lambda_o = \lambda_t$ or λ_c) x 10^{-6}	Time (t_i in hrs) or Cycles (C_i)	$\lambda_t t_i$ or $\lambda_c C_i$ x 10^{-6}	Mission Failures $x_i = \lambda_t t_i + \lambda_c C_i$ x 10^{-6}
					K_E	K_A				
7	Thermal blanket	1	0.001	a)	900	0.001	0.0009	0.2 hr.	0.0002	
			0.001	c)	1	1	0.001	168 hrs.	0.17	
			0.001	e)	90	0.001	0.00009	0.5 hr.	0.00005	0.2
8	Elect. connector	5 pins	0.002	a)	900	0.001	0.009	0.5 hr.	0.0018	
			0.002	c)	1	1	0.01	168 hrs.	1.68	1.8
			0.002 per pin	e)	90	0.001	0.0009	0.2 hr.	0.0005	
9	Thermocouple	1	0.05	a)	900	0.001	0.045	0.2 hr.	0.009	8.4
				c)	1	1	0.05	168 hrs.	8.4	
				e)	90	0.001	0.0045	0.5 hr.	0.0023	
10	Structure	1	0.01	a)	900	1	9.0	0.2 hr.	1.8	
			↕	b)	1	0.001	0.0001	168 hrs.	0.0017	2.3
				c)	1	0.5	0.05	0.278 hr.	0.0014	
			0.01	e)	90	1	0.9	0.5 hr.	0.45	
	INSTRUMENTATION***									
	Press. transducer	1								
	Thermocouple	1								
	Thermistor	1								
	TCV position indicator switch	1								
	Connector	1								

Mission Phase Code: a, launch; b, orbit nonoperating; c, orbit operating time dependent; d, orbit operating cycle dependent; e, deorbit and landing

NOTES: ***Instrumentation is not included because it is not essential to mission success.

APPENDIX 7.2

TEST FACILITIES

APPENDIX 7.2 TEST FACILITIES

Two separate test facilities were used for the RCS test firings – a sea-level test cell and an altitude facility. Sea-level firings were conducted using the RRC high energy test cell located in Redmond, Washington. The 400-ft^2 cell was equipped with full instrumentation lead connectors to the laboratory data center. A schematic of the test setup is shown in Figure 7.2-1. Two temperature conditioned propellant tanks were used. The 400-gallon tank was used for steady-state firings and most of the pulse-mode firings. The smaller 35-gallon tank was used for selected pulse-mode tests to measure propellant consumption during pulsing operation of the RCS.

All RCS altitude simulation tests were conducted at the Boeing Tulalip test site located 35 miles north of RRC's Redmond, Washington, facilities. The Area 34 altitude test facility includes a 10,000-ft^3 environmental chamber, a 640-ft^3 environmental chamber, two steam ejector systems, a cooling tower, a steam generating plant, a 2,500-ft^2 assembly area, and an adjoining control area.

The vacuum system for altitude simulation consists of two steam ejector systems. One system is a five-stage ejector capable of evacuating the tank to a simulated altitude of 230,000 feet, under no-flow conditions. To accommodate test specimen out-gassing, the same system can evacuate the chamber at a constant rate of 135 pounds per hour to maintain a consistent 200,000-foot altitude simulation. The second vacuum system consists of a two-stage ejector system capable of exhausting 1,350 pounds per hour at 96,000-foot altitude simulation or 9,600 pounds per hour at 25,000-foot altitude simulation. This system is used during tests on high flow test specimens.

Long duration engine firings were conducted at fully expanded, balanced nozzle exhaust flow conditions by augmenting the vacuum pumping characteristics of the Tulalip test facility with RCS second throat exhaust diffuser as shown in Figure 7.2-2. A schematic of the altitude test setup is presented in Figure 7.2-3.

SPACE SHUTTLE RCS SEA LEVEL TEST FIRING SCHEMATIC

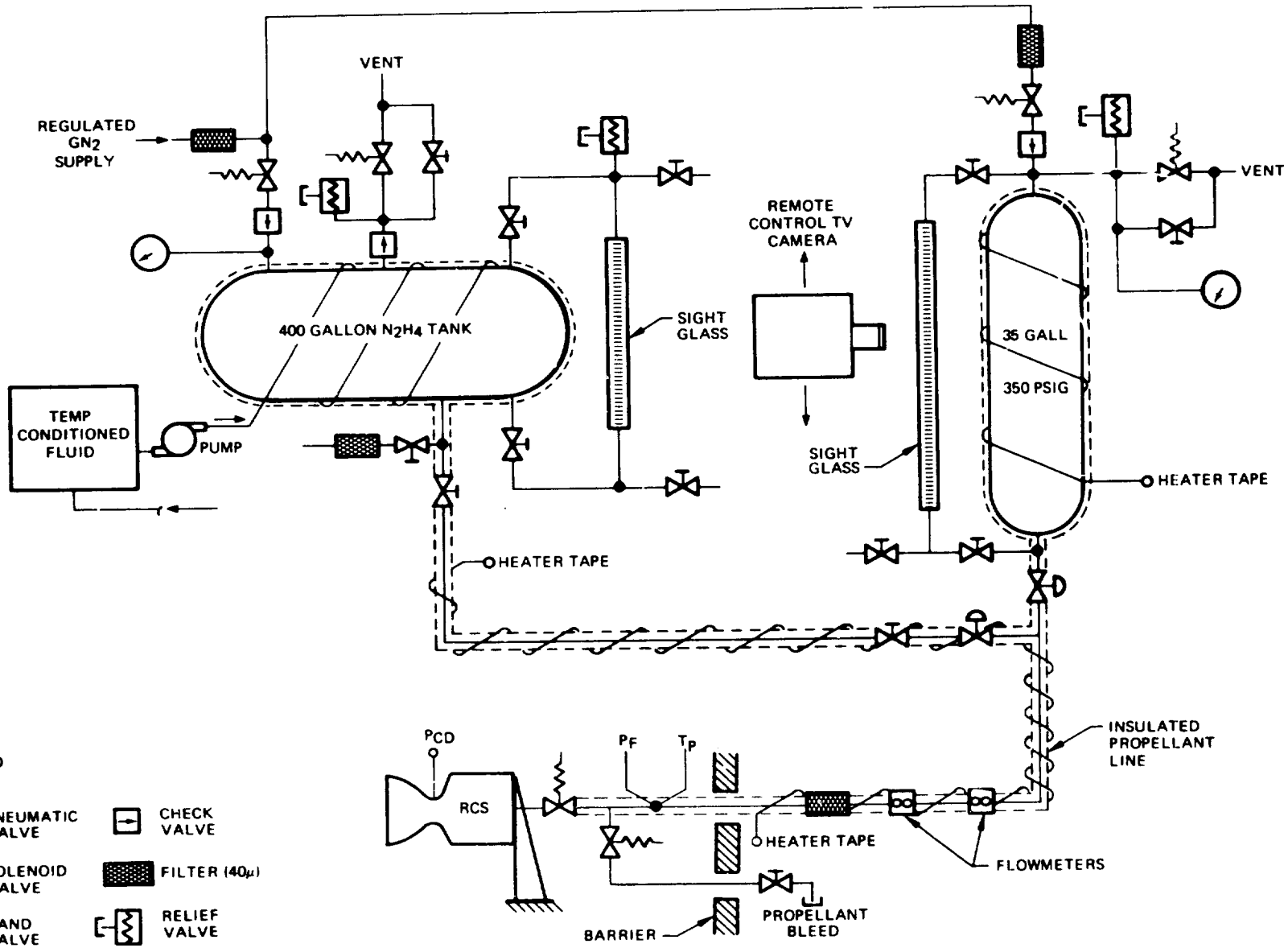

Figure 7.2-1

SPACE SHUTTLE RCS ALTITUDE TEST CELL ESTIMATED OPERATING PRESSURES

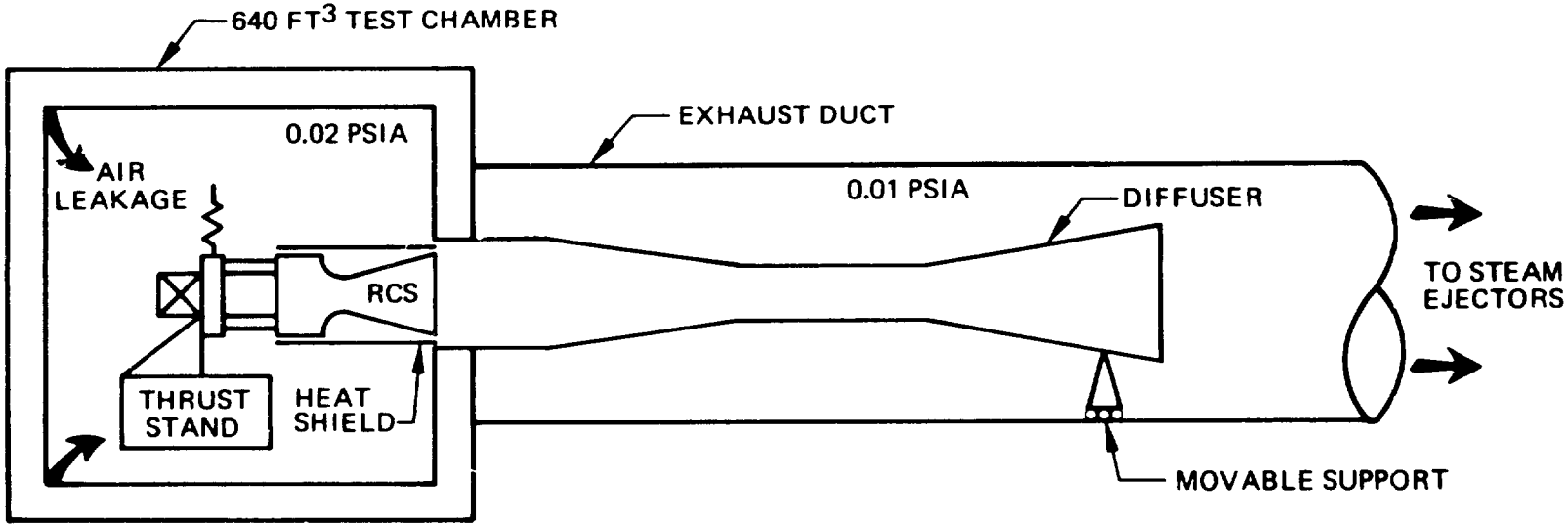

a) PRETEST CONDITIONS IN ALTITUDE TEST CELL

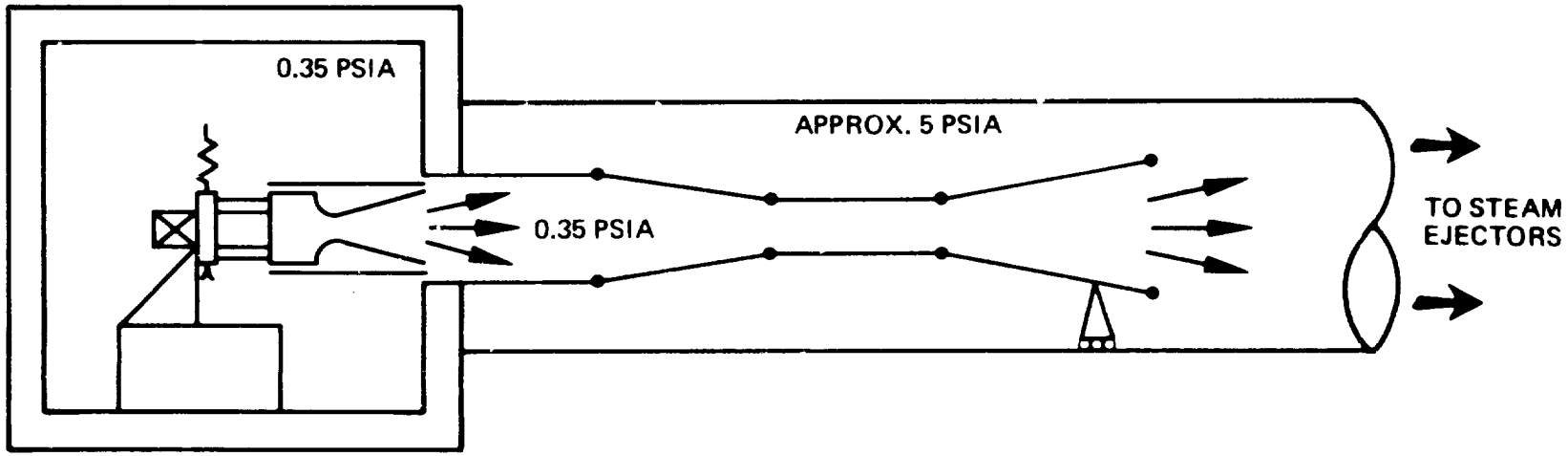

b) STEADY STATE FLOW CONDITIONS FOR 490 lbf THRUST RCS

Figure 7.2-2

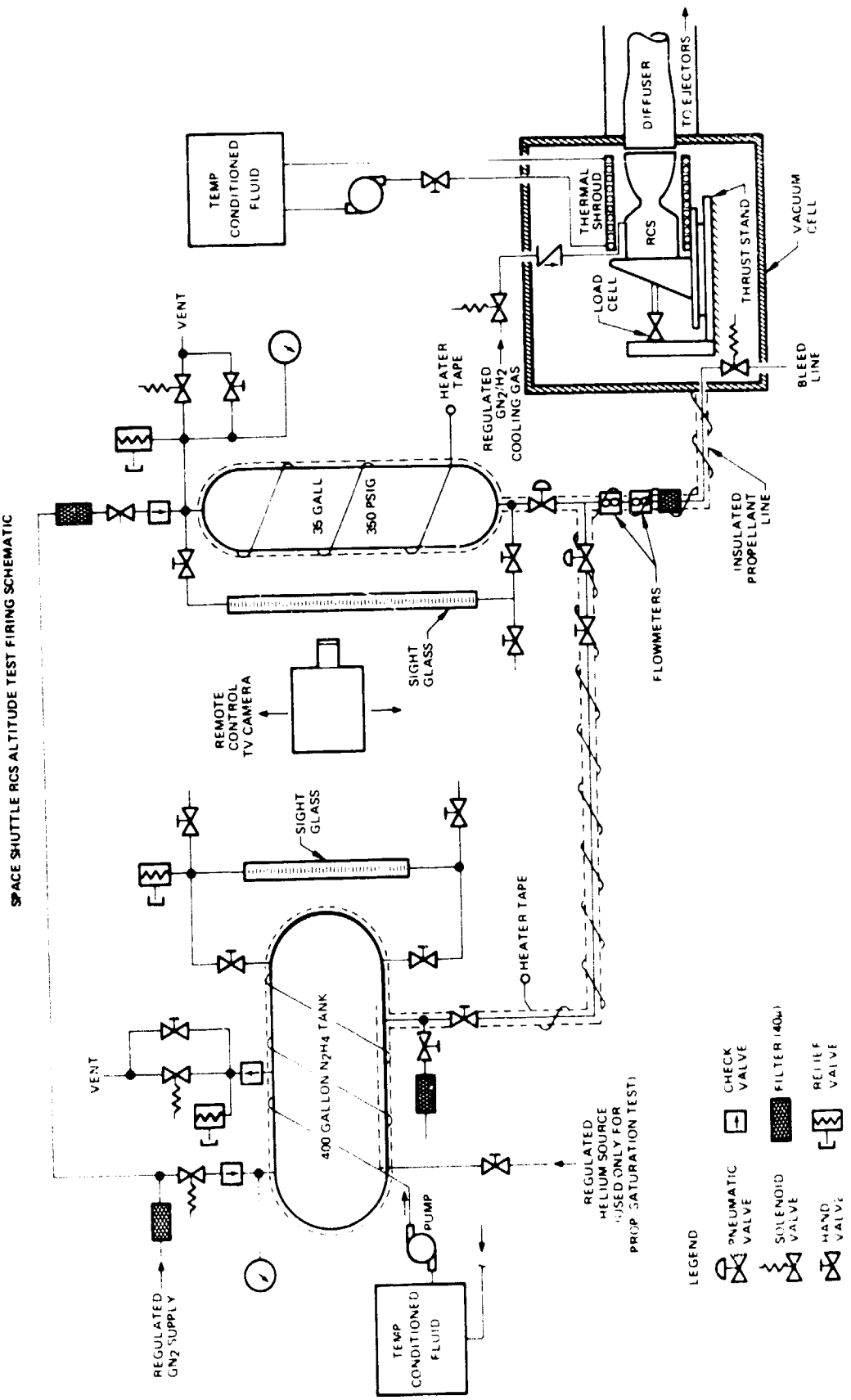
SPACE SHUTTLE RCS ALTITUDE TEST FIRING SCHEMATIC
TEMP CONDITIONED FLUID
DIFFUSER
TO EJECTORS
THERMAL SHROUD
RCS
VACUUM CELL
THRUST STAND
LOAD CELL
BLEED LINE
VENT
HEATER TAPE
REGULATED GN2/H2 COOLING GAS
35 GALL
350 PSIG
INSULATED PROPELLANT LINE
FLOWMETERS
SIGHT GLASS
REMOTE CONTROL TV CAMERA
SIGHT GLASS
HEATER TAPE
400 GALLON N2H4 TANK
VENT
REGULATED HELIUM SOURCE (USED ONLY FOR PROP SATURATION TEST)
PUMP
REGULATED GN2 SUPPLY
TEMP CONDITIONED FLUID
LEGEND
PNEUMATIC VALVE
CHECK VALVE
SOLENOID VALVE
FILTER (40μ)
HAND VALVE
RELIEF VALVE

Figure 7.2-3

REFERENCES

1-1 Nyberg, D. G., *Test Report – Viking Duty Cycle Demonstration Using a Space Shuttle (Wedge) Engine*, RRC 74-R-406, December 12, 1973

1-2 Marshal, G. H., *Post-Test Inspection Results of the MR-3A 26.5-lbf Thrust Rocket Engine Assembly*, RRC-73-R-350, 1974

3-1 Roubidoux, T. O. and Monrad, F. O., *Space Shuttle Materials Report*, RRC-73-R-373, April 27, 1973

3-2 Schmidt, E. W. and Krug, J. W., *Oxygen Damage to Hydrazine Decomposition Catalysts*, RRC-73-ES-75, November 27, 1972

4-1 Eggers, R. F. and Jorgenson, W. E., *Preliminary Analysis of the Preflight Checkout, Maintainability, and Post-Test Service Requirements of the Space Shuttle RCS Engine*, RRC-73-R-358, February 23, 1973

5-1 *Test Plan – Monopropellant Engine Investigation for the Space Shuttle RCS*, RRC-TP-0258, April 1973